Electrical Degradation of Crystalline Silicon PV Modules in Indian Climates and its Correlation with Cell Cracks: Field and Laboratory Studies

Submitted in partial fulfillment of the requirements
for the degree of

Doctor of Philosophy

by

Rajeev Dubey

(Roll no. 113190014)

Supervisors
Prof. Anil Kottantharayil
Prof. Juzer Vasi

Department of Electrical Engineering

INDIAN INSTITUTE OF TECHNOLOGY BOMBAY

2020

Dedicated to my teachers…

Thesis Approval

The Thesis entitled

Electrical Degradation of Crystalline Silicon PV Modules in Indian Climates and its Correlation with Cell Cracks: Field and Laboratory Studies

by

Rajeev Dubey
(Roll No.113190014)

is approved for the degree of

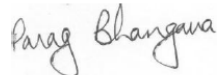Doctor of Philosophy

_____
Prof. Anil Kottantharayil

_____
Prof. J. Vasi

_____
Prof.Narendra Shiradkar

_____
Dr. Dirk Jordan

_____
Prof. Parag Bhargava

Date:(19/05/2021)

Place: IIT Bombay, Mumbai

Declaration

I declare that this written submission represents my ideas in my own words and where others' ideas or words have been included, I have adequately cited and referenced the original sources. Some parts of Chapters 4, 5 and 6 have been published in the form of All-India survey reports by the National Center for Photovoltaic Research and Education (NCPRE) at IIT Bombay, and also in various international conferences and journals, as listed at the end of this thesis.

I hereby declare that I have adhered to all principles of academic honesty and integrity and have not misrepresented or fabricated or falsified any idea/data/fact/source in my submission. I understand that any violation of the above will be cause for disciplinary action by the Institute and can also evoke penal action from the sources which have thus not been properly cited or from whom proper permission has not been taken when needed.

Rajeev Dubey
(113190014)

Date: 20th May, 2021

Abstract

An understanding of degradation mechanisms and the impact of the harsh climate on modules' durability is important for assessing the reliability of PV modules in India. Although the modules sold in the market are certified as per the IEC 61215 standard or equivalent, this does not guarantee the 25-year field life claimed by the manufacturers. The available literature on degradation rates of solar panels installed in different parts of the world shows that there are differences in the degradation rates depending on the location of the system. Furthermore, from the available literature, it is evident that there is a lack of information regarding the degradation rates reported from the fielded modules of India, especially in the hot climatic zones. Considering the lack of information with regard to the long-term performance of PV systems in different climatic conditions of India with respect to different degradation modes (like cell cracks, PID), it has been the objective of the All India Surveys of PV Module reliability, carried out in 2014 and 2016. This includes a study of the dependence of performance on the climatic zone, system size, module technology, age, and type of installation. An exhaustive error analysis has been done and it has been assessed that the maximum possible total error in the P_{max} degradation rate is 9% and 5% for crystalline silicon modules measured at irradiance above 500 W/m^2 and 700 W/m^2 respectively. The field-aged PV modules have been characterized with the help of lighted *I-V*, dark *I-V*, insulation resistance measurement; interconnect breakage test, infrared thermography, and Electroluminescence (EL). The analysis of survey data shows that there is wide variability in the annual module degradation rate, and it is generally higher than international benchmarks. It can be seen from the survey results that there is a lot of variability even in the performance of crystalline silicon modules. Almost half of the surveyed sites of c-Si modules are performing reasonably well (classified as Group X), while the rest of the c-Si sites (classified as Group Y) are not. These observations point to problems regarding module quality and/or installation procedures. It has also been found that degradation rates are higher in hot climates. Furthermore, the average power degradation rate for large installations is significantly lower than that for small/rooftop installations. In addition, cell cracks are the main reason for the high degradation rate in young modules falling in Group Y. Around 88% of Group Y and 80% of the 'Outlier' modules are in the young age category which implies a low quality of these young

modules and / or improper installation practices in recent years. There is a good correlation between the total number of cell cracks in the module and the power degradation of the module. In old crystalline silicon modules, the main contributor to P_{max} degradation is I_{sc} followed by *FF*, whereas in the case of young crystalline silicon modules the main contributor to the P_{max} degradation is *FF* degradation.

A method to measure the temperature coefficients of voltage (*β*) and current (*α*) for the PV modules in the field has been developed, and based on this methodology a dedicated instrument that can measure the temperature coefficients has been built. One of the key findings from the field surveys was that many modules were suffering from a large number of cell cracks. To achieve a statistically large number of EL images with high throughput in the field, a portable and inexpensive EL camera was developed by modifying a normal digital camera. This has been compared with the laboratory-grade EL camera as per the procedure defined in IEC TS 60904-13. Furthermore, an image difference technique was developed to capture the EL image in presence of ambient light.

To understand the impact of cracks generated due to the mechanical loading on the degradation seen in the field, it was needed to be studied more systematically in the laboratory. To meet this requirement, a novel lab-based Dynamic Mechanical Loading (DML) tool was developed. The major advantages of this tool are (1) the pressure applied is uniform, and (2) the front side of the solar panel is available for *I-V* and EL when the DML testing is in progress. These advantages were not available in the existing mechanical loading tool like 'suction cup'. This novel tool can subject the PV module to static and dynamic loads simulating a variety of conditions seen in the field and used to conduct detailed accelerated tests on PV modules. The results of the accelerated tests show that as the severity of crack (in terms of total dark area in the cell and the number of crack) increases, there is a reduction in P_{max}, and this is different for different interconnect designs. The degradation in the P_{max} is mainly due to the degradation in *FF*. There is good agreement in the trends seen in field and laboratory studies. Furthermore, the degradation in power and the number of Mode C cracks show a saturating trend with number of cycles used in the DML accelerated testing. Mechanical loading at a lower frequency (slow DML) requires more number of cycles to create cracks as compared to a higher frequency (fast DML). Therefore the recommended recipe for the dynamic mechanical loading for accelerated testing is 1000 Pa pressure at 8 cycles/min and 1000 number of cycles.

In summary, the work reported in this thesis describes the reliability, durability, and performance of the PV modules deployed in the field, and the development of tools and techniques suitable for field characterization. The study has shown that the cracks in the solar cell are one of the most common degradation modes in young modules. Hence, it became important to carry out a systematic laboratory study to understand the origin and the impact of cracks on the performance of the PV module. As a result, a novel laboratory tool and special accelerated methods were developed to study the effect of cracks in a systematic manner.

Contents

List of Figures

power supply at IIT Bombay.

List of Tables

Abbreviations Notations and Nomenclature

a-Si	Amorphous silicon
AR	Anti-reflecting
ASTM	American Society for Testing and Materials
ASU-PRL	Arizona State University Photovoltaic Reliability Lab
BoM	Bill of Materials
c-Si	Crystalline silicon
CdTe	Cadmium Telluride
CIGS	Copper Indium Gallium Selenide
CMOS	Complementary Metal–Oxide–Semiconductor
DML	Dynamic Mechanical Loading
DUT	Device Under Test
E_a	Activation Energy (eV)
EL	Electroluminescence
FMEA	Failure Modes, Effects, and Criticality Analysis
FSEC	Florida Solar Energy Center
G	Plane of array irradiance at the time of IR measurement (W/m^2)
GW	Giga Watt
IEA	International Energy Agency
IEC	International Electrotechnical Commission
I_L	Photo-generated current (A)
I_o	Reverse saturation current (A)
IPCC	Intergovernmental Panel on Climate Change

IR	Infrared Thermography
I_{sc}	Short circuit current, (A)
$I\text{-}V$	Current voltage
J_{02}	Space-charge region current density (A/m^2)
J_o	Reverse leakage current density (A/m^2)
JPL	Jet Propulsion Laboratory
LID	Light Induced Degradation
mono c-Si	Mono crystalline silicon
multi c-Si	Multi crystalline/polycrystalline silicon
MW	Mega Watt
NCPRE	National Centre for Photovoltaic Research and Education
NIR	Near Infra-red
NISE	National Institute for Solar Energy
NREL	National Renewable Energy Laboratory
PERC	Passivated Emitter Rear Cells
PL	Photoluminescence
PLC	Programmable Logic Controller
$P_{LID\_discounted}$	LID discounted power rating
P_{max}	Maximum rated power (W)
$P_{Nominal}$	Nominal Power Nameplate
$P_{Present}$	Measured Power at STC
PR	Performance Ratio
PV	Photovoltaics
RPN	Risk Priority Number
R_s	Series resistance (Ohms)

R_{sh}	Shunt resistance (Ohms)
USA	United States of America
UV	Ultra-Violet
V_{oc}	Open circuit voltage (V)
V_T	Thermal equivalent voltage
η	Electrical efficiency of the solar cell
n	Ideality factor
τ	Minority carrier lifetime
α	Temperature coefficient for current (A/°C)
β	Temperature coefficient for voltage (V/°C)
k	Curve correction factor

Chapter 1

Introduction

1.1   Background

The term 'energy demand' is utilized to describe the total consumption of energy by human activities. It guides the entire energy system. It influences the usage of total amount of energy, type of energy source and it also influences the energy consumption by the end use technologies. The energy demand has been rising very fast since the industrial revolution in 1760, and will continue to do so in the future. It has been estimated by the Energy Information Administration [1] that the total energy consumption of the world will increase by 50% between 2018 and 2050. Currently and in the past, most of the energy demand is met from fossil fuel sources resulting in harmful greenhouse gases (like methane, carbon dioxide etc). As a result, meteorological measurements indicate that the earth's surface temperature has increased by 0.8 ℃ on average in

the last 140 years [2]. It has been estimated that global energy-related carbon dioxide emissions increased by 1.7% to 33 Gigatonnes (Gt) in 2018 [3]. Coal alone contributes 10 Gt, standing third in the rank in greenhouse gas emission [3]. A majority of these emissions came from recently developed coal power plants in Asia [3]. In an attempt to reduce these emissions, the Paris Climate Agreement was signed by 197 countries in 2015. They set a target to limit global temperature rise well below 2 ℃ above the pre-industrial levels to avoid catastrophic climate change [4]. In order to restrict the average global temperature rise from exceeding 1.5 ℃, the Intergovernmental Panel on Climate Change (IPCC) has suggested in a special report in 2018 that global net emission of carbon dioxide should fall by 45% from 2010 level and become "net zero" by 2050 [5]. According to a report [1] published in 2019, it is projected that renewable (solar, wind and hydroelectric) would be the fastest growing energy sources between 2018 and 2050. It also projects that the worldwide renewable energy consumption would increase by 3.1%/year between 2018 and 2050 as compared with 0.6%/year growth in fossil based energy sources. India's National Solar Mission has set a target of installing 100 GW of solar power in India by 2022 [6], in addition to 75 GW from non-solar based renewable energy sources. In recent times, due to the rapid progress in installation, the Indian Government has revised the targets to 227 GW of renewable energy capacity [7]. Of all the renewables, solar energy, and especially solar photovoltaic, has seen the greatest deployment in recent years. Figure 1.1 shows the rapid growth in solar photovoltaic capacity worldwide in the last decade [8]. This expeditious growth is due to a significant drop in the prices of solar panels. From the figure, it is evident that from the year 2008 there is a continuous and rapid reduction in the price of the solar PV module and as a result, there is a boost in the PV module installed capacity.
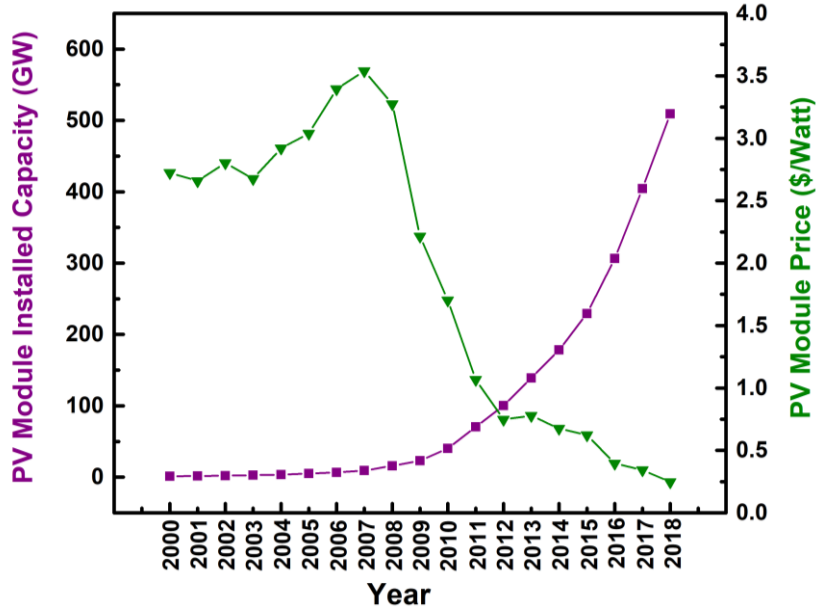
Fig. 1.1: Total installed capacity of solar photovoltaic systems in the world [8] and corresponding solar panel prices [9] [10].

1.2   Solar Photovoltaics

Solar radiation is the most abundant source of energy on earth [11]. Solar Photovoltaics is defined as the process of converting light (photons) to electricity (voltage), which is called the photoelectric effect. In 1954 scientists at Bell Laboratories were the first to utilize this phenomenon to create a working solar cell (made from silicon) that could generate an electric current when subjected to sunlight [12]. This section presents a very brief overview of solar cells and modules. Photons having energy higher than the band gap of the energy of the semiconductor are absorbed by the solar cell. Electrons in the valence band get excited into the conduction band as shown in Fig. 1.2. By this phenomenon an electron-hole pair is generated, which gets separated by the p-n junction [13]. Silicon based solar cells typically have 1 μs recombination lifetime [13]. If these carriers are collected by contacts before the recombination then an external current is extracted from the device [14].

3
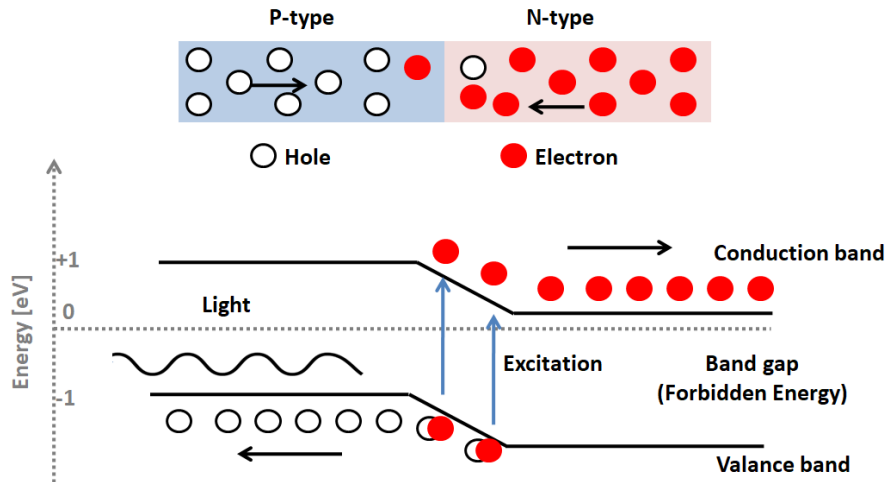
Fig. 1.2: Electron-hole pair generation due to light absorption. Red solid circle are electrons and white hollow circles are holes.

The 'single diode model' is the most common equivalent circuit model for a solar cell. Figure 1.3 shows the circuit for a single diode model. It is represented by five parameters: photo-generated current (I_L), reverse saturation current (I_o), series resistance (R_s), shunt resistance (R_{sh}), and ideality factor (n). Equations 1.1 and 1.2 represent the current voltage (I-V) relationship for the equivalent circuit.

$$I = I_L - I_D - I_{sh} \tag{1.1}$$

$$I = I_L - I_o \left[\exp\left(\frac{V+IR_s}{nV_T}\right) - 1 \right] - \frac{V+IR_s}{R_{sh}} \tag{1.2}$$
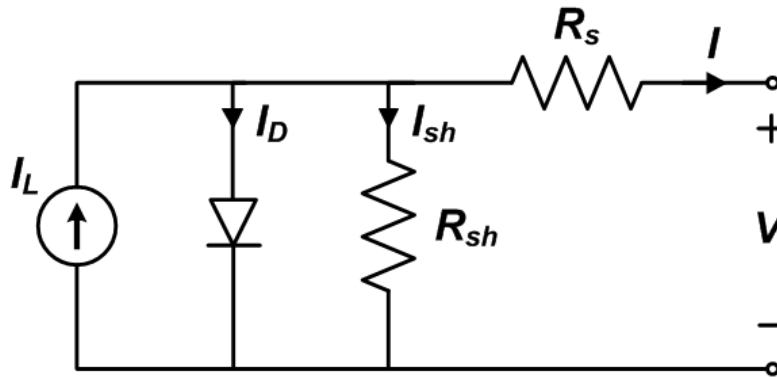
Fig. 1.3: Single diode equivalent circuit of a solar cell.

4

Crystalline silicon PV modules are manufactured by encapsulating solar cells using glass and different polymers. Currently in the market, most commercially available crystalline silicon PV modules consist of 60 or 72 series connected solar cells. This type of PV module design typically consists of three bypass diodes. Bypass diodes prevent the overall power loss in generation due to partial shading. Figure 1.4 shows the structure of a 60 cell crystalline silicon PV module technology [15].
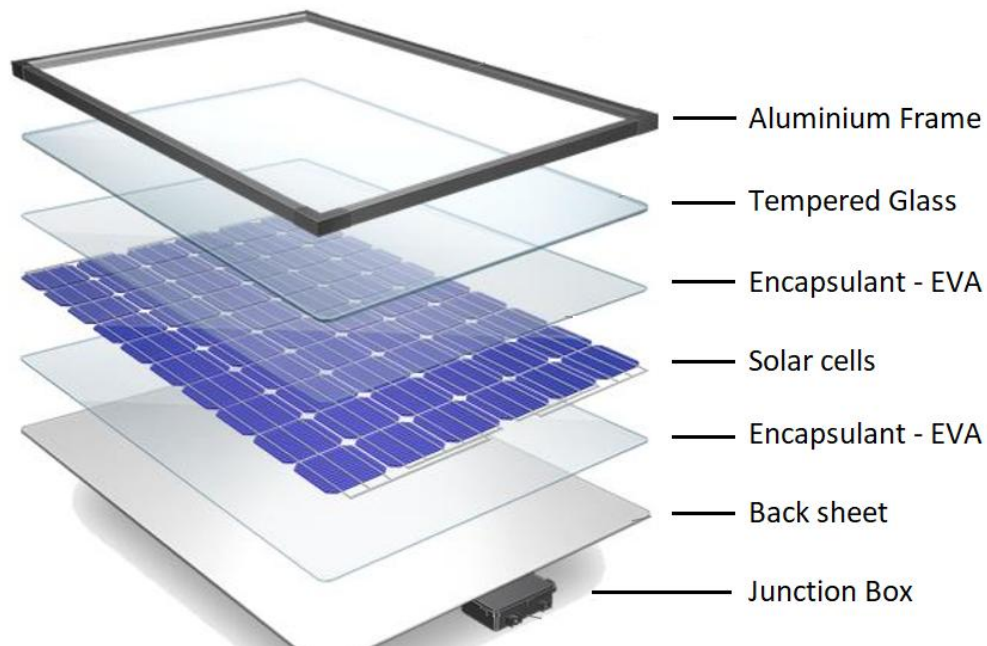
Fig. 1.4: Various components of the crystalline silicon PV module [15].

The function of various components is described in Table 1.1. From a reliability point of view (which will be the main thrust of this thesis) every component is important. Degradation in any component can leads to reduction in overall power output of the PV module and can also cause catastrophic failure.

Table 1.1: Different components of PV module and their purpose [16].

Components	Function
Junction Box	Includes bypass diodes and fuse to protect the solar cells. Protects the bypass diode, the fuse and external terminals from harsh environmental factors like dust and moisture.
Backsheet	Helps in electrical isolation and prevents moisture ingress.
Ribbon	Electrically connects the solar cell to the external circuit.
Encapsulant	Provides cushioning for the solar cells. It also provides electrical isolation, and adhesion between the glass, solar cell and backsheet while allowing maximum light to transmit.
Solar cell	Converts incident light energy into electrical energy.
Glass	Gives mechanical rigidity and protect from harsh environmental factors like dust and moisture.
Frame	Gives mechanical rigidity and holds all the components together

1.3 Motivation, Aim & Objectives of this Work

India's National Solar Mission has set a target of installing 100 GW of solar power in India by 2022. This is resulting in significant investment in the solar energy sector. The actual success of this mission will depend on energy generation from the power plants over the long term. Given the continued price pressure on PV module manufacturers in recent years, it is important to keep a constant watch on the performance of the installed modules, and to assess their long-term durability and reliability. At the same time, it is also important to understand the impact of the harsh climatic zones of India on modules' durability. Although the modules sold in the market are certified as per the IEC 61215 standard [17], this does not guarantee the 25-year field life claimed by the manufacturers. This IEC certification is mainly suited to screen the modules for infant mortality [18]. Any change in the design and the bill of material (BoM) can impact the reliability and durability of the modules. Considering the lack of information with regard to the long-term performance of PV systems in different climatic conditions of India, the National

Centre for Photovoltaic Research and Education (NCPRE) and the National Institute for Solar Energy (NISE) have jointly undertaken 3 surveys in 2013 [19], 2014 [19] and in 2016 [20] [21] across the whole country to understand the reliability and the performance of the solar panels deployed in the field. This includes a study of the dependence of performance on climatic zone, system size, module technology, and age and type of installation. The details of these surveys have been described in more detail in the Chapter 4 of the thesis. This chapter will mainly focus on the electrical performance of the field-aged PV modules, which has been characterized with the help of lighted *I-V*, dark *I-V* and Electroluminescence (EL).

The power output of photovoltaic modules depends on the temperature of operation and irradiance. In order to estimate the performance of a module from an *I-V* data measured in the field, it is necessary to have precise values of temperature coefficient of the module, since the measured data needs to be translated to standard test condition (STC) which is 1000 W/m^2 and 25 ºC [22], so that it could be compared with the name plate values (measured at STC in lab). Manufacturer's datasheet and literature are typically the source to obtain the values of temperature coefficient of the module. But these values are very generic and can introduce errors during the STC translation. Hence, it was deemed necessary to develop a methodology to obtain the temperature coefficient of the module in the field, so that error in the translation could be reduced. Moreover, it was also felt that a dedicated field portable tool should be developed which can measure the temperature coefficient in a faster and in an efficient way.

One of the key findings from the All India Survey 2014 data was that young modules (age less than 5 years) were suffering from a large number of cell cracks. These cracks may have been produced during cell or module manufacture, or may have developed later due to transportation or poor handling and installation. Therefore, it was important to obtain a large number of EL images of modules, in order to identify the origin of these cell cracks. This could be achieved by using a portable and inexpensive EL camera, so that multiple such cameras could be deployed in the field during surveys. Therefore, it was felt necessary to develop a portable and inexpensive EL camera. We developed such a camera by modifying a normal digital camera. During its operation in the field, it was felt that some enhancement (like using IR lamp to focus) should be done in order to ease its operation and also to improve the quality of the EL images. Furthermore, image difference technique was developed to capture the EL image in presence of ambient light, in order to avoid the limitation of capturing the EL images in the dark at night.

The technique we developed is capable of capturing the EL images at low irradiance, suitable for operating during evenings in the field.

Consistent results were obtained from both the surveys done in 2014 and 2016 that young modules (age less than 5 years) were suffering from a large number of cell cracks. In order to understand the physical reason for the development of cracks and how much they can impact on the performance of the PV module, it was felt necessary to develop a stress test tool which will simulate and accelerate the same effects on the PV module in the laboratory which it experiences in the real field conditions. Thus a dynamic mechanical tool was developed which can subject the PV module to static and dynamic loads simulating a variety of conditions seen in the field. Moreover, we have performed accelerated tests to determine the impact of cracks on the performance of the PV module. Also, we have tried to obtain parameters like pressure, frequency (number of cycles/min) and total number of cycles for dynamic mechanical loading that can give similar effects obtained in thermal cycling.

In summary, this work focuses on the reliability, durability, and performance of the PV modules deployed in the field. The individual components of the PV module undergo degradation by different modes when deployed in the field. Consequently, to have mature growth for the PV industry the ability to accurately predict the output power is of key importance. Module manufacturers claim 25 years warranty, with only a 20% reduction in power output. Hence, it becomes necessary to undertake long term field studies in different climatic conditions to evaluate the reliability and the durability of the PV modules and validate the warranty terms. Testing the modules deployed in the field would serve an important role in determining the PV modules performance and lifetime for basically two reasons, one it helps in correlating the indoor test result with the outdoor results, and secondly, it is the normal operating conditions. Based on the field experiences and failure analysis done on the degraded modules would help in designing more and more rigorous accelerated tests. Subsequently, it would help in designing a conclusive qualification standard that would ensure the long term reliability of the PV module. In order to, effectively understand the degradation mode prevalent in any climatic zone, it is important to collect quality and statistically large numbers of data. As a result, unique characterization tools and methodologies are needed to develop to collect data efficiently and effortlessly in the field. Cracks in the solar cell are the most common degradation mode. It has been found that cracks cause severe degradation in power loss. These cracks are developed due

8

to snow loading, wind loading, during installation, or transportation. Hence, it is important to carry out a systematic laboratory study to understand the origin and the impact of cracks on the performance of the PV module. As a result, special accelerated methods and types of equipment which can replicate exact similar conditions that a PV module experience in the field are needed.

1.4   Thesis structure

The work done in this thesis focuses on the reliability, durability, and performance of the PV modules deployed in the field. This thesis consists of 7 chapters. Chapter 2 presents a brief literature review of degradation rates and modes reported internationally and from India. It also provides some information on the development of various characterization tools like inexpensive EL cameras and mechanical loading tools and techniques.

Chapter 3 provides an overview of the various characterization tools and methodologies used in the outdoor (or field surveys) and indoor. An analysis of the 2014 and 2016 survey data is presented in Chapter 4. In this chapter comparison of 2014 and 2016 survey data is also presented. It has been found that the modules in hot climate degrade at a faster rate than non-hot zones. It is also evident from the analysis that cell cracks are the major reason for the degradation in young modules (age less than 5 years). Several other conclusions are also drawn from the data and analysis presented in this chapter.

Chapter 5 contains a description of some of the new characterization tools which we needed to develop for simulating mechanical stresses with different kinds of load on the PV modules. It also describes the development of inexpensive camera and temperature coefficient measurement devices. Some of the new field characterization methodology which we developed, like daylight EL imaging, is also presented in this chapter.

Accelerated aging of the cracked cell PV modules and its impact on performance is presented in Chapter 6. This chapter also compares the modules of different make and their power reduction when subjected to similar kinds of stresses.

Finally, the conclusions and scope of future work are outlined in Chapter 7. The outcome of two All India Surveys has been summarized, and recommendations have been presented to

achieve the ambitious target of 100 GW (and beyond). The results from the indoor accelerated tests have been summarized and relevant future work has been outlined in this chapter.

Chapter 2

Literature Review

In this chapter, the significance of the reliability and the durability in the long term performance of the PV module is illustrated. Several factors affecting the reliability of the PV module are discussed. The PV design and structure has undergone several changes and improvements since the days of its genesis. These design improvements were adapted in order to improve its durability and performance. In 1955 Bell Laboratories of USA developed the first PV module by encapsulating a 3 cm diameter solar cell in silicone oil within a plastic case which has an efficiency of around 6% [23]. Over the past several years, the solar cell efficiency was progressively enhanced from 6% to over 25% today for single junctions [24]. The solar module, which we are primarily concerned with, also underwent modifications so as to enhance its reliability and durability in the extreme outdoors environment. As a result, for many decades, degradation of PV modules under outdoor deployment has been an important focus of scientific

research [25]. The concept of laminating the solar cells to a glass coversheet using a polymer Polyvinyl butyral (PVB) with Mylar as a backsheet was introduced by Spectrolab Inc. of the USA in 1976 [26]. Although PVB had cost lower than silicone encapsulant which had been used earlier, it showed faster degradation when deployed outdoors. Finally, Ethyl Vinyl Acetate (EVA) replaced PVB in the 1980s since it was more stable and also lower in cost as compared to expensive silicones [27] [28]. Also Tedlar/polyester/Tedlar replaced Mylar backsheet since it has better resistance to UV rays and moisture penetration. Currently, most PV module designs have a multi-layered structure with high transmissivity glass followed by encapsulant that encloses the solar cells and interconnect ribbons, and then the back-sheet polymer. These entire components are held together by an aluminum frame on four sides to provide rigidity to the module (refer Fig. 1.4 in Chapter 1 of the thesis).

These individual components undergo degradation by different modes when deployed in the field. Module manufacturers offer a 25 year warranty, with only 20% reduction in power output. Hence, it becomes necessary to undertake long-term field studies in different climatic conditions to evaluate the reliability and the durability of the PV modules to assess their performance and validate the warranty terms. The relevant literature related to field and laboratory studies on performance degradation in PV modules and relevant characterization methodology and tools to quantify this performance degradation is reviewed in this chapter, and summarized in the following sections.

2.1   Electrical Degradation Reported in Field Surveys

In order to estimate the electrical degradation from various systems and be consistent in reporting the parameters, it is necessary to standardize the process of surveying the health and performance of the PV installations. This would then help in the comparison of the data from different sources. Current-Voltage characterization (*I-V*) is one of the most important characterizations done in the field to estimate the performance of the PV modules in the field. Similarly, EL and IR also assist in the estimation of the performance of the PV module. Constantly researchers have been reporting innovative techniques and tools for better estimation of reliability and durability of the PV modules. C.E. Packard *et al.* from the National Renewable

Energy Laboratory (NREL) have come up with a Visual Inspection Data Collection Tool in the form of a checklist [29]. This checklist mainly focuses on the visual degradation of PV modules like discoloration and delamination. Characterization methodology and tools play an important role in determining the quality of the results of a survey on field performance. Kazuhiko Kato of AIST Japan used an innovative equipment like the Cell Line Checker, apart from regular characterization equipment like an infrared camera, automatic *I-V* tracer, and insulation tester [30]. This innovative tool helps in detecting faults in the interconnect circuit and bypass diodes. Similarly, we tried to develop several characterization tools and methodologies which could assist in measuring useful data in the field and help in a better understanding of the various degradation modes prevalent in different climatic zones. It has been described in more detail in Chapter 5 of the thesis.

To estimate the electrical performance of PV modules, current-voltage (*I-V*) characteristics of PV modules measured in the field need to be translated to Standard Test Conditions (1000 W/m^2. irradiance and 25° C module temperature) and compared with the nameplate values. W. Herrmann of TÜV Rheinland identified several factors affecting the uncertainty in final translated parameters which also includes the measurement uncertainties [31]. His research shows that error in translated results for power output could be as high as 4% from the data collected from various laboratories in the European Union. D. Dirnberger *et al.* have shown the main sources of error in measurement and *I-V* curve translation from the data collected from field [32]. They describe that uncertainty in calibration of the *I-V* curve tracer, irradiance, and temperature sensor can cause the uncertainty in measured power. Furthermore, they indicate that out of the four model parameters (temperature coefficient of current, temperature coefficient of voltage, curve correction factor, and series resistance) the uncertainty in temperature coefficient of voltage and current has an extreme effect on the overall uncertainty. They have also recommended that the *I-V* measurement should be performed during clear sky conditions or at irradiance more than 800 W/m^2. Jordan *et al.* have mentioned and emphasized accuracies in degradation rate calculations [33]. Degradation rate in power is calculated using equation 2.1.

$$P_{max} \ Degradation \ Rate \ (\%/year) = \frac{(P_{Initial} - P_{Present})*100}{P_{Initial}*Age} \qquad (2.1)$$

In order to calculate the long term performance of a system, Jordan *et al.* have recommended that Year on Year (YOY) method has a lesser value of uncertainty since the method does not depend on the effect of seasonality [34]. Jordan *et al.* have also shown how the uncertainty in power estimation can lead to a financial risk [35]. The literature mentioned above establishes the importance of understanding the uncertainty and sources of error associated with measurements and translated values. To investigate the aspect of error further, we did laboratory experiments and performed detailed error analysis which has been described in more detail in Chapter 4 (Section 4.4.2).

2.1.1 Degradation Rates Reported Internationally

In order to have mature growth for the PV industry the ability to accurately predict the output power is of key importance [36]. Testing the modules deployed in the field has served an important role in determining the PV modules performance and lifetime for basically two reasons, firstly it helps in correlating the indoor test result with the outdoor results [34] and secondly, it is the usual operating conditions [37]. Jet Propulsion Laboratory (JPL) started the block buy program under which they used to procure the state-of-the-art PV modules and test them [38]. As a result, based on their field experiences and failure analysis done on the degraded modules, they designed more and more rigorous accelerated tests, which became the background knowledge for the later design and qualification standard IEC 61215 [39] [17]. High degradation rates were reported for pre Block-V modules by Roesler *et al.* [40]. After a remarkable improvement in PV design, Rosenthal *et al.* reported that there is a significant decrease in the failure rate from 45% for pre-Block V to 0.1% for Block V PV modules [41]. Furthermore, for Block IV and V mono c-Si modules, degradation rates were found to be well below 1%/year by Atmaram *et al.* [42] which were deployed in Florida. In 1982, researchers at National Renewable Energy Laboratory (NREL) reported degradation rates to be higher than 1%/year for outdoor tested modules [43]. The reason for high degradation was suspected to be Light Induced Degradation LID, since these modules were having an age of around one year [44].   Berman *et al.* reported in 1995 from the data collected from 200 multi c-Si modules installed in the Negev desert of Israel that the degradation rates were less than 1%/year [45]. Furthermore, publications

14

from Italy [46], Finland [47] and Spain [48] reported similar degradation rates. Fukae *et al.* presented the data from Japan and showed that a-Si modules perform better at higher temperatures [49]. Similar results were shown by Akhmad *et al.* and they mentioned that during summers the performance of a-Si modules is better than c-Si [50]. Japan Quality Assurance Organization reported degradation data on a-Si modules from two different locations by Ikisawa *et al.,* and they found degradation rates below 1%/year [51]. In another report published by Machida and Yamazaki, it was shown that multi c-Si modules degrade faster than mono c-Si [52]. One of the significant recent reports in the literature by Jordan *et al.* on "Photovoltaic Degradation Rates—an Analytical Review" showed the average degradation rate to be 0.8%/year based on 1920 reported degradation rates in prior literature [53]. This paper also presents the analysis based on the modules installed before (pre-2000) and after (post-2000) the year 2000 for c-Si is shown in Fig. 2.1. The report mentions the average degradation rate for c-Si modules (0.7%/year) to be lower than the average degradation rate for thin film modules (1.5%/year). One of the key findings of this report is the degradation rate grouping based on outdoor exposure duration. The modules having outdoor exposure of 10 years show a median degradation rate of 0.7%/year. The one with outdoor exposure between 10 to 20 years show a median degradation of 0.46 %/year. It shows that the modules having lesser age degrade at a faster rate. This report clearly indicates that all technologies installed prior to the year 2000 show lower degradation as compared to post-2000.
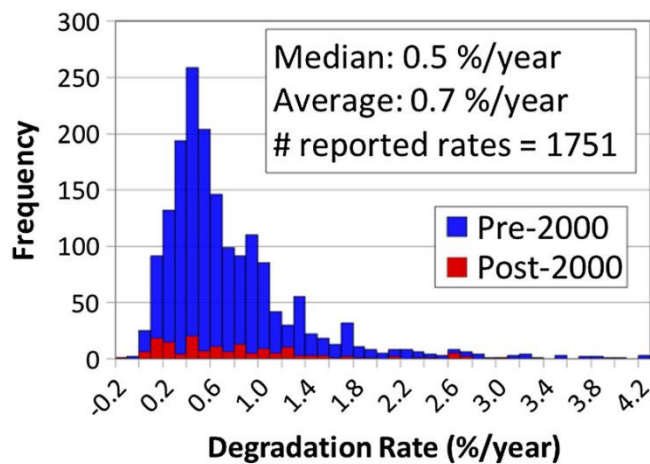
Fig. 2.1: Degradation rate histogram grouped by outdoor exposure duration [25].

Cereghetti *et al.* published a report on various technologies and showed a very low degradation rate of 0.3%/year [54]. PVUSA reported a degradation rate of less than 1%/year for c-Si modules and slightly more than 1%/year for thin film modules [55]. Based on the results obtained from reliability modeling in 2008, Vázquez and Rey-Stolle illustrated that degradation rates less than 0.5%/year are required to assure long term warranties [56]. The degradation rate of 0.5%/year was reported by Vaassen for modules deployed in the temperate climate of Germany [57]. Similar results were reported by Becker and Bettinger of overall degradation rates around 0.5%/year [58]. Jordan *et al.* have reported an average degradation rate of 0.7%/year for 44 modules of different technologies deployed at NREL [59]. A study done by Reis *et al.* presented an average degradation rate of 0.4/year for 162 modules deployed in Arcata, CA, USA over a period of 11 years [60]. Further investigation shows the main reason for the degradation was a reduction in short circuit current (I_{sc}). Similar results were obtained by Sakamato *et al.* by inspecting more than 2000 modules and finding the degradation rates less than 0.5%/year and the main reason for the degradation was losses in *FF* and I_{sc} [61]. Another study done by King *et al.* found the median degradation to be 0.5%/year and it was due to the degradation in solder joints [62]. Wohlgemuth *et al.* reported that 90% of a field failure is due to interconnection breakage and corrosion based on the study done on more than 4000 modules returned from the field [63] [64]. A study done in Spain by Friera *et al.* found a relatively high degradation rate of 1.1%/year, which was mostly due to the degradation in antireflection coating and delamination [65]. Several degradation studies were done in Switzerland by Realini *et al.* [66] [67] and in Sweden by Hedstrom *et al.* [68] that showed a fairly low degradation of around 0.2%/year in systems deployed for more than 20 years in the field. Saleh *et al.* reported 1%/year degradation rate for a 30 year old system deployed in deserts of Libya [69]. Vignola *et al.* reported degradation values in range 0.6%/year to 1.5%/year for modules in Oregon, USA [70]. Similar results were reported by Alonso-Abella *et al.* from data measured over 3000 modules deployed in Toledo, Spain [48] [71]. Dhere *et al.* found the degradation rates for triple junction a-Si system which was installed in the hot and humid climate of Florida, USA to be 0.5%/year. McNutt *et al.* and Gregg *et al.* both reported the degradation rate of 1%/year for multi junction modules for systems deployed in USA [72] [73] [74]. Multiple reports published the degradation rate of around 1%/year for thin film modules deployed in Italy and Poland [75] [76]. In the moderate climate of Germany, Dirnberger *et al.* reported degradation rates close to zero for CdTe modules [77]. Another study

done on CdTe modules at NREL by Marion *et al.* reported a degradation rate of around 0.6%/year [78]. Similar, results were reported by Ross *et al.* for system deployed in Arizona, USA [79]. Foster *et al.* measured degradation rates between 0 to 1%/year for several systems located in Mexico [80].

In another important report in the literature by Jordan *et al.* on "Technology and Climate Trends in PV Module Degradation" the authors present the statistical analysis of the degradation rate data reported in prior literature, showing its dependence on technology and climatic zones [81]. Extensive literature search has been done by the authors on more than 2128 data points on the degradation of *I-V* parameters. Figure 2.2 show that the average degradation of the data reported in prior literature to be 0.8%/year. In Fig. 2.3 it can be seen that for c-Si technology the degradation rates to be approximately steady at around 0.5%/year for installations before and after the year 2000. However, for thin-film technologies, there is a significant move towards stability for post-2000 installations. The authors reported that the largest contributor of power degradation in the case of crystalline silicon technology is the short circuit current reduction, to a lesser degree the loss in fill factor and it depends least on the reduction of open circuit voltage as shown in Fig. 2.4 (a). But in the case of thin film technology, the reduction in power output is mainly due to the degradation in the fill factor as shown in Fig. 2.4 (b). Increase in series resistance for CIGS and light induced degradation in case for a-Si was reported as the reason for high value of degradation by the authors.
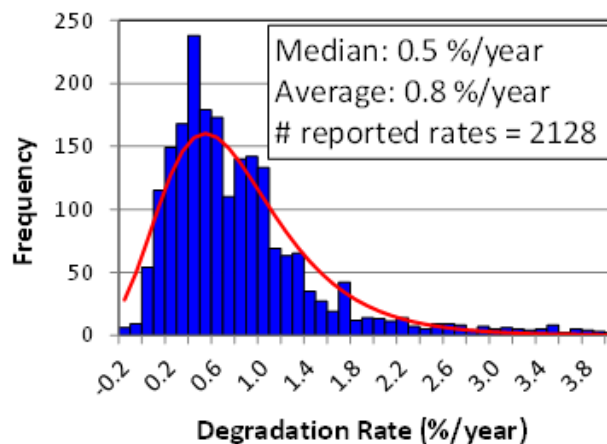
Fig. 2.2: Histogram of published degradation rates (blue bars) with an extreme value distribution fit (red line). The average degradation rate of the previous reported values in literature to be 0.8%/year [81].
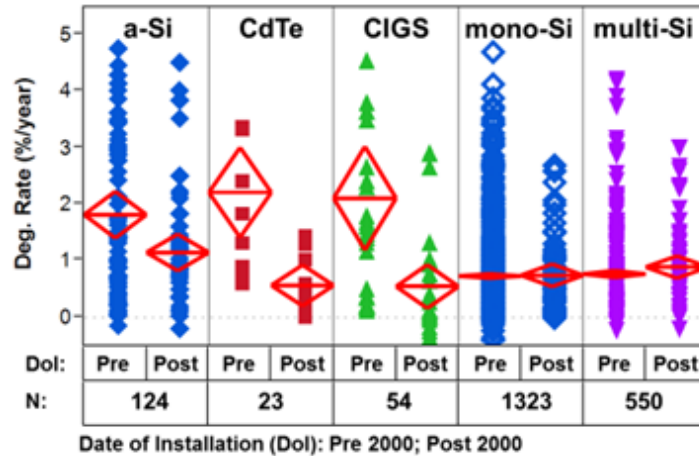
Fig. 2.3: Data shows for thin-film modules there is a significant change in degradation in pre and post 2000 installation. The number in each category indicates the number of data points. The 95% confidence interval is denoted by the diamonds with the mean as the crossbar [81].

(a)   (b)
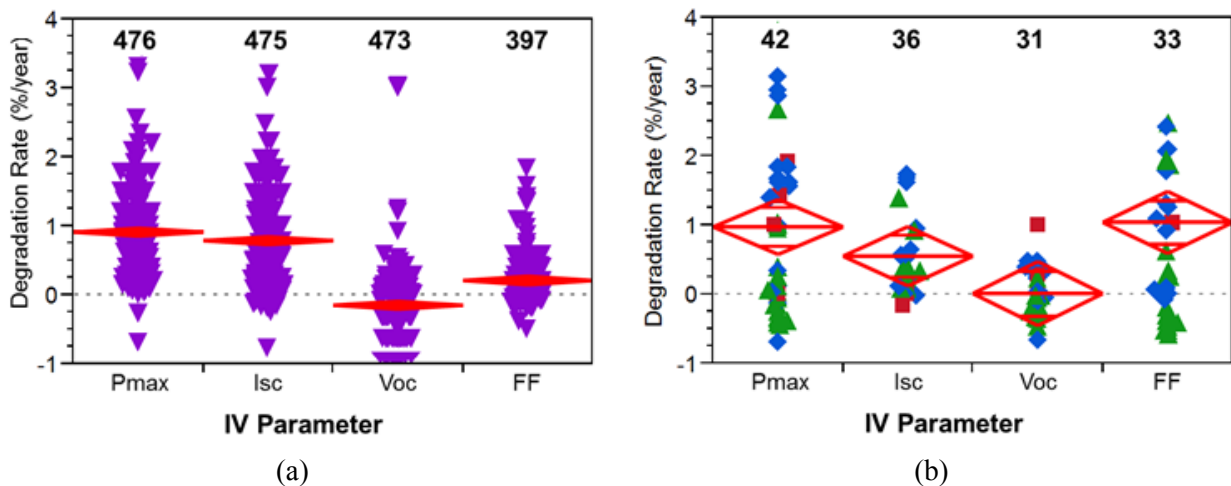
Fig. 2.4: P_{max}, I_{sc}, FF and V_{oc} degradation rates for (a) c-Si and (b) thin-film. The thin-film part is an overlay of a-Si (filled blue diamond), CIGS (filled green triangles), and CdTe (filled red squares). As a guide for the eye, no degradation is indicated by a dashed line. The numbers at the top indicate the number of data points [81].

Jordan and Kurtz analyzed more than 50,000 PV systems deployed in different locations in USA, ranging in installation capacity from 0.5 kW to 25 MW [82]. The cumulative installed capacity of these systems was more than 1.7 GW. They reported the degradation rates between 0.5%/year and 1%/year. They mentioned that excessive high degradation rates of 2-3 %/year were not observed. Deceglie *et al.* presented an analysis of PV system energy production from hundreds of residential and non-residential PV systems [83]. They emphasized the importance of

18

the difference between module degradation and energy yield degradation. They reported the energy yield degradation rates to be higher than 0.5%/year according to their study. Suleske has investigated the degradation of modules installed in a grid-tied power plant in Arizona, for 10 to 17 years, and has reported degradation rates ranging from 0.9%/yr to 1.9%/yr for non-hot spot modules [84]. Raupp *et al.* from Arizona State University Photovoltaic Reliability Laboratory (ASU-PRL) conducted extensive degradation rates analysis on more than 59,000 indivisible and string modules from different configuration systems and reported degradation rates between 0.7%/year and 1%/year [85]. Figure 2.5 shows the reported degradation rate from different countries in the world.
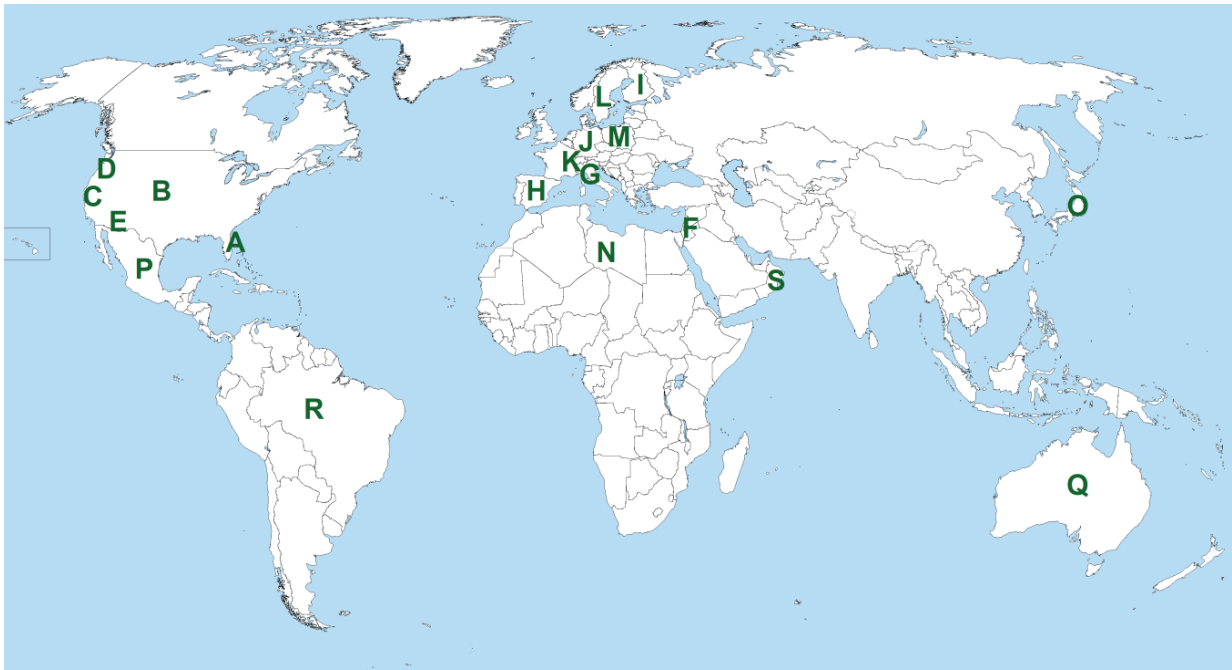
A- Florida, USA 1%/year [72][73],**0.5%year** [74]. **B-Golden, CO, USA 1%/year** [43], **0.7%/year**[59]
C- California, USA 0.3%/year [60], **0.4%/year** [60]. **D- Oregon, USA 0.6%/year** [70].
E- Arizona, USA 1.8%/year [84], **4.9%/year** [84]. **F-Israel 1%/year** [45]. **G- Italy 1%/year** [46]
H- Spain 0.6%/year [48][74]. **I-Finland 1%/year** [47]. **J-Germany 0.5%/year** [57].
K-Switzerland 0.2%year [67]. **L-Sweden 0.2%/year** [68]. **M- Poland 1%/year** [76].
N-Libya 1%/year [69]. **O- Japan 1%/year** [51]. **P-Mexico 0.5%/year** [54].
Q-Australia 0.4%/year [54]. **R-Brazil 0.7%/year** [54]. **S-Oman 1.96%/year** [86]

Fig. 2.5: Overall degradation rate reported from different countries around the world.

It can be seen from the above survey that there is variation in the observed degradation rates, and most of the rates seem to fall between about 0.5 %/year and 1 %/year. This probably explains why, until recently, a degradation rate of 0.8%/year was considered to be the international benchmark. It should be mentioned here, however, that in recent years, a value of 0.5-0.6 %/year has also been used. It can also be noticed that degradation rate reported from most of the countries fall in the cold climatic zone and the degradation rates are in between 0.5%/year to 1%/year.

2.1.2 Degradation Rates Reported from India

In the previous section, degradation rates reported internationally have been discussed. In this section, studies on degradation rates reported from India would be reviewed. Wohlgemuth *et al.* [87] presented a study on the performance of thin film modules deployed at the Solar Energy Centre, Gurgaon since 2002. Cadmium Telluride (CdTe), Copper Indium Selenide (CIS), and three different types of amorphous silicon (a-Si) were characterized using visual inspection, infrared thermography, electroluminescence (EL), wet Hi-pot tests and *I-V* measurements. Results show that the triple junction a-Si module (without the double glass) had the best performance with less than 5% power loss from specification in 8 years. Major power loss was reported for a-Si on glass (double junction a-Si) if the module suffered bar graph corrosion (where the TCO peels off the glass). On the other hand, modules that do not show any sign of bar graph corrosion still met their original power specifications. The reason for the high reduction in the power loss for CdTe and CIS modules was due to the degradation in the fill factor. EL images confirm that the CIS modules are inactive around the edges where moisture would be expected to penetrate. Moreover, at high irradiances, the *I-V* curve of the CIGS module shows significant series resistance. According to the authors, the reason may be that the back contact is no longer fully ohmic, but rather has a reverse junction that impedes or offers high resistance to the current flow. In another study done by O.S. Sastry *et al.* on the performance of c-Si PV modules deployed for ten years under Indian field conditions shows that degradation in the performance of PV modules is higher than the expected level [88]. Furthermore, they reported that PV modules of some IEC 61215 qualified module designs have degraded more than the

guaranteed level in actual field conditions. Authors concluded that the current IEC standards need to be revised to account for the harsh Indian conditions in order to ensure reliable field performance of the modules so as to survive for more than 20 years in field operations. O.S. Sastry *et al.* have done a study on the performance ratio (PR) which will help in identifying site-specific PV technology that offers maximum energy yield [89]. The yield in energy depends on the irradiance and temperature while the PR values mainly depend on the ambient temperature and the spectral response of the solar cells. Therefore we can conclude that PR values are site specific and depend on technology. This forms the foundation for identifying site-specific technology which can result in high energy yield. The authors collected the data of the monthly and yearly energy yield for the three different technologies (HIT, amorphous silicon and multi crystalline silicon) installed at the Solar Energy Centre in Gurgaon. They reported that HIT and a-Si single junction modules have performed much better as compared to multi c-Si modules in the similar climatic conditions of Gurgaon. Sinha *et al.* have reported on the performance of some of the PV modules used with street lighting systems installed at Solar Energy Centre in 1990 and showed that these modules have only 10% degradation in power output (even less than specified in IEC 61215) even though they were deployed in field for more than 20 years, and hence they were termed as "champion modules" [90]. Further studies were done by NISE on the performance analysis of different photovoltaic technologies (a-Si, multi c-Si and HIT) installed in similar outdoor conditions and showed that HIT and a-Si performs better than multi c-Si modules [91] [92] [93] [94] [95] especially during the months of summer. This may be due to the thermal annealing effect in a-Si technology [96]. A systematic study done by Singh *et al.* on the HIT modules showed the performance degradation of these modules to be around 0.6%/year which is mostly coming from the degradation of fill factor. This is attributed to the increase in the series resistance by 3.5%. In extension to these studies researchers from NISE (erstwhile Solar Energy Centre) have also reported the effect of seasonal spectral variation on the performance on these technologies and for the composite zone, they have found that HIT is least affected while a-Si is most affected [97] [98] [99]. O.S. Sastry *et al.* presented a study on the performance of c-Si and thin film modules which were under operation in the field for ten years at SEC/NISE, Gurgaon [100]. Authors presented that there is 4.2%/year reduction in power from the initial measured power CIS modules, 3.8% for double junction a-Si, 0.91%/year for CdTe, and 1.8% for the c-Si module. Furthermore, they showed that mono c-Si modules have

21

performed much better as compared to thin film modules. Further investigation showed that the reason for the high degradation of thin film modules can be attributed due to the material degradation and adhesion degradation or delamination in the module encapsulant. It should be mentioned here that most of the studies done by SEC/NISE are on their outdoor test bed, and are not truly 'field' studies, that is, studies in the field on real-life installations Several studies done on PV plant performance benchmarking based on annual Energy Yield (EY) and Performance Ratio (PR) reported that thin film modules perform slightly better than c-Si modules [101] [102] [103] [104] [105] [106]. One of the major concerns these reports present is that a large portion of the installed PV plants is performing below their potential. This raises the concern about the quality of the installed plant for the long term performance. However, they also report that there are a few PV plants showing very minimal degradation.

We see from this section that generally the degradation rates observed in India are higher than the international benchmark. Furthermore, the number of true 'field' studies is small. This thesis will address these gaps. The primary object of this work is to obtain the degradation rate of the modules deployed in the field.

2.1.3 Effect of Hot Climate

The climatic condition of India tends to be hotter as compared to European countries. Therefore during any study on PV module reliability and durability in India, the study of the impact of hot climate on the performance of the PV module can't be ignored. Findings on the degradation mode dominant in hot climates can help in making testing and qualification standards (IEC 61215) more and more stringent. The impact of high temperature on the degradation of cells and modules has been well documented [107]. Understanding the temperature effects on the performance of the PV module and its long term reliability has been studied by several researchers [108] [109]. Suleske *et al.* have reported the degradation rate for the grid-tied modules installed in the deserts of Arizona to be 1.8%/year for modules that don't show any sign of hot-spot whereas modules having hot-spots show a very high value of degradation rate of 4.9%/year [84]. Several researches have shown that performance in hot climate also depends on the module technology [92] [94]. A recent study was done in Ghana on

the reliability and degradation of PV module showed P_{max} degradation rates in the range of 1.31%/year to 1.84%/year [110]. Rehaman *et al.* conducted a study in Saudi Arabia and reported a high degradation value in the energy output from the PV modules [111]. Similar results were reported by Mohandas *et al.* from Qatar and showed a loss in 0.8% in PR for a one year old system. Honnurvali *et al.* have published a case study on the output power degradation rates in the hot climate of Oman [112]. They reported that the discoloration of the encapsulant is the major cause of the reduction in I_{sc} and P_{max} and a discoloration has been noticed in modules having an age of less than 2 years which raises the concern regarding the quality of the PV modules. Furthermore, they showed the overall mean power degradation rate of 1.96%/year which is twice the degradation rates reported in European countries. Regarding the multi c-Si modules they reported a higher degradation rate of 2.54%/year for modules in Hot and Dry climate. In addition, authors also showed that CdTe modules perform better than c-Si modules in Hot and Dry climatic conditions.

Several large power plants investigated by ASUPRL which were deployed in hot and dry climatic zone reported degradation rates between 0.6%/year to 2.5%/year [113]. The dominant degradation modes reported by them are solder bond deterioration and encapsulant discoloration [114]. Solder bond deterioration is due to the thermo-mechanical fatigue leading to increase in series resistance which reduces the fill factor. On the other hand encapsulant discoloration reduces the short circuit current. Besides, they reported that P_{max} degradation in glass/glass module is due to the reduction in voltage which is attributed to the triggering of bypass diode due to current mismatch caused by the delamination over the cells. Yedidi *et al.* [115] from ASU PRL evaluated for safety failure, reliability failure and degradation rates in hot climate and showed that 0.5% -1.7% modules qualify for the safety returns, 73-76% of the modules qualifies for the warranty claims and around 25% of the modules were meeting the warranty terms. Another study from ASU PRL by Belmont *et al.* reports the degradation rate from a 26 year old power plant in Arizona to be 2.3%/year and the reason for this high degradation is reported to be encapsulant discoloration and interconnect failure [116] [117] [118] [119]. Kuitche *et al.* have developed an innovative methodology for ranking failure mode based on the FMEA and data mining technique [120]. It is evaluated that solder bond failures and encapsulant discoloration are the two most dominant modes under the hot and dry desert climatic conditions of Phoenix, Arizona, USA.

Jordan *et al.* mention that a hotter climate causes higher PV degradation. However, it also depends on quality and technology [121]. Authors have reported V_{oc} degradation in the module which shows the cell changing behavior in hot climates. In addition, they have reported higher degradation in bifacial PERC modules in hotter climates. Weham *et al.* have reported that elevated temperature induced degradation (LeTID) can cause serious effects on the degradation of PERC modules, hence finding the reasons and developing mitigation strategies have been the subject of rigorous research [122]. Kurtz *et al.* [123] presented the concept of equivalent temperature and mentioned the technique to determine from the metrological data. They evaluated the thermal exposure and aging rate of PV modules for different mounting configuration assuming degradation mechanisms with high, average, and low activation energies. They found the Arrhenius-weighted average aging (equivalent) temperatures (T_{eq}) to be significantly lower than the temperature expected for an ambient temperature of 40 ⁰C and 1000W/m^2 irradiance. The authors emphasized that further work is needed to understand the degradation occurring upon increased temperature. Sinha *et al.* have reported that I_{sc} degradation rate for hot and dry Arizona climate to be 0.28±0.05%/year by using a modified Arrhenius equation model [124]. One of the most commonly reported models for the temperature dependence of the degradation process is the Arrhenius equation. In the case of a temperature dependent process, the Arrhenius law in equation 2.2 and 2.3 can be applied to estimate the increase in rate as consequences of an increase in temperature as given by Cocca *et al.* [125].

$$K = Ae^{-\frac{E_a}{Rt}} \tag{2.2}$$

$$\frac{K_1}{K_2} = e^{\frac{E_a}{R}\left(\frac{1}{T_2}-\frac{1}{T_1}\right)} \tag{2.3}$$

The workshop held on the "PV Module Reliability in Hot Climates" at the Indian Institute of Technology Bombay, establishes the importance of the study of different degradation modes prevalent in hot climates [126]. Researchers from NREL, ASUPRL, NISE, Qatar, UAE, Saudi Arabia, and Japan presented the data on the effect of hot climate on the performance and

reliability of the PV modules. They also presented that the modules in the hotter climates are degrading at a faster rate.

The literature mentioned above establishes the importance of understanding the degradation modes which are dominant at high temperatures and the reason for high degradation rates. Researchers around the world have emphasized further examining the degradation mechanism and developing the mitigation techniques which could enhance the reliability and durability of PV modules when deployed in hot climates.

To investigate this aspect further, we have performed, in this thesis, a detailed analysis focusing on the issues of hot climate which has been described in more detail in Chapter 4.

2.1.4 Effect of System Age

Jordan *et al.* [25] have compiled data from published literature regarding the degradation rates of solar power plants, and have compared the degradation rates for different age groups of the installations – (1) Less than 10 years, (b) 10 – 20 years and (c) More than 20 years. Figure 2.6 show the median degradation rates for these age groups are 0.7 %/year, 0.46 %/year and 0.43 %/year respectively. This indicates that the degradation rates of the PV systems tend to be higher in the initial years but stabilize to lower values in later years.

Mikofski *et al.* [127] at SunPower Corporation of USA have worked on developing a physics based model for degradation of solar panels, by taking into consideration the various degradation modes that can affect the long-term field performance. They have collected data of 179 crystalline silicon (non-IBC) sites which show an almost linear degradation up to 5 years of operation (rate: 1.25 %/year), followed by a sudden dip in power output (thereby indicating an even higher degradation rate).
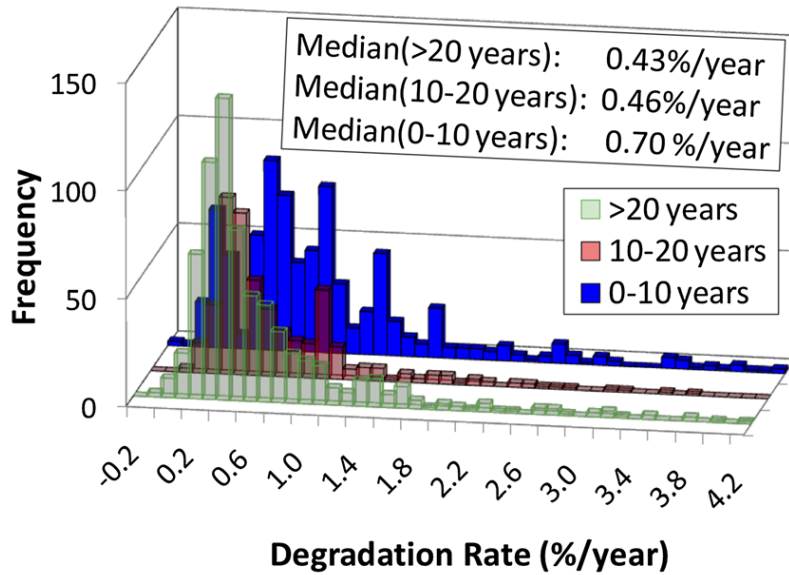
Fig. 2.6: Degradation rate histogram grouped by outdoor exposure length. The median rate for exposure length up to 10 years is significantly higher than for studies of 10 years and longer [25].

Jordan *et al.* [128] have studied the non-linearity in the degradation rate associated with different failure modes of the solar panels. They have reported that most of the available PV technologies show a rapid decay in the first year of installation which is due to light induced degradation or other meta-stabilities inherent in the PV technology. Beyond this, they have observed that the power degradation of solar panels is in general linear (i.e. a constant degradation rate) for panels affected by encapsulant discoloration. On the other hand, for panels affected by solder bond fatigue, the degradation curve is concave in nature. Furthermore, in the case of wear out degradation modes like solder bond failure, the power output can drop rapidly upon the onset of the degradation mode, which introduces non-linearity in the degradation curve.

Kang *et al.* [129] presented a study on the degradation of the PV modules depending on the usage period installed at different locations in Korea. The modules inspected were sorted with respect to their installation time. They were divided into four different categories: age greater than 20 years, age more than 10 years but less than 20 years, age more than 5 years but less than 10 years, and age less than 5 years. They presented that modules older than 20 years showed degradation of 1.75%/year, modules having age greater than 10 years showed a degradation rate of 1.23%/year, modules in age category greater than 5 years showed degradation rate of 2.73%/year, and degradation rate of around 5%/year were shown by modules age less than 5

years. The reason for the high degradation rates in the case of modules aged less than 5 years was found to be a significant reduction in the fill factor. These data are not in agreement with those of Jordan *et al.* Hossion has reported a very high degradation rate of 6.86%/year for 5 year old multi c-Si modules deployed in Dakha [130]. This shows that modules having age less than 5 years show a very high value of degradation.

2.1.5 Effect of Light Induced Degradation

Light-induced degradation (LID) is attributed to a decrease in the solar cell efficiency that is detected during excess carrier injection by above bandgap illumination [131] or due to forward biasing [132]. LID is observed as a reduction in the solar cell short circuit current and the open circuit voltage. During the 1970s, LID was first noticed in the boron doped Float Zone (FZ) silicon solar cells [133] [134] [135]. It was found that the light induced defect density increases with the increase in the boron and oxygen concentration. Degradation was associated with the formation of boron-oxygen complex and the effect became known as boron-oxygen LID (BO-LID) [136] [137]. Initially, it was assumed that reducing boron or oxygen concentration would ensure LID free silicon solar cell [138]. However, in 1998, Henley *et al.* observed LID in boron doped FZ silicon solar cell deliberately doped with copper [139]. LID was also found in phosphorus [139] and gallium doped silicon [140] having copper impurities and this phenomenon became known as Cu-LID. In recent times, strong LID has been reported by several manufactures in Passivated Emitter Rear Cells (PERC) and Al-BSF silicon solar cells, which is difficult to explain by BO-LID theory [141] [142] [143]. Similar meta-stabilities are found in various thin-film technologies due to which there is a decrease in the power output upon outdoor exposure (for example Staebler-Wronski effect in a-Si modules [144] [145]), or even increase initially followed by long term degradation (in the case of CdTe modules [146] [147]). There can be up to 10% enhancement due to light soaking effect in the case of CdTe modules and it also shows strong temperature dependence [148].

Since LID is commonly seen in c-Si modules from almost all manufacturers, the manufactures generally incorporate this in their warranty terms, as a 2% to 3% initial rapid degradation in power output during first year of operation [149] [150] [151]. The extent of LID

depends on the quality of wafer and cell manufacturing process as it is primarily caused due to the present impurities like boron, iron, copper and oxygen in the silicon ingot [142]. Though the degradation due to LID varies from manufacturer to manufacturer, PVSyst software recommends a value of 2% LID for energy generation simulation [152], which we have also adopted in our present analysis (this has been described in more detail in Chapter 4). LID can have a significant effect when we compare degradation rates of modules of different ages.

It is suspected that the LID can be fully recovered by annealing [135] [153]. It has been reported by many researchers that in the case of Cu-LID, there can be a full recovery at 200 ºC for 30 minutes. Table 2.1 shows the data of degradation in power, short circuit current, open circuit voltage and fill factor, in LID affected samples, compiled from the literature [142] [154] [155] [156]. Sopori *et al.* [157] have carried out a detailed study on the LID of c-Si solar cells to understand the bulk and the surface components. They have reported that the LID degradation mechanisms are related to bulk and surface. The bulk effect is due to the Boron-Oxygen complex and full recovery is possible through annealing. Furthermore, they showed that the surface effect is primarily related to SiN:H/Si interface. It has been found that there is a very small indication in the lighted *I-V* characteristic but it can be easily identified in the J_{02} component of the dark *I-V* (this motivated us to perform dark *I-V* characterization in 2014 and 2016 Surveys). Besides, they have also reported that 40% of the degradation in power output is due to short circuit current (I_{sc}) degradation, another 40% due to open circuit voltage (V_{oc}) degradation, and the rest 20% is coming from fill factor (*FF)* degradation. Accordingly, for the purpose of our analysis, we have divided the 2% LID in power output into 0.8% for V_{oc}, 0.8% for I_{sc} and 0.4% for *FF*.

PERC modules are very acute to strong but slow LID, known as LeTID [158] [142] [159]. It has been reported that the degradation rate [158] and the defect density [159] increase with an increase in temperature, usually these values are reported at 50º to 80º C. It has been found that LeTID of over 10% in PERC Cz-Si cells with partial recovery at 200º C and almost complete regeneration at 70 ºC. It indicates that the cell structure and definitely the back surface passivation layer cause degradation. Although it has been reported earlier that aluminum oxide (Al_2O_3) passivation has improved during illumination [160] [161], no remarkable LeTID difference is detected between PERC multi c-Si with an Al_2O_3/SiN_X [162]. It has been found that LeTID is observed in Ga-doped Al-BSF multi c-Si [158], and it cannot be explained by either

passivation degradation or BO-LID. Krauss *et al.* have reported that in AlOx-passivated PERC multi c-Si cells a low LeTID-related lifetime correlate with high dislocation densities [143].

Table 2.1: Typical values of LID reported in literature.

Cell Technology	Typical Relative LID reported in Literature				Reference
	P_{max}	V_{oc}	I_{sc}	*FF*	
Mono c-Si	3-4%	5-6%	2.5-3%	- 0.5%	[155]
	5%	NA	NA	NA	[156]
	2.8%	1.1%	1.1%	0.6%	[142]
	2.5%	1%	0.9%	0.5%	[157]
Multi c-Si	1%	NA	NA	NA	[156]
	2%	0.4%	0.9%	0.5%	[142]
	2.5%	0.7%	1.5%	-0.5%	[162]

2.1.6 Effect of Potential Induced Degradation

In recent years Potential Induced Degradation (PID) has acquired significant importance as it could lead to a catastrophic failure of the PV modules operating in outdoor conditions at high voltages [163] [164]. A high electric potential difference is developed between the module frame and solar cell which results in leakage current flowing from module frame to solar cell (or vice-versa, depending on the module position in the string) resulting in PID. PID would be more drastic in the future, as the solar industry is moving towards high voltage systems (1500 V) to minimize the overall cost [165].   In 1985, JPL were the first to report PID in c-Si and in thin film modules [166] [167]. To investigate further, during the early 2000s, NREL, Florida Solar Energy Center (FSEC), and BP Solar started examining the risk of high voltage stress [168] [169] [170]. Subsequently, in 2005, Sunpower reported PID in their rear-junction n-type silicon modules deployed in Germany [171]. After 2010, there has been a huge thrust in the research on PID of the conventional p-type c-Si PV modules [163] [164] [172] [173] [174], through which

the term PID was formulated by Pingel *et al.* [163]. There are several factors which could influence PID such as properties of antireflective coating on solar cell, encapsulant, module design (like frame or frameless) and even system topologies [163] [175] [176]. It has been reported that even the same type of modules undergo different extent of power degradation depending on the environment (temperature, humidity and moisture) in which they are deployed, grounding condition (dry or wet), and even the deposition of soil on the top of PID susceptible modules [173] [174] [176] [177] [178] [179]. PID is attributed to the leakage current caused by the high electric field induced between the module frame and the solar cells. Figure 2.7 shows several different pathways through which the current can flow between the module's frame to the solar cells [163] [178] [180]. These paths are summarized below:

1. Along the surface of the glass and through the bulk of glass and the encapsulant.
2. Through the bulk of glass and encapsulant.
3. Laterally through the interface between glass and encapsulant.
4. Through the bulk of encapsulant.
5. Laterally through the interface between encapsulant and backsheet.
6. Along the surface of the backsheet and through the bulk of the backsheet and the encapsulant.
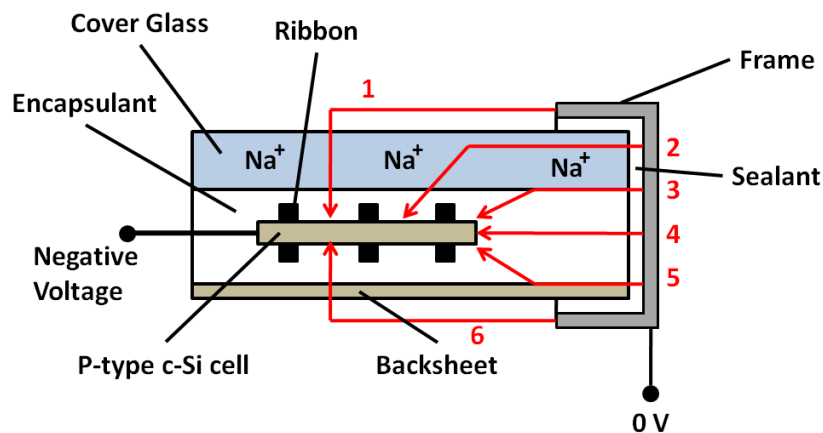
Fig. 2.7: Cross sectional view of a typical c-Si PV module (frame-glass-encapsulant-cell-encapsulant-backsheet). Solar cell is at negative potential with respect to the frame. Red arrows show the modeling of possible leakage paths [179].

Leakage current path 1 is reported to be the most lethal among all the leakage current paths mentioned above, since the conductivity of the front glass gets enhanced under rainy or wet condition [178] [181]. The most common type of PID in the conventional p-type c-Si PV module is PID-shunting (often termed as PID-s). Substantial research has shown that PID of a conventional p-type silicon PV module is either due to reduction in shunt resistance (R_{sh}) [163] [182] [183] or due to the increase in the dark saturation current (due to recombination in the space-charge region J_{02}) and the ideality factor of the second diode term (n_2) [184]. In the case of PID-s, Na plays a signification role. Under the influence of negatively biased condition, Na$^+$ ions drift from the silicon nitride AR coating towards the interface of silicon and AR coating, and penetrating the crystal, through interstitial crystal defects (like stacking faults and grain boundaries). As a consequence, this results in significant shunting (both ohmic and non-linear) [174] [185] [186]. Subsequently, it degrades the cell efficiency [174] [186]. One of the physical models of PID-s says that there is an accumulation of positive charge in the AR coating, and as a result, it inverts n$^+$ region into the p+ conduction region thus creating a shunting path across the p-n junction [185]. Extensive studies have shown that the Na contamination is originating from the soda-lime glass sheet. Naumann *et al.* reported that SiN$_x$ could be another potential source for Na contamination [187]. PID has also been reported in thin-film modules (a-Si, CdTe, and CIGS) and it is primarily due to the Na ion migrations [167] [168] [169] [175] [186].

To test PID at a module level two most common methods, namely the climatic chamber and the conductive layer on the glass top is used worldwide. In the case of a climatic chamber test, the PV module is biased at a high voltage in high temperature and humid environment (to achieve this module is kept inside an environmental chamber) [173] [174]. On the other hand, the conductive layer PID test is done by placing a conductive layer (it could be Al foil, Cu foil, water, or carbon paste) on the top glass layer and then biasing the module at a high voltage. This method has been included in the IEC 62801-1 standard [188]. Al or Cu foil provides the conductive path on the glass top which simulates the equivalent effect of high humidity conditions. The advantage of using this method is that it eliminates the use of the expensive environmental chamber.

Xiong *et al.* performed PID test on various commercial PV (both c-Si and thin film) module by applying ±1000V between the module frame and solar cell for 650 hours at 85 ℃ and 85% relative humidity. They reported that PV modules at positive bias had nearly no effect

31

whereas negative bias showed significant power degradation [175] [189]. Hattendorf *et al.* [190] presented a study in which they negatively biased two types of p-type c-Si modules at 250V, 500V, and 750V. They reported that for both types of PV modules, the ones biased at –750V showed the maximum power degradation and modules biased at –250V showed the least power degradation. Furthermore, they reported that the extent of PID increases with the increase in the applied voltage. However, a definite linear relationship between power loss and applied voltage was not reported. Based on classic Peck and exponential equations, Hacke *et al.* proposed an acceleration model [191]. In their study, they took 20 sample PV modules (60 cell p-type c-Si) biased at a constant voltage of – 1000V. They analyzed P_{max}/P_{max_0} as a function of time, temperature, and relative humidity. The model shows that power degradation follows a linear relationship with the square of time. The acceleration model proposed is given in Eq.2.4.

$$\frac{P_{max}}{P_{max\_0}} = 1 - A * e^{\frac{-E}{kT}} * RH\%^B * t^2 \qquad (2.4)$$

where: A is pre-exponential factor, E is thermal activation energy, B is a constant, and *k* Boltzmann constant and T as the temperature.

Since PID has catastrophic effects on PV modules, several preventive methods have been developed to reduce the PID effect in the case of conventional p-type c-Si or thin film modules deployed in the field. Kambe *et al.* have reported that the PV module having aluminosilicate as the top glass showed very less PID degradation [192]. Similar results were obtained in the case of borosilicate and quartz glass [177] [193]. Since this PID resistant glass has a higher cost, hence it is not desirable by the module manufacturers, as it would increase the overall cost of the PV module. Hara *et al.* introduced an alternate method for preventing PID by applying a thin film of TiO_2 on the cell side of the glass [194]. It showed an excellent protection against high voltage stress. However, it adversely affected the optical performance as this extra TiO_2 layer scatters, absorbs, and reflects the incident light. Several reports have presented that polyolefin, ionomer, and silicon based encapsulant which possess high bulk resistivity is the best substitute EVA for PID resistant modules [177] [195]. At the system level, one of the simplest methods to

reduce PID-s is to ground the negative pole of the transformer based inverters. In the case of transformerless inverter applying reverse bias voltage (+1000V) at night can recover PID.

This review of PID shows that it can be an important degradation mechanism, and since it is accelerated by temperature and humidity, can adversely affect modules in the field in India's hot/humid conditions.

2.1.7 Motivation for Field Survey

The available literature on degradation rates of solar panels installed in different parts of the world shows that there are differences in the degradation rates depending on the location of the system. Most of the reported literature is coming from US and European countries which were the early adopters of the PV technology. As a consequence, the available data is mostly from moderate and cold weather conditions whereas there is very little data reported from hotter tropical climates. The few data from Hot climates like that of Oman and Arizona indicates higher degradation rates than that reported for the cold climates, and in fact this data is higher than the warranty provided by many of the module manufacturers. India has Hot and Humid climate in most parts, but much of the country also sees cold winters, leading to a composite type of climate. It is important to ascertain the degradation rate and the degradation modes prevalent in these tropical climatic conditions. Some of the published literature from SEC in Gurgaon indicated higher than expected degradation rates, but these were from PV systems installed at the test bed at one location in Gurgaon and they are not the true representative of the fielded modules. Furthermore, from the available literature it is evident that there is lack of information regarding the degradation rates reported from the fielded modules of India, especially in the hot and humid climatic zones. Hence, it was felt necessary to undertake field surveys to get a better picture of the degradation of solar panels in different parts of the country. Considering the lack of information with regard to the long-term performance of PV systems in different climatic conditions of India, the High Powered Task Force of MNRE had in March 2013 requested the National Centre for Photovoltaic Research and Education (NCPRE), at the Indian Institute of Technology Bombay (IITB) to survey the performance of older PV systems already installed in the country. NCPRE requested the National Institute of Solar Energy (NISE) to partner in

conducting the survey, keeping in view the wide experience which NISE (formerly Solar Energy Centre) had in monitoring PV system performance. This was the genesis of the 'All-India Surveys of PV Module Reliability' conducted in 2013, 2014, 2016 and 2018. The present author was the lead investigator in the 2013 and 2014 Surveys, and the co-lead in the 2016 Survey. This thesis presents the results and analysis of the 2014 and 2016 Surveys, in which the author played the major role. (The 2013 Survey data is not presented, as it assessed comparatively few modules.)

2.2 Electroluminescence (EL)

2.2.1 Principle of Radiative Recombination

Photovoltaic devices convert the incident light energy into electricity. Under forward-biased electrical excitation, these PV devices behave like a Light Emitting Diode (LED), and emit wavelengths corresponding to the bandgap. For silicon devices (and this section will focus on silicon devices only), the wavelengths are in the near IR. Kirchartz *et al.* showed that the LED quantum efficiency of the PV device is reciprocal to its electrical efficiency [196]. The radiative recombination for electron-hole pairs in silicon is extremely weak, since silicon is an indirect bandgap material where most of the recombination emits phonons, but it exists nevertheless, and can be detected. EL characterization is done by injecting a forward current equivalent to short circuit value through the electrical contacts. Therefore EL can only be applied to the devices having metallization contacts. Figure 2.8 shows the band diagram of silicon, for the illustration of the luminescence process.
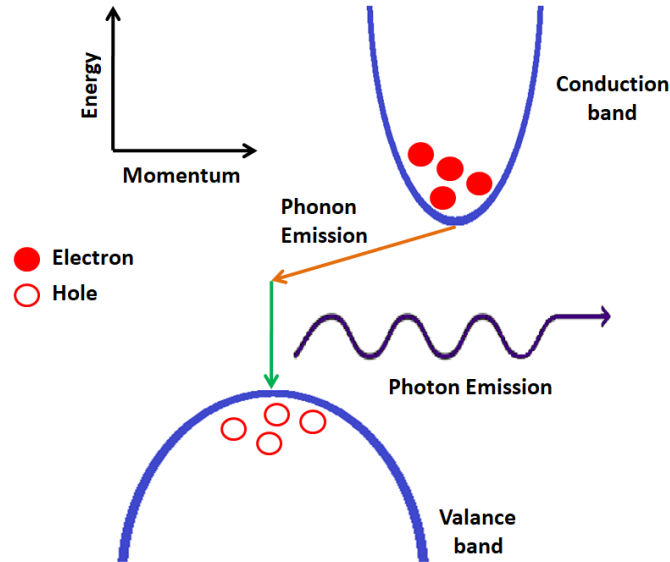
Fig. 2.8: Schematic of the band diagram, illustrating of the luminescence process.

In the case of c-Si solar cell the photons emitted are around the wavelength of 1150 nm, equivalent to 1.1 eV. The photons emitted are distributed between 950 nm and 1250 nm. The probability of EL emission is reduced due to the indirect bandgap nature of silicon [197]. External sensors such as silicon CCD, silicon CMOS or InGaAs detector can detect the emitted photons since these sensors are sensitive to wavelengths higher than 900 nm. Regions in the solar cell which have a lower carrier density due to shunts, interconnect breakages, and contaminations decrease the probability of the band-to-band recombination and thus these defects could be easily identified in the EL images [198] [199].

2.2.2 Principal Setup

A classic representation of an EL setup is shown in Fig. 2.9. The setup consists of a near infrared sensitive camera with a visible blocking filter, a DC power supply, the PV module under test, and a dark room. Device Under Test (DUT) is forward biased by injecting DC current equivalent to the short circuit current of the DUT under illumination [200]. The light emitted due to the radiative recombination is captured by the near infrared sensitive camera. Temperature of

the sample is monitored to ensure thermal stability. The EL testing is done inside a dark room to reduce the impact of external (stray) lights, since the EL signal itself is very weak. This is a drawback of the standard EL imaging procedure since it prevents us from performing the test outdoors in field conditions in the presence of ambient light. Stoicescu *et al.* [201] [202] have come up with a system which enables measurement of EL images of PV modules in the field during daytime. This system, called the 'DaySy' utilizes a modulating device to vary the working point of the system periodically. A high quality video stream of the modulated system is captured, and an algorithm then eliminates the static background image and obtains the EL signature of the module. However, this system is very expensive. In order to overcome this limitation, we developed an inexpensive and simple methodology by using the technique of image difference to capture the EL images in the presence of ambient light (this has been described in more detail in Chapter 5). The effect of ambient light on the EL image could be further reduced in case of c-Si solar cell by putting an additional 850 nm long IR pass filter in front of the lens.

Different physical properties of the device could be extracted by capturing EL images at different test conditions. Intrinsic defects of the device such as crystal defects and grain boundaries can be detected by capturing EL images at different DUT temperatures (from 25 º C to 100 ºC) [199]. Series resistance mapping of the DUT can be obtained by utilizing the EL images captured at different bias currents. EL imaging acquisition time can vary from milliseconds to minutes as it depends on multiple factors such as quantum efficiency of the camera sensor, signal to noise ratio, lens aperture, and the field of view. It has been found that the EL image captured by the camera could be different from the actual EL emitted by the DUT [203]. This difference may be due to the pixel-smearing caused by the camera lens and sensor [204]. Image correction needs to be done before analyzing the EL images to make meaningful conclusions.
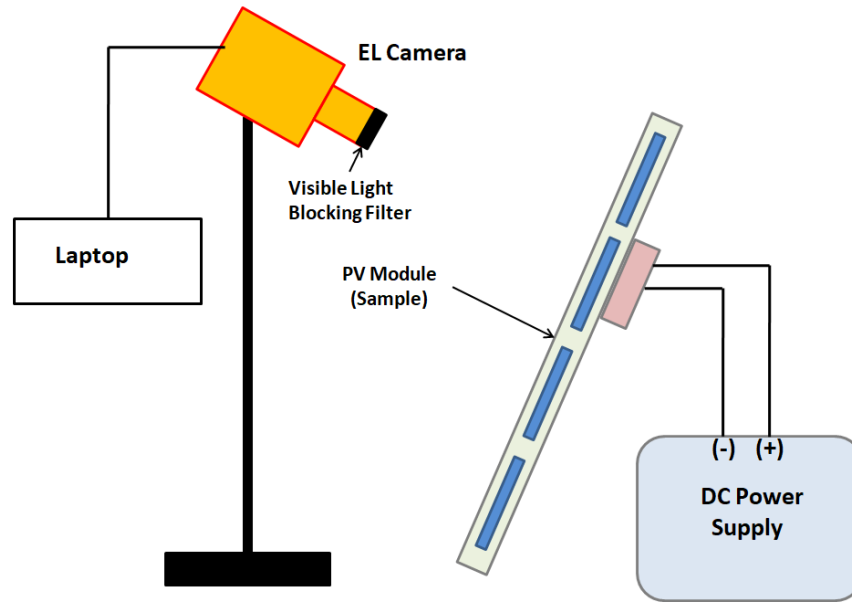
Fig. 2.9: Schematic of an EL setup.

2.2.3 Camera Type

Indium gallium arsenide (InGaAs), silicon charged-coupled devices (CCD), mercury cadmium telluride (MCT), and silicon Complementary Metal Oxide Semiconductor (CMOS) are the most commonly used sensors for EL imaging camera [205]. These sensors have different spectral responses and they also differ in the cost. InGaAs and MCT are the most expensive sensors whereas silicon-based CCD and CMOS are the cheapest. Although InGasAs and MCT are the most expensive, they cover the entire EL spectrum emitted from a Si solar cell, whereas CCDs or CMOS sensors, being made of silicon themselves, cover only a part of the EL spectrum. Figure 2.10 shows the spectral response of different sensors. Due to the difference in their spectral responses, they differ in the exposure time required to capture the EL images. InGaAs sensor requires milliseconds to capture the EL images whereas the CCD sensor requires a few seconds. As a result, InGaAs sensors are suitable for capturing EL videos. Since, CCD sensors have a lower cost and satisfactory performance; therefore, CCD sensors are preferable choice for the EL cameras.
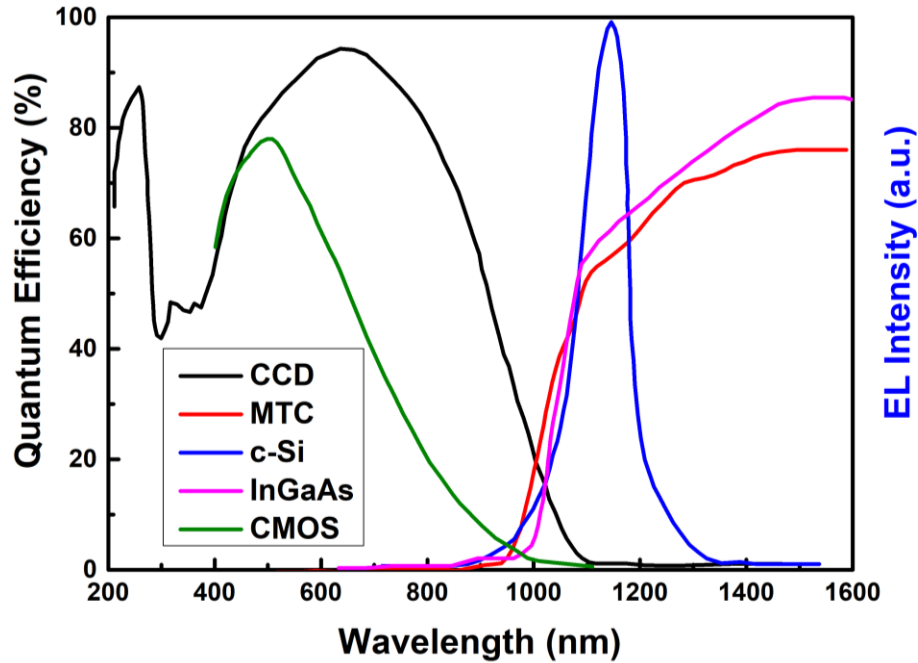
Fig. 2.10: Quantum efficiency of different types of sensors (CCD, MTC, InGaAs, and CMOS), compared with the typical emission of c-Si solar cell device (blue line) [205].

2.2.4 EL imaging as an Electrical Characterization Tool

EL imaging is a powerful, quick and reliable inspection technique to get information on defects in solar cells and modules. These defects, particularly cracks and inactive regions, appear as dark parts in the EL image of the PV cell or module [206]. Figure 2.11 show an example of all the 3 types of cracks [207]. Out of these 3 classifications, Mode C and Mode B types of cracks can lead to significant power loss since the dark areas mean that electrical connection to the affected area has been broken, whereas Mode A cracks does not lead to any loss in power output. Figure 2.12 (a) shows EL image of a healthy PV module, whereas Fig. 2.12 (b) shows EL image of a defective PV module.
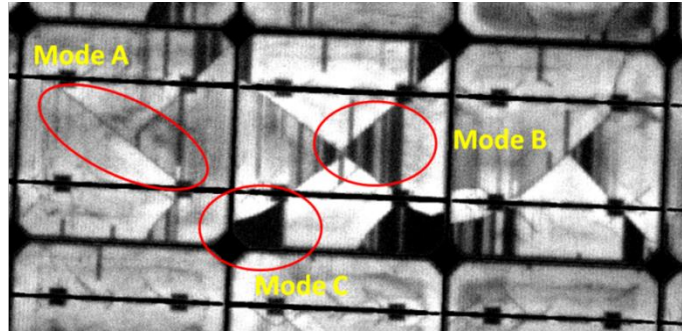
Fig. 2.11: Different types of cracks as visible in EL images [207].

EL intensity has been found to correlate well with the minority carrier diffusion length of crystalline silicon solar cells, and hence can serve as a tool for diffusion length mapping [199] [208] [209]. Ideality factor "n" can also be deduced by measuring the EL intensity as a function of the forward injection current [209]. Takamoto *et al.* have worked on the detection of crystal defects by analyzing the variation in the EL intensity with temperature [210]. Khatavkar *et al.* have used modulated EL for determination of the carrier lifetime in HIT solar cells [211]. Gazuz *et al.* have shown that EL imaging can also serve as a fast characterization technique to analyze the power loss in the bus bars of cells and modules [212]. High resolution EL imaging can help detect cracks and broken finger contacts in PV modules [213] [214].

(a)   (b)
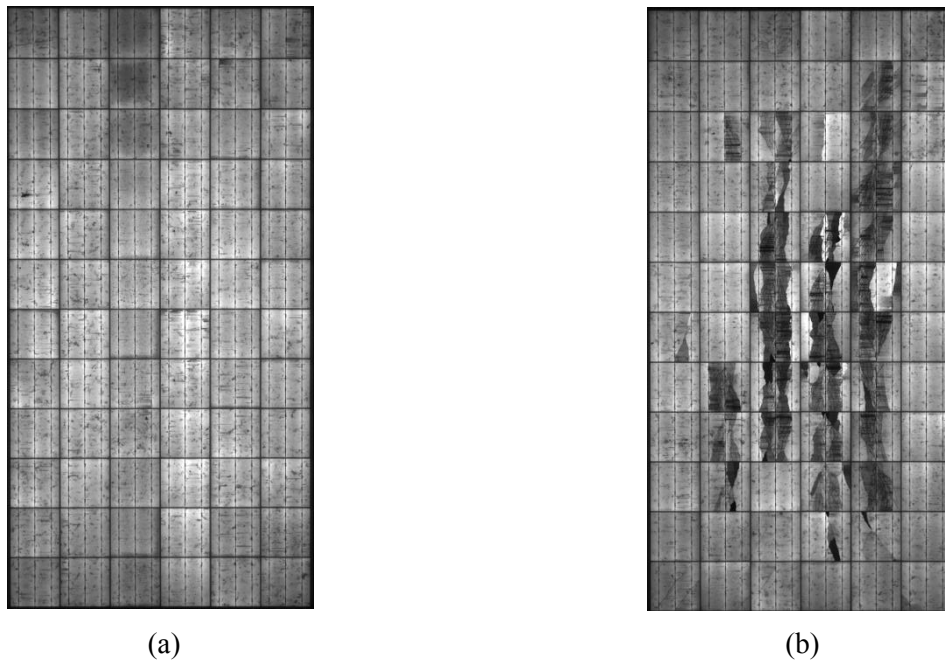
Fig. 2.12: EL image of (a) defect free, (b) defective PV module.

Köntges *et al.* [203] have demonstrated that EL imaging can be used to determine the operating voltages of each cell of a PV module accurately, and they refer to this technique as Voltage Imaging of Modules (VIM). Much work has also been done in digital image analysis of the EL images with the aim of extracting quantitative information from the images. Mansouri *et al.* [206] have found that a linear relation exists between the size of the cell breakages and the power drop in crystalline silicon modules. Also, EL imaging has helped in verifying the reduction in the size of the localized shunts in CdTe modules after light soaking, which explains the increase in the efficiency of these modules after stabilization. Kitiyanan *et al.* have utilized image subtraction technique to differentiate between intrinsic and extrinsic defects, by taking multiple EL images at low and high temperatures [215]. Wurfel *et al.* have used the ratio of two EL images taken using different spectral filters to determine the minority carrier diffusion lengths [216]. This procedure is much faster than the spectrally resolved LBIC [217] technique generally used for determining the diffusion lengths. Similarly, in [218], the authors have used the ratio method to determine the recombination and optical parameters (like diffusion length and back surface reflectance) from the electroluminescence images. Waltera *et al.* [219] have proposed a technique to map the local series resistance by taking EL images at high and low bias voltages. Tsai *et al.* [220] have discussed a technique to single out the defect in an EL image by using Fourier image reconstruction process and image subtraction technique. The signature of the defects in the Fourier transform is removed in order to generate the corresponding EL image of a defect-free solar cell (by reverse Fourier transform), which is then subtracted from the actual EL image to leave behind just the defect.

As seen from this survey, EL imaging has proved to be an excellent tool to characterize the defects in the solar cells and modules. Although it has generally been used only in the laboratory, its relevance for field surveys is very high, especially for detecting micro-cracks in installed modules. A number of improvements in EL imaging for field assessment has been done, and were used in the All India Surveys.

2.3   Impact of Mechanical Loading in PV Modules

2.3.1 Mechanical Loading Tool Types

There are two types of mechanical loading tests currently in vogue in the PV industry – static and dynamic. The static loading test is primarily a test to ensure a module's ability to endure snow loads and other static loadings. The IEC 61215 standard requires the solar panels to pass a static load test of 5400 Pa [221]. On the other hand, the dynamic loading test is primarily to check module's ability to endure strong winds. In the Indian context, this test is also very important since transportation and installation of modules produce a significant amount of dynamic loading. Dynamic loading is an essential part of standardized accelerated testing defined in IEC TS 62782. This test requires ±1000 Pa at a rate of 3 to 7 cycles per min for 1000 cycles with current flow.

The static mechanical load testing is performed to test the mechanical strength of the PV design as per IEC 61215. One of the simplest methods used to perform static loading is by manually placing weights, such as sandbags, on the top surface of the PV modules [222]. This is a cost effective method; however, it cannot be used for cyclic dynamic loading. This method is time consuming and it has high chances for non-uniform forces as it depends on the placement of sandbags. Figure 2.13 shows the schematic of the static loading using the sandbag method.

Another popular method for doing static mechanical loading is using the compressed-air bladder or the airbag method [222]. In this method, a bladder is filled with compressed air, and it applies a uniform load in static mode. This method is slightly better than the sandbag method due to better uniformity of the applied load. However, near the junction box region the loading maybe still non-uniform [222]. Both of these methods cannot be used for dynamic loading. Figure 2.14 shows the schematic of the static loading using the airbag method.
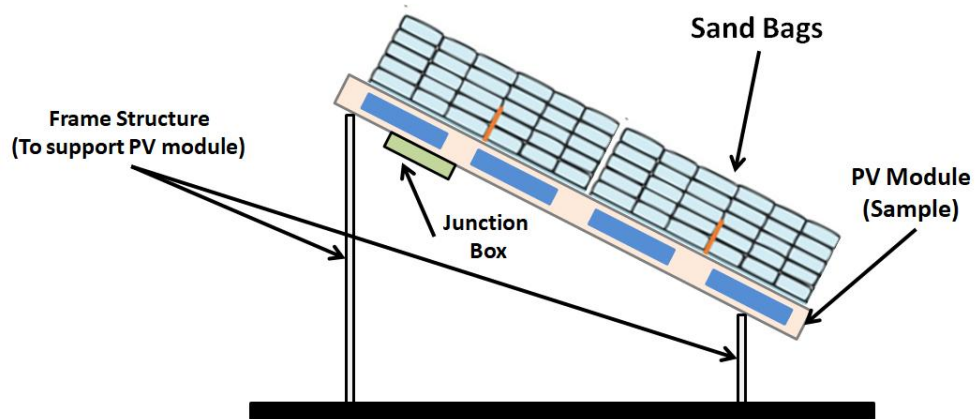
Fig. 2.13: Schematic of Static Mechanical Loading tool using sand bag method [222].
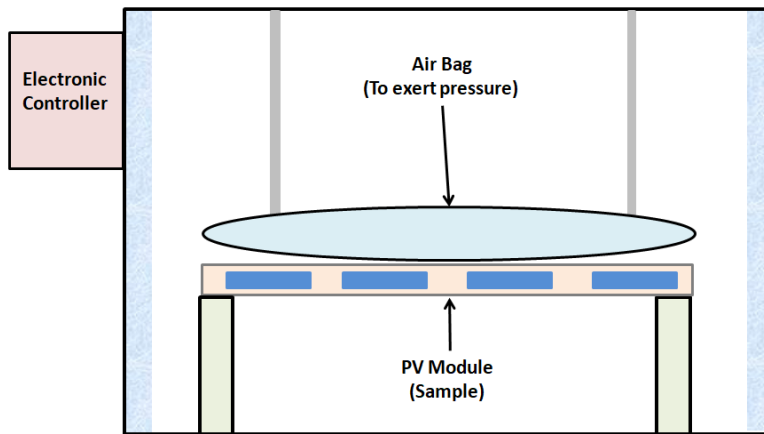
Fig. 2.14: Schematic of Static Mechanical Loading tool using air-bag method [222].

The Dynamic Mechanical Load tester almost universally in use currently in various research and testing laboratories like Fraunhofer ISE, PI Berlin, Sinovoltaics etc. [223] [224] is based on vacuum cups connected to pneumatic cylinders. The vacuum cups exert push-pull pressure on the solar panel in order to simulate the effect of variable mechanical loading on the panel. The pneumatic cylinders are controlled using a computer program which sets the cycling rate and pressure range. A basic schematic diagram of such a setup is given in Fig. 2.15. Two major drawbacks of this arrangement are that: (1) The pressure is not truly uniform but is

concentrated at the vacuum cups, and (2) the front side of the solar panel is not available for *I-V*, EL or any other measurements when the DML testing is going on.

An alternative type of DML Tester developed at NREL (USA) [225] uses an air-tight seal at the backside of the solar panel and exerts air pressure (blowing or suction) on the backside in order to flex the panel, simulating the effects of mechanical loading due to wind forces. Vacuum pumps and blowers are used in this setup, as shown schematically in the Fig. 2.16. The drawbacks of the vacuum cup based design are completely overcome in this design. However, the NREL tool has one limitation that it is incapable of accommodating PV modules of different sizes in a single air-tight seal.

Since the PV modules are manufactured in different sizes, hence it was felt necessary to develop a universal tool which can hold a PV module of any dimension. Also, it is desirable to develop a single tool that can perform both static and dynamic tests which can apply uniform load throughout the PV module. Hence we developed a mechanical loading tool by extending the design developed by NREL by introducing a universal fixture that can accommodate any commercially available PV module in the market. This has been described in more detail in Chapter 5.
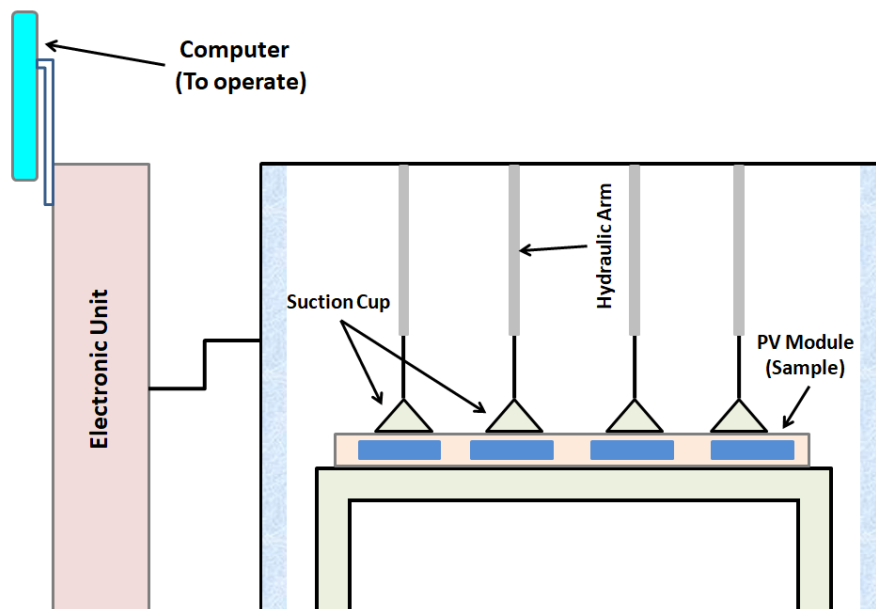
Fig. 2.15: Schematic of Dynamic Mechanical Loading tool using suction cup method [223].
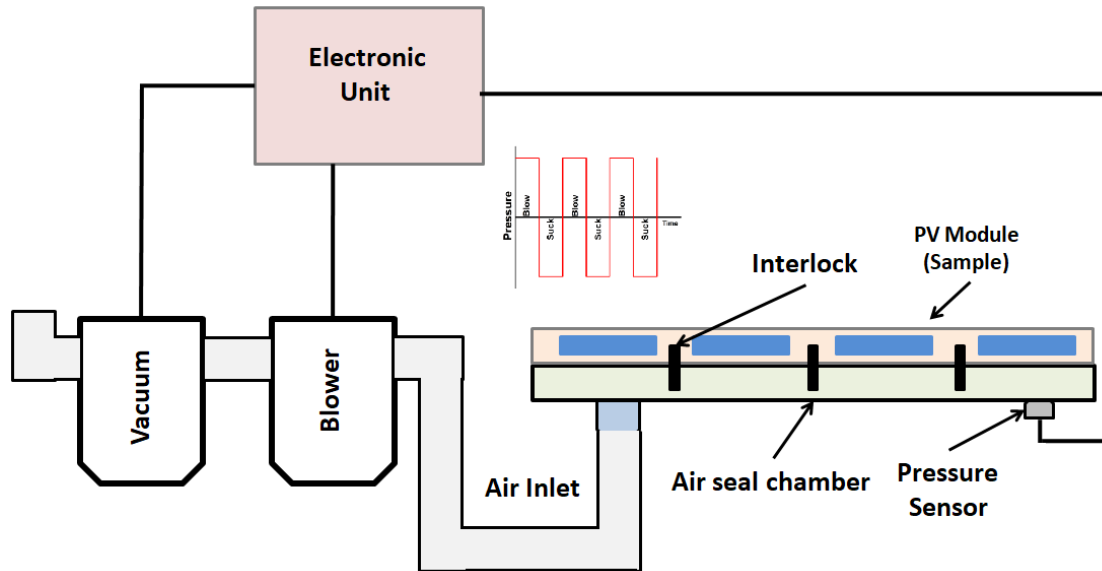
Fig. 2.16: Schematic of Dynamic Mechanical Loading tool using vacuum pumps and blowers. Blower and vacuum switch are turned ON and OFF in a cyclic manner to create positive and negative pressure on DUT [225].

2.3.2 Effect of Mechanical Load Tests on Electrical Performance

Bosco *et al.* [225] have performed DML tests on 42-cell solar panels to evaluate the suitability of DML tests as an accelerated test for interconnect ribbon fatigue. They have reported that the ribbons fail in a few hundred to thousands of DML cycles, which can be completed within a matter of few hours. One ±1 kPa DML cycle has been found to be equivalent to one thermal cycle and 175 such cycles are equivalent to 25 years exposure in Colorado, with respect to ribbon fatigue failure.

Mickiewicz *et al.* [226] have looked at the effect of different encapsulants on the degradation of solar panels in static and dynamic load tests, at three different temperatures (–30 °C, RT, 85 °C). A maximum power loss of 2% was observed for the 160 μm cell-based EVA-encapsulated solar panels, after the DML test of 10000 cycles at 5400 Pa (0.5 Hz). They have observed that the cells tend to crack more in the EVA encapsulated panels as compared to Silicone based panels, particularly when operated at low temperatures. Silicone is found to better protect the thinner cells (thickness of 160 μm), which are more fragile in nature.

Koch *et al.* [224] subjected 15 crystalline silicon modules to static and dynamic loading tests followed by Damp Heat. They have reported that the power loss of panels subjected to static loading is higher than those subjected to dynamic loading, because the static loading is done at a much higher pressure than the dynamic loading. Solder joint failure was observed in some of the panels subjected to dynamic loading, but no such contact problem was observed in panels subjected to static loading.

Seigneur *et al.* [227] have conducted a systematic study in Florida to investigate the effect of cyclic loading events in the field and to understand its effect on the modules having cracked cells. They have shown that under extreme wind loading (for example hurricane) the center of the module undergoes 10,000 cycles in roughly 24 hours duration with amplitude reaching 0.9 cm or equivalent to 250 Pa load. Furthermore, they showed that cyclic loading can lead to power degradation in the field over time as a result of the crack opening. This was confirmed by reproducing similar results in the lab. The study also highlighted that modules with prior cracks present can suffer higher power degradation if subjected to cyclic loading. The authors also observed that there is a small daily displacement at the center of the module due to thermal expansion. They emphasized that the range of such displacements needs to be studied since a daily displacement corresponds to about 10,000 cycles over 30 years.

Vasudevan *et al.* [228] showed that the vibration profile data obtained for the transportation of PV modules on Indian roads are substantially higher than the values defined in ASTM D4169 Assurance level II [229], the main reference of IEC 62759-1:2015 [230]. Furthermore, power spectral density (PSD) data has shown that even manual handling can result in high values of acceleration, up to 15 kg. The authors recommended further investigation by performing laboratory simulations to understand better the impact of mechanical loading on the durability of the PV modules during transportation.

The literature mentioned above establishes the importance of investigating the impact of variety of factors that cause mechanical loading and bending of the PV modules. These loading can occur during handling, shipping, installation, and also during deployment from snow and wind loading. In particular, for India, the former stresses appear to be responsible for generation of cracks, as seen in our Surveys. Thus it was deemed important to understand how this mechanical loading impacts the performance of the PV module and we did a systematic

laboratory study to investigate it further. The results of this study have been presented in detail in Chapter 6 of the thesis.

2.4   Summary

From the literature survey, it can be noticed that the various components of the PV module undergo degradation by different modes when deployed in the field. It is deemed important to measure the performance of the fielded PV modules at regular intervals to understand the degradation modes frequent in different climatic conditions. It is also felt important to develop innovative characterization tools and methodologies which could assist in measuring useful data in the field and help in a better understanding of the various degradation modes prevalent in different climatic zones. The above literature also presents that the degradation rates observed in India are higher than the international benchmark and the number of true 'field' studies is less. Furthermore, PV modules deployed in hot climates degrade at a higher rate. LID and PID are the most prevalent degradation modes commonly observed in power plants and this issue is addressed by many researchers around the world. It has been found that EL imaging is a useful tool for determining electrical and various useful parameters of the solar cell. The literature above also suggests that various loading occurs during handling, shipping, installation, and also during deployment from snow and wind loading causing mechanical loading and bending of the PV modules. Subsequently causing cell crack and power loss.

Chapter 3

Characterization Techniques Used in this Work

3.1   Introduction

In the previous chapter a comprehensive overview of the available literature on the degradation modes frequently seen in PV modules has been presented. In the course of the All India Surveys of PV power plants installed in different locations of India, we have performed various characterization tests in the field. In addition, laboratory experiments have also been conducted to understand the impact of cracks on the performance of PV modules of various designs when subjected to mechanical stress. Hence, before moving on to the results from both field and laboratory investigations, which are presented from Chapter 4 onwards, we shall describe the various characterization techniques in this chapter.

3.2   Electrical Characterization

3.2.1 Lighted Current-Voltage Measurement (Outdoor)

The current-voltage (*I-V*) characteristic is one of the most common electrical characteristics of the PV module since it directly indicates the performance of the module. Utilizing the *I-V* characteristic several important parameters (as shown in Fig. 3.1) of the PV module could be estimated (at any given condition of temperature and irradiance).
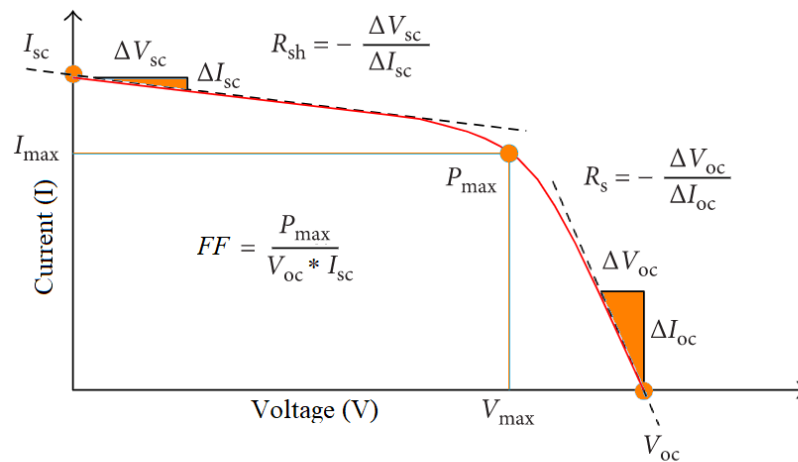
- Maximum current generation (the short circuit current) I_{sc}
- Maximum voltage generation (the open circuit voltage) V_{oc}
- Maximum power generation (the maximum power point) P_{max}
- Series R_s and Shunt resistances R_{sh}
- Fill factor *FF*

Fig. 3.1: Current-Voltage (*I-V*) characteristic of a PV module, showing various parameters of the *I-V* curve.

The Solmetric portable *I-V* tracer (model: PVA 1000S) was used to measure *I-V* characteristic of the module in the field (outdoor). It has an accuracy of 0.5% (±0.04 A) in current and 0.5% (±0.25 V) in voltage [231]. This instrument has a provision of Solsensor unit which has an integrated silicon photodiode for measuring irradiance and two ports for connecting

thermocouple to measure the PV module backsheet temperature. The Solsensor has to be fixed in the plane of the array (POA) for accurate measurement of incident irradiance on the module. Solsensor has an accuracy of 2% in irradiance and 1 °C in temperature measurement. Figure 3.2 (a) shows the schematic diagram for *I-V* measurement in field (outdoor), and the Solmetric *I-V* tracer along with the Solsensor unit is shown in Fig. 3.2(b).
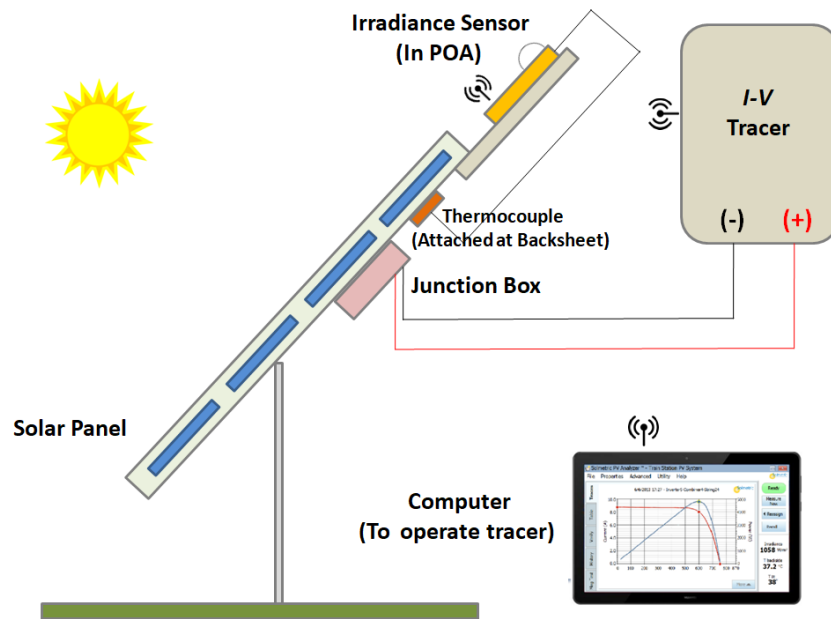
(a)

(b)

Fig. 3.2: Field lighted *I-V* characterization (a) schematic diagram of the setup, (b) Solmetric PVA-1000S *I-V* tracer used for field characterization of PV modules.

49

3.2.2 Lighted Current-Voltage Measurement (Indoor)

The Spire Solar Simulator (model: SPI-SUN 5600 SLP BLUE) which has a Class A+A+A+ certification from the equipment manufacturer [232] was used to characterize PV modules in the laboratory (indoor). As per IEC 60904-9, the requirement for a class AAA simulator is mentioned in Table 3.1 [233]. Spire Corporation has defined a special A+ classification as within 50% of the limit band accepted by IEC standard for Class A. One of the unique features of this simulator is that it can generate a light spectrum from 300 nm to 1100 nm. The capability of generating a light spectrum from 300 nm to 400 nm is not owned by many conventional solar simulators.

Table 3.1: IEC 60904-9 classification for class AAA solar simulator.

Parameters	IEC Requirements
Spatial non-uniformity	Within 2%
Spectral mismatch	Within 25% in the different wavelength bands
Temporal Instability	Within 2%

Throughout the study, a c-Si reference module was used to calibrate the solar simulator by using the short circuit current value of the reference module as the calibration parameter. The reference which is used for the calibration has a tolerance of 5% in its calibrated current rating mentioned by the solar simulator manufacturer. To confirm the repeatability of the measurements, in the case of test samples measured before and after the applied stress, the solar simulator was calibrated using the same reference module. The specifications of the Spire simulator are shown in Table 3.2. The solar simulator is calibrated every year in order to ensure the class AAA classifications. Figure 3.3 (a) shows the schematic diagram for indoor measurements of *I-V* characteristics on the Spire solar simulator and Fig. 3.3 (b) shows the photograph of the Spire simulator at NCPRE, IIT Bombay.

Table 3.2: Accuracy values for the Class A+A+A+ Spire simulator.

Parameters	Values
Accuracy in current	0.2%
Accuracy in voltage	0.2%
I-V resolution	0.003%
Repeatability in current	0.15%
Repeatability in voltage	0.15%
Repeatability in power	0.15%

3.2.3 Dark Current-Voltage Measurement (Indoor)

In dark *I-V* characterization of a solar module, carriers are injected electrically by a positive bias, rather than being generated by light. In dark, the solar cell or module behaves like a large flat diode and dark *I-V* can provide additional information about the cell for various diagnostic purposes. A simple dark *I-V* measurement generates the exponential curve of a diode. The plot of current on a linear scale versus voltage reveals very little information about the diode (except its 'exponential' nature). However, a semilog plot of current versus voltage can generate much more information, which can be used to interpret different loss mechanisms dominant in distinct regions of the *I-V* curve. Figure 3.4 shows the dark *I-V* plot of a solar cell on (a) linear scale and (b) on a semilog scale showing different parameters of the dark *I-V*. The quality of the junction, the ideality factor, and the grid and contact resistance could be estimated easily by utilizing the dark *I-V* characteristics. It is very effective in defining parameters like series resistance, shunt resistance, diode saturation currents, and diode ideality factors which determine the performance of any photovoltaic device.
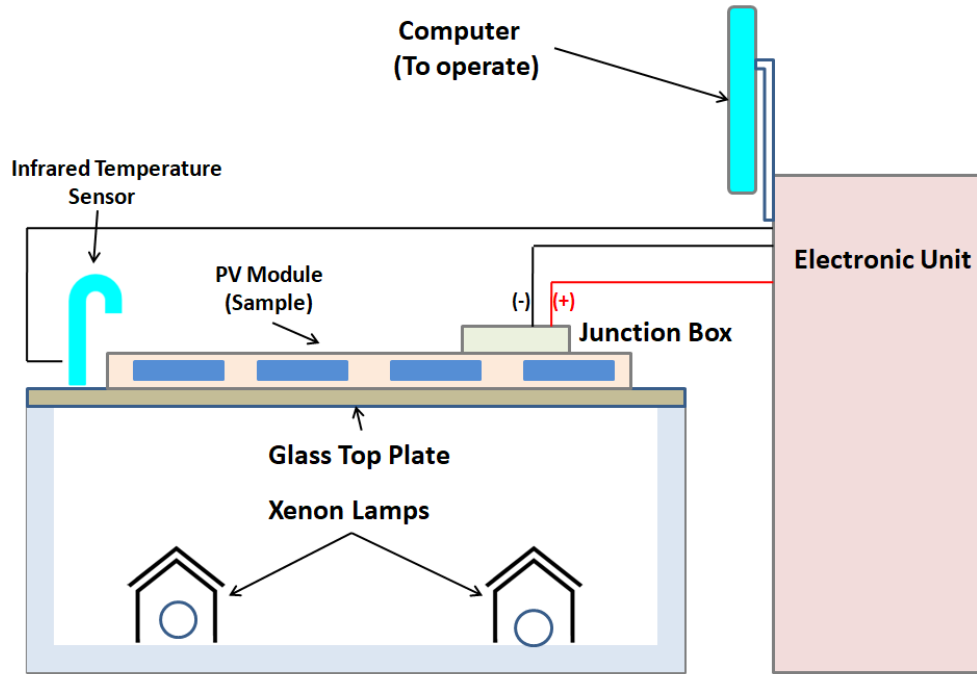
(a)

(b)

Fig. 3.3: Indoor lighted *I-V* characterization (a) schematic diagram of the setup, (b) side view of Spire Solar Simulator at NCPRE Solar Module Lab at IIT Bombay.
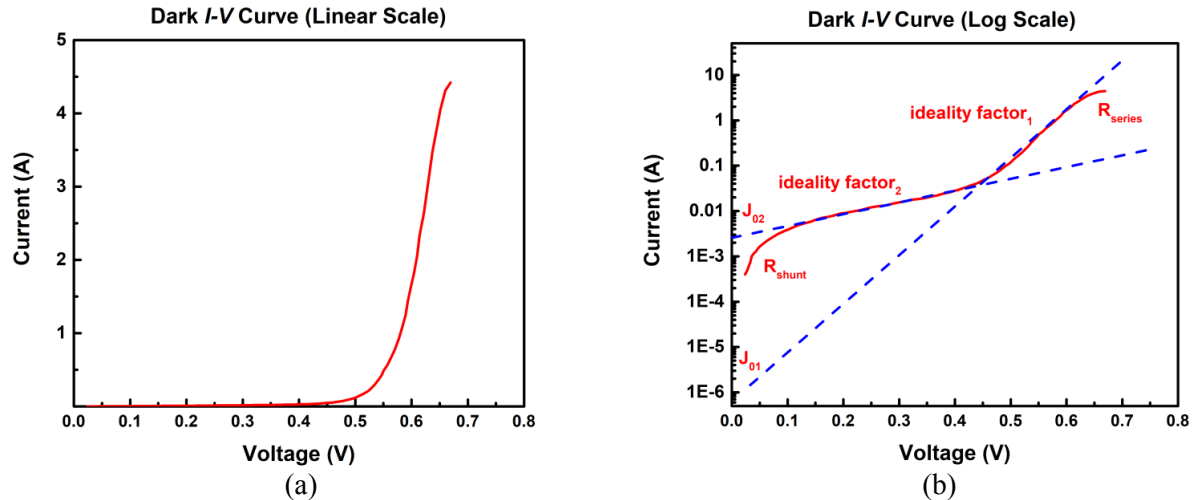
Fig. 3.4: Dark *I-V* characteristic of PV module (a) on linear scale (b) on semilog scale showing various parameters of dark *I-V* curve.

Dark *I-V* of the module is measured by an in-house dark *I-V* setup. The setup consists of a Keysight 34465A DMM for measuring current, GWInstek PSW-720W as a DC voltage source and NI USB TC-01 for recording the temperature of the PV module during the voltage sweep. The Instrument 'panel' developed in-house in Matlab was used to control instruments in a pre-programmed manner and log the data measured. Voltage and current values along with the test sample backsheet temperature at the start and the end of the voltage sweep were recorded. Table 3.3 presents the specification of dark *I-V* setup. Figure 3.5 (a) shows the schematic diagram for indoor measurements of dark *I-V* characteristics, Fig. 3.5 (b) shows the instrument panel of the setup as seen on the computer screen, and Fig. 3.5 (c) shows the photograph of the dark *I-V* setup at IIT Bombay.

Table 3.3: Specification of in-house dark *I-V* setup.

Parameters	Values
Current measurement range	1μA to 10A
Voltage source range	0 V to 140 V
Current measurement accuracy	± (0.12% of reading + 0.01% of range)
Voltage programming accuracy	100 mV
Voltage programming resolution	3 mV
Temperature measurement accuracy	1 ºC
Temperature measurement resolution	0.0625 ºC
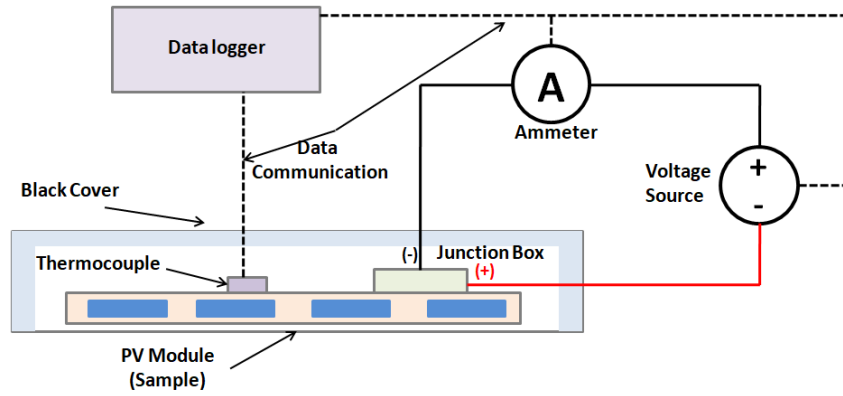
(a)
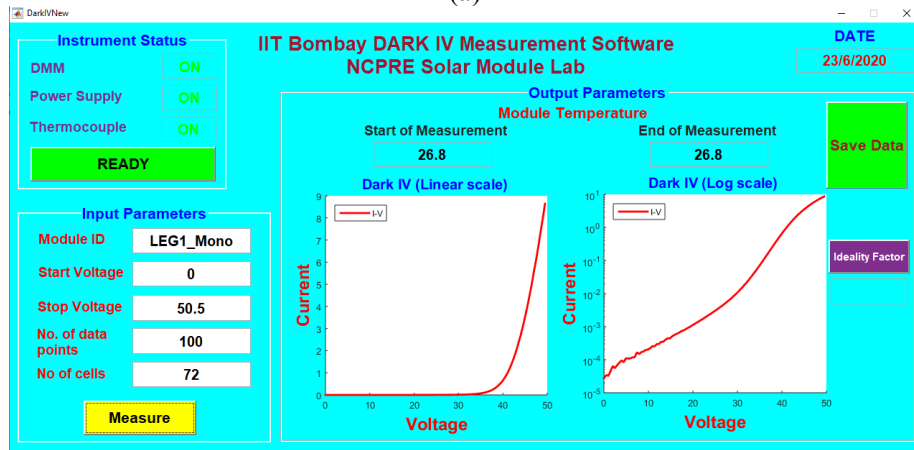
(b)
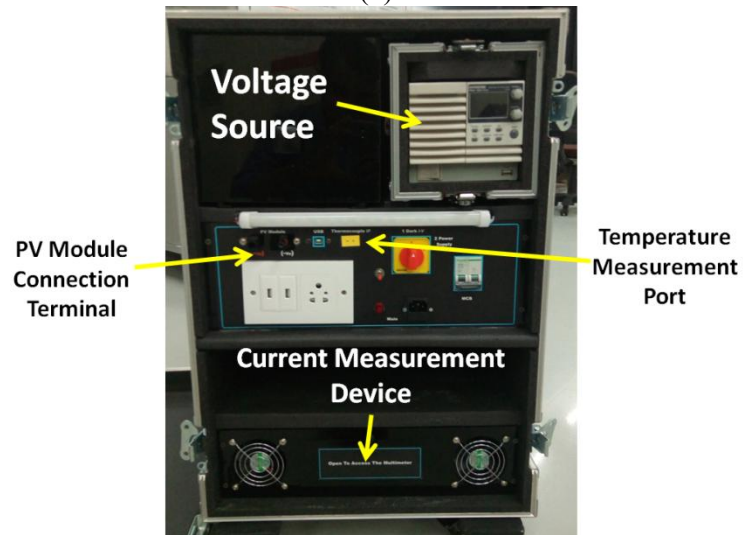
(c)

Fig. 3.5: Indoor dark *I-V* characterization (a) schematic diagram of the setup, (b) instrument panel screenshot and (c) front view of the in-house dark *I-V* setup at NCPRE Solar Module Lab.

3.2.4 Interconnect Failure Measurement (Outdoor)

The Cell Line checker by Togami Corporation of Japan (refer Fig. 3.6 (b)) can be used to detect open circuit faults in the solar panels due to the breakage of solder bonds or interconnect ribbons. This equipment consists of two components – (1) Transmitter which has to be connected to the solar panel or the string, and (2) Receiver unit which has to be placed on the top glass over the solar panel interconnects ribbon (that is swept on the front side of the module over the interconnect ribbons). The strength of the signal received by the receiver unit indicates the current flow through the ribbon. If the signal strength is very poor (or absent) it can be inferred that the ribbon's connection to the solar cell is damaged. This device can be used in two different modes: (1) magnetic field mode for detecting module faults and (2) Electric field mode for detecting open-circuited modules in a PV array. Figure 3.6 (a) shows the schematic of the outdoor interconnect breakage test setup, Fig. 3.6 (b) shows the picture of Cell Line Checker (Togami SPLC-A-Y1) (1) receiver, and (2) transmitter.

(a)   (b)
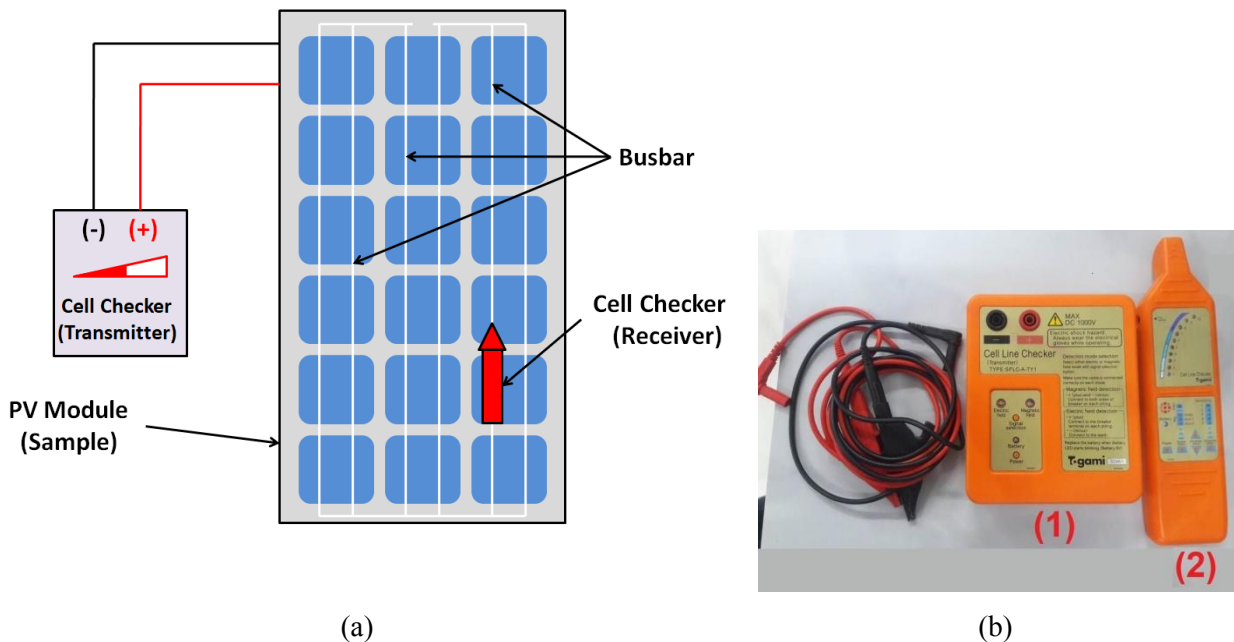
Fig. 3.6: Outdoor interconnect breakage characterization (a) schematic diagram of the setup, (b) picture of Cell Line Checker (Togami SPLC-A-Y1) (1) transmitter, and (2) receiver at NCPRE Solar Module Lab, IIT Bombay.

3.2.5 Insulation Resistance Measurement (Indoor)

Insulation resistance is an important measure of the quality of insulating materials used in the module, like the encapsulant and backsheet. Low values of insulation resistance can be a cause of concern with regard to the safety of the personnel handling such modules. The insulation resistance of the modules was checked indoor (laboratory) under both dry and wet condition. The insulation resistance is measured between the shorted output terminals and the module frame. If the insulation resistance measurement is done keeping the test module in dry condition then it is called dry insulation resistance test, whereas if the test module is submerged in water during the test then it is known as a wet insulation resistance test. Insulation resistance of the modules in the field survey was done using FLUKE 1550C. FLUKE 1550C can apply insulation test voltage values of 250 V, 500 V, 1000 V, 2500 V, and 5000 V. It can measure leakage current in the range between 1 nA and 2 mA. Figure 3.7 the schematic of the indoor insulation resistance test (a) dry, Fig. 3.7 (b) wet, and Fig 3.8 (c) picture of FLUKE 1550C instrument used in field surveys.

(a)

(b)

(c)
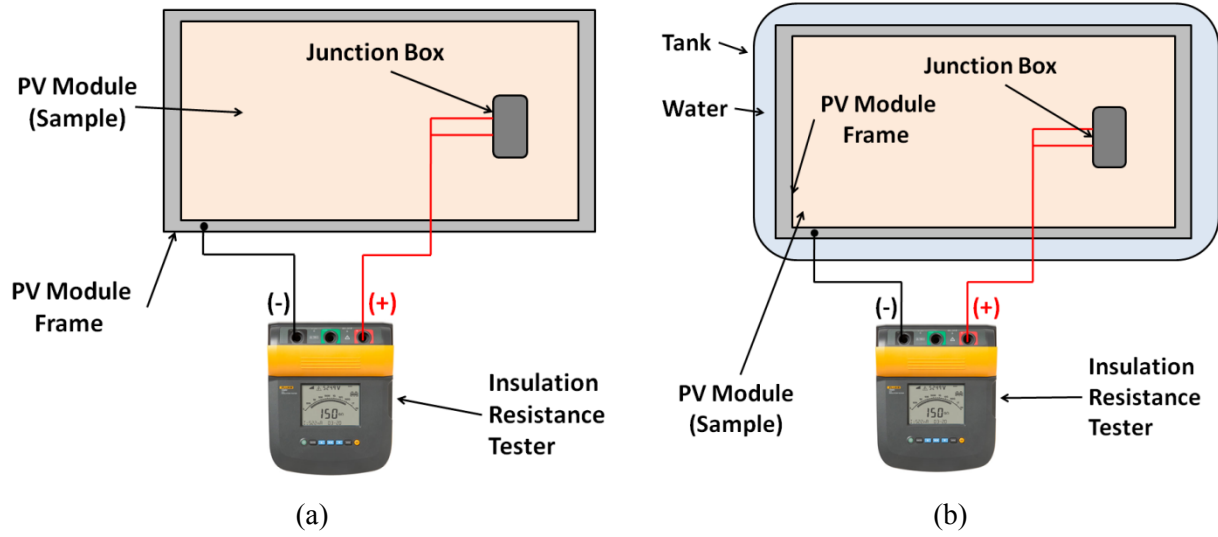
Fig. 3.7: Indoor insulation resistance characterization (a) schematic diagram of dry insulation resistance measurement setup, (b) schematic diagram of wet insulation resistance measurement setup and (c) picture of FLUKE 1550C (at NISE Gurgaon) used in field surveys.

3.3 Optical Characterization

3.3.1 Electroluminescence Imaging

Electroluminescence (EL) imaging is based on the same principle as of a light emitting diode. The solar module is forward biased through a DC power supply (GWInstek PSW-720W) by injecting current and radiative recombination of carriers that cause light emission. Since the silicon PV module is an indirect bandgap semiconductor, most of the recombination occurs through the defects or Auger recombination. There is a very low amount of band to band recombination producing radiative emission which can be captured by an external detector. EL imaging of the PV modules was done by using a Sensovation coolSamBa HR-830 [234] and a modified 24Mega Pixel SONY (model alpha 5100) mirrorless digital camera. The advantages of using a portable, compact modified digital camera for capturing EL images in the field are manifold (as been described in more detail in Chapter 5, Section 5.2). Specifications of the Sensovation coolSamBa HR-830 and modified 24Mega Pixel SONY mirrorless digital camera are given in Table 3.4. Since the same DC power supply was used for EL as for dark *I-V* measurements, the reader is referred to Table 3.3 for its specifications. Figure 3.8 shows (a) the schematic diagram for doing EL imaging, (b) the Sensovation HR-830 EL setup, (c) the modified digital EL camera setup, and (d) GWInstek PSW-720W power supply at IIT Bombay.

Table 3.4: Specification of EL camera used in study.

Parameters	Sensovation HR 830	SONY alpha 5100
Resolution	8.3 Mpixels	24.2 Mpixels
Sensor Image Type	Cooled CCD	CMOS
Number of Pixels	3326 x 2504	6000 x 4000
Pixel size	5.4 μm x 5.4 μm	3.88 μm x 3.88 μm
Sensor Area	14.9 mm x 12.3 mm	15.6 mm x 23.5 mm
Readout Rate	5 MHz High Quality Mode	8 MHz
Frame rate	1.5 fps	6 fps
Digital resolution	16 bit	14 bit
PC interface	USB	USB/ WIFI
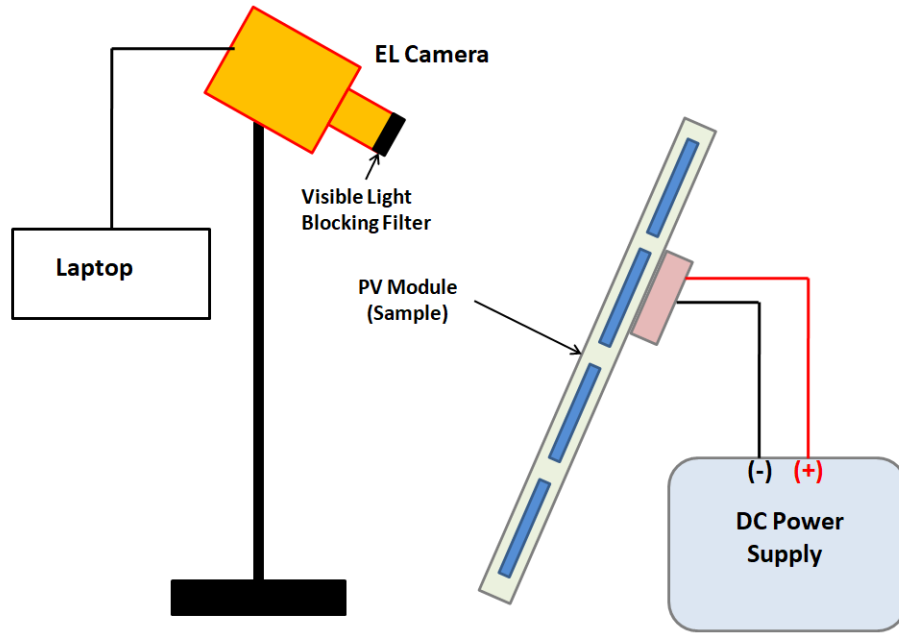
Fig. 3.8: (a) Schematic diagram for doing EL imaging, (b) Sensovation HR-830 EL setup, (c) modified digital EL camera setup, and (d) GWInstek PSW-720W power supply at IIT Bombay.

59

To understand the origin of cracks, it is important to capture the EL images while the PV module is under any external force when these cracks get generated. As a result, we need to capture the EL images of the module in milliseconds. Subsequently, we used Sensors Unlimited InGaAs (model: SU320CSX) detector EL camera to capture the EL videos when the PV module is under any mechanical load or stress. Table 3.5 shows the specification and Figure 3.9 (a) shows the image of Sensors Unlimited (SU320CSX) InGaAs camera and Fig. 3.9 (b) shows the screenshot of camera controlling software.

Table 3.5: Specification of Sensors Unlimited (SU320CSX) camera.

Parameters	Values
Dynamic range	1700:1
Digital Output Frame Rate	30 fps
Pixel Pitch	12.5μm
Spectral Response	700 nm to 1700 nm
Quantum Efficiency	≥65% from 1000 nm to 1600 nm
Noise (RMS)	≤ 35 electrons
Exposure time	200 μs to 32 ms
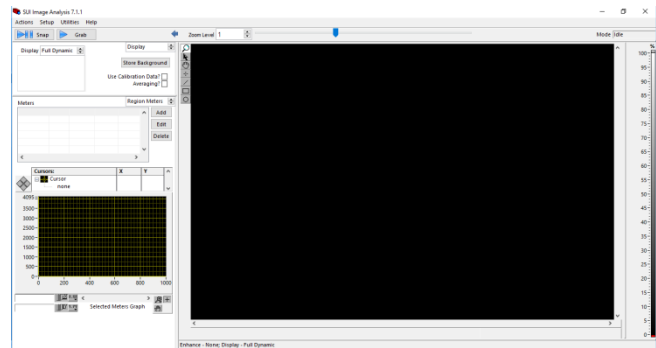
(a)   (b)

Fig. 3.9: (a) Sensors Unlimited (SU320CSX) camera used for capturing EL videos, (b) screenshot of camera controlling software.

The quantum efficiency of the InGaAs detector is more than 65% in the spectrum range of 700 nm to 1700nm. Due to high quantum efficiency in the EL emission spectrum for c-Si, hence InGaAs detectors can easily capture the EL videos. However, InGaAs detector cameras are very expensive. Consequently, we developed an inexpensive alternative to capture EL videos by modifying a CMOS detector DSLR camera. Figure 3.10 (a) shows the modified CMOS camera to capture EL videos and Fig. 3.10 (b) screenshot of the in-house control software to capture EL video.

(a)
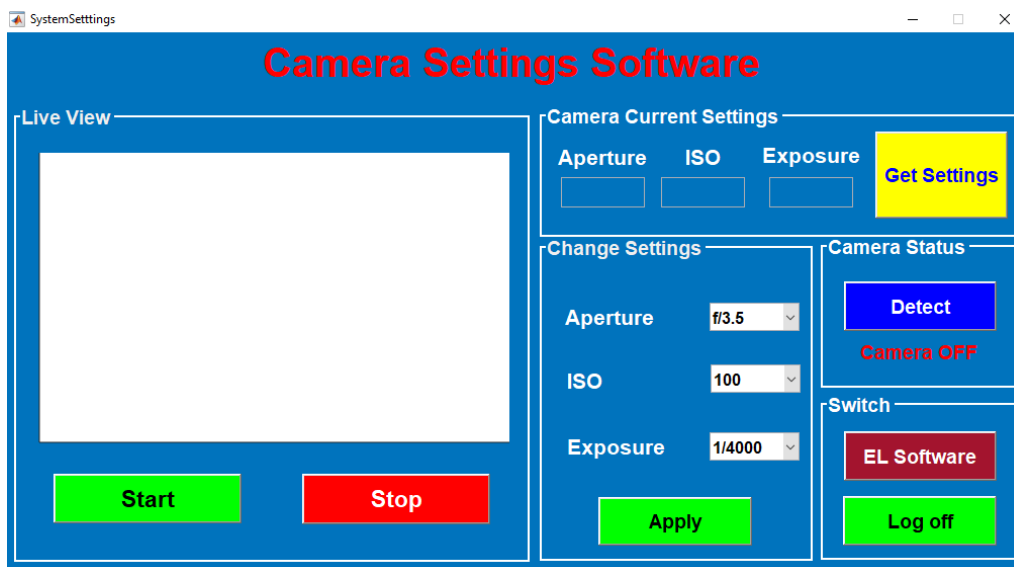
(b)

Fig. 3.10: (a) Modified CMOS detector DSLR camera at NCPRE, IIT Bombay, (b) screenshot of in-house control software to capture EL video.

3.3.2 Photoluminescence Imaging

Photoluminescence imaging is one of the most resourceful characterization techniques of silicon samples across the entire PV value chain. Photoluminescence occurs due to the recombination of excess carriers which are generated by absorption of light of energy greater than the bandgap. Minority carrier lifetime (τ) is one of the most important parameters in a solar cell. The short circuit current (I_{sc}) depends on the excess carrier lifetime. A good solar cell is also a good photodiode. Therefore, PL monitoring at different stages of solar cell processing is very beneficial. PL helps in identifying the recipe which is favorable in enhancing the final efficiency of the solar cell. This is possible because PL monitoring does not require any contacts. Typical PL equipment consists of a light source to excite electron-hole pair in the test sample and a camera (having detector which is sensitive in the emission spectrum of the test sample) with a suitable filter attached in the front of the detector to cut off the excitation light. Figure 3.11 shows (a) the schematic diagram for doing PL imaging, (b) picture of an in-house PL setup for a solar cell at NCPRE, IIT Bombay.

(a) (b)
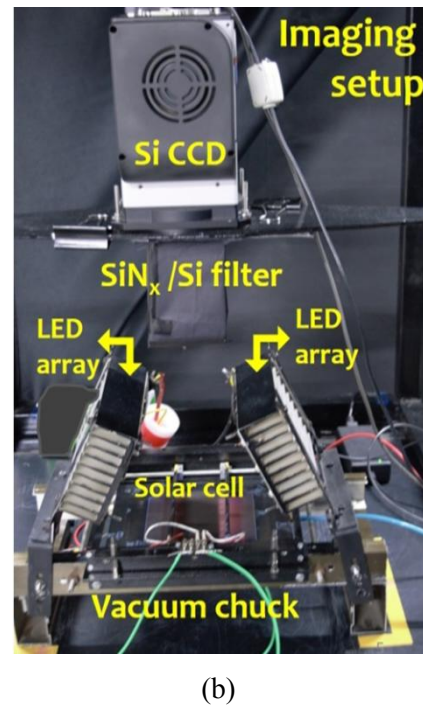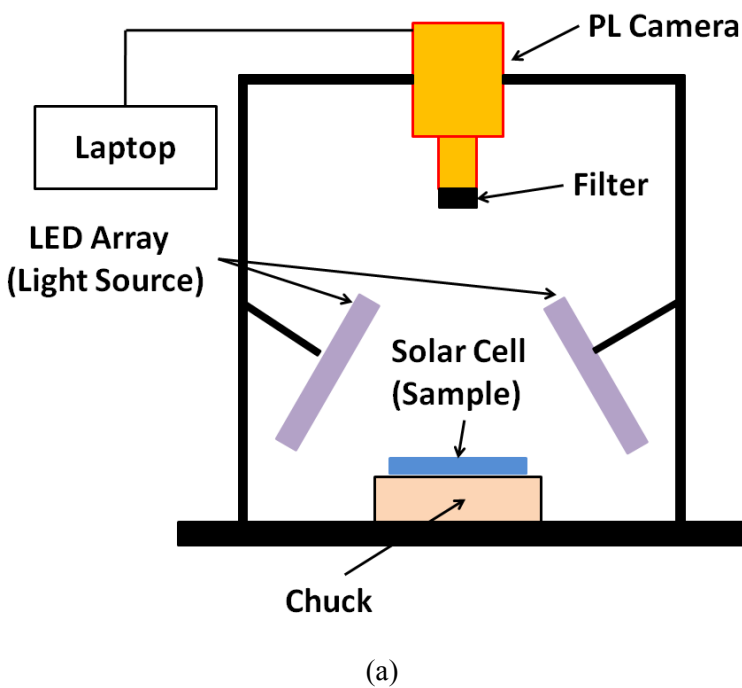
Fig. 3.11: (a) Schematic diagram for doing PL imaging, (b) picture of an in-house PL setup for a solar cell at NCPRE, IIT Bombay.

3.4   Thermal Characterization

3.4.1 Infra-red Thermography

Temperature measurements of the PV modules in the field were done through a contactless measurement technique known as infrared thermography (IR). IR images of the modules in the field were captured by using FLIR E60 [234]. This instrument utilizes the un-cooled micro-bolometer for recognizing the temperature on the infrared signature released by the test sample. Usually, the IR images in the case of c-Si modules were captured from the backside at an irradiance value greater than 700 W/m^2. Kontges *et al.* [235] have suggested that the emissivity value of 0.95 should be set for capturing IR images from the backside of the PV module while 0.85 should be used when capturing from the front surface [235]. Table 3.6 shows the specification of the FLIR E60.

Table 3.6: Specification of FLIR E60.

Parameters	Values
Resolution	320 x 240 pixel
Temperature sensitivity	< 0.05 K
Temperature Accuracy	± 2 °C
Temperature Range	-4 to 1202°F (-20 to 650°C)
Field of View	25° x 19°
Frame Refresh	60 Hz
Visual Camera	3.1 Mega Pixels

Figure 3.12 shows (a) the schematic diagram for capturing IR images outdoor and also presenting the recommended view of the angle as per Kontges *et al.* [235] and (b) a photograph of the FLIR camera (model E60) used for capturing IR images in the field surveys.
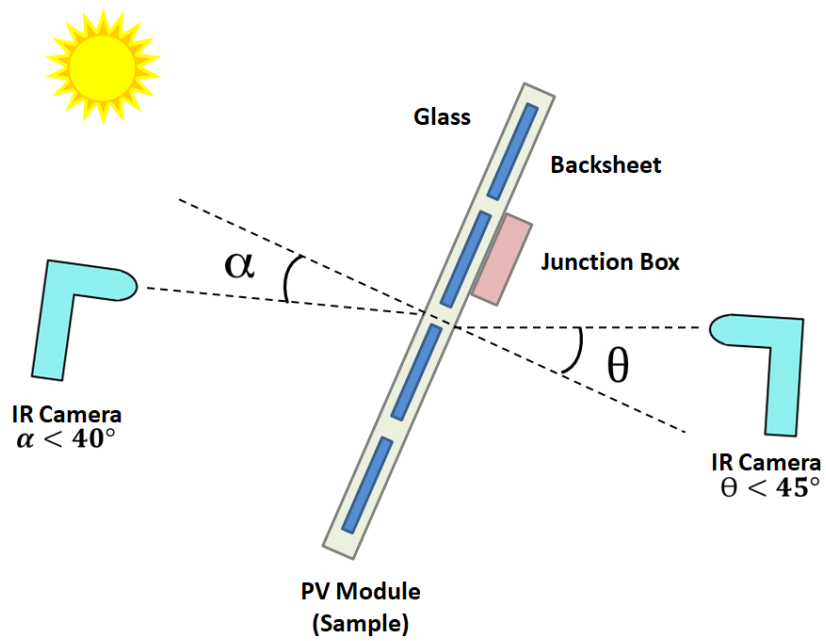
(a)

(b)

Fig. 3.12: (a) Schematic diagram for doing IR imaging and recommended view of angle [235], (b) FLIR camera (model E60) used for capturing IR images in field survey.

3.5   Accelerated Test Equipments

3.5.1 Environmental Chamber

To enhance the reliability and durability of PV modules, it is important to understand the failure and degradation modes prevalent in any climatic condition. To identify the long-term performance and design issues researchers and test lab utilizes indoor accelerated tests. Accelerated tests can be designed according to the environmental stressors of a specific climate. Environmental stresses like humidity, temperature, and UV can be replicated inside an environmental chamber to perform climate specific accelerated testing.   An environmental chamber supplied by Ballice (BS 4500WC) was used to perform thermal and humidity freeze tests on the PV modules. This chamber can perform all the IEC 61215 [221] tests. Table 3.7 shows the specifications and Fig. 3.13 shows the front view of the Ballice (BS 4500WC) walk-in chamber.

Table 3.7: Specification of Ballice (BS 4500WC) walk-in chamber.

Parameters	Values
Temperature range	-40 ℃ to 100 ℃
Temperature rate of change	1 ℃ (or higher)
Humidity range	10 to 90% RH
Refrigeration system	Double stage water cooled

Fig. 3.13: Front view of Ballice (BS 4500WC) walk-in chamber at NCPRE, IIT Bombay.

3.5.2 Dynamic Mechanical Tool

A PV module undergoes several kinds of mechanical stresses during its life cycle. These mechanical stresses get generated either due to snow loading, wind loading, or during installation and transportation. Subsequently, these mechanical stresses cause cracks in the solar cell. As a result, these cracks cause power degradation in the PV modules. To understand the genesis of the cracks and to co-relate the amount of crack with the mechanical load, in laboratory PV modules are artificially subjected to similar loading, as they observe outdoors. To subject the PV modules under various kinds to mechanical stresses, we developed an in-house dynamic mechanical loading (DML) tool. This tool can exert a positive pressure of 10,000 Pa and negative pressure of 2500 Pa. DML tool can perform static and dynamic loading tests as defined in IEC 61215 [221] and IEC TS 62782 respectively. Testing of any size of commercially available PV modules can be done on this DML tool. The design, features, and specifications of the DML tool have been

66

described in more detail in Chapter 5 of this thesis. Figure 3.14 shows the photograph of the DML tool at NCPRE, IIT Bombay.
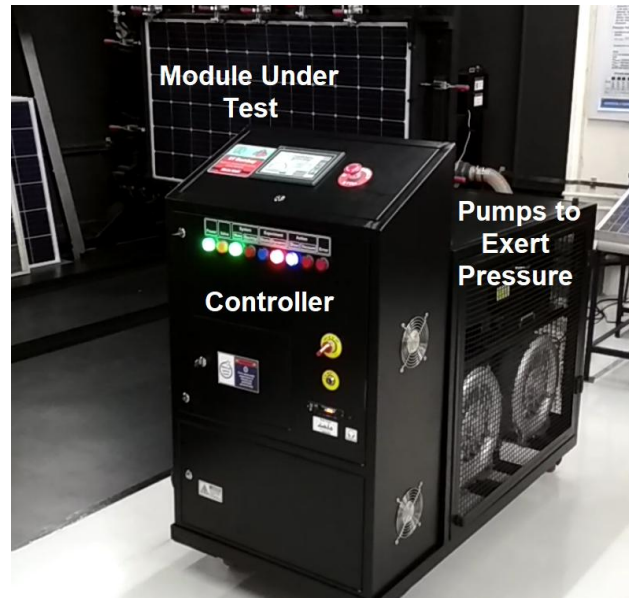
Fig. 3.14: Photograph of the DML tool at NCPRE, IIT Bombay.

3.6 Summary

In this chapter, a description of the wide range of equipment which we have utilized for doing electrical, optical, and thermal characterization of the PV modules during the course of this work has been presented. Portable outdoor field types of equipment have been used in the All-India surveys of PV module reliability. The analysis of the data captured in these surveys, as well as in the laboratory is presented in the subsequent chapters.

This page is intentionally left blank.

Chapter 4

Performance Analysis of Fielded PV Modules

4.1   Introduction

Currently, there is a worldwide push for renewable energy. As a result, utility-scale solar PV installations have increased significantly. These PV modules undergo degradation upon exposure to the outdoor environment. Environmental factors like high operating temperature, humidity, and UV content of the incident solar radiation cause degradation in the individual components of the PV module. As a result, it affects the long term reliability and the durability of the PV module. The module manufactures provide the expected lifetime of PV modules to be 25 years in the field. Hence, it is important to accurately measure the power generation of the

69

deployed modules and determine the degradation which can help us to predict the actual performance over the long term. To improve the reliability and the service life of the PV modules in various climatic conditions, it is beneficial to understand the degradation modes prevalent in the fielded PV modules. Subsequently, it would also help in designing and improving the accelerated tests, which can improve the reliability of the PV modules, and indeed improve the modules themselves. Given the lack of information about the long-term performance of PV modules installed in different climatic conditions of India, a joint team from the National Centre for Photovoltaic Research and Education (NCPRE) and National Institute of Solar Energy (NISE) has conducted surveys of PV systems deployed in different locations of the country. The joint team conducted its first PV module survey in the summer of 2013 [236] and performed measurements on 63 'visually degraded' PV modules spread across India. The analysis of the 2013 Survey is presented in Appendix I. Interested readers are requested to refer to Appendix I for the degradation rate and visual data analysis results of 'visually degraded' PV modules. The survey conducted in 2013 was a learning exercise that enabled us to set up more organized surveys on a much broader scale in 2014 [237] and 2016 [20]. It may be mentioned here that the present author was the lead person for the 2013 and 2014 Surveys and the co-lead for the 2016 Survey. The electrical performance analysis and EL analysis presented in this chapter were carried out solely by the present author. Current-voltage (*I-V*) measurement and visual inspection were the two primary characterizations done on the PV module during the 2013 Survey. However, as mentioned above for the later surveys, both the number of characterization techniques and the number of modules inspected were expanded significantly. The field assessment of the modules in 2014 and 2016 Surveys included a visual inspection (using NREL visual inspection checklist [29], condensed into 2 pages), a detailed electrical characterization of the modules (illuminated *I-V*, dark *I-V*, insulation resistance test, interconnect breakage test, off-grid inverter performance test, electroluminescence imaging), thermal characterization (illuminated *IR* and dark *IR*), and measurement of the relevant weather and irradiance data. In addition to these characterizations, for the first time, on-site measurement of the temperature coefficients of the modules was performed using a technique (described in more detail in Chapter 5) that had been specifically developed for the purpose [238]. A total of 925 modules were inspected in the 2016 Survey and 1148 in the 2014 Survey. Measurement of some of the repeat modules was done in the 2014 and 2016 Surveys. To understand the climatic effect on the

70

performance and the long term reliability of the PV modules, the modules have been grouped based on the climatic zone. There have been multiple climatic zones classifications present in literature, and the classification criteria proposed by Bansal and Minke for India has been used for this work [239] (the criteria are described in Table 4.1).

Table 4.1: Climatic Zone Classification criteria as per Bansal and Minke [239].

Climate	Mean Monthly Temperature (°C)	Mean Relative Humidity (%)
Hot & Dry	> 30	< 55
Warm & Humid	> 30	> 55
Moderate	25 – 30	< 75
Cold & Cloudy	< 25	> 55
Cold & Sunny	< 25	< 55
Composite	This applies when six months or more do not fall within any of above categories	

Figure 4.1 shows the various climatic zones in India, along with the sites where the survey (a) in 2014 and (b) in 2016 has been conducted (represented in black dots). It is evident from the figure that all climatic zones have been covered in the survey. Furthermore, it has been reported that many degradation modes get activated at high temperatures. To understand the effect of high temperature on the reliability and durability of the PV modules, we have specifically classified the six climatic zones into two groups namely 'Hot zone' (grouping Hot & Dry, Warm & Humid and Composite zone together) and 'Non-hot zone' (grouping Moderate, Cold & Cloudy and Cold & Sunny zones together) and analyzed the degradation rates in 'Hot' and 'Non-hot' zones. Therefore, the six climatic zone classifications would sometimes be classified into Hot and Non-Hot zones for the sake of analysis wherever found necessary. Figure 4.2 shows the distribution of technology of the modules surveyed (a) in 2014 and (b) in 2016. Most of the modules surveyed are, as expected, of c-Si technology. Figure 4.3 shows the distribution of modules surveyed in each climatic zone (a) in 2014 and (b) in 2016. Figure 4.4 shows the statistics regarding the various characterization tests performed during the survey (a) in 2014 and (b) in 2016. The extensive characterization tests like current-voltage (*I-V*) characterization (in daylight), infrared (*IR*) thermography, visual inspection, insulation resistance and interconnect breakage tests were performed on all inspected modules at each site. Based on these characterizations in the daytime,

a few modules were selected for further testing, and dark current-voltage (dark *I-V*) characterization, dark *IR* thermography, and electroluminescence (EL) testing was performed in the late evening or at night.

(a)   (b)
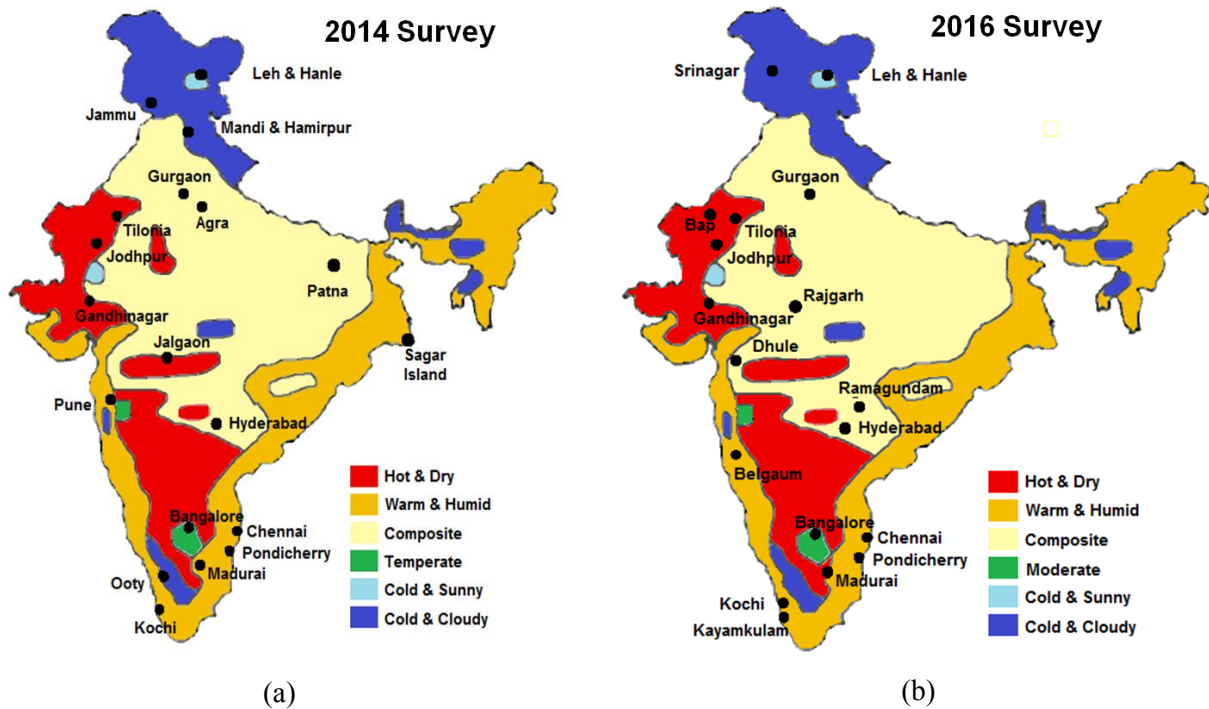
Fig. 4.1: Climatic zones of India and sites visited during the All-India Surveys in (a) 2014 [237], and (b) 2016 [20]. A total of 51 PV systems were surveyed in 2014 while 37 systems were surveyed in 2016.

(a)   (b)
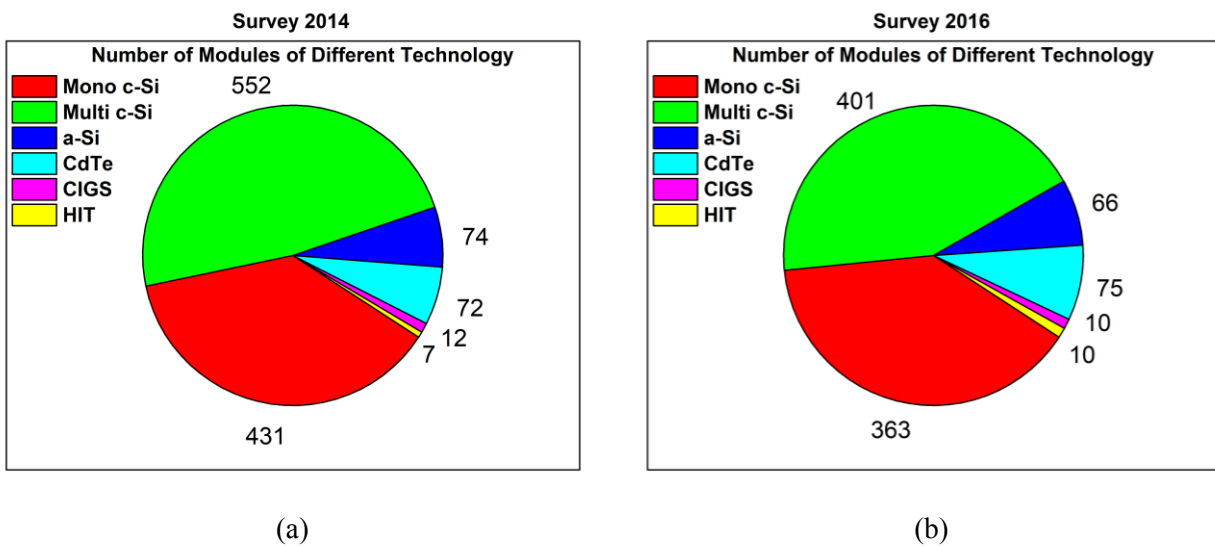
Fig. 4.2: Distribution of technology of the modules surveyed (a) in 2014 Survey, and (b) in 2016 Survey.

72

Survey 2014
Number of Modules in Different Climatic Zones

308 · 135 · 56 · 122 · 333 · 194

- Hot & Dry
- Warm & Humid
- Composite
- Moderate
- Cold & Sunny
- Cold & Cloudy

Survey 2016
Number of Modules in Different Climatic Zones

184 · 94 · 243 · 106 · 20 · 278

- Hot & Dry
- Warm & Humid
- Composite
- Moderate
- Cold & Sunny
- Cold & Cloudy

(a)   (b)
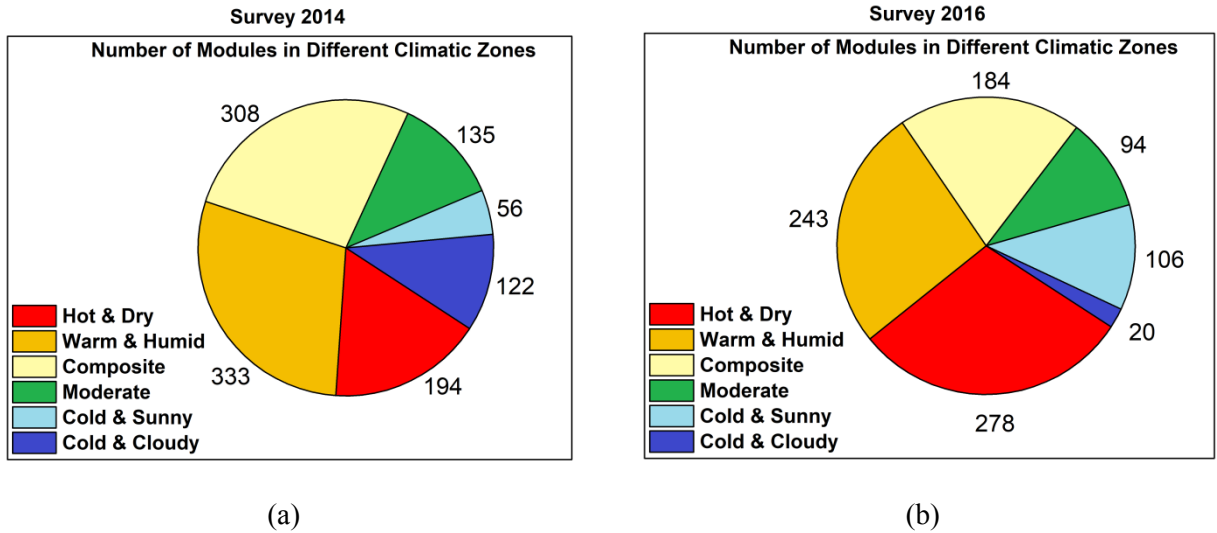
Fig. 4.3: Distribution of modules surveyed in each climatic zone (a) in 2014 Survey, and (b) in 2016 Survey.

Survey 2014 — Number of Modules vs Characterization Test Conducted at Site: I-V (1148), IR (1148), Visual (1148), Insulation Resistance (1148), Interconnect Breakage (1148), Dark I-V (56), Dark IR (56), EL (49).

Survey 2016 — Number of Modules vs Characterization Test Conducted at Site: I-V (925), IR (882), Visual (882), Insulation Resistance (882), Interconnect Breakage (882), Dark I-V (177), Dark IR (177), EL (273).

(a)   (b)
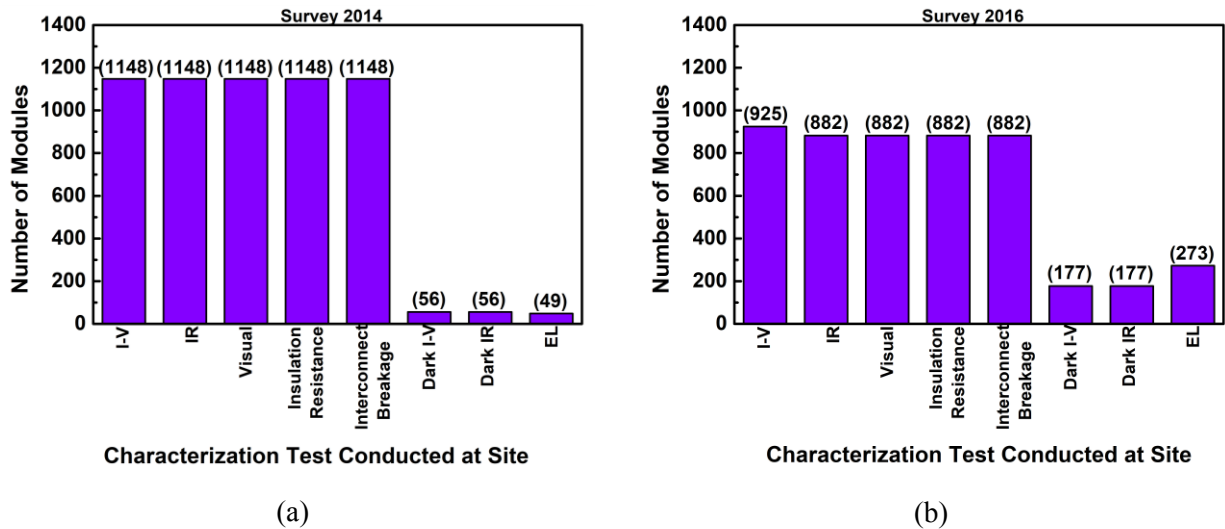
Fig. 4.4: Statistics regarding the various characterization tests performed during the (a) 2014 Survey and (b) 2016 Survey.

In the subsequent section, a modified version of IEC 60891 correction procedures (to translate from field conditions to STC) used in the analysis would be discussed. Also, the error associated with measurements, translating from high temperature, and the uncertainty in the maximum power rating of the module would be presented. The definition of 'Linear Degradation

73

Rate', which discounts the rapid initial light-induced degradation (LID) seen in many modules and the data plotting format with different error bars would be discussed. The various degradation modes observed during the survey are analyzed and presented in the various sub-sections of Section 4.5 based on age, climatic zone, and installation size. The age classification was done by dividing the modules into two categories: (1) Young (modules installed less than 5 years ago), and (2) Old (modules installed more than 5 years ago). Inspected sites have been classified into two categories based on the installed capacity: (1) Small/Medium (installed capacity < 100 KW), and (2) Large (installed capacity > 100 KW). Analysis of dark *I-V*, insulation resistance and the interconnect breakage data and the suspected reason for the degradation in those parameters would be discussed in the subsequent sub-sections. A detailed comparison of electrical data obtained in 2014 and 2016 Survey has been done and the performance of the modules installed at sites which were repeated in the 2014 and 2016 Survey have been presented in Section 4.10.

4.2 Correction Applied to Survey (2014 and 2016) Survey Data

4.2.1 Correction Procedure 1a

In the field measurement, *I-V* data of the PV modules were measured at the existing conditions of module temperature and irradiance, which naturally varied from place to place. The IEC 60891 standard defines three procedures to translate the measured *I-V* characteristics of photovoltaic devices to standard test conditions (STC) i.e. 1000 W/m^2 irradiance and 25 ℃ module temperature. Translating the *I-V* data to STC is necessary for comparing the performance of different PV modules, and in finding out how much the module has degraded. The IEC 60891 first procedure ('Procedure 1') involves two equations, one for correcting current and the other for voltage (as shown in Eq. 4.1 and Eq. 4.2).

$$I_2 = I_1 + I_{sc} * \left(\frac{G_2}{G_1} - 1\right) + \alpha * (T_2 - T_1) \qquad (4.1)$$

$$V_2 = V_1 - R_s * (I_2 - I_1) - k * I_2 * (I_2 - I_1) + \beta(T_2 - T_1) \qquad (4.2)$$

where:

I_1, V_1	Co-ordinates of points on the measured characteristics.
I_2, V_2	Co-ordinates of the corresponding points on the corrected characteristics.
G_1	Irradiance measured on the reference device.
G_2	Irradiance at the standard or the other desired irradiance.
T_1	Measured temperature of the test specimen.
T_2	Standard or the other desired temperature.
I_{sc}	Measured short circuit current of the test specimen at G_1 and T_1
α and β	Temperature co-efficient of current and voltage of the test specimen.
R_s	Internal series resistance of the test specimen.
k	Curve correction factor.

As a result, each point of the entire *I-V* curve is corrected. This procedure requires four correction parameters for translating the entire *I-V* curve. Those parameters are: α (temperature coefficient for current), β (temperature coefficient for voltage), R_s (internal series resistance of the test specimen) and k (curve correction factor). In order to have high accuracy, all four parameters are required in the translating equation. However, obtaining the values of R_s and k requires measurements of temperature and irradiance dependency of the current and voltage. A detailed analysis has been done to understand the loss of accuracy by neglecting these parameters (R_s and k), and this is presented below.

To determine the values of k, we need three *I-V* curves at constant irradiance but different temperatures, whereas the value of R_s of a module is determined by using three *I-V* curves at a constant temperature but different irradiances. During our All India Field Survey, due to the lack of enough field data to determine the values of R_s and k, only two parameters i.e. α (temperature coefficient for current) and β (temperature coefficient for voltage) have been used while keeping

R_s and k equal to zero in the correction Procedure 1. Furthermore, the value of the temperature coefficient used in the correction Procedure 1 was determined in the field (the procedure of obtaining the temperature coefficients have been described in detail in Chapter 5). Nameplate values of I_{sc} and V_{oc} were used in order to convert the values of α (temperature coefficient for current) and β (temperature coefficient for voltage) from %/°C to A/°C and V/°C respectively. Thus, the equations of Correction Procedure 1 will get modified as follows:

$$I_2 = I_1 + I_{sc} * \left(\frac{G_2}{G_1} - 1\right) + \alpha * (T_2 - T_1) \tag{4.3}$$

$$V_2 = V_1 + \beta(T_2 - T_1) \tag{4.4}$$

The above two equations were used for correcting the measured *I-V* curve to the STC condition. This modified correction procedure has been named as Correction Procedure 1a. A MATLAB code has been developed in order to perform the translation in an automated way. To understand the level accuracy of Correction Procedure 1a (compared to the more accurate Procedure 1, where R_s and k are not ignored), an exhaustive set of experiments and error analysis has been done and described in the Section 4.4.1.

4.3   Degradation Rate Calculation

To calculate the degradation rate, the initial performance data is needed. Generally, the initial *I-V* curves were not available during the surveys, so the performance data was computed based on the nameplate data. Usually, there is tolerance for the nameplate power rating, hence Nominal Power rating is used instead of Nameplate rated power, which is obtained as the nameplate power plus average of the tolerance band. Equation 4.5 defines the 'Overall Degradation Rate'. Since most manufacturers of crystalline silicon modules provide for an initial rapid degradation in their modules, which is usually 2% - 3% in the first year or less of field exposure mostly due to the Light Induced Degradation (LID), followed by a linear power

warranty, therefore while calculating the 'linear' degradation rates the effect of LID has been adjusted. This is necessary so that the rates for old and young modules can be compared. To accommodate this initial LID loss in the modules, 2% LID loss has been assumed in the Nominal Power and it has been named as 'LID discounted power rating'. Although the LID loss in modules can vary depending on the wafer quality, the value of 2% has been taken, as described in detail in Section 2.1.5. Equation 4.6 shows the procedure to calculate the Linear Power degradation based on this LID discounted power rating. Figure 4.5 graphically shows the calculation of Linear Degradation Rate for a 15 – year old module. For example, if a module is rated at 100 W and has a tolerance of -0% to 5%, then its Nominal Power will be 102.5 W. Adjusting 2%LID on Nominal Power, we get 100.4 W and this is considered to be $P_{LID\_discounted}$. It should be noted here that the positive degradation rate means a decrease in power.

$$\text{Overall } P_{max} \text{ Degradation Rate (\%/year)} = \frac{(P_{Nominal} - P_{Present})*100}{P_{Nominal}*\text{Age}} \qquad (4.5)$$

$$\text{Linear } P_{max} \text{ Degradation Rate (\%/year)} = \frac{(P_{LID\_discounted} - P_{Present})*100}{P_{LID\_discounted}*\text{Age}} \qquad (4.6)$$
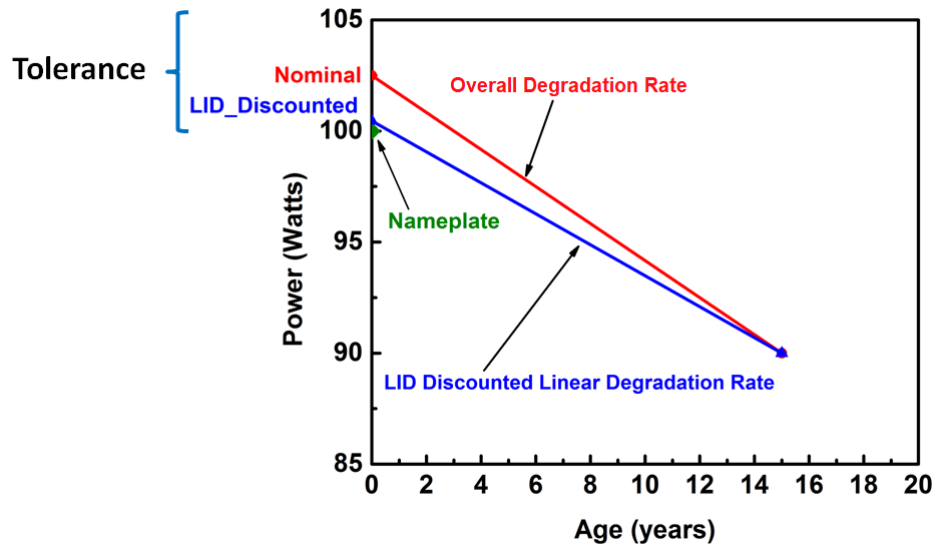
Fig. 4.5: Graphical representation of 'Linear Degradation Rate', and comparison with 'Overall Degradation Rate'.

4.4   Error and Statistical Analysis Applied to Survey Data

The *I-V* parameters of the module under test at STC are obtained from the field measurement followed by the Correction Procedure 1a. Therefore, any uncertainty in the STC data of a particular module depends on the uncertainty introduced by the measurement equipment plus the uncertainties or errors due to the correction procedure (refer to Fig. 4.6). It is important to assess the uncertainties and errors because, as seen from Eq. 4.6, even small errors in measurement or translation can result in large errors in the degradation rate. We therefore undertook a detailed study of the errors and uncertainties.
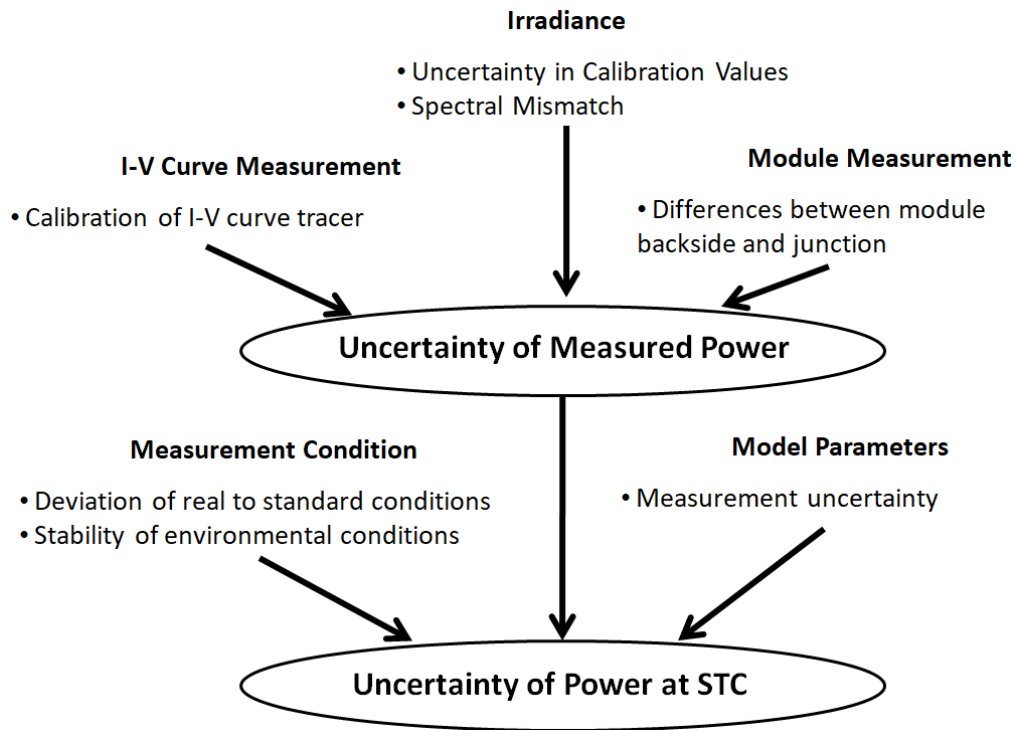
Fig. 4.6: Factors affecting on the combined uncertainty of power at STC [32].

4.4.1 Error Analysis of Correction Procedure 1a

To determine the level of accuracy of Correction Procedure 1a, the following experiment was performed. The characteristics of a crystalline silicon module were measured at STC condition on the Spire Solar Simulator Model 5600 SPL Blue. Afterwards, this module was taken outdoors and allowed to heat up in the sunlight. When the module temperature got stabilized at around 60 °C, it was quickly brought back inside the laboratory. As the laboratory temperature was set at 25 °C, the module temperature started reducing, and its *I-V* was taken at regular intervals on the Spire until the module reached room temperature. The simulator was set in such a way that it could take *I-V* data at three different irradiance levels (1000 W/m^2, 800 W/m^2, and 600 W/m^2) in a single flash. The temperature coefficients of current (α) and voltage (β) were obtained by calculating the slope of I_{sc} with temperature and V_{oc} with temperature respectively. The values of R_s and k were computed by utilizing the procedure described in IEC 60891 (since we had available three *I-V* curves at a constant temperature but different irradiances and three *I-V* curves at a constant irradiance but different temperatures). Next, an *I-V* data set obtained at 800 W/m^2 and 47 °C was translated to STC using four different parameter combinations: (a) using only α and β measured experimentally (R_s and k set to 0), (b) using only α and β obtained from literature (R_s and k set to 0), (c) using α, β and R_s measured experimentally (k set to 0) and (d) using α, β, R_s and k measured experimentally. *I-V* parameters such as P_{max}, V_{oc}, I_{sc} and *FF* were computed for one module and the comparison is shown in Table 4.2. From the data shown in the table it is evident that not much error – about 1.5% in P_{max}– is made by using only α and β obtained from the literature (i.e., Correction Procedure 1a). For the high-capacitance module these numbers may be different.

Table 4.2: Comparison of P_{max}, V_{oc}, I_{sc} and *FF* translated to STC using different parameters.

Parameter	STC Values measured directly on Spire	Translated from 800 W/m^2 and 47 °C to STC using			
		α,β (measured)	*α,β* (from literature)	*α,β&R* (measured)	*α,β, R & k* (measured)
V_{oc} (Volts)	44.2	44.6	44.94	43.96	44.05
I_{sc} (Amp)	5.2	5.17	5.19	5.18	5.17
P_{max} (Watts)	170.1	171.2	172.7	167.6	169.6
FF (%)	74.0	73.9	74.02	73.6	74.3

The experiment was repeated on four other samples, and the full *I-V* curves are shown in Fig. 4.7 for all the five samples. From the results obtained it is evident that Spire-measured STC *I-V* data and the translated *I-V* data (considering one example of *I-V* data measured at 800 W/m^2 and 47 °C) using only $α$ and $β$ obtained from literature (i.e., using Procedure 1a) match very well, and the RMS error is between 1.4% and 5.4%.

RMS Error: 1.4%   RMS Error: 3.1%

RMS Error: 5.4%   RMS Error: 3.6%
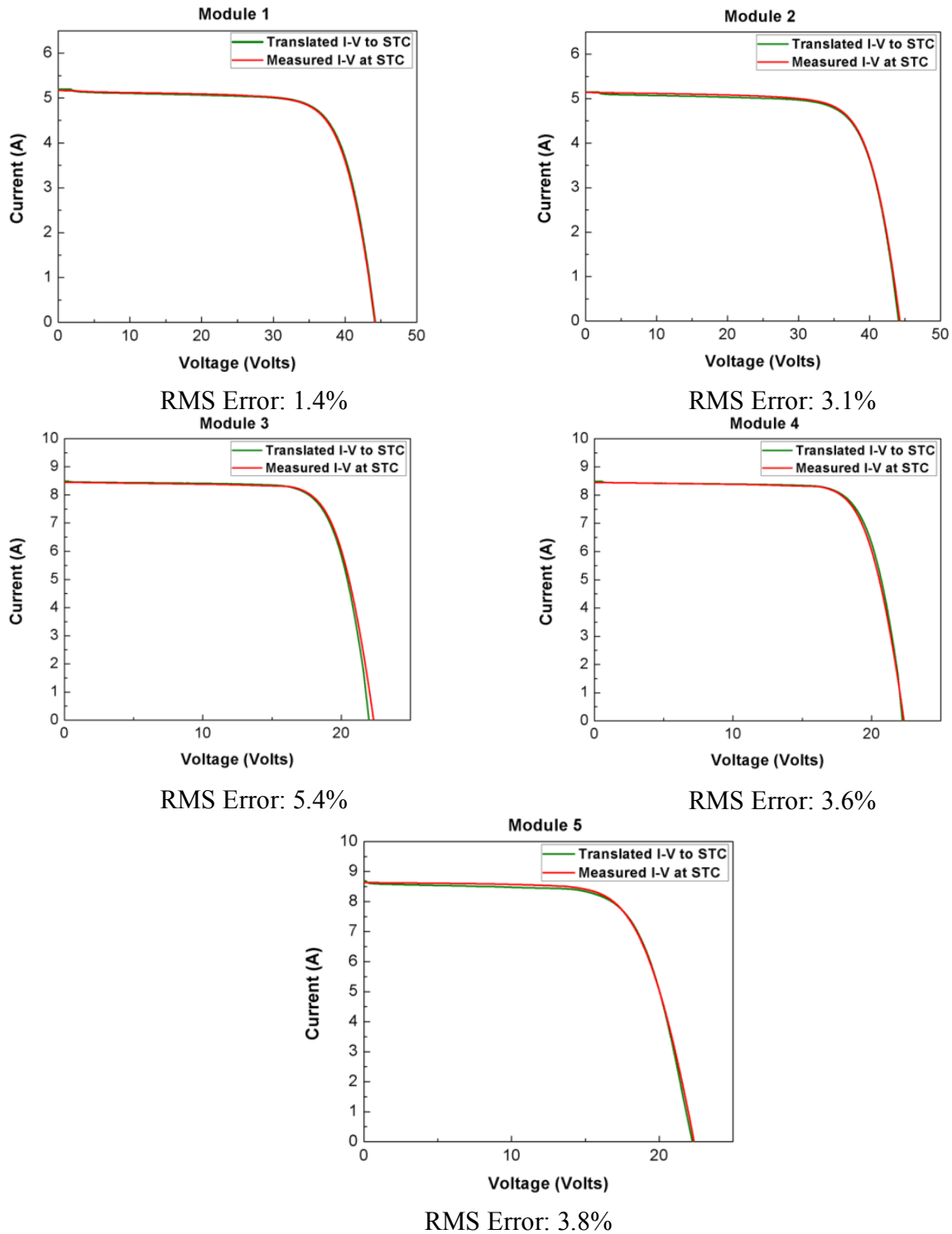
RMS Error: 3.8%

Fig. 4.7: Comparison of R.M.S error for the measured *I-V* data at STC and translated *I-V* using only *α, β* obtained from literature.

In the 2016 Survey the measured *I-V* data were translated using the temperature co-efficient (*α* and *β*) measured in the field, however, in the 2014 Survey the measured *I-V* data was translated

by using the temperature coefficient obtained from the literature. Extending, the results shown in Table 4.3 by presenting the percentage error in P_{max} in two cases: (1) translating using measured α and β and (2) translating using α and β obtained from the literature. From the Table 4.3, it can be seen that the percentage error in P_{max} using measured α and β is 0.65% and it is 1.53% by using literature α and β.

Table 4.3: Comparison of P_{max}, V_{oc}, I_{sc} and FF translated to STC using α, β measured and from literature.

Parameter	STC Values measured directly on Spire	Translated from 800 W/m² and 47 °C to STC using			
		α,β (measured)		α,β (from literature)	
		Value	% Error	Value	% Error
V_{oc} (Volts)	44.2	44.6	0.90	44.94	1.67
I_{sc} (Amp)	5.2	5.17	0.58	5.19	0.19
P_{max} (Watts)	170.1	171.2	0.65	172.7	1.53
FF (%)	74.0	73.9	0.14	74.02	0.03

During the 2014 and 2016 Survey, though most of the I-V data were taken around 700 – 800 W/m², some of the data were measured at much lower irradiance (around 500 W/m²) due to overcast or smoggy weather especially during the 2014 Survey (which was conducted during the months of September-November). In order to learn whether we can include these data in our analysis, we experimentally determined the error in translating I-V data measured at low irradiances (down to 500 W/m²) to STC using Correction Procedure 1a. To calculate the error in translating I-V data measured down to 500 W/m² to STC using Correction Procedure 1a, I-V data of a crystalline silicon module at different values of irradiance (ranging from 500 to 1000 W/m²) and temperature (ranging from 25 ºC to 70 ºC) were measured followed by translating to STC by using Correction Procedure 1a. Table 4.4 shows the P_{max} value when translated to STC from the given set of irradiance and temperature for a crystalline silicon module. Table 4.5 shows the percentage error associated with P_{max} (the error is estimated with respect to the P_{max} at STC) when translated to STC from the given set of irradiance and temperature. Table 4.6 and Table 4.7 show the number of surveyed modules in 2014 and 2016 respectively which fall in different categories of irradiance and temperature. Using Table 4.5, Table 4.6, and Table 4.7 we obtained modified error tables – Table 4.8 (for 2014 Survey) and Table 4.9 (for 2016 Survey). The

shaded region in the tables means that no *I-V* data was measured in these categories. From Table 4.8 and Table 4.9 it can be concluded that the maximum error in P_{max} translation (using Procedure 1a) is 4.59% in 2014 Survey data and 3.58% for 2016 Survey data. This experiment was further repeated for 4 more modules and comparable results were obtained. The conclusions obtained from this experiment allowed us to use data obtained at irradiance levels above 500 W/m^2 with reasonable accuracy. However, the errors in translation of the actual field data may be marginally higher than the values obtained in this experiment, since the spectral changes associated with overcast (low irradiance) conditions could not be simulated in our controlled laboratory experiment.

Table 4.4: P_{max} value at STC obtained by translating using Procedure 1a.

P_{max} (Watts)	Temperature (°C)									
Irradiance (W/m^2)	25.00	30.00	35.00	40.00	45.00	50.00	55.00	60.00	65.00	70.00
500	150.43	149.74	149.64	149.72	150.11	150.42	150.86	151.12	151.59	152.32
550	149.70	148.97	148.83	148.87	149.20	149.47	149.89	150.11	150.56	151.25
600	149.12	148.37	148.18	148.24	148.49	148.67	149.06	149.25	149.67	150.31
650	148.25	147.58	146.38	146.08	145.81	145.68	145.55	145.36	145.17	145.03
700	147.59	146.92	145.69	145.32	144.99	144.86	144.67	144.45	144.21	144.05
750	147.01	146.29	144.99	144.56	144.22	144.01	143.80	143.54	143.26	143.08
800	146.27	145.51	145.21	145.16	145.30	145.53	145.62	145.71	145.26	145.66
850	145.62	144.86	144.45	144.38	144.53	144.68	144.73	144.77	144.32	144.39
900	145.06	144.24	143.81	143.71	143.77	143.91	143.92	143.92	143.40	143.41
950	144.35	143.28	142.46	142.03	141.57	141.41	140.94	140.27	139.89	139.65
1000	143.82	142.96	141.80	141.30	140.80	140.59	140.09	139.38	138.99	138.67

Table 4.5: Percent error in P_{max} value at STC obtained by translating using Procedure 1a.

ΔP_{max} (%)	Temperature (°C)									
Irradiance (W/m^2)	25.00	30.00	35.00	40.00	45.00	50.00	55.00	60.00	65.00	70.00
500	4.59	4.12	4.05	4.10	4.37	4.59	4.90	5.08	5.41	5.91
550	4.09	3.58	3.48	3.51	3.74	3.93	4.22	4.37	4.69	5.17
600	3.69	3.17	3.03	3.07	3.25	3.37	3.65	3.78	4.07	4.51
650	3.08	2.61	1.78	1.57	1.38	1.29	1.20	1.07	0.94	0.84
700	2.62	2.16	1.30	1.04	0.82	0.72	0.60	0.44	0.27	0.16
750	2.22	1.72	0.82	0.52	0.28	0.13	-0.01	-0.19	-0.39	-0.51
800	1.70	1.18	0.96	0.94	1.03	1.19	1.25	1.32	1.00	1.28
850	1.25	0.72	0.44	0.39	0.49	0.60	0.63	0.66	0.35	0.40
900	0.86	0.29	0.00	-0.07	-0.03	0.07	0.07	0.07	-0.29	-0.28
950	0.37	-0.37	-0.94	-1.24	-1.56	-1.67	-2.00	-2.47	-2.73	-2.90
1000	0.00	-0.60	-1.40	-1.75	-2.10	-2.24	-2.59	-3.08	-3.36	-3.58

Table 4.6: Number of modules surveyed in 2014 in different categories of irradiance and temperature.

# of Modules	Temperature (Deg. C)								
Irradiance (W/m^2)	25 – 30	30 – 35	35 – 40	40 – 45	45 – 50	50 – 55	55 – 60	60 – 65	65 – 70
500 – 550	2	16	7	17	13	4	0	0	0
550 – 600	0	2	4	22	14	13	0	0	0
600 – 650	0	1	6	26	34	13	0	0	0
650 – 700	1	4	3	14	30	8	1	1	0
700 – 750	2	0	4	16	20	12	3	3	2
750 – 800	0	1	4	14	32	19	4	3	6
800 – 850	0	3	1	7	25	22	23	8	1
850 – 900	0	0	1	8	25	25	37	21	0
900 – 950	0	0	3	8	10	21	47	66	8
950 – 1000	0	4	19	39	47	42	30	28	8

Table 4.7: Number of modules surveyed in 2016 in different categories of irradiance and temperature.

# of Modules	Temperature (°C)								
Irradiance (W/m^2)	25 – 30	30 – 35	35 – 40	40 – 45	45 – 50	50 – 55	55 – 60	60 – 65	65 – 70
500 – 550	0	0	0	0	0	0	0	0	0
550 – 600	0	0	0	0	0	0	0	0	0
600 – 650	0	0	0	0	0	0	0	0	0
650 – 700	0	0	0	0	0	0	0	0	0
700 – 750	0	0	0	0	0	0	0	0	0
750 – 800	0	0	0	0	0	0	0	0	0
800 – 850	0	0	1	9	7	11	51	13	9
850 – 900	0	0	0	3	12	29	43	70	30
900 – 950	0	0	0	16	22	52	66	101	29
950 – 1000	0	0	7	8	8	20	38	76	59

Table 4.8: Modified error in P_{max} value at STC obtained by translating using Procedure 1a for modules surveyed in 2014.

ΔP$_{max}$ (%)	Temperature (Deg. C)									
Irradiance (W/m^2)	25.00	30.00	35.00	40.00	45.00	50.00	55.00	60.00	65.00	70.00
500	4.59	4.12	4.05	4.10	4.37	4.59				
550			3.48	3.51	3.74	3.93				
600			3.03	3.07	3.25	3.37				
650			1.78	1.57	1.38	1.29				
700	2.62	2.16	1.30	1.04	0.82	0.72	0.60	0.44	0.27	0.16
750	2.22	1.72	0.82	0.52	0.28	0.13	-0.01	-0.19	-0.39	-0.51
800			0.96	0.94	1.03	1.19	1.25	1.32	1.00	1.28
850				0.39	0.49	0.60	0.63	0.66	0.35	0.40
900				-0.07	-0.03	0.07	0.07	0.07	-0.29	-0.28
950				-1.24	-1.56	-1.67	-2.00	-2.47	-2.73	-2.90
1000			-1.40	-1.75	-2.10	-2.24	-2.59	-3.08	-3.36	-3.58

Table 4.9: Modified error in P_{max} value at STC obtained by translating using Procedure 1a for modules surveyed in 2016.

ΔP_{max} (%)	Temperature (°C)									
Irradiance (W/m²)	25.00	30.00	35.00	40.00	45.00	50.00	55.00	60.00	65.00	70.00
500	4.59	4.12	4.05	4.10	4.37	4.59	4.90	5.08	5.41	5.91
550	4.09	3.58	3.48	3.51	3.74	3.93	4.22	4.37	4.69	5.17
600	3.69	3.17	3.03	3.07	3.25	3.37	3.65	3.78	4.07	4.51
650	3.08	2.61	1.78	1.57	1.38	1.29	1.20	1.07	0.94	0.84
700	2.62	2.16	1.30	1.04	0.82	0.72	0.60	0.44	0.27	0.16
750	2.22	1.72	0.82	0.52	0.28	0.13	-0.01	-0.19	-0.39	-0.51
800	1.70	1.18	0.96	0.94	1.03	1.19	1.25	1.32	1.00	1.28
850	1.25	0.72	0.44	0.39	0.49	0.60	0.63	0.66	0.35	0.40
900	0.86	0.29	0.00	-0.07	-0.03	0.07	0.07	0.07	-0.29	-0.28
950	0.37	-0.37	-0.94	-1.24	-1.56	-1.67	-2.00	-2.47	-2.73	-2.90
1000	0.00	-0.60	-1.40	-1.75	-2.10	-2.24	-2.59	-3.08	-3.36	-3.58

4.4.2 Uncertainties in Measurements

The Solmetric PVA-1000S portable *I-V* curve measurement tool was used during the surveys. This instrument has a silicon photodiode as the irradiance sensor and a K-type thermocouple as the temperature sensor. According to the manufacturer's datasheet, measurement uncertainty is ±2% for irradiance measurement, ±2 °C for temperature measurement, and the maximum measurement uncertainty in both voltage and current ±0.5%.To estimate the errors caused by the instrument on the *I-V* parameters at STC the following analysis was performed. Utilizing the equations used for Correction Procedure 1a (replicated below as Eqs. 4.7 and 4.8), it can be concluded that the maximum positive deviation in the translated current at STC (I_2) is obtained if there is a maximum positive deviation in current measurement (I_1, I_{sc}), maximum

negative deviation in irradiance measurement (G_1) and maximum negative deviation in temperature (T_1) measurement (refer Eq. 4.7). Equivalently, maximum positive deviation in voltage at STC (V_2) occurs if there is a maximum positive deviation in voltage measurement (V_1) and maximum positive deviation in temperature (T_1) measurement (refer Eq. 4.8).

$$I_2 = I_1 + I_{sc} * \left(\frac{1000}{G_1} - 1\right) + \propto * (25 - T_1) \tag{4.7}$$

$$V_2 = V_1 + \beta * 25 - \beta * T_1 \tag{4.8}$$

Examining, all possible combinations of measurement error in voltage, current, irradiance, and temperature, the maximum possible error caused by the instrument in the P_{max} value at STC is shown in Table 4.10 for the 2014 Survey data and Table 4.11 for the 2016 Survey data for different combinations of temperature and irradiance. The shaded region in the table again indicates that no I-V data was measured in these categories (refer to Table 4.6 and 4.7). From Table 4.10 and Table 4.11 it is evident that the maximum error caused by the instrument is 4.05% in the case of 2014 Survey data and 4.10% in the case of 2016 Survey data. Note that these are the *maximum* errors possible, and not the expected errors, which may well be considerably less.

Table 4.10: Error caused by the instrument on P_{max} at STC (2014 Survey).

Error (%)	Temperature (Deg. C)									
Irradiance (W/m²)	25	30	35	40	45	50	55	60	65	70
500	4.05	4.05	4.04	4.03	4.01	4.00				
550			4.03	4.03	3.97	3.95				
600			4.04	4.03	3.97	3.95				
650			4.01	3.99	3.97	3.95				
700	4.04	4.04	4.01	3.99	3.97	3.95	3.93	3.92	3.91	3.89
750	4.04	4.05	4.00	3.99	3.97	3.95	3.93	3.92	3.90	3.89
800	4.04	4.04	3.99	3.97	3.96	3.94	3.92	3.91	3.89	3.88
850			4.00	3.98	3.96	3.94	3.93	3.91	3.90	3.89
900				3.98	3.97	3.95	3.93	3.92	3.91	3.89
950				3.99	3.98	3.96	3.95	3.94	3.93	3.88
1000			4.00	3.99	3.98	3.96	3.95	3.94	3.93	3.92

Table 4.11: P_{max} Error caused by the instrument on P_{max} at STC (2016 Survey).

Error (%)	Temperature (°C)									
Irradiance (W/m²)	25	30	35	40	45	50	55	60	65	70
500	4.05	4.05	4.04	4.03	4.01	4.00	3.99	3.97	3.96	3.93
550	4.05	4.05	4.03	4.03	3.97	3.95	3.94	3.91	3.90	3.88
600	4.05	4.05	4.04	4.03	3.97	3.95	3.94	3.92	3.91	3.88
650	4.05	4.05	4.01	3.99	3.97	3.95	3.93	3.92	3.90	3.89
700	4.04	4.04	4.01	3.99	3.97	3.95	3.93	3.92	3.91	3.89
750	4.04	4.05	4.00	3.99	3.97	3.95	3.93	3.92	3.90	3.89
800	4.04	4.04	3.99	3.97	3.96	3.94	3.92	3.91	3.89	3.88
850	4.04	4.04	4.00	3.98	3.96	3.94	3.93	3.91	3.90	3.89
900	4.03	4.03	4.00	3.98	3.97	3.95	3.93	3.92	3.91	3.89
950	4.03	4.03	4.01	3.99	3.98	3.96	3.95	3.94	3.93	3.88
1000	4.03	4.03	4.00	3.99	3.98	3.96	3.95	3.94	3.93	3.92

4.4.3 Uncertainties in Power at STC

The total uncertainty in the corrected P_{max} is the combination of uncertainties in the measurement of the *I-V* data, temperature and irradiance in the field, and the error due to the translation procedure. Table 4.12 shows the worst-case error in the corrected P_{max} to be around 8.64% in the case of 2014 Survey data, considering all the errors and uncertainties. Similarly, Table 4.13 shows the combined error in the corrected P_{max} to be around 5.83% in the case of the 2016 Survey.

Table 4.12: Total error due to instrument and Correction Procedure 1a on P_{max} at STC for 2014 Survey.

ΔP_max (%)	Temperature (Deg. C)									
Irradiance (W/m²)	25	30	35	40	45	50	55	60	65	70
500	8.64	8.17	8.09	8.13	8.38	8.59				
550			7.51	7.54	7.71	7.88				
600			7.07	7.1	7.22	7.32				
650			5.96	5.73	5.63	5.64				
700	6.66	6.2	5.48	5.25	5.12	5.1	5.06	4.83	4.52	4.18
750	6.27	5.77	5.02	4.76	4.6	4.55	4.5	4.12	3.89	3.54
800	5.74	5.22	4.95	4.91	4.99	5.13	5.22	5.33	5.54	5.83
850			4.44	4.43	4.52	4.7	4.77	4.86	5.06	5.33
900				3.93	4.03	4.16	4.21	4.28	4.45	4.68
950				4.13	4.33	4.67	4.73	5.05	5.35	5.56
1000			3.55	3.66	3.85	4.15	4.21	4.51	4.75	5.01

Table 4.13: Total error due to instrument and Correction Procedure 1a on P_{max} at STC for 2016 Survey.

ΔP_max (%)	Module Temperature (°C)									
Irradiance (W/m²)	25	30	35	40	45	50	55	60	65	70
500	8.64	8.17	8.09	8.13	8.38	8.59	8.89	9.05	9.37	10.44
550	8.14	7.63	7.51	7.54	7.71	7.88	8.16	8.28	8.59	9.05
600	7.74	7.22	7.07	7.1	7.22	7.32	7.59	7.7	7.98	8.39
650	7.13	6.66	5.96	5.73	5.63	5.64	5.63	5.3	5.12	4.83
700	6.66	6.2	5.48	5.25	5.12	5.1	5.06	4.83	4.52	4.18
750	6.27	5.77	5.02	4.76	4.6	4.55	4.5	4.12	3.89	3.54
800	5.74	5.22	4.95	4.91	4.99	5.13	5.22	5.33	5.54	5.83
850	5.3	4.76	4.44	4.43	4.52	4.7	4.77	4.86	5.06	5.33
900	4.92	4.32	4	3.93	4.03	4.16	4.21	4.28	4.45	4.68
950	4.43	3.66	3.99	4.13	4.33	4.67	4.73	5.05	5.35	5.56
1000	4.03	3.43	3.55	3.66	3.85	4.15	4.21	4.51	4.75	5.01

4.4.4 Uncertainties in Nameplate Data

In the case of field surveys like the ones done for this study, it is usually not practical to obtain the initial performance data of the module when it was first installed, so the nameplate data has to be used instead. Hence, an extra uncertainty in the linear degradation rate is created by the tolerance band provided by the module manufacturers in the name plate power ratings of the modules (generally it is +/– 3% but also, in a few cases –0% / +5%). Therefore, the true value of the initial power rating could have been anything within the tolerance band. To calculate the error due to the name plate uncertainty, actual initial STC data of 45 numbers of CdTe modules from a PV power plant was obtained. The distribution of the power output of these 45 modules is shown in Fig. 4.8. The power rating of these modules was 85 Watt (–0%/ +5%), however from the figure it is evident that the modules are evenly distributed around a mean value of 86.5 W.
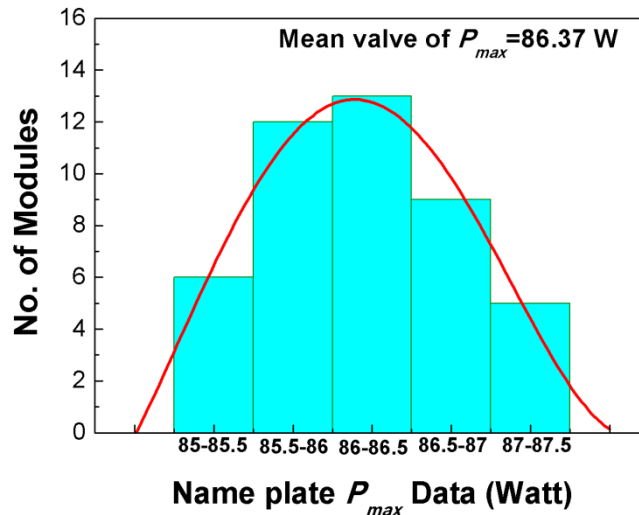
Fig. 4.8: Distribution of name plate P_{max} data of CdTe modules (45 numbers).

If the higher end value (nameplate rating plus the maximum tolerance) is used to calculate the degradation rate, then the computed degradation rate would be higher compared to the degradation rate obtained using the lower end value (nameplate rating plus minimum tolerance). This has been graphically shown in Fig. 4.9 for a hypothetical 15 year old 100 W PV module. This would create a discrepancy in the calculated degradation rate, and we have tried to

minimize this by defining the "nominal" value of the electrical parameters. These nominal electrical parameters are calculated by taking an average of the higher and lower end values of the electrical parameters (For the CdTe module mentioned above, the "nominal" value would be 87.1 W.). Uncertainty in the nameplate value is referred to as error due to nameplate, this adds up a significant fraction of the error in the degradation rates for younger modules (but its effect decreases as the module's age increases). Figure 4.10 graphically demonstrates this effect.
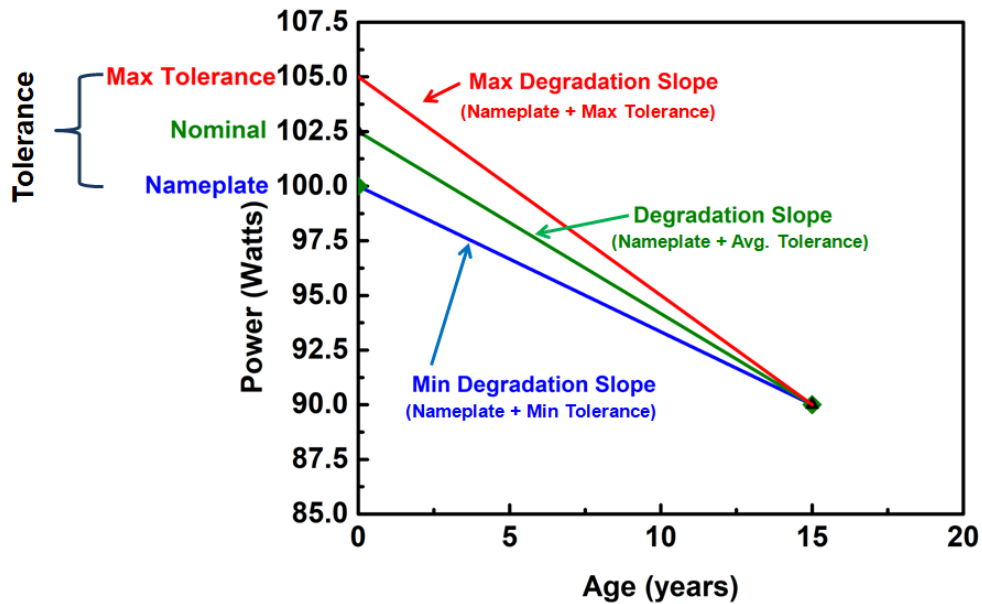
Fig. 4.9: Graphical representation of uncertainty due to nameplate error.
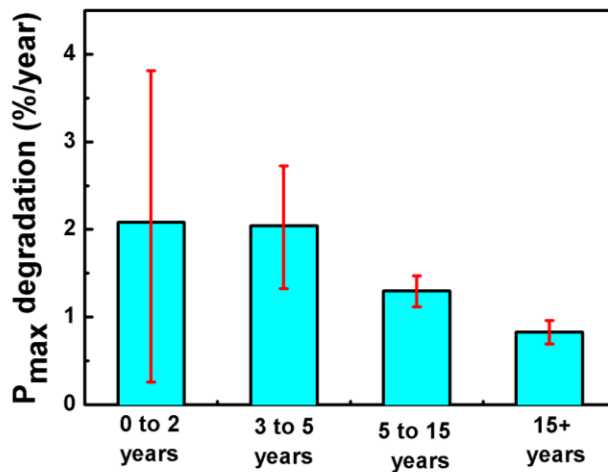
Fig. 4.10: Error due to nameplate uncertainty of ± 2.5%.

4.4.5 Graph Templates

In this section, the templates of the graphs used in this chapter have been presented in Fig. 4.11, Fig. 4.12 and Fig. 4.13 (please note that the data presented are indicative only). Figure 4.11 shows the histogram in which the two vertical dashed red lines indicate the average and the median value of the data set.

Figure 4.12 shows the template for the degradation rate plotted for several groups. Young modules (age less than 5 years) are indicated by hollow symbols whereas the solid symbols indicate Old modules (age greater than 5 years). The mean of each group (value in parentheses) is shown by the red horizontal line, while the red diamond shows the 95% confidence interval. The number of samples (modules) is presented above in square brackets. The error bar due to measurement and STC correction for each group is shown on the right side of the plotted data in green. The error bar due to uncertainty in name plate for each group is shown on the left side of the plotted data in pink. On the right side of the figure, the cumulative probability distribution for the data points has also been shown. Since it would impair the readability of the plot, the symbols for all the data points are not marked in the cumulative probability.

Figure 4.13 shows the graph with single data point per group and shows the errors due to measurement and STC correction in green and error due to uncertainty in name plate in pink. However, there would be no mean value or confidence interval presented in such plots.
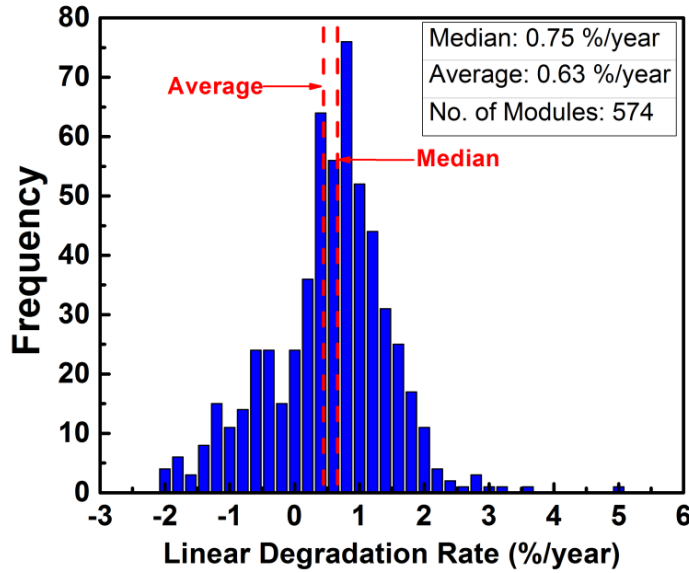
Fig. 4.11: Graph template showing histogram for group of data. Two dashed red lines indicate the average and the median value of the data set.
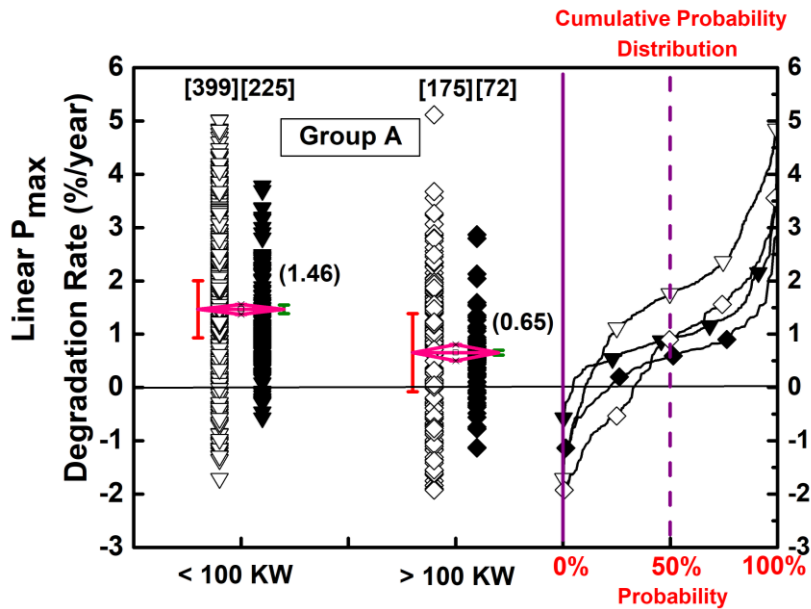
Fig. 4.12: Graph template showing various uncertainties and cumulative probability for group of data. The error due to measurement and STC correction shown on the right side of the plotted data in green. The error due to uncertainty in name plate shown on the left side of the plotted data in pink.
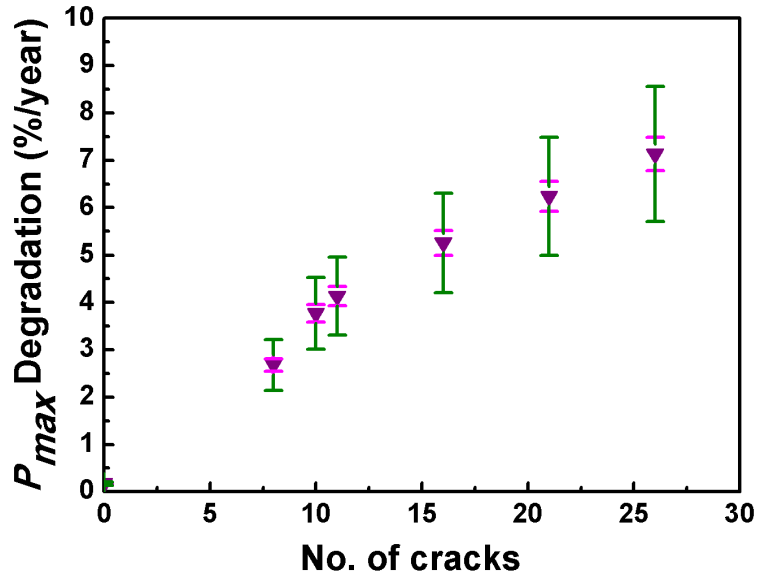
Fig. 4.13: Graph template showing various uncertainties for a single point data. Error due to measurement and STC correction is in green and error due to uncertainty in name plate is in pink.

4.4.6 Statistical Analysis

In this section, the statistical methods used for the analysis of the survey data are presented. The primary step in the statistical analysis is to remove outliers present in the data. These outliers represent modules with extraordinarily high degradation rates, which are not representative of the group. The outliers in the degradation rate data are identified based on the inter-quartile range. The data is arranged in the ascending order and then split into two halves (with median included in both halves if the total number of sample points is odd). After that, the lower fourth (lf) and the upper fourth (uf) are obtained as the median of the lower and upper half respectively. Inter-quartile ranges are given by the difference between the upper fourth and lower fourth. We have defined outlier as any data point beyond 1.5 times of inter-quartile range. In 2016 Survey data, all data points above 5.12 %/year and for 2014 Survey data, all data points above 5.02%/year degradation rate are identified as outliers, as shown in Fig. 4.14 (a) for 2014 Survey and Fig. 4.14 (b) for 2016 Survey. The subsequent analysis of the data presented in this section is carried out after eliminating the outliers from the original data set.
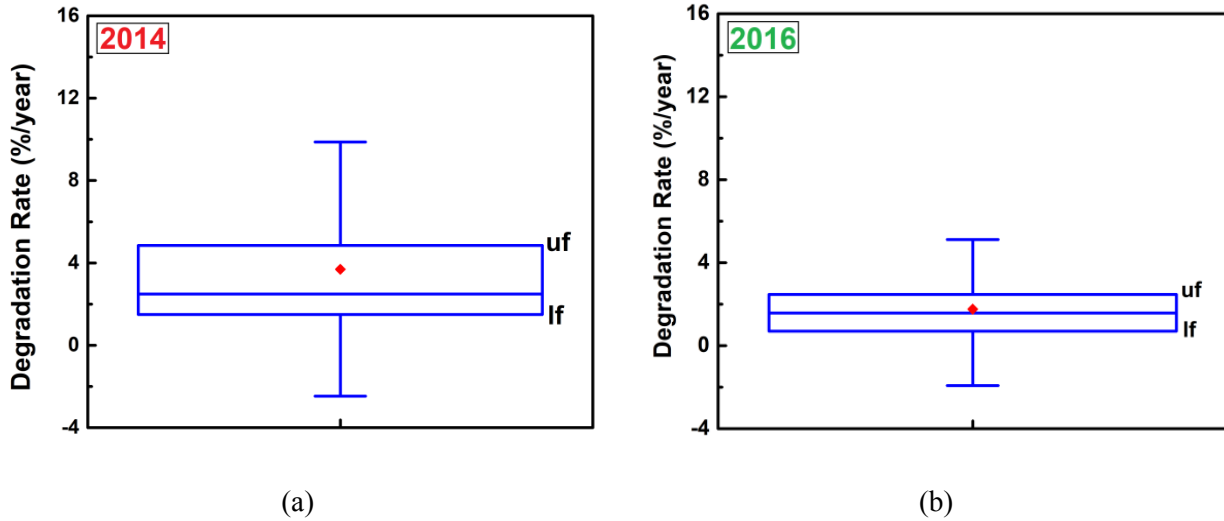
Fig. 4.14: Box plot for P_{max} degradation rates for c-Si modules in all sites in (a) 2014 Survey and (b) 2016 Survey. (The red dot indicates the samples mean).

To reach meaningful conclusions the overall trends in the measurements from the huge set of data collected need to be presented using suitable summary statistics. The sample mean has been used as an estimator of the central tendency. Mean could be a good estimator of the central tendency provided the data is close to normal distribution. As per George and Mallery [240], a distribution can be considered to be normal if the values for asymmetry (skew) and kurtosis are between –2 and +2. In order to test the data, whether, it is normal, P_{max} degradation rate distribution of data collected in the 2014 Survey and 2016 Survey are shown in Fig. 4.15 (a) and Fig 4.15 (b) respectively. The skew and kurtosis of the data set were found to be 0.16 and – 0.30 for 2014 Survey data and 0.13 and 0.24 for 2016 Survey data and these values lie well within the range specified. Hence the mean was used to represent the central tendencies of the data sets. Moreover, some of the important statistical parameters like confidence interval CI, as given in Eq. 4.9 below are defined based on the mean values.

(a)   (b)
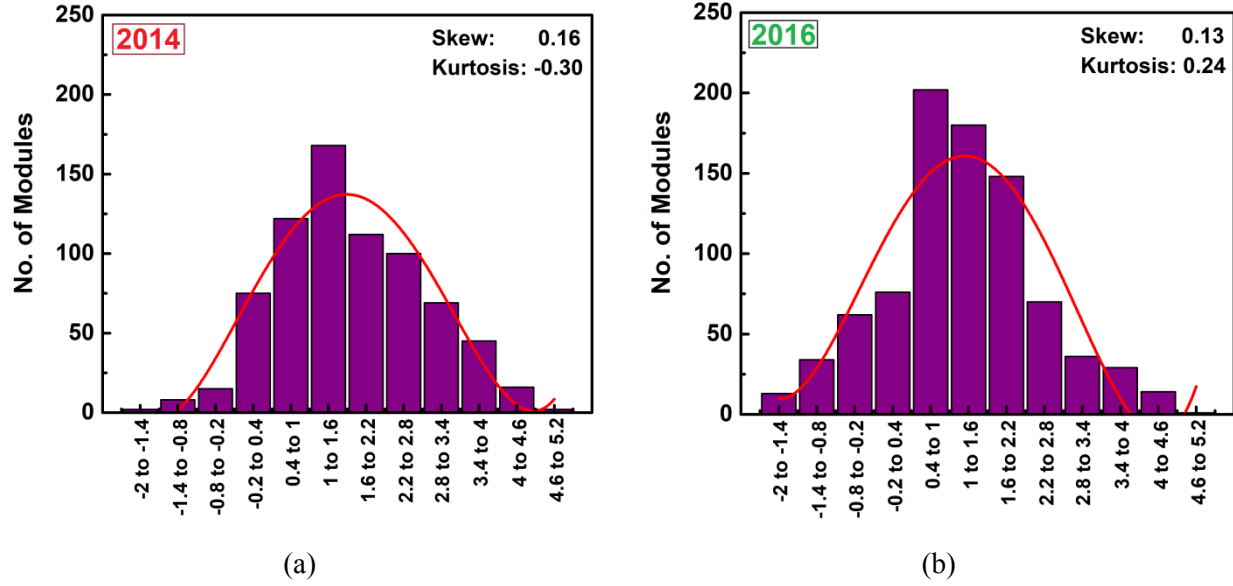
Fig. 4.15: P_{max} degradation rate distribution of data collected in (a) 2014 Survey and (b) 2016 Survey (excluding the outliers). Skew and Kurtosis are 0.16 and -0.30 respectively for 2014 Survey. Skew and Kurtosis are 0.13 and 0.24 respectively for 2016 Survey.

$$x - 1.96 * \frac{s}{\sqrt{n}} < CI < x + 1.96 * \frac{s}{\sqrt{n}} \tag{4.9}$$

where:
x: Mean of the sample
s: Standard deviation of the sample
n: Number of data points in the sample
CI   95% confidence interval

The bootstrap method has been used to construct the confidence interval. In this method, a large number of bootstrap samples of size N are drawn with replacement from the original sample of size n. Subsequently, for each of the bootstrap samples, test statistics of interest (the average degradation rate in the present context) is computed. This, in turn, is utilized to compute the percentile points which are then used to obtain the requisite $100(1-\alpha)$ % confidence interval for the unknown parameters. The histogram of the bootstrap means and the 95% bootstrap confidence interval (CI) for the population mean of P_{max} degradation rates are shown in Fig. 4.16. For the data presented below, 95% confidence interval is calculated to be (1.15, 1.30). These calculations are based on the sample size n equal to 925 and the number of bootstrap samples N equal to 10,000.

The logistic regression has been performed on the degradation data with R software package and the p-values of the results are used to judge whether the explanatory variables are statistically significant or not. An explanatory variable x_i is considered to be statistically significant if the p-value corresponding to the estimator, of its unknown parameter, is less than 0.05.
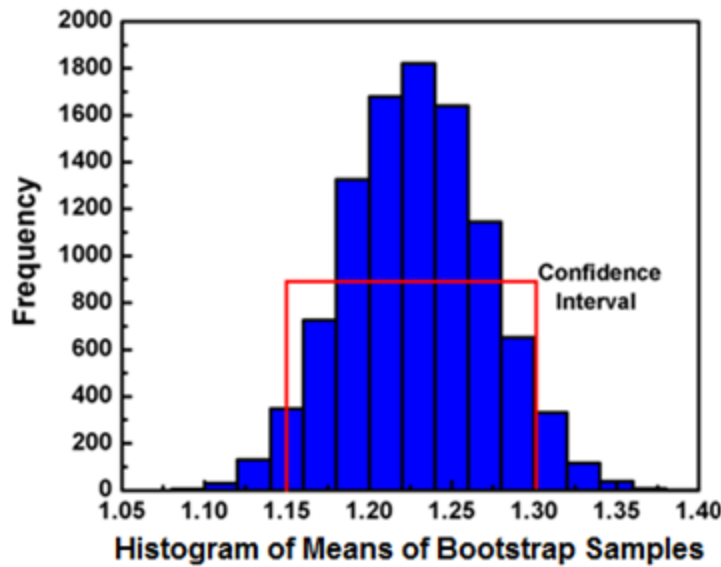
Fig. 4.16: Sampling distribution of P_{max} degradation means based on bootstrap samples. The 95% confidence interval is calculated to be (1.15, 1.30). These calculations are based on the sample size n equal to 925 and the number of bootstrap samples N equal to 10,000.

4.5   Analysis of Electrical Degradation on 2014 and 2016 Survey Data

The translation of *I-V* parameters of the module to STC enables us to compare its current performance with its initial performance at the time of installation, and thus computed the Overall Degradation Rate (%/year) of the output power (P_{max}) and other important electrical parameters like short-circuit current (I_{sc}), open-circuit voltage (V_{oc}) and fill factor (*FF*). In the case of those modules whose initial performance was unavailable, "Nominal" values of the

97

electrical parameters (average of the higher and lower end nameplate values, as defined in Section 4.4.4) have been used to compute the degradation rates. The effect of LID has been incorporated by discounting 2% LID on the Nominal value for crystalline silicon modules to arrive at the Linear Degradation Rate as explained in the previous Section 4.3. A 2% LID discounting has been done for power rating, split up as 0.8% discounting for I_{sc} and V_{oc}, and 0.4% for *FF*. The value of 2% LID and its split-up has been arrived at after a literature survey (detailed in Chapter 2). The outliers have been removed from the initial dataset of degradation rates using the statistical technique as described in the previous section and then the data of the remaining modules have been analyzed. For thin-film modules, the *I-V* data has been presented after irradiance and module temperature corrections but *without considering any spectral mismatch or light soaking effects*.

4.5.1 Overall P_{max} Performance and Classification of c-Si Sites

A total of 1148 modules have been measured during the 2014 Survey, out of which 160 modules' *I-V* were rejected since these were measured at irradiance lower than 500 W/m^2. Out of the remaining 988 modules, 254 modules showed high overall P_{max} degradation rates above 5.02 %/year and these have been deemed as 'outliers'. In the 2016 Survey a total of 925 modules have been measured, out of which the *I-V* of 26 modules could not be translated to STC due to a problem in temperature measurements. From the remaining 899 modules, 34 modules showed high P_{max} degradation rates above 5.12 %/year and these have been deemed as 'outliers'. Analysis of 734 modules from 2014 Survey and 856 modules from 2016 Survey has been presented in this chapter. Figure 4.17 shows the histogram of (a) Overall P_{max} Degradation Rate (having a mean degradation rate of 2.10%/year) for 2014 Survey and (b) Overall P_{max} Degradation Rate (having a mean degradation rate of 1.55%/year) for 2016 Survey data. Figure 4.18 shows the histogram of (a) Linear P_{max} Degradation Rate (having a mean degradation rate of 1.66%/year) for 2014 Survey and (b) Linear P_{max} Degradation Rate (having a mean degradation rate of 1.20%/year) for 2016 Survey. Although the initial rapid degradation (LID) of the c-Si modules is already taken care of, this is still higher than the normal warranty conditions (20% degradation in 25 years implying a Linear Degradation Rate in P_{max} of less than 0.8 %/year). It is

98

evident from Fig. 4.17 that there is a wide variability in the degradation rates. The reason for this wide variability is due to the wide variation in the quality of the modules, climatic conditions, and/or installation procedures among the PV power plants inspected. From Fig. 4.17 it can be seen that many modules have a *negative* degradation rate. These negative degradation rates are mainly due to the thin-film (especially CdTe) modules. The probable reason for this could be the spectral mismatch and light-soaking effects described earlier, and also perhaps due to conservative under-rating. Figure 4.19 and Fig. 4.20 shows the histograms for c-Si modules *only*, which constitute the majority of modules inspected during both the surveys. Group A in the figure refers to 'All' c-Si modules. It is evident from the figure that c-Si modules show a wide variance in degradation rates. Now, for only the c-Si modules, the average value is 2.20 %/year for 2014 Survey and 1.90 %/year for 2016 Survey for the Overall Rate. Similarly, from Fig. 4.20 for the c-Si modules, the average value is 1.82%/year for 2014 Survey and 1.47 %/year for 2016 Survey for Linear Rate for the c-Si modules. From Fig. 4.19 and Fig. 4.20 it is evident that in the cases, the average of the Overall and the Linear degradation rates are quite high, and cause for concern. (However, it should be noted that there are many modules with reasonable degradation rates less than 1%/year also.)
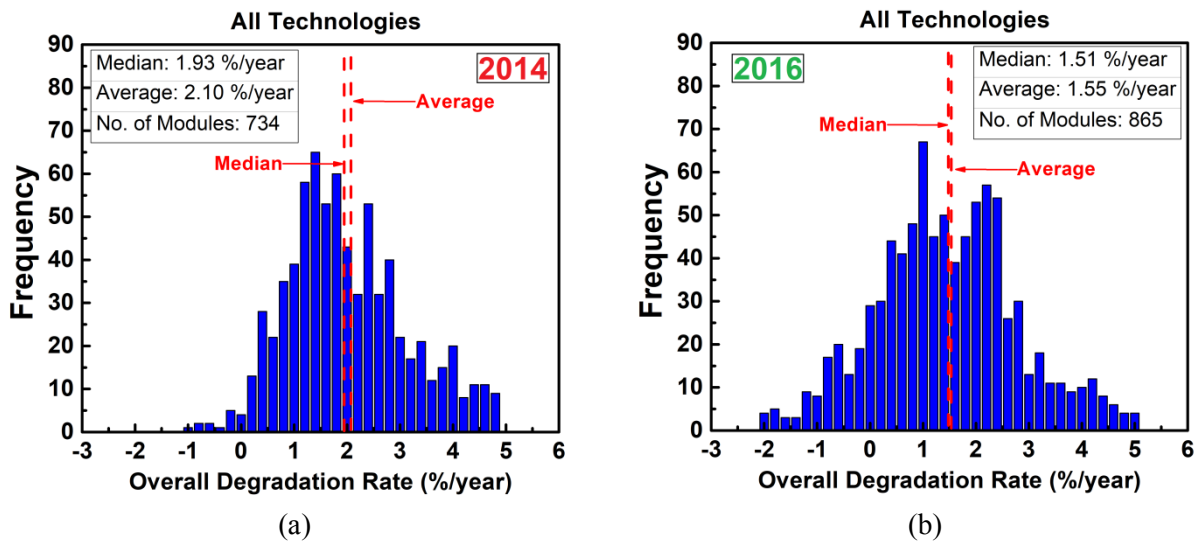
Fig. 4.17: (a) Histogram of Overall P_{max} Degradation Rate of 2014 Survey data (mean value of 2.10%/year), and (b) Histogram of Overall P_{max} Degradation Rate of 2016 Survey data (mean value of 1.55%/year).

99
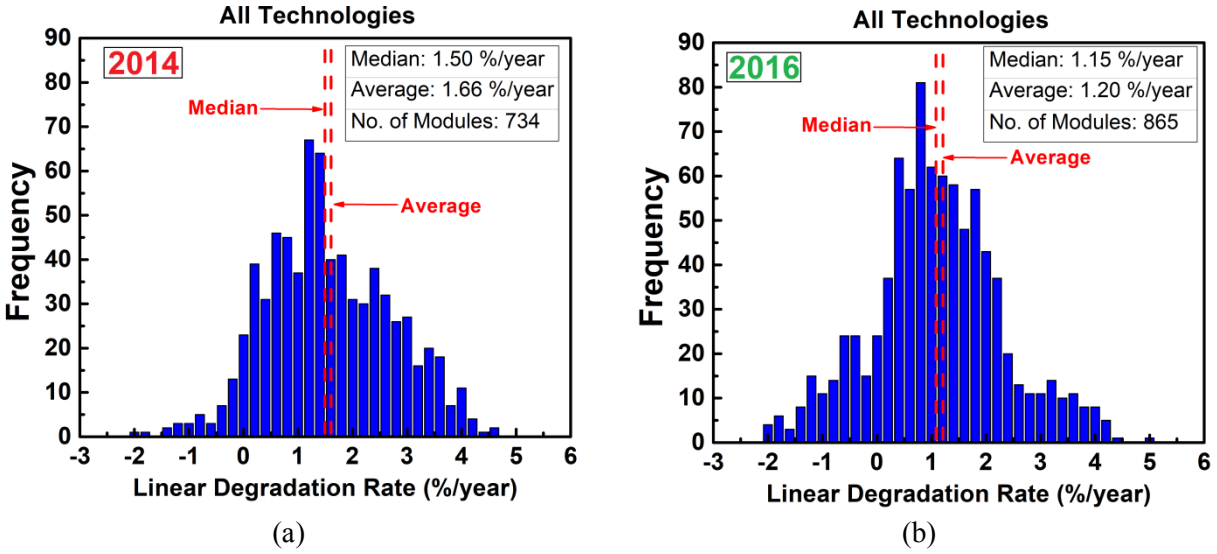
Fig. 4.18: (a) Histogram of Linear P_{max} Degradation Rate of 2014 Survey data (mean value of 1.66%/year), and (b) Histogram of Linear P_{max} Degradation Rate of 2016 Survey data (mean value of 1.20%/year).
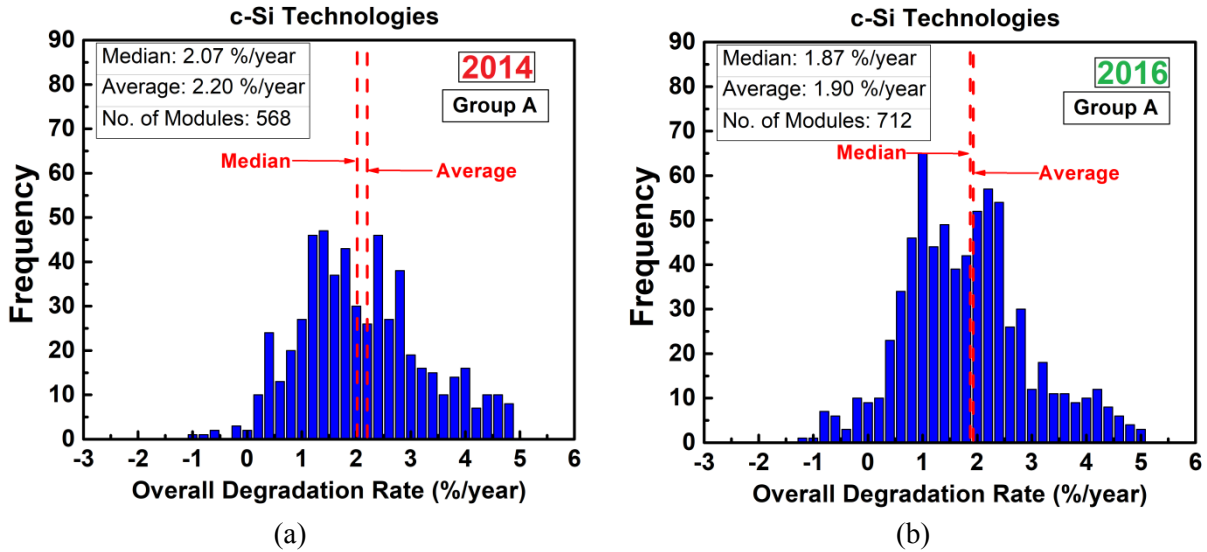
Fig. 4.19: (a) Histogram of Group A Overall P_{max} Degradation Rate of crystalline silicon modules for 2014 Survey, and (b) Histogram of Group A Overall P_{max} Degradation Rate of crystalline silicon modules for 2016 Survey.

100
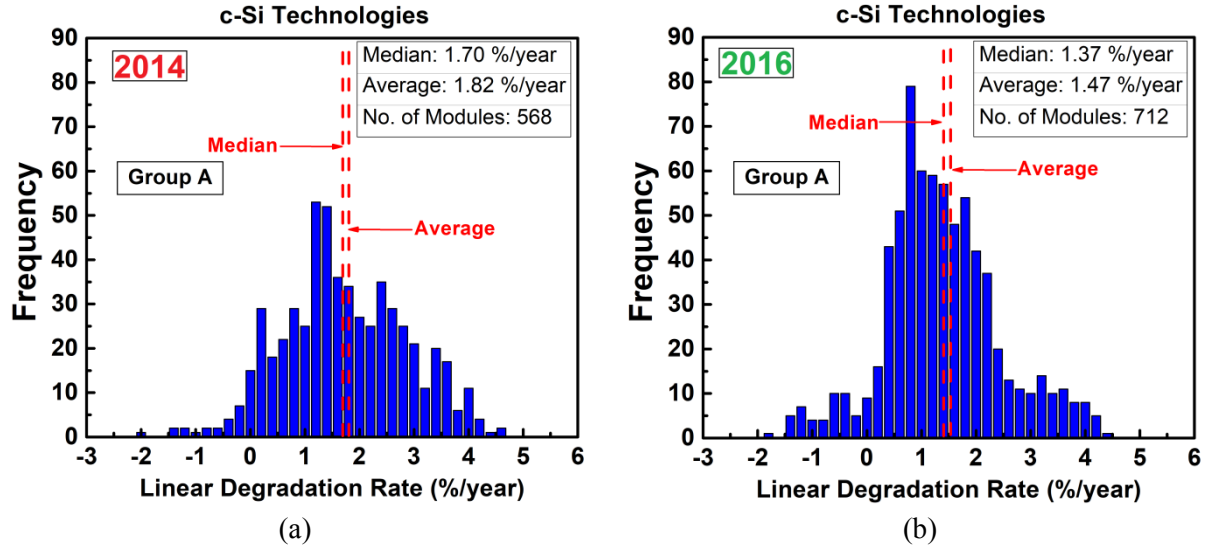
Fig. 4.20: (a) Histogram of Group A Linear P_{max} Degradation Rate of crystalline silicon modules for 2014 Survey, and (b) Histogram of Group A Linear P_{max} Degradation Rate of crystalline silicon modules for 2016 Survey.

From Fig. 4.19 and Fig. 4.20, it could be noted that some of the c-Si modules are performing quite well, whereas others are not; there are some 'good' sites and some 'problematic' sites. Therefore the c-Si sites inspected have been divided into Group X ('good') sites, where the average Overall Degradation Rate is < 2 %/year; and Group Y ('problematic') sites, where the average Overall Degradation Rates is > 2 %/year. The probable reason for the Group X sites to perform well could be the use of better quality modules and/or correct installation procedures than the Group Y sites. It should be noted that for this study this division of Group A (is the superset comprising of both Group X and Group Y) into Group X and Group Y sites has been done only for c-Si, since they constitute the majority, do not suffer from uncertainties of thin-film, and represent the present mainstream technology. In order to understand the influence of the climatic zone on the performance of the modules, data of only 'good' Group X sites has been considered, to avoid any extraneous factor. For all the further analysis presented in this section, the Linear P_{max} Degradation Rate will be used and the Overall P_{max} Degradation Rate will be provided only for a few cases.

The data for each manufacturer of c-Si modules and c-Si sites are shown in Fig. 4.21 (a) for 2014 Survey and Fig. 4.21 (b) for 2016 Survey. To preserve the anonymity of the manufacturers, module manufacturers names have been coded using alphabets (A through V, shown along the x-axis in the figure) and the different sites of each of these manufacturers have

101

been indicated using numbers (1, 2, 3, etc.), which is shown at the top of the figure and the data are color-coded to represent the different climatic zones. Also, the age of the modules has been presented in the figure, with closed symbols representing old modules (age greater than 5 years) and open symbols indicating young modules (age less than or equal to 5 years). It is seen that there is a wide variability at most of the sites having crystalline silicon modules, with only a few showing a tight distribution. Moreover, the average degradation rate (indicated by the red horizontal bar) varies a lot from one site to another. We believe that the installation seems to have an impact on performance even if one accounts for manufacturer and climate, as seen, for example, in the varying degradation rates for Manufacturer C in composite climate (refer Fig. 4.21 a). The demarcation value of 2%/year has been chosen, since 2%/year was the mean value of Overall Degradation rate for the all the modules surveyed in 2014.

Figure 4.22 (a) and (c) for 2014 Survey and (b) and (d) for 2016 Survey show the Overall Power Degradation Rate for crystalline silicon modules belonging to Group X and Group Y sites. From Fig. 4.22 (a) and (b) it could be seen that the average Overall Degradation Rate for Group X modules is 1.55%/year for the 2014 Survey and 1.22 %/year for the 2016 Survey, which again is higher than the value promised in warranty contracts. A total of 271 modules fall in the category of Group X for the 2014 Survey, which represents 24% of all the surveyed modules, and 37% of the 734 modules taken for the detailed electrical analysis after discarding outliers. For 2016 Survey, a total of 397 modules fall in the category of Group X, which represents 40% of all the surveyed modules, and 45% of the 865 modules taken for detailed electrical analysis after discarding outliers. It can be observed that a higher percentage of modules fall in the category of Group X for the 2016 Survey as compared to 2014 Survey. The reason for the higher percentage of Group X modules is attributed to the inclusion of more large sites (System size > 100kW) in 2016 Survey as compared to 2014 Survey. Conversely, Fig. 4.22 (c) and (d) shows that histogram of the Overall Power Degradation Rate for sites in Group Y is 2.79%/year for the 2014 Survey and 2.75%/year for the 2016 Survey. The reason for this difference would be more evident in the subsequent sections.
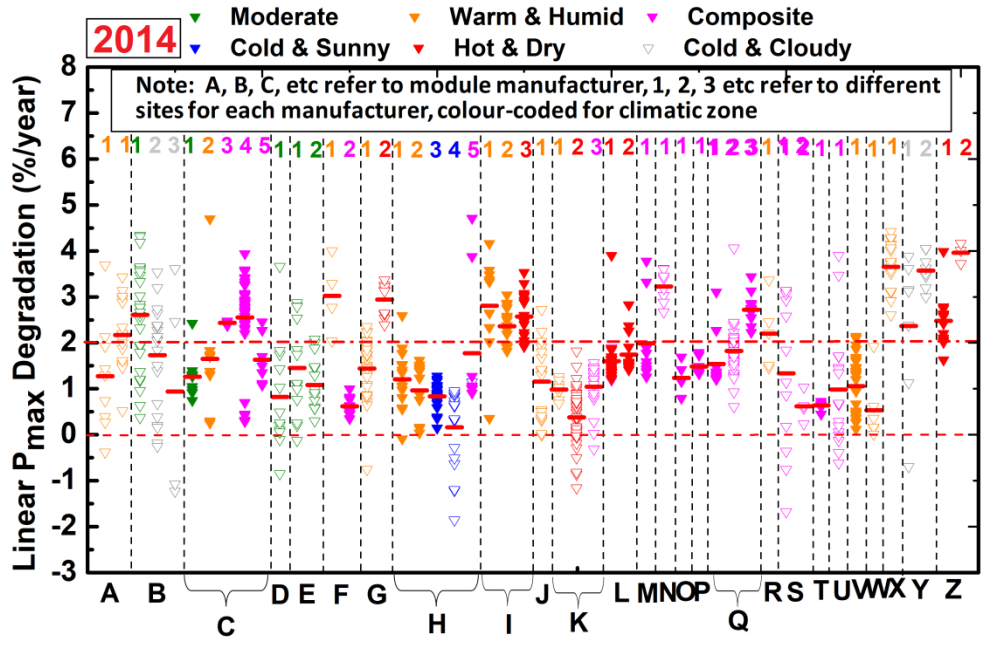
(a)
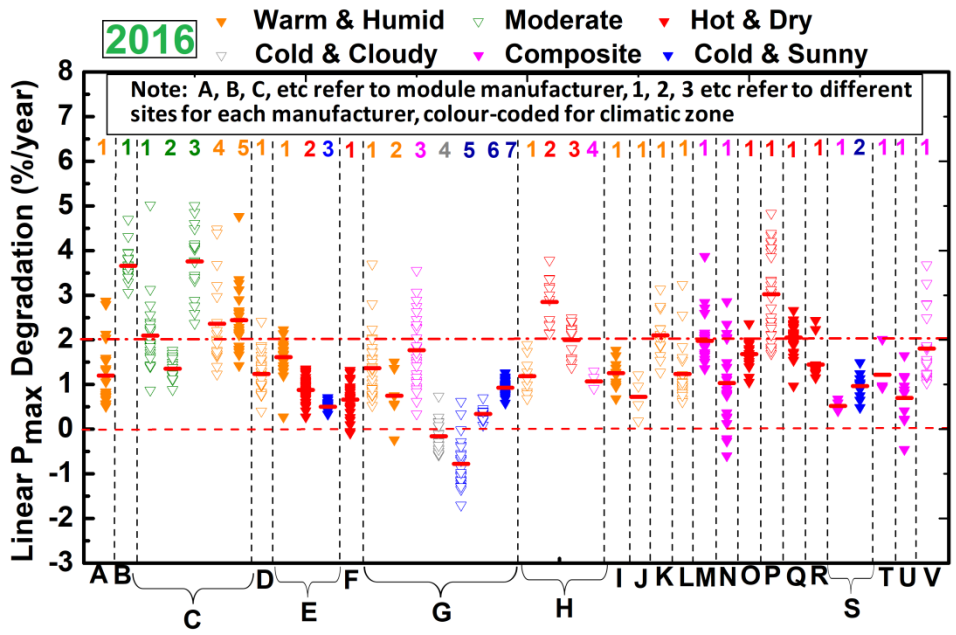
(b)

Fig. 4.21: Manufacturer wise and site wise P_{max} degradation rates (a) for 2014 Survey and (b) for 2016 Survey, incorporating climatic zone data and age of the modules.
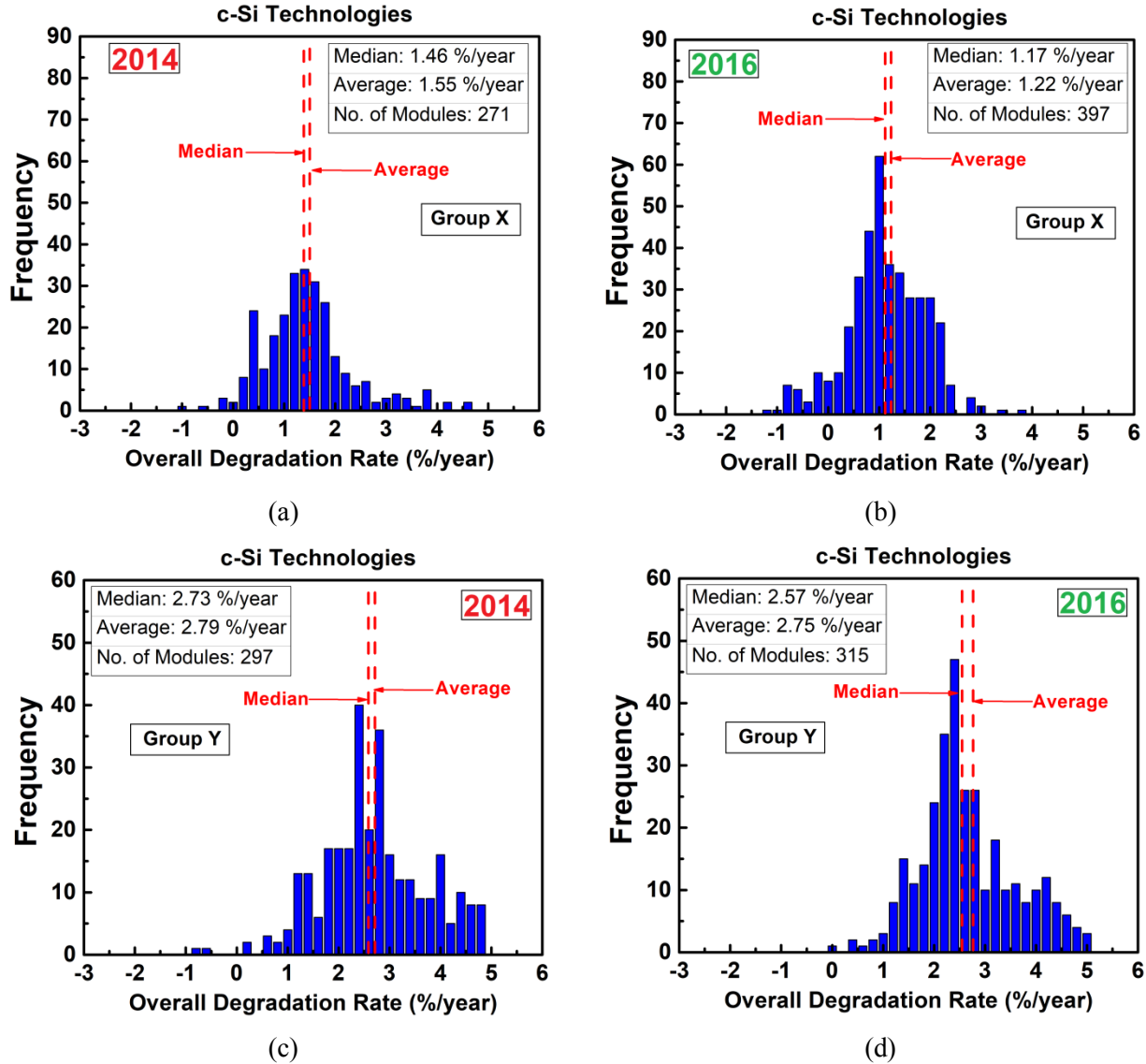
Fig. 4.22: Histogram of Overall P_{max} Degradation rate for (a) 2014 Survey Group X modules, (b) 2016 Survey Group X modules, (c) 2014 Survey Group Y modules and (d) 2016 Survey for Group Y modules.

The histograms are shown in Fig. 4.23 for the Linear Degradation Rates, and lead to similar conclusions stated above (though the absolute values have come down due to LID discounting). In the case of Group X sites, the average Linear Degradation Rate is 1.25%/year for 2014 Survey and 0.89 %/year for 2016 Survey, which, though still high, but for the case of 2016 Survey is acceptable. However, the average degradation rate even after LID discounting for the Group Y sites is high – 2.34%/year for 2014 Survey and 2.21%/year for 2016 Survey which is a matter of concern, since it would affect the long term reliability and durability of the PV

modules. The modules installed in the Group Y sites show poor performance, which may be due to material quality issues, poor manufacturing processes, poor transportation and/or handling, or other causes such as over-rating of modules. This has been explored in more detailed in Section 4.8. Incorrect rating of modules may result from poorly calibrated measurements in the PV module manufacturing facilities or deliberately over-rating the modules. As discussed before, the effect of the climatic zone has been checked only for the Group X sites, and not for Group Y sites, in order to avoid any extraneous factors like manufacturing quality and installation procedures from influencing our conclusions. However, technology and age variation analysis is done for both Group X as well as Group A modules (Group A is the superset comprising of both Group X and Group Y), in addition to the thin film modules. Data analysis based on Group A modules or Group-wise modules has be done and presented was ever deemed appropriate.

4.5.2 Climatic Zone Variation

Climatic conditions have a major impact on the performance degradation of the PV modules [33]. As mentioned before, the effect of the climatic zone would be analyzed for Group X modules, and six climatic zone classifications done by Bansal and Minke would be used for this work. The six climatic zones have been color coded to facilitate the understanding, using orange for Warm & Humid, red for Hot & Dry, green for Composite, magenta for Moderate, blue for Cold & Sunny and grey for Cold & Cloudy. The impact of high temperature on the module performance has been presented by clubbing the climatic zones into Hot zone (Warm & Humid, Hot & Dry and Composite zones) and 'Non-Hot' zone (Cold & Sunny, Cold & Cloudy and Moderate zones). In addition to the P_{max} degradation rate, degradation rates of the various other I-V parameters are also presented as a function of climatic zone.

105
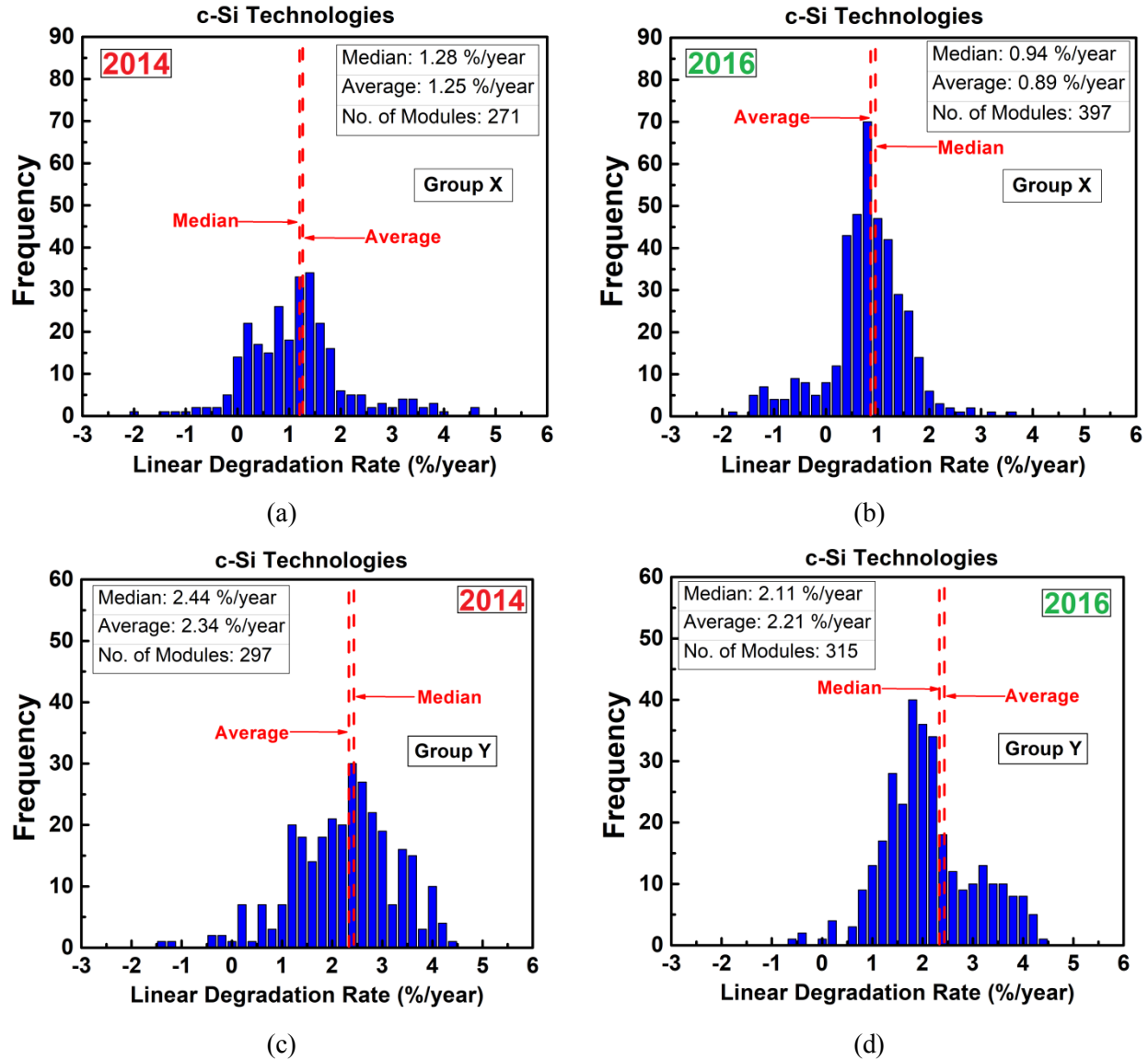
Fig. 4.23: Histogram of Linear P_{max} Degradation rate for (a) 2014 Survey Group X modules, (b) 2016 Survey Group X modules, (c) 2014 Survey Group Y modules and (d) 2016 Survey for Group Y modules.

As mentioned before, for all the figures shown in this section, red horizontal lines represent the mean of the data set, error due to measurement and STC correction has been shown using the green bar on the right side, and the error due to uncertainty in name plate has been shown using a pink bar on the left side of the datasets. The 95% confidence interval is represented by the red diamond and the number of data points (modules) is indicated inside the square bracket at the top of the respective category. Consistently, inverted triangles have been used for data illustrating the 6 Indian climatic zones, circles for Hot and Non-Hot zones, hollow symbols for the young

106

modules (age less than or equal to 5 years), and solid symbols for the old modules having age more than 5 years.

Influence of Climate on P_{max} Degradation

Figure 4.24 (a) for 2014 Survey and Fig. 4.24 (b) for 2016 Survey show the Linear Power Degradation Rate (after 2% LID discounting) of the Group X modules with respect to the six-zone climatic classification system. It is evident from the figure that the average Linear Degradation in the power is highest in Warm & Humid and Hot & Dry climate (neglecting the 20 modules from the Moderate climate in the 2016 Survey, as the number of samples is too low and least in the cooler climates (Moderate and Cold & Dry). Overall, the climatic zone trend is similar in 2014 and 2016 Survey. The explanations for the highest degradation rates in the Warm & Humid and Hot & Dry zone maybe that discoloration, delamination, corrosion and breakage in interconnect are accelerated at higher temperatures and humidity. It is evident from the Fig 4.24 that the P_{max} degradation rate variation is tight for the Group X modules, and this lends confidence to our assurance that climatic variation is well captured for Group X. Also, some of the young modules show a negative Linear Degradation Rate, which may be due to over-discounting of LID, under-rating of the nameplate, and/or error due to STC translation.

Figure 4.25 (a) for 2014 Survey and Fig. 4.25 (b) for 2016 Survey show Linear power degradation rate of Group X modules with respect to Hot and Non-Hot zones. Also, the cumulative probability distribution has been plotted to understand the nature of distribution and the points on the 50% probability line represent the median values. It is clear that the modules deployed in the Hot zones are degrading at a faster rate than the modules in the Non-Hot zones in both the surveys. It is evident from the figure that degradation rate for 2014 Survey is higher as compared to 2016 Survey which is due to the inclusion of more large sites in the 2016 Survey. It may also be noted that the degradation rates in the Non-Hot zones (< 0.8 %/year) are very much in consonance with international and warranty values. This firstly gives confidence in our measurements, and further implies that hot climates accelerate degradation. This obviously has grave consequences for performance in typical Indian conditions.
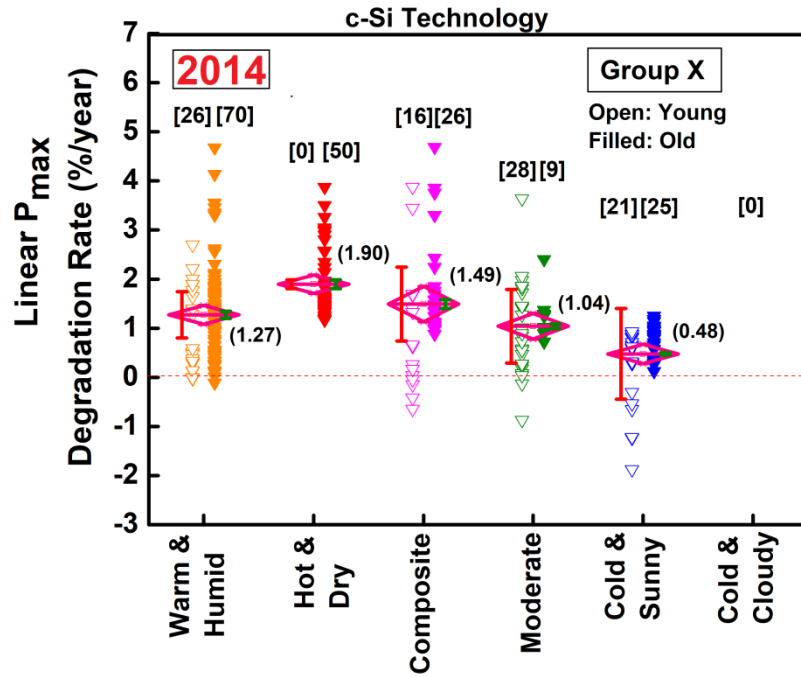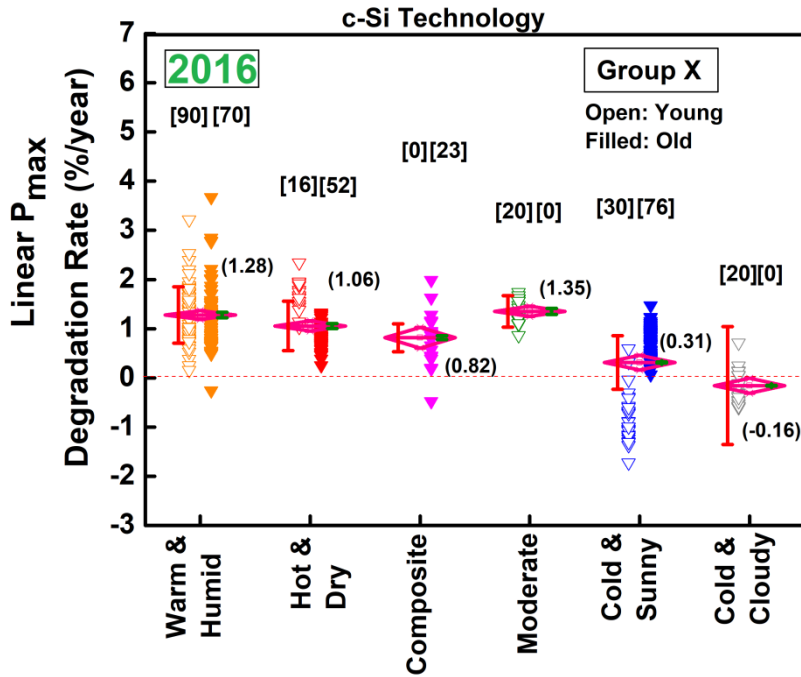
Fig. 4.24: Comparison of Linear P_{max} Degradation Rate with respect to six-zone classification system for Group X modules (a) 2014 Survey and (b) 2016 Survey. Warm and Humid and Hot and Dry have the highest degradation and Cold zones have the least value of degradation.
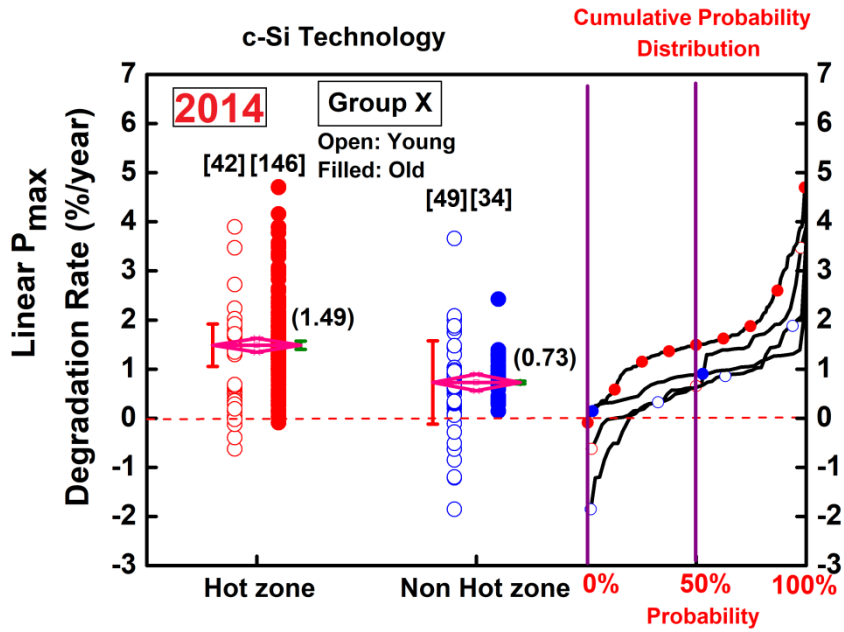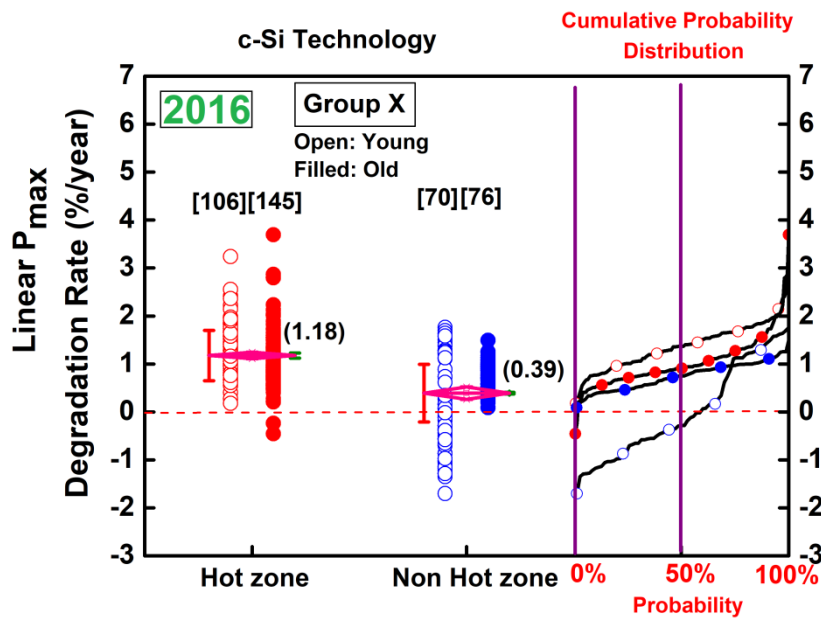
Fig. 4.25: Comparison of Linear P_{max} Degradation Rate with respect to Hot and Non-Hot zone for Group X modules (a) 2014 Survey and (b) 2016 Survey. Young modules in Hot zones have higher degradation rate and young modules in Non-hot zones are showing the least degradation.

109

<u>Influence of Climate on *I-V* Parameters (I_{sc}, V_{oc} and *FF*)</u>

Figure 4.26 (a) for 2014 Survey and Fig. 4.26 (b) for 2016 Survey show the Linear Degradation Rates for the various *I-V* parameters (P_{max}, I_{sc}, V_{oc}, and *FF*) for Group X modules with respect to climatic-zone. It is evident from the figure that for most climate zones *FF* degradation is the largest contributor to P_{max} degradation, though for the Hot & Dry and Composite zones, the I_{sc} degradation rate is also significant. The probable reason for the high *FF* degradation is due to cell to cell mismatch in the module caused by cracks as evident from the EL images (this is explained in more detail in Section 4.7). The reason for the higher I_{sc} degradation is due to the high temperature in these climates (especially Hot & Dry), leading to an increased encapsulant browning which reduces the light transmission to the solar cells (which is discussed later in this section where I_{sc} degradation and encapsulant browning are correlated).
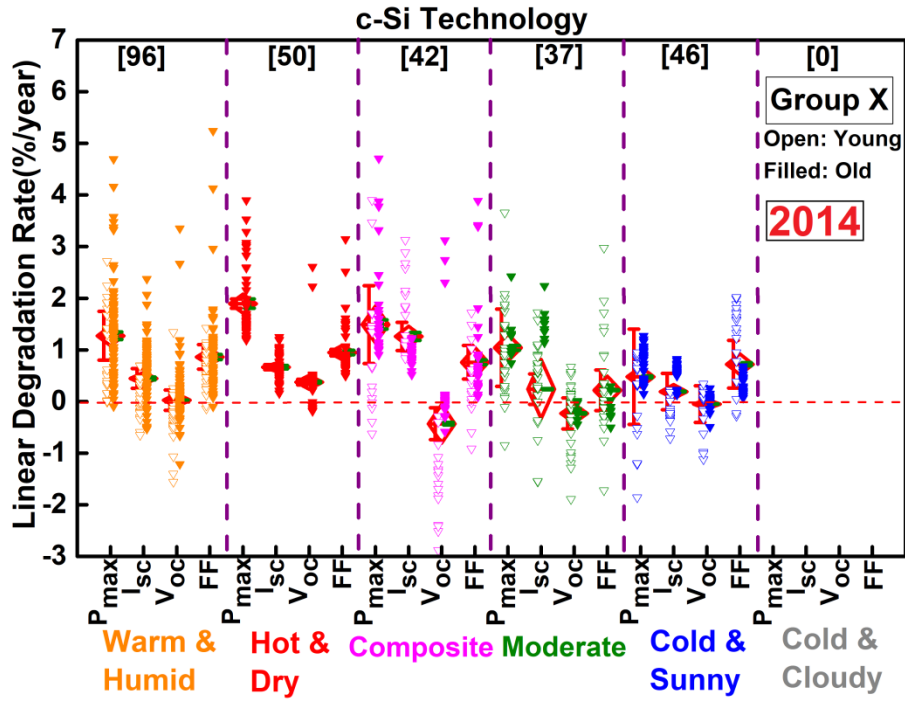
(a)
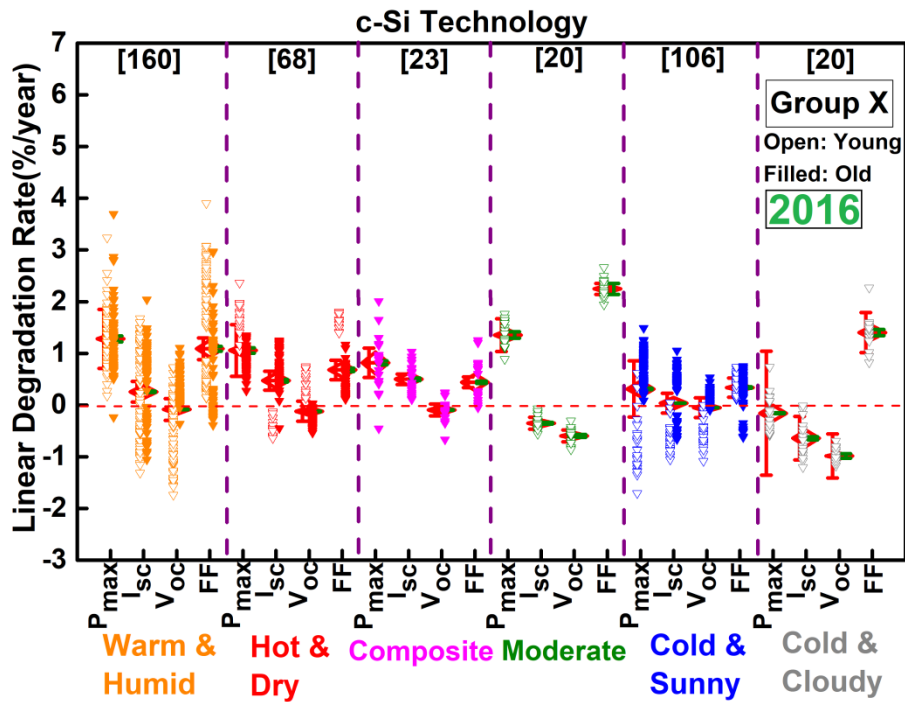
(b)

Fig. 4.26: *I-V* parameter degradation distribution with respect to six-zone classification system for Group X modules (a) 2014 Survey and (b) 2016 Survey. *FF* is the degradation is the largest contributor to P_{max} degradation, though for the Hot & Dry and Warm & Humid, Composite zone the I_{sc} degradation rate is also significant.

4.5.3 Technology Based Variation

Influence of Technology on P_{max} Degradation

     The Linear P_{max} Degradation Rate (%/year) for Group X c-Si and thin film modules are shown in Fig. 4.27 (a) for 2014 Survey and Fig. 4.27 (b) for 2016 Survey. It can be seen that among the thin-film modules, CdTe modules are degrading the least. It should be noted that generally, CdTe modules are under-rated (as a standard practice) to take care of the stabilization effects. Also, thin-film modules are usually from internationally well-known manufacturers who have strict control over their production (and sometimes installation) quality. Besides, many c-Si module manufacturers are new to module manufacturing. Therefore, it is not surprising to find that the average degradation rates of the thin film modules are lower than that of the crystalline silicon modules. Whether this is an intrinsic technology effect (i.e. that c-Si as a technology performs worse than thin-film), or due to the reasons mentioned above, cannot be asserted at this stage. It is difficult to comment on the performance of CIGS and HIT technologies, due to an insufficient number of samples. It is evident from the figure that the degradation rate for a-Si in 2014 Survey (1.52 %/year) is higher as compared to the 2016 Survey (-0.11). This is attributed to the inclusion of more a-Si large power plants and excluding the small rooftop installation of a-Si in 2016 Survey. Linear P_{max} Degradation per year for Group A ('All') c-Si and thin film modules are shown in Fig. 4.28 (a) for 2014 Survey and Fig. 4.28 (b) for 2016 Survey. In both the figures color-coding is not used, since the technologies are not differentiated by climatic zone.
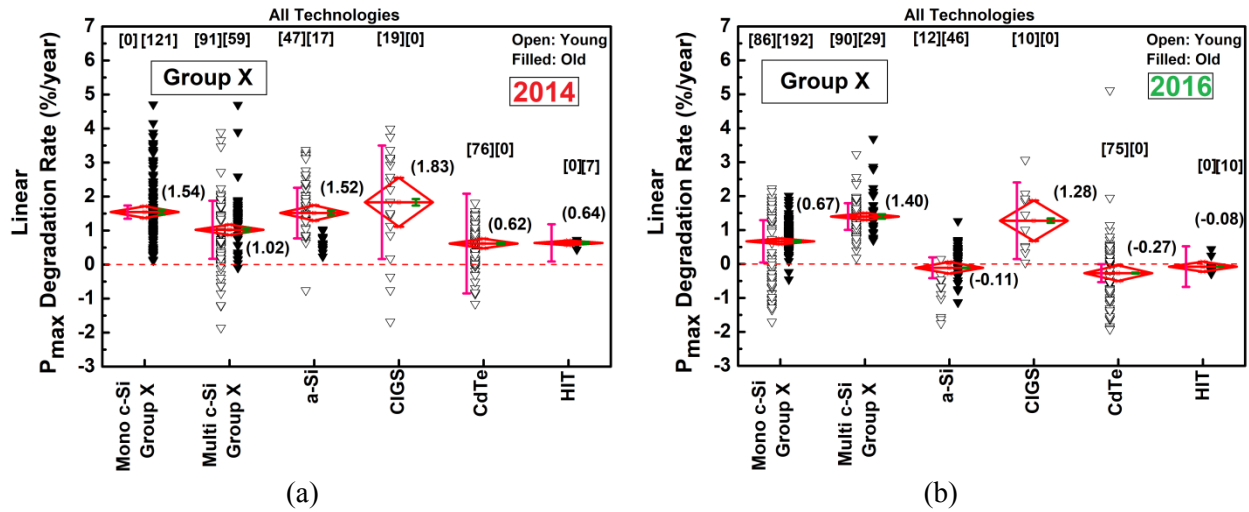
Fig. 4.27: Linear P_{max} Degradation per year for modules of different technologies (for c-Si, only Group X modules are considered) (a) 2014 Survey and (b) 2016 Survey. Crystalline silicon modules are degrading at a faster rate than thin-film modules.
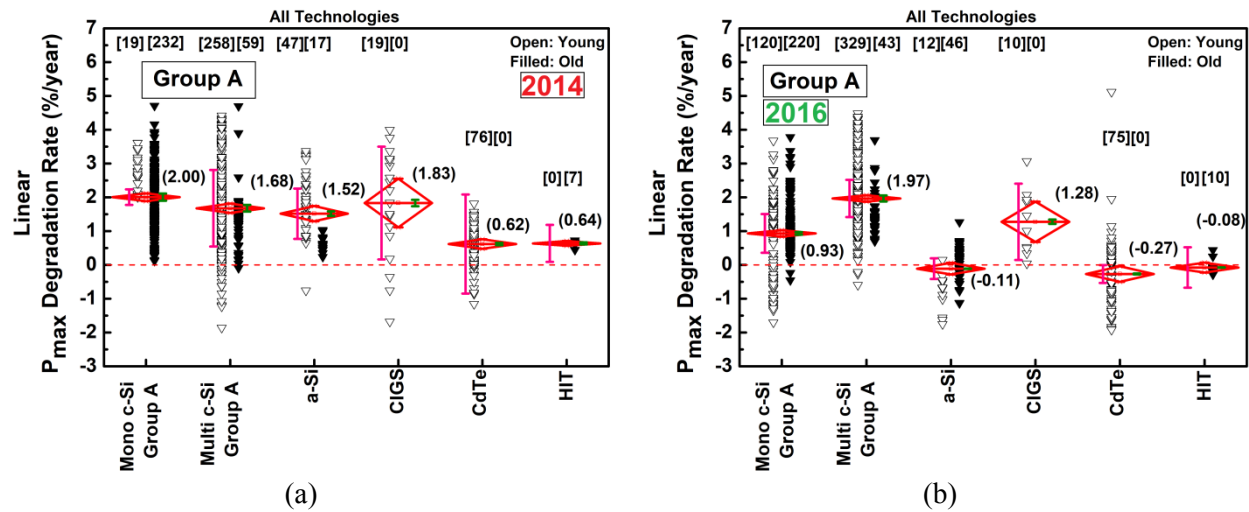
Fig. 4.28: Linear P_{max} Degradation per year for modules of different technologies (all (Group A) c-Si modules are considered) (a) 2014 Survey and (b) 2016 Survey. Crystalline silicon modules are degrading at a faster rate than thin-film modules.

Influence of Technology on *I-V* Parameters (I_{sc}, V_{oc} & *FF*)

The reduction in the power output of the PV module is caused by degradation in one or more of the electrical parameters. The Linear P_{max}, I_{sc}, V_{oc} and *FF* degradation rates for Group X c-Si and thin-film category modules are shown in Fig. 4.29 (a) for 2014 Survey and Fig. 4.29 (b) for 2016 Survey. It can be seen from the figure that for crystalline silicon modules P_{max} degradation is mainly due to degradation in *FF* and I_{sc}. It is least affected by the degradation in V_{oc}. For the thin film modules, P_{max} degradation is mostly associated with the degradation in *FF* followed by the I_{sc} for 2014 Survey. In case of 2016 Survey thin film modules, P_{max} degradation is mostly associated with the degradation in V_{oc} followed by the *FF*. Similar conclusions can be drawn from Fig 4.30 which shows the P_{max}, I_{sc}, V_{oc}, and *FF* degradation for Group A c-Si and thin-film PV modules.
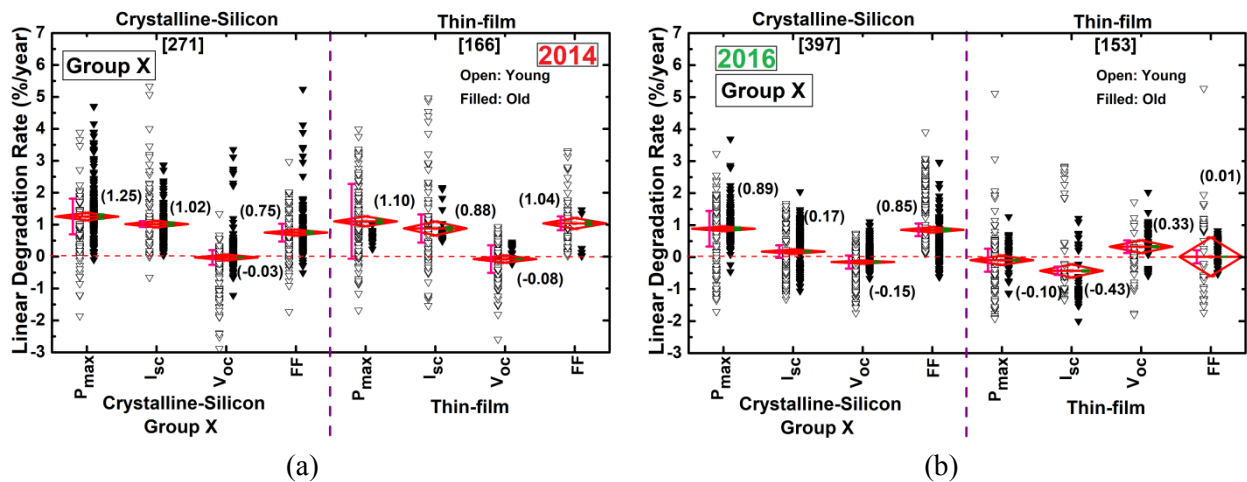
Fig. 4.29: Linear P_{max}, I_{sc}, V_{oc} and *FF* degradation for Group X c-Si and thin-film modules (a) 2014 Survey and (b) 2016 Survey.

114
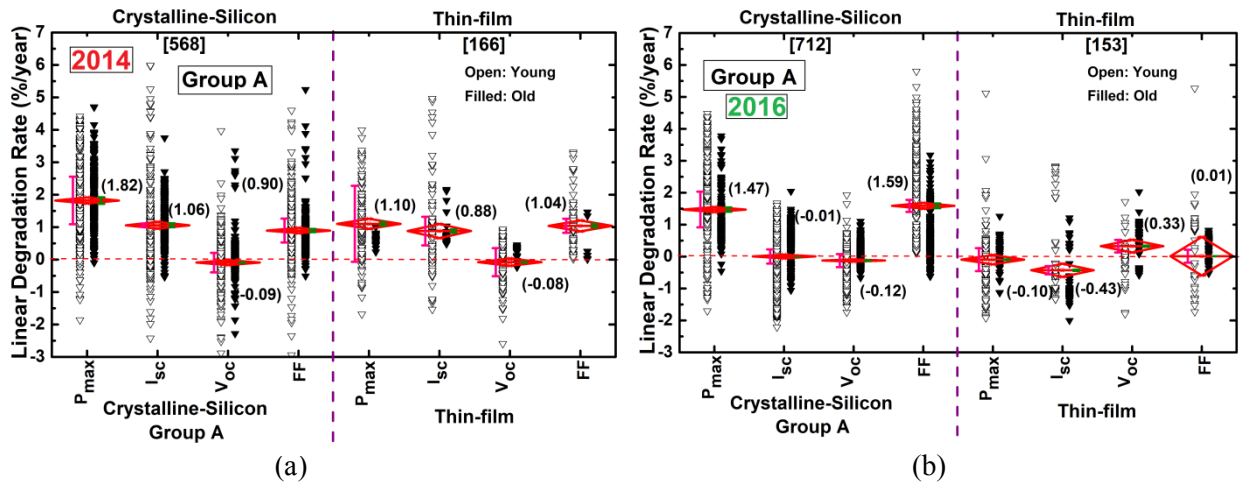
Fig. 4.30: Linear P_{max}, I_{sc}, V_{oc} and FF degradation for Group A c-Si and thin-film modules (a) 2014 Survey and (b) 2016 Survey.

4.5.4 Age Based Variation

In order to ascertain the effect of age on the P_{max} degradation rate (% per year), the modules inspected have been separated into young (installed in/after 2011, so age ≤ 5 years) and old (installed before 2011, so age > 5 years) categories. Since the sample size of thin film modules in the old age category was insufficient, the analysis of age variation has only been done for c-Si modules. The histograms of Linear P_{max} Degradation of young and old c-Si modules in Group A for 2014 and 2016 Surveys are shown in Fig. 4.31 (note that use of the Linear rate is vital here for a fair comparison). It is quite evident from the figure that the average Linear Degradation Rate for 2014 Survey is less than for 2016 Survey in both young and old categories. The spread of the degradation rates is much wider in young modules as compared to old modules for both the 2014 and 2016 Surveys. It is quite evident from the figure that for the 2016 Survey, the average Linear Degradation Rate for young modules is much greater (1.68 %/year) than for the old modules (1.11 %/year). However, for the 2014 Survey the averages Linear Degradation Rate the young and old modules both have the same value of 1.82%/year.

From Figure 4.31 it can be seen that for the 2014 Survey the average Linear Degradation Rate the young and old modules both have the same value of 1.82%/year. However, it should be noted that out of 254 modules that have been deemed as outliers (degradation rate more than

115

5.02%/year), 231 c-Si modules fall in the Young category (age less than 5 years), which means 91 percent of the modules in the outlier are young modules. Similarly, from the 2016 Survey data analysis shows that 80 percent of the outlier modules fall in the Young category. Hence it can be concluded that the young modules are degrading at a higher rate than old modules.
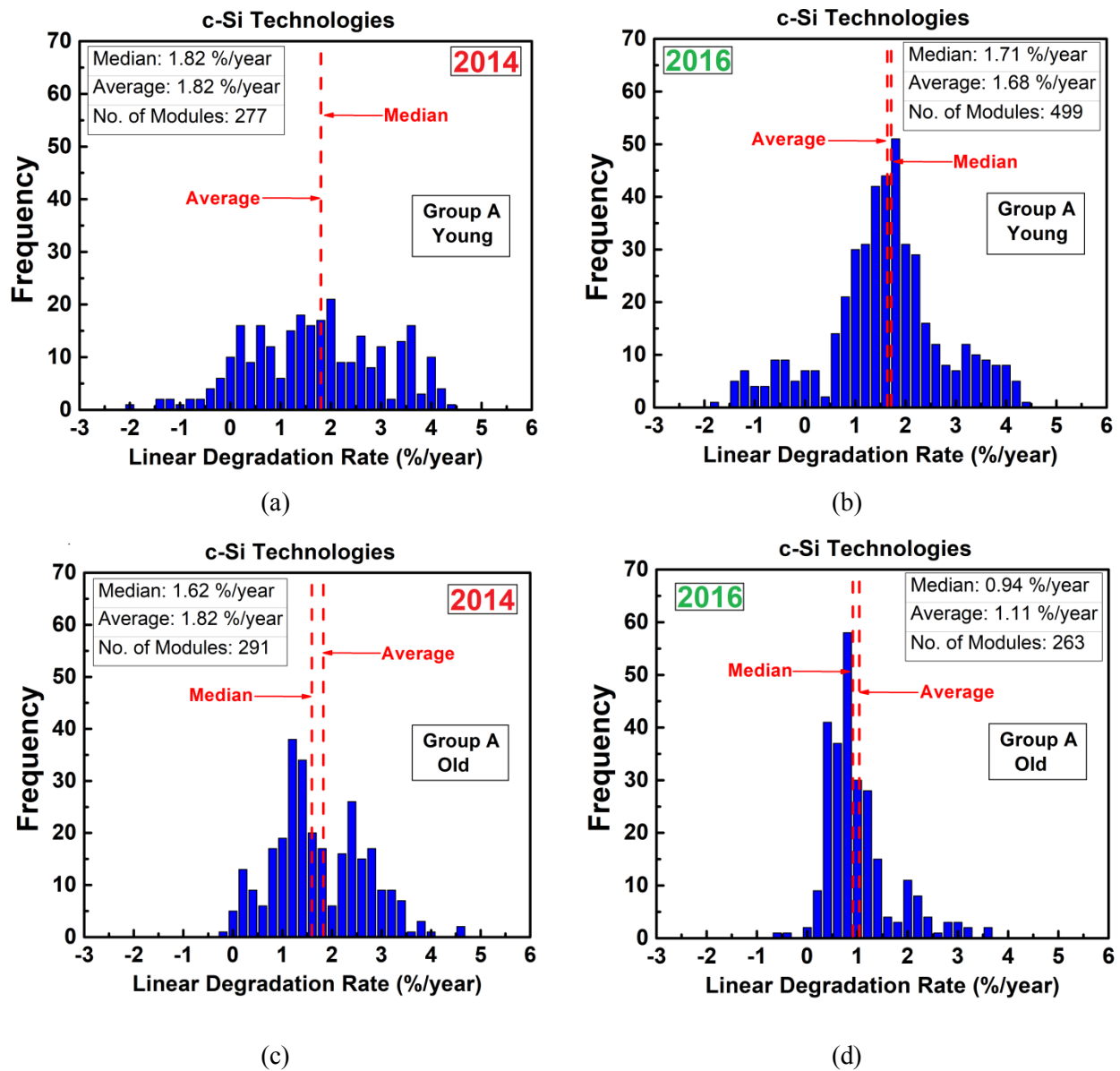
Fig. 4.31: Histogram of Linear Degradation Rates of c-Si modules in Group A, for young modules (a) 2014 Survey, (b) 2016 Survey and for old modules (c) 2014 Survey and (d) 2016 Survey.

The effect of module age on the degradation of the *I-V* parameters of the crystalline silicon modules only from Group X sites has been shown in Fig. 4.32 (a) for 2014 Survey and Fig.4.32 (b) for 2016 Survey. From the figure, it can be noticed that old modules are degrading at a higher rate as compared to young modules (though marginally *slower* for 2016 Survey). It is evident from the figure that for the old modules, for both 2014 and 2016 Survey, the degradation in P_{max} is due to degradation in both I_{sc} and *FF*. It could be concluded that the old modules degrade mainly due to encapsulant browning (which reduces I_{sc}), cell cracks, and corrosion (both of which reduce the *FF*). In the case of young modules, for 2014 Survey, the degradation in P_{max} is mainly due to degradation in both I_{sc} and *FF,* however, for 2016 Survey, modules degrade due to decrease in *FF*, possibly caused by cracks generated during installation (this is discussed in more detail in the next section).

The effect of age on the degradation of the *I-V* parameters of Group Y crystalline silicon modules has been shown in Fig. 4.33 (a) for 2014 Survey and Fig.4.33 (b) for 2016 Survey. It can be clearly noticed from the figures for Group Y modules, the degradation in P_{max} is slightly higher for young modules. It can also be due to the poorly calibrated measurements in the module manufacturing facilities. Similarly, for Group Y young modules, the degradation in power is mainly due to fill factor (*FF*), whereas, for old modules, degradation is due to both I_{sc} and *FF*. The reason for high *FF* degradation can be ascribed to cracks caused by poor installation. It can be noted that the *FF* degradation rate is much higher in Group Y as compared to Group X young modules, which indicates that the problem of cracks is more severe in Group Y modules as compared to Group X modules (this is confirmed by EL analysis as described in a Section 4.7).
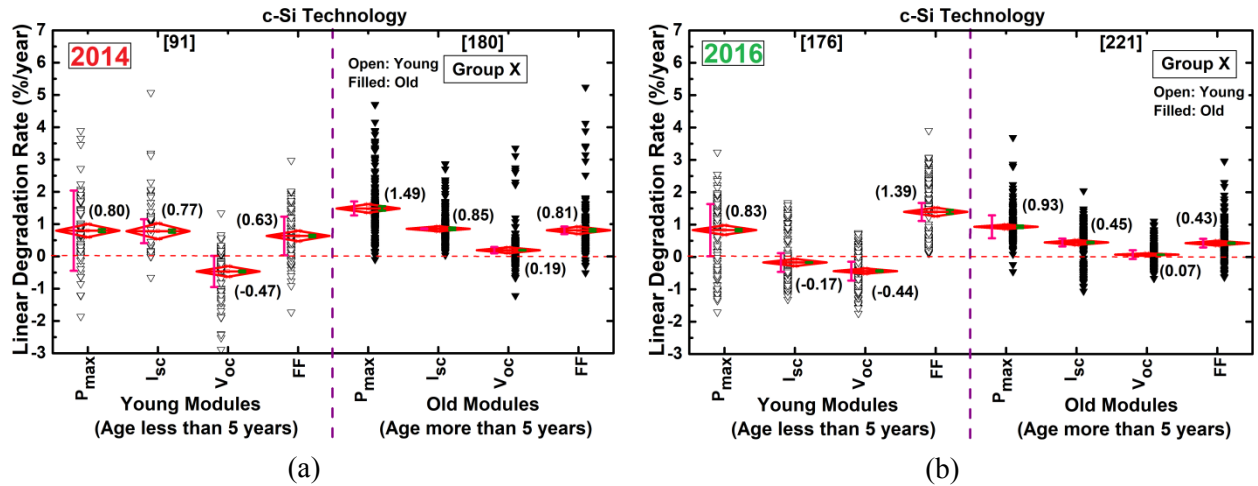
Fig. 4.32: Linear P_{max}, I_{sc}, V_{oc} and FF Degradation for young and old crystalline silicon modules in Group X (a) 2014 Survey and (b) 2016 Survey.
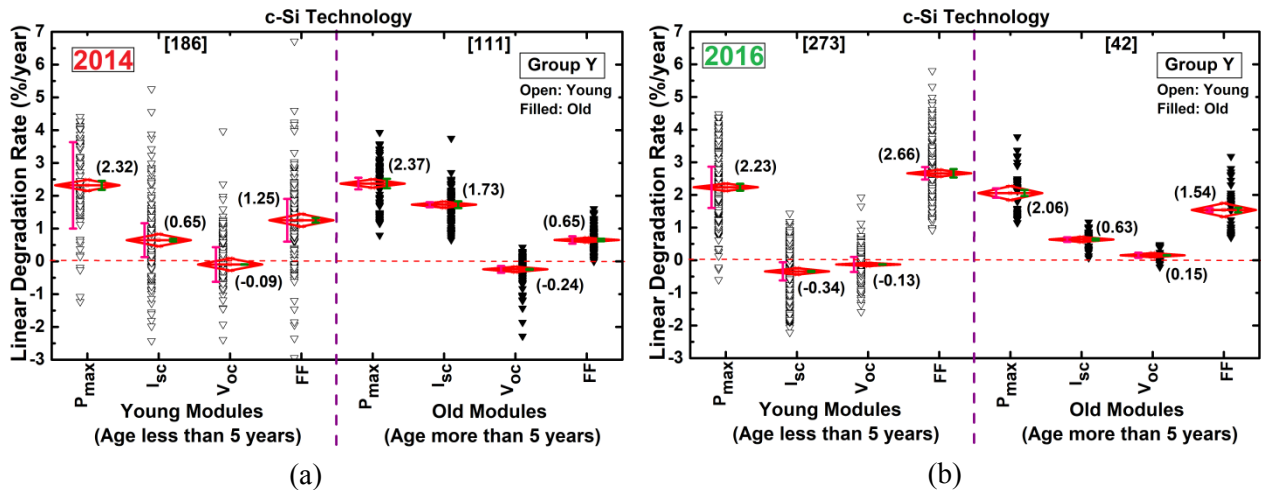
Fig. 4.33: Linear P_{max}, I_{sc}, V_{oc} and FF Degradation for young and old crystalline silicon modules in Group Y (a) 2014 Survey and (b) 2016 Survey. In case of Young modules FF is the main reason for degradation and for the old modules FF and I_{sc} both are responsible.

4.5.5 System Size and Installation Based Variation

In order to understand the effect of the size of the installation the sites surveyed have been separated into two categories based on the size of the installation – small/medium size (less than

118

or equal to 100 kW) and large size (greater than 100 kW capacity). The choice of 100 kW as a demarcation can be understood from Fig. 4.34 (a) for 2014 Survey and Fig. 4.34 (b) for 2016 Survey (which show the average Linear P_{max} Degradation Rate for different Group A sites with respect to respective system size). From the figure, it is evident that the site-wise average Linear P_{max} Degradation Rate is concentrated on either side of the 100 kW line. From the Fig. 4.34 (b) it is noticeable that more number of large systems have been included in the 2016 Survey as compared to 2014 Survey (refer Fig. 4.34 (a)).
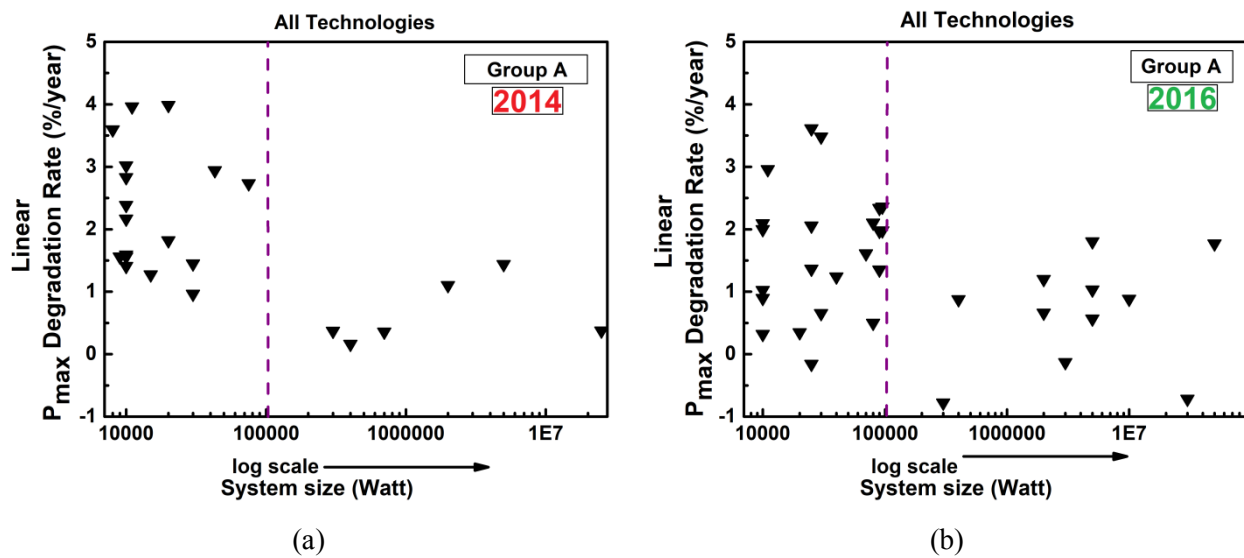
Fig. 4.34: Average Linear P_{max} Degradation rates of Group A sites with respect to system size (a) 2014 Survey and (b) 2016 Survey. It can be seen the site-wise average Linear P_{max} Degradation Rates are concentrated on either side of the 100 kW line.

The Linear P_{max} Degradation Rate for these categories, for Group A and Group X have been shown in Fig. 4.35 (a) for 2014 Survey and Fig. 4.35 (b) for 2016 Survey and Fig. 4.36 (a) for 2014 Survey and Fig. 4.36 (b) for 2016 Survey respectively. It can be clearly seen from the figures that modules installed in large PV systems (including MW scale power plants) are degrading at a much lower rate than the modules in the smaller installations. The cumulative probability plots on the right side of the figures indicate that the data distributions are different from each other (so the differences are statistically significant). From the above important result, it could be concluded that the large commercial and utility scale installations (even in Group A) are performing better (0.62%/year for 2014 Survey and 0.99 %/year for 2016 Survey) than

119

smaller installations, but also flags a warning about the poor performance of small and medium sites (1.93%/year for 2014 Survey and 1.68 %/year for 2016 Survey). In contrast, for the installations in the Hot zone, the large sites in Group A have an average degradation rate of 1.16%/year for 2014 Survey and 1.28 %/year for 2016 Survey (refer Fig. 4.37 (a) and Fig. 4.37 (b)), which is quite high. Even for Group X the average degradation rate for large installations in Hot zones is high at 1.16%/year for 2014 Survey and 1.12 %/year for 2016 Survey as shown in Fig. 4.38 (a) and (b).
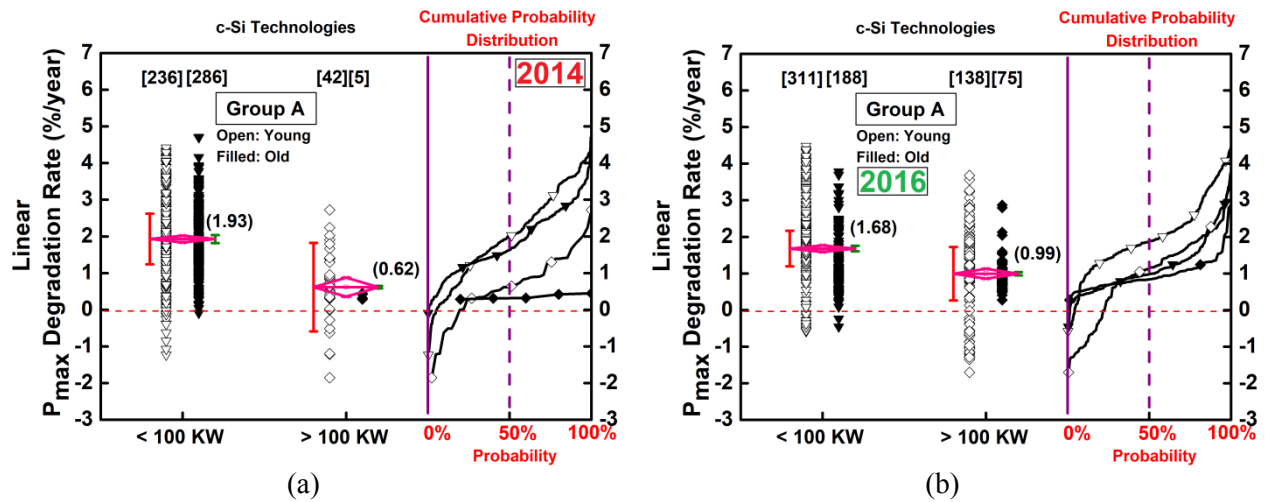
Fig. 4.35: Effect of system size on Linear P_{max} Degradation for Group A modules (a) 2014 Survey and (b) 2016 Survey.
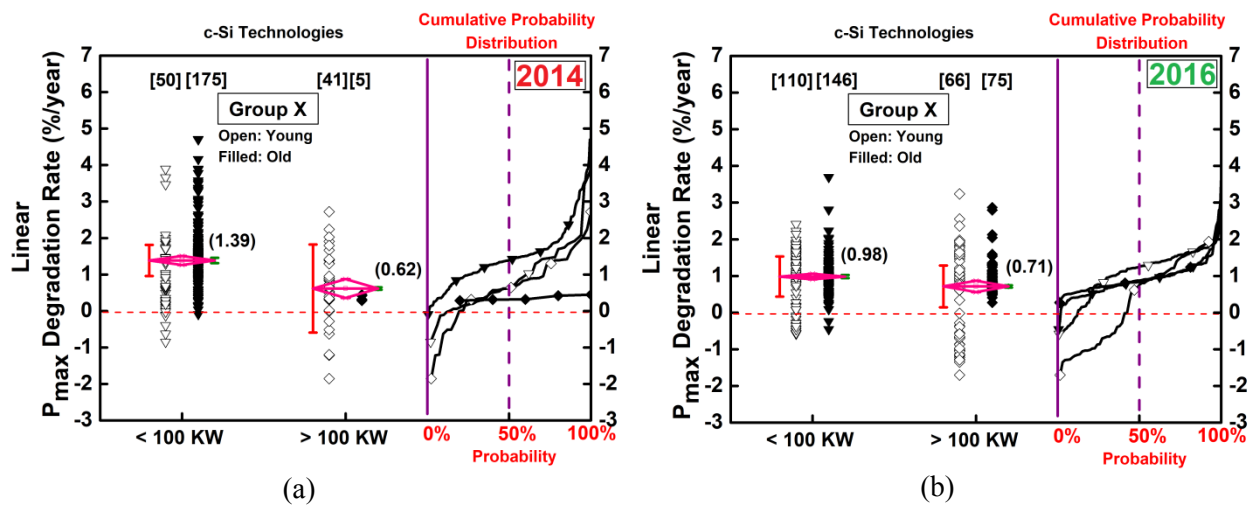
Fig. 4.36: Effect of system size on Linear P_{max} Degradation for Group X modules (a) 2014 Survey and (b) 2016 Survey.

120
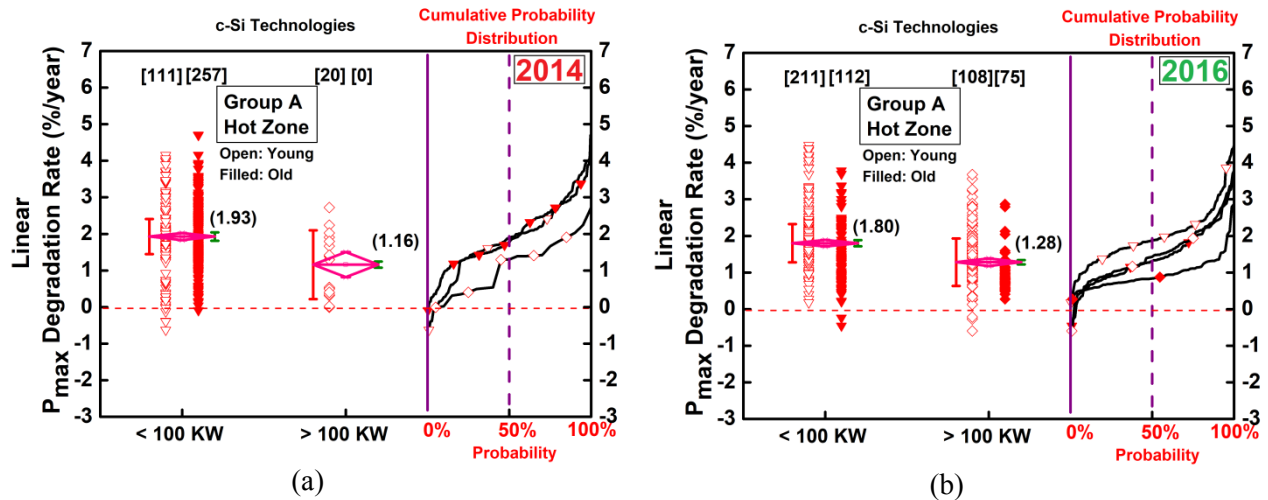
Fig. 4.37: Effect of system size on Linear P_{max} Degradation for Group A modules in Hot zones (a) 2014 Survey and (b) 2016 Survey.
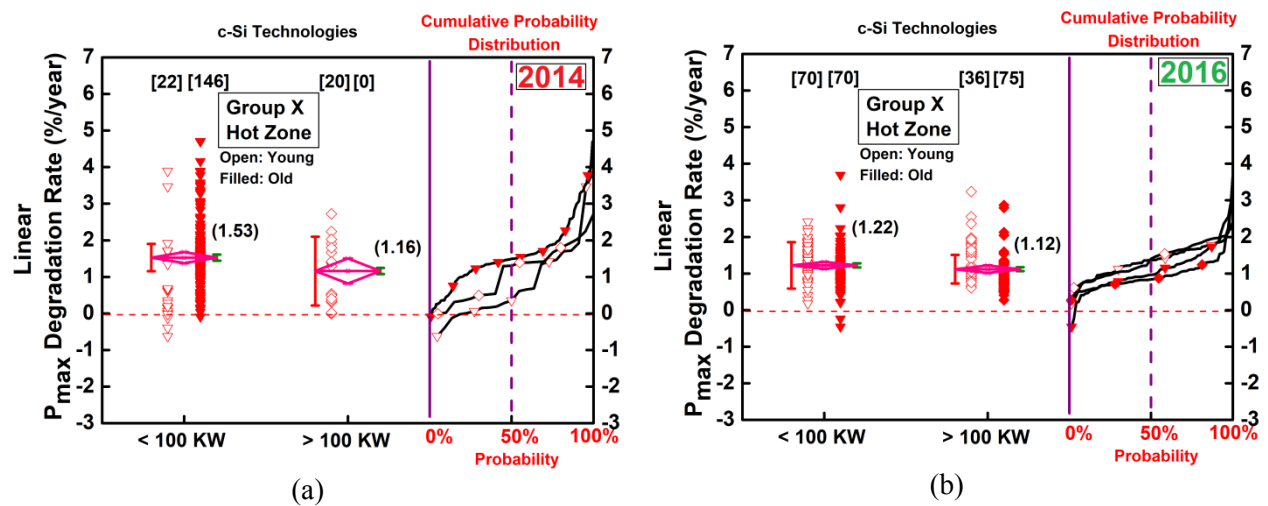
Fig. 4.38: Effect of system size on Linear P_{max} Degradation for Group X modules in Hot zones (a) 2014 Survey and (b) 2016 Survey.

An attempt to capture the effect of roof-mounted (note that most 'roof-mounted' are actually rack mounted installations deployed on flat roofs) and ground-mounted installation on the Linear P_{max} Degradation Rate has been done. The Linear P_{max} Degradation Rate for roof and ground mounted modules for Group A sites has been shown in Fig. 4.39 (a) for 2014 Survey and (b) for 2016 Survey. It is evident from the figure that the ground-mounted modules are degrading at a lower rate than the roof-mounted panels for the small size category. This may be due to the

module quality and installation related issues in the smaller rooftop sites. The corresponding plot for Group X modules has been shown in Fig. 4.40, and a similar conclusion could be drawn.

From the above analysis, the following conclusions could be drawn for c-Si modules. Large installations overall, especially the Group X sites, are performing reasonably well, however, large sites in the Hot zones are showing relatively high degradation rate. The analysis clearly shows that (a) hot climates accelerate degradation; (b) rooftop sites perform worse than ground-mounted.
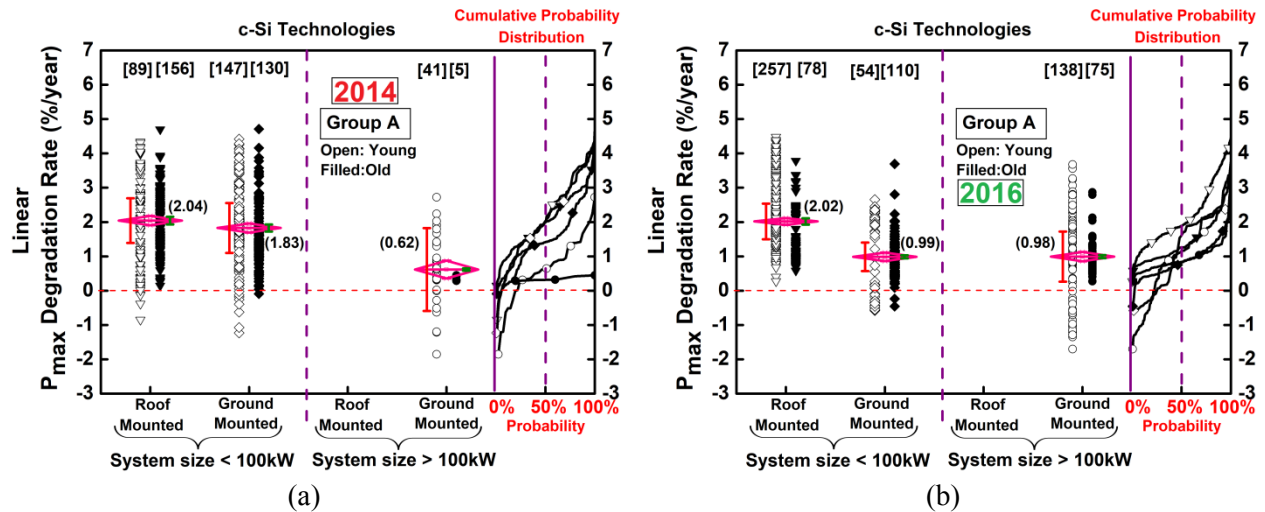
Fig. 4.39: Effect of installation type on Linear P_{max} Degradation for Group A modules (a) 2014 Survey and (b) 2016 Survey.
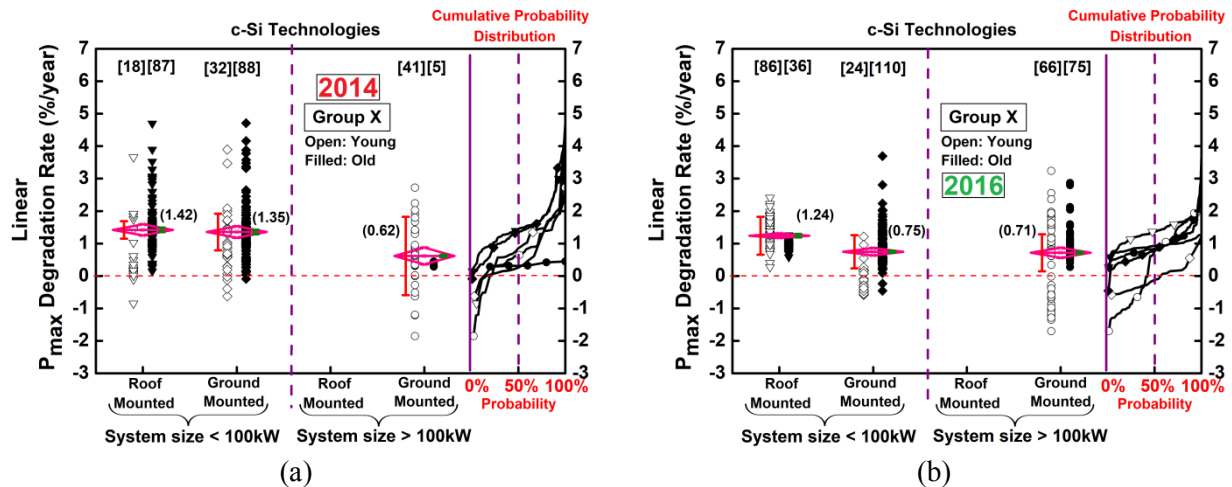
Fig. 4.40: Effect of installation type on Linear P_{max} Degradation for Group X modules (a) 2014 Survey and (b) 2016 Survey.

122

4.6 Analysis of Miscellaneous Electrical Data and Correlation with Visual & Infrared (IR) Data

4.6.1 Analysis of Visual Degradation and Infrared (*IR*) Data Analysis

Different components of the PV modules get degraded upon exposure to the outdoor environment. Most of these degradation modes show visible signs which make it easy to identify. Visible degradation modes act as an early indicator of an imminent loss in electrical power output and this visual degradation analysis helps in identifying the root cause of electrical degradation. One of the most common characterization techniques is Infra-red (IR) imaging technique which shows the temperature distribution in the PV module, and helps to identify the hot spots. In this section correlation of visual degradation and IR data with output power loss has been done.

4.6.1.1 Correlation with Visual Degradation Modes

The visual degradation observed in the field survey has been recorded using a visual inspection checklist (which is a modified version of the NREL Visual Inspection Checklist [29]). The extent of snail tracks, encapsulant discoloration, delamination, corrosion, backsheet defects etc. have been analyzed based on climatic zone, size of installation and other characteristics of the inspected sites. The discoloration of the encapsulant has been quantified from the digital images and correlated to the short circuit current and power degradation of the solar panels, as shown in Fig. 4.41. The discoloration of the encapsulant has been categorized into 5 categories and the average I_{sc} degradation has been found to correlate well with the discoloration category [241]. The analysis of the visual degradation modes has been presented in detail in a separate thesis [241], and is also available in the public domain as part of the report "*All India Survey of Photovoltaic Module Reliability 2016*" [20]. The main purpose of briefly introducing it here is in order to correlate it to the electrical performance (which is the focus of this thesis).
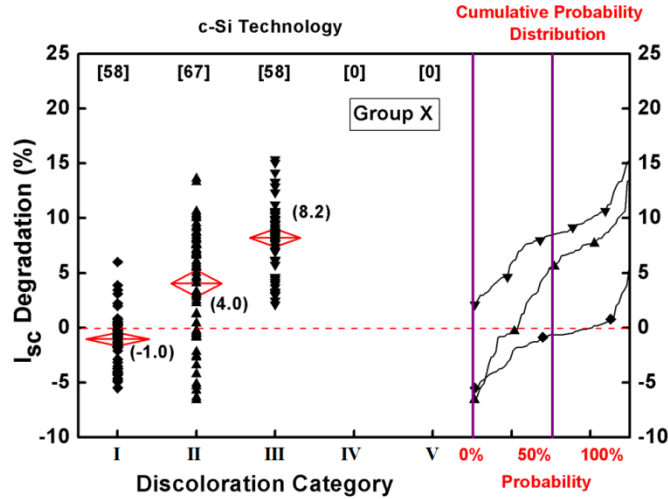
Fig. 4.41: Plot of short circuit current degradation versus severity of discoloration for Group X modules.

4.6.1.2 Correlation with Hot Spots

Infrared thermography has been performed in the field surveys in order to record the temperature profiles of the solar panels under both short circuit and MPPT conditions. About 13% of the panels have shown localized elevated temperatures (Hot Spots) in the 2016 Survey (more details are given in [241]) and the electrical performance of the panels have been correlated with the extent of thermal mismatch in the panels, as shown in Fig. 4.42. In Fig. 4.42, the Thermal Mismatch Index (TMI) has been defined based on the thermal anomaly in the panel, normalized by the panel efficiency and number of cells in the panel defined in Eq. 4.10 [241]. The analysis of the thermal imaging data and correlations are explained in detail in a separate thesis [241], and is also available in the public domain as part of the report "*All India Survey of Photovoltaic Module Reliability 2016*" [20].

$$TMI = \frac{Module \ \Delta T}{\eta * N} \qquad (4.10)$$

where:

Module ΔT: Temperature mismatch between the cells in a module

η: Initial efficiency of the PV module

N: No. of cells in the PV module

124
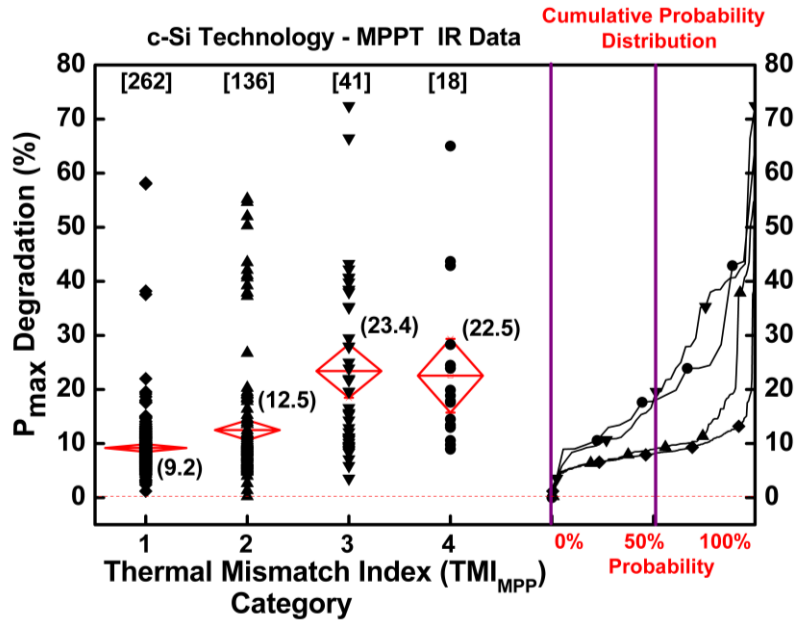
Fig. 4.42: Plot of P_{max} degradation (%) versus the *TMI* category for IR images taken at MPPT condition

4.6.2 Analysis of Dark *I-V* on Survey Data

In the field, the dark *I-V* characterization was done by covering the module with a black cloth and then sweeping the forward-biased voltage from zero to the open circuit voltage and measuring the output current. It should be noted that during the measurement of all the PV modules the *I-V* curves were consistently swept from I_{sc} to V_{oc}. Further analysis on the dark *I-V* data of module thus obtained was converted into the dark *I-V* of an equivalent solar cell by dividing the voltage (at each *I-V* data point) by the number of cells in the module [242]. The concept of dark *I-V* of the equivalent cell is graphically demonstrated in Fig. 4.43. The advantage of utilizing this technique is that it enables us to directly use the one diode model to obtain the dark *I-V* parameters such as ideality factor (*n*) and reverse leakage current (J_o) [243]. Since the ideality factor estimated using this method is impacted by dark *I-V* curve, therefore it is referred to as the 'Overall ideality factor'. This technique to obtain the dark *I-V* parameters has been described in detail and discussed in Appendix IV.

125
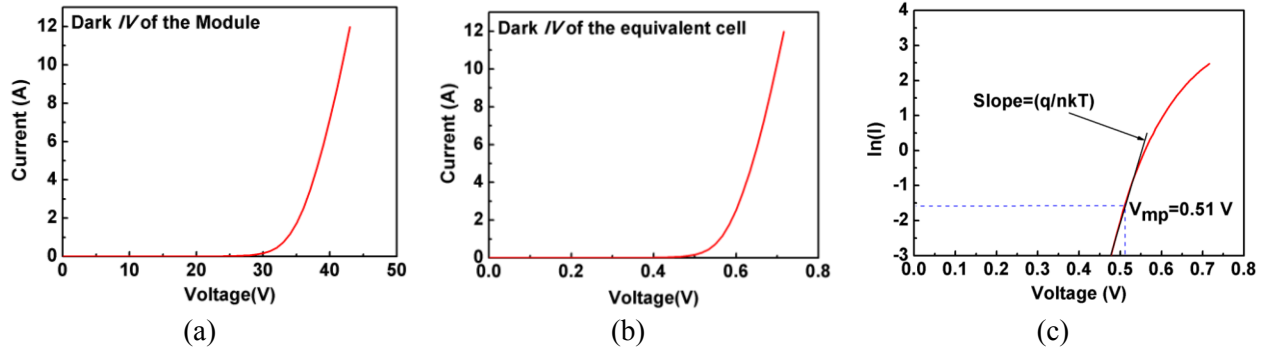
Fig. 4.43: (a) Measured dark *I-V* of the module and, (b) dark *I-V* of the equivalent cell obtained by dividing the module *I-V* voltages by number of cells (here 60), (c) *ln(I)* vs. voltage plot, showing also the tangent at V_{mp}, from which *n* can be found.

4.6.2.1 Correlation of Overall Ideality Factor with Age

At the maximum power point, the Overall ideality factor *n* of the equivalent cell was calculated. The variation in Overall ideality factor with age has been shown in Fig. 4.44 (a) for 2014 Survey and Fig. 4.44 (b) for 2016 Survey. It can be seen from the plot that the Overall ideality factor *n* increases with an increase in the age of the module. This demonstrates that the solar cell itself, and not only the packaging material of the PV modules, degrade over the years. Since, as the age of the diode increases, its characteristics degrade (for, example due to increased leakage), hence it is reasonably expected that the Overall ideality factor *n* would increase. Besides, Fig. 4.45 (a) for 2014 Survey and (b) for 2016 Survey shows the series resistance for those modules increases with age and Overall ideality factor *n* has an increasing trend with the series resistance (as shown in Fig. 4.46). This leads to the conclusion that the Overall ideality factor may be degrading partly due to increased series resistance. Due to the corrosion in the metallization, it is expected that there will be an increase in the series resistance. The correlation between the series resistance and the corrosion has been described in more detail in a separate thesis [241].

126
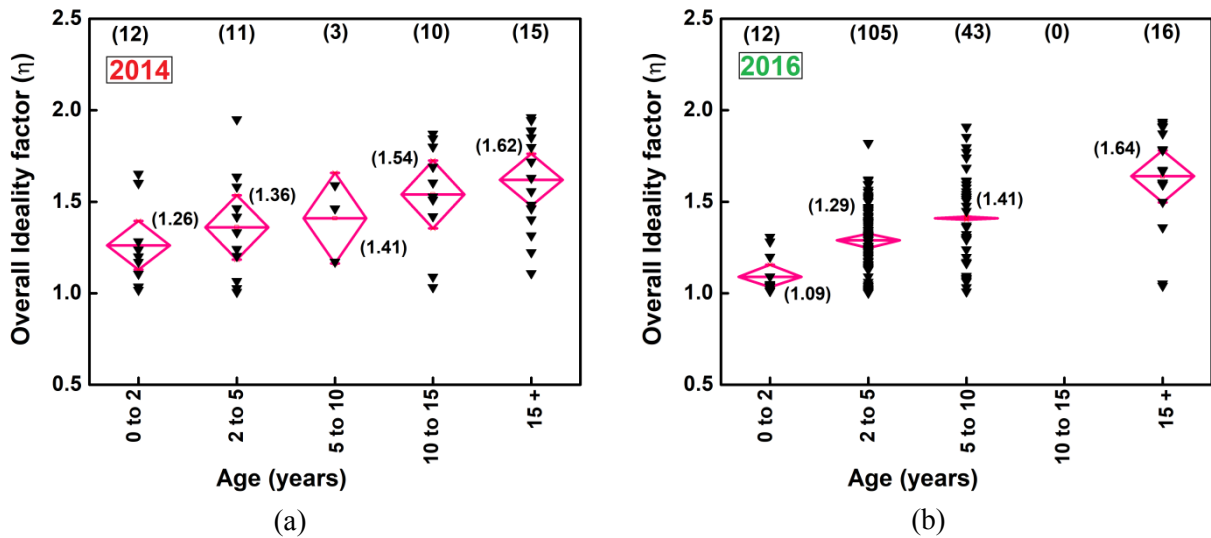
Fig. 4.44: Correlation of Overall ideality factor *n* with age (a) 2014 Survey and (b) 2016 Survey. The red diamond represents the 95% confidence interval. The red diamond represents the 95% confidence interval.
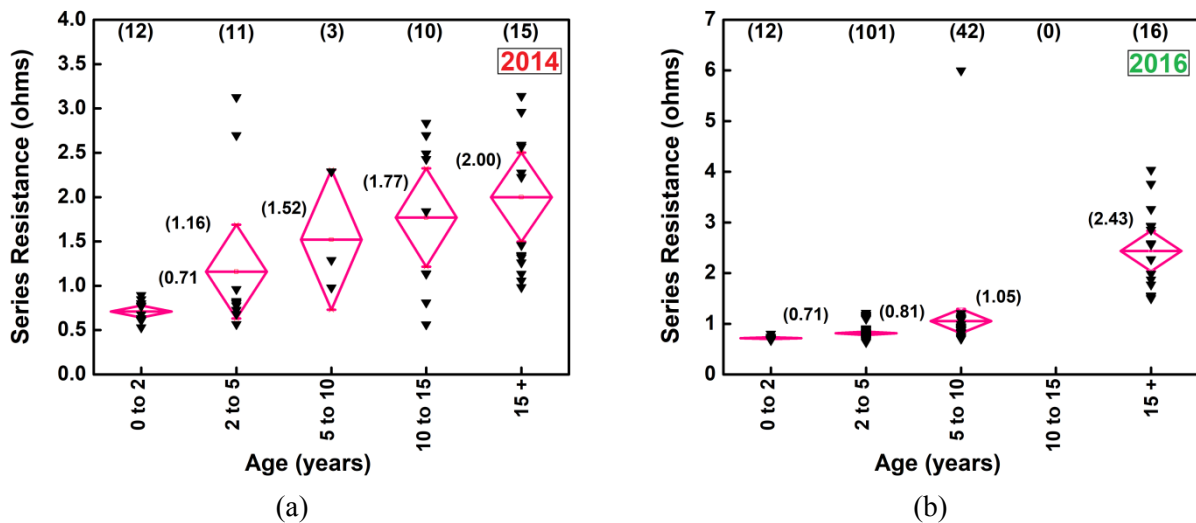
Fig. 4.45: Correlation of series resistance with age (a) 2014 Survey (b) 2016 Survey. The red diamond represents the 95% confidence interval.
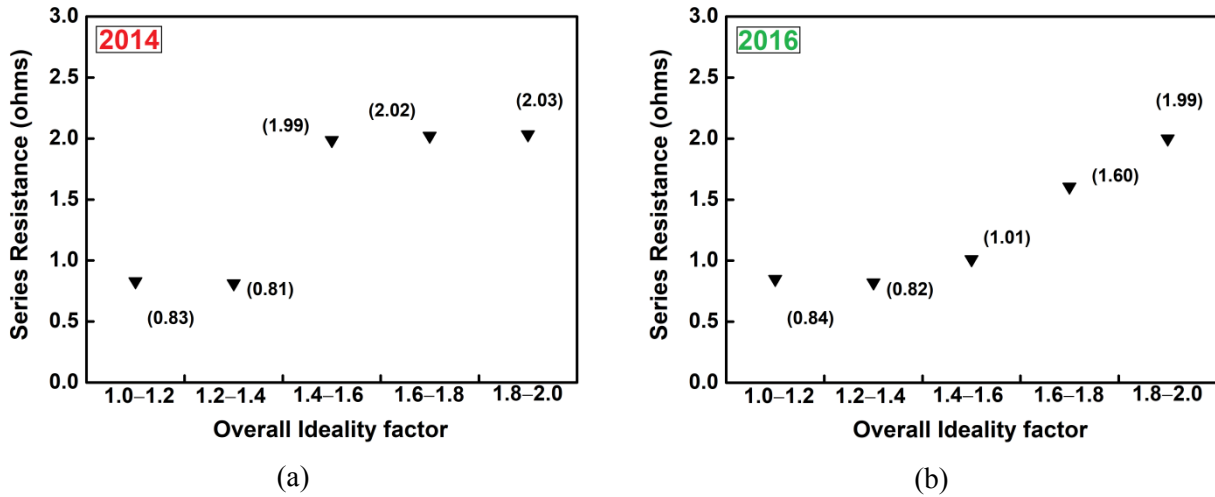
Fig. 4.46: Correlation of series resistance with Overall ideality factor (a) 2014 Survey and (b) 2016 Survey. The red diamond represents the 95% confidence interval.

4.6.2.2 Variation of Overall Ideality Factor with Climate

The age-averaged Overall ideality factor variation with respect to Hot and Non-Hot Zones has been shown in Fig. 4.47 (a) for 2014 Survey and Fig.4.47 (b) for 2016 Survey. It indicates that the modules in the Hot zones have a slightly higher value of n as compared to modules in Non-Hot zones. The degradation in the value of the Overall ideality factor can be ascribed to the higher operating temperature and/or humidity of the PV modules, which may accelerate degradation. An increase in the value of the Overall ideality factor causes a decrease in the value of the FF which eventually results in the degradation in P_{max} [244]. Also, it can be seen in Fig. 4.47 that the average Overall Ideality factor for Hot and Non-Hot zones for 2014 Survey is higher than for 2016 Survey. The reason for the higher value is due to the presence of more small and rooftop sites as compared to the 2016 Survey. Therefore, it can be concluded that in Hot zones the P_{max} degradation is not only due to degradation in packaging materials, but also to a small extent, due to the degradation in the solar cell. But it should be noted that due to the insufficient number of data set for n, reaching a definitive conclusion for climatic zone variation is difficult.

128
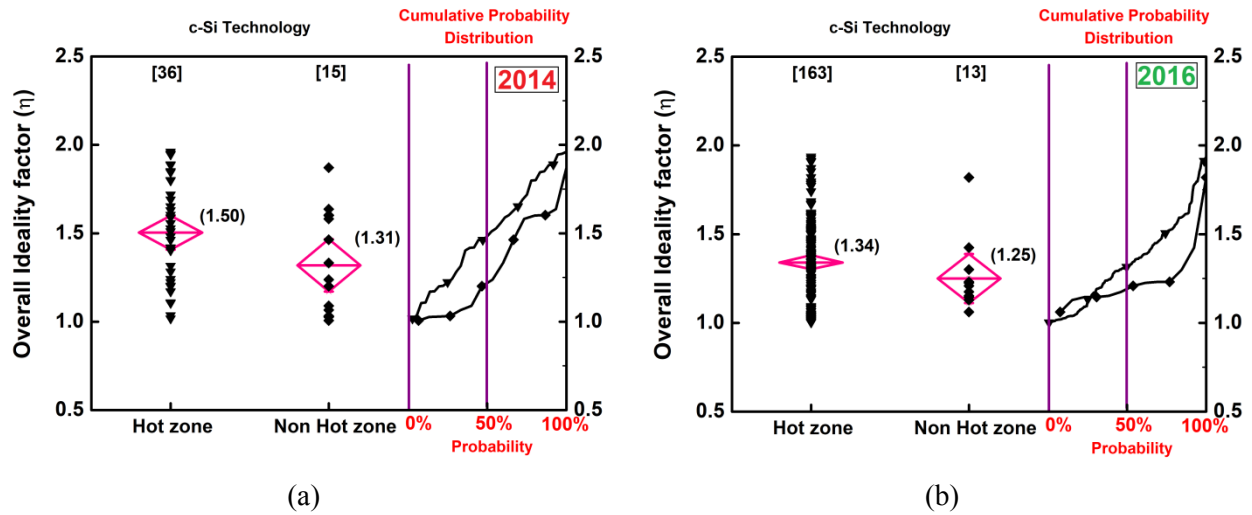
Fig. 4.47: Correlation of Overall ideality factor with respect to Hot and Non-Hot zones (a) 2014 Survey and (b) 2016 Survey. The red diamond represents the 95% confidence interval.

4.6.2.3 Correlation of Overall Ideality Factor with Linear P_{max} Degradation

The correlation between the Overall ideality factor n and the (total) percentage Linear P_{max} Degradation Rate for Group A modules has been shown in Fig. 4.48 (a) for 2014 Survey and Fig. 4.48 (b) for 2016 Survey. It can be seen from the figure that an increase in n causes a decrease in the *FF* value which finally decreases the power output of the module. Therefore, the output power clearly correlates with the quality of the semiconductor device. It should be noted that in Fig 4.48 the total power degradation is plotted and not the annual degradation rate.

129

(a)   (b)
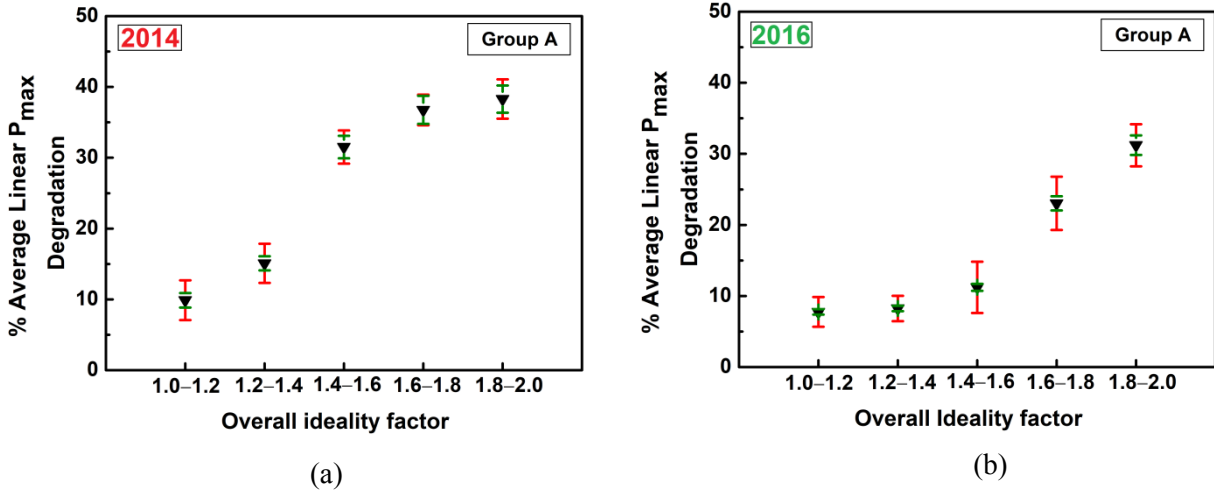
Fig. 4.48: Correlation of Overall ideality factor n with the percentage Linear P_{max} degradation (a) 2014 Survey and (b) 2016 Survey.

4.6.3 Analysis of Insulation Resistance on Survey Data

The Fluke Insulation Tester was used to measure the insulation resistance of the PV modules. The test was conducted by shorting the output terminals of the PV module and connecting to the positive terminal of the instrument, while the negative terminal of the instrument was connected to the frame of the module. The data thus obtained was called dry insulation resistance. To measure the 'wet' insulation resistance, the top glass of the module was fully covered by a wet cloth. The procedure adopted to measure the wet insulation resistance test in the field survey differs from the IEC prescribed method which is used for indoor testing and certification of modules. As per IEC 61215 test procedure, the wet insulation resistance is measured by submerging the module in water. Since the 'wet' insulation resistance methodology adopted in the field survey is not as per the procedure defined in the IEC, the interpretation of the data will not be comparable to the IEC standard but is presented here because of importance in terms of safety. Furthermore, the insulation resistance measured in field in our case was not measured at 25º C.

4.6.3.1 Analysis of Dry Insulation Resistance

The criterion for passing the dry or wet insulation test (as per the IEC 61215) is that the product of insulation resistance and area of the module be more than 40 MΩ m^2 (for module area more than 0.1 m^2). Figure 4.49 (a) shows that 94% and (b) shows that 99.5% of the surveyed modules passed the dry insulation test in 'All' category for 2014 Survey and 2016 Survey respectively. Figure 4.49 (c) 2014 Survey and (d) 2016 Survey show the percentage of the young and old modules which passed the Dry insulation resistance test in all the categories (All, Group X and Group Y). From the figure it can be seen that the percentage of modules which has passed the Dry insulation resistance test for the 2014 Survey is marginally lower than the 2016 Survey.

(a)   (b)

(c)   (d)
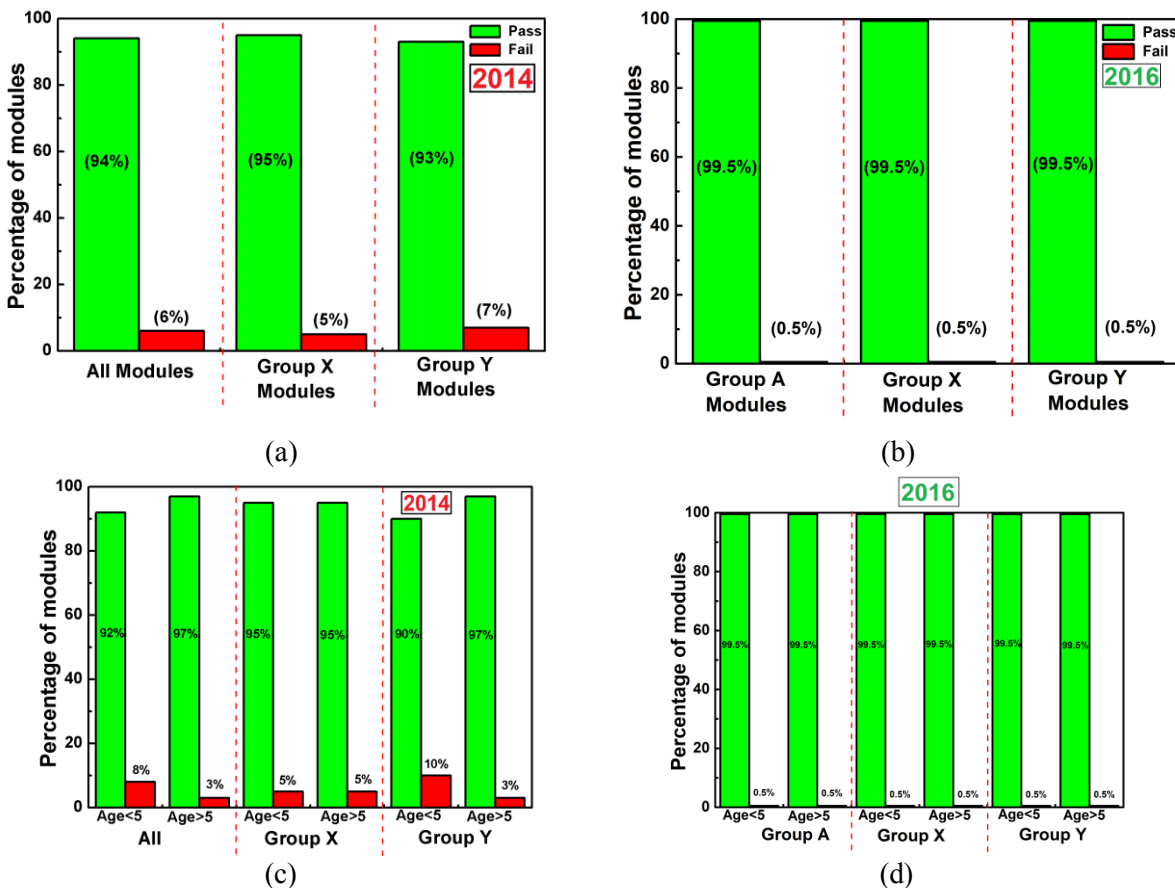
Fig. 4.49: Percentage of modules passed or failed in the dry insulation resistance test for different groups – Group A, Group X, and Group Y (a) 2014 Survey and (b) 2016 Survey. Percentage of modules passed or failed in dry insulation resistance test for 'All', Group X, and Group Y modules for young and old category (c) 2014 Survey and (d) 2016 Survey.

131

4.6.3.2 Correlation of Linear P_{max} Degradation with Insulation Resistance

The Linear P_{max} Degradation Rate (%/year) increases with decrease in dry insulation resistance for Group A modules which has been shown in Fig. 4.50. It can be seen that there is a correlation of the output power degradation of the PV modules with the insulation resistance may result in safety related issues. It should be noted that the insulation resistance measured in the field has not been translated to 25º C. However, similar trend was obtained when translated to 25º C described in a separate work.

(a)   (b)
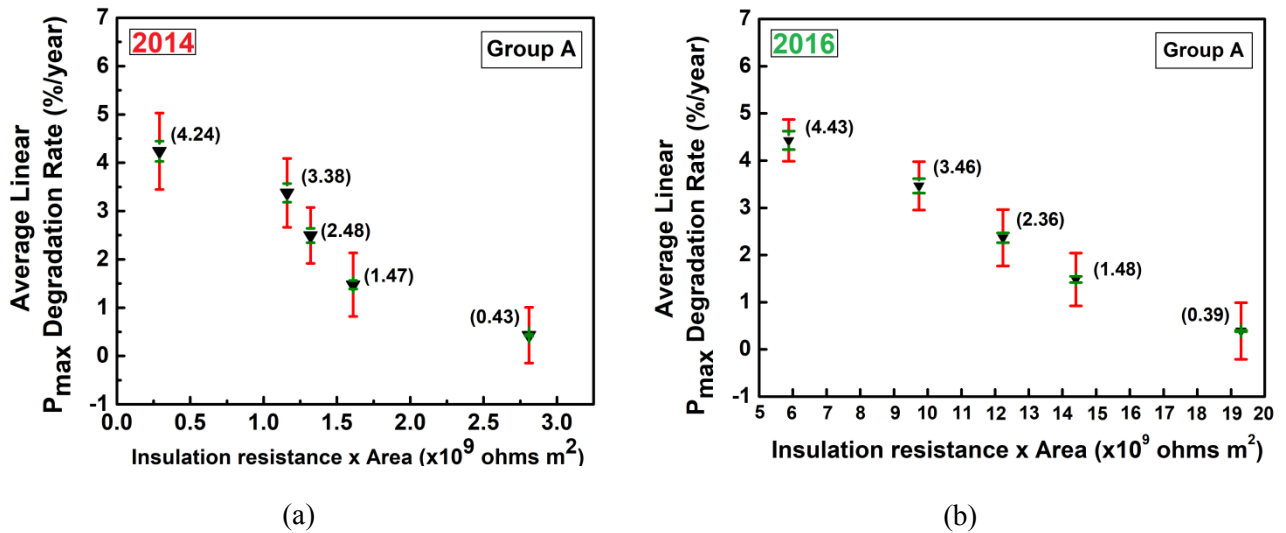
Fig. 4.50: Correlation of P_{max} degradation rate (%/year) with insulation resistance for Group A modules (a) 2014 Survey and (b) 2016 Survey.

4.6.4 Analysis of Interconnect Breakage on Survey Data

Interconnects in PV modules are used to provide a connection between the cells, and they conduct the electrical current from cell to the external load. Generally, for necessary redundancy in case of breakage, there are 2 to 5 interconnects in each cell. However, even if one interconnect is broken, the whole cell's current would be conducted by the other interconnects, and this leads

132

to current crowding and increase in series resistance. An increase in series resistance degrades the fill factor and finally the output power. The interconnect breakage in the PV module in field survey was tested by using the Togami Cell Line Checker [241] [20]. The place where the interconnect breakage was found was marked with a red marker pen on the PV module. The breakage found on the PV module has been categorized into two categories: 1 – Line breakage if it continues over a length, 2 – Point breakage if the breakage is at a single point. An example of line and point breakages is shown in Figure 4.54. The term severity in interconnect breakage is defined as the ratio of the number of cells affected by the interconnect breakage to the total number of cells in the module [241].
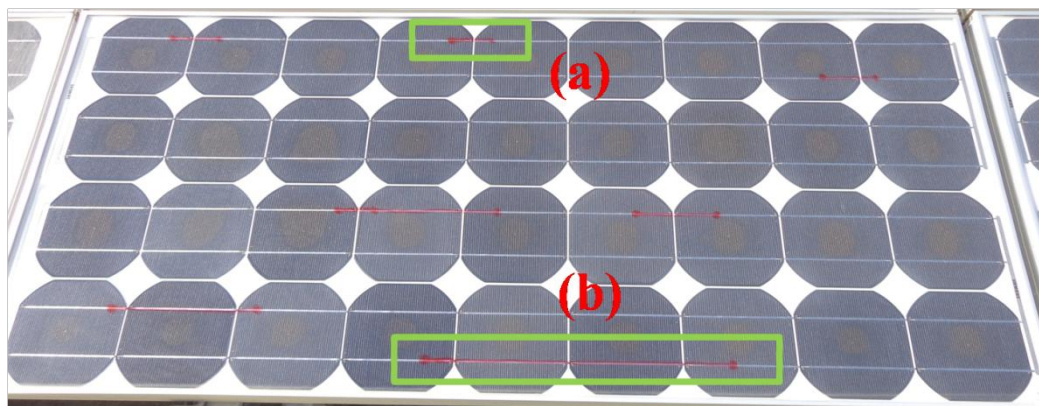
Fig. 4.51: An example of (a) point breakage and, (b) line breakage.

4.6.4.1 Correlation of Interconnect Breakage with Series Resistance

The correlation of series resistance with the severity of the interconnect breakage has been shown in Fig. 4.52 (a) for 2014 Survey and Fig.4.52 (b) for 2016 Survey. It indicates that as the severity of the interconnect breakage increases, the series resistance (expectedly) also increases which reduces the *FF* and consequently decreases the P_{max}. In Fig. 4.53 shows (a) for 2014 Survey and Fig. 4.56 (b) for 2016 Survey that the severity of interconnect breakage is more in

Hot zones, so this is one more reason why modules in Hot zones have higher degradation rates as compared to the Non-Hot zones. It is also evident from the figure that severity of interconnect breakage for 2014 Survey is higher as compared to 2016 Survey which is due to the inclusion of more large sites in the 2016 Survey.

(a)   (b)
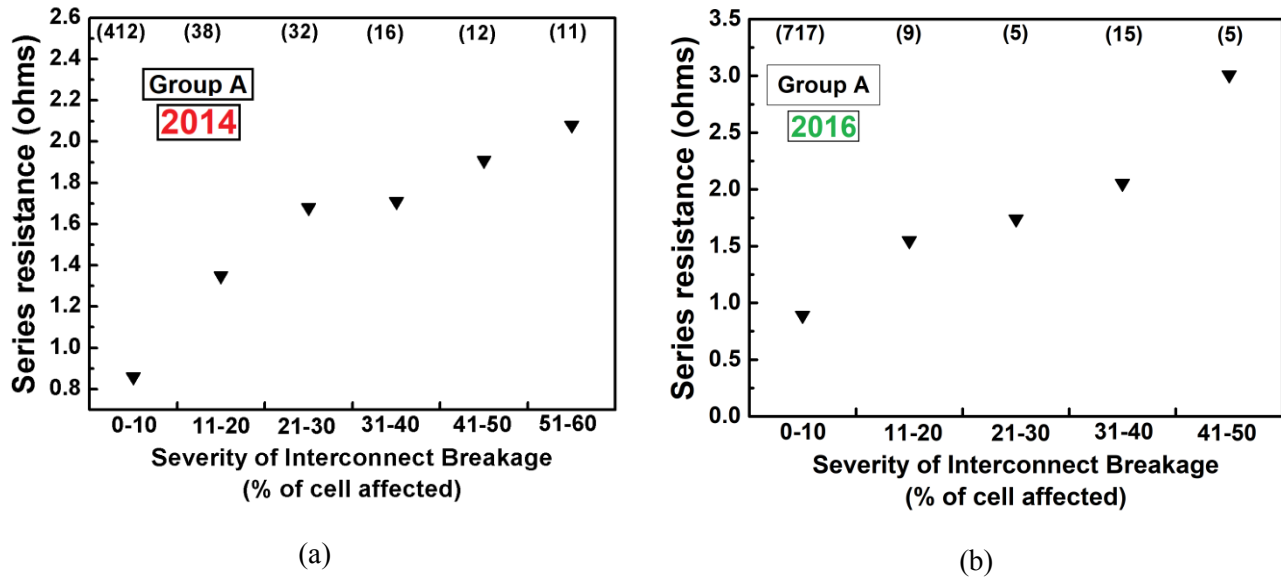
Fig. 4.52: Correlation of average value of series resistance with severity of interconnects breakage (numbers on top represent the number of modules in each category) (a) 2014 Survey and (b) 2016 Survey. As the severity increases the series resistance increase.

(a)   (b)
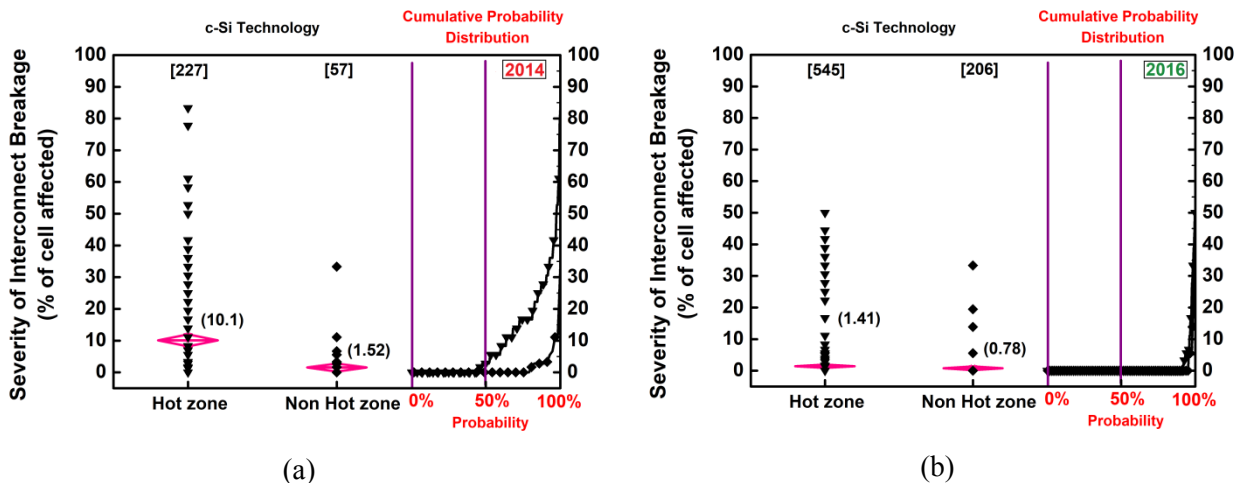
Fig. 4.53: Severity of interconnects breakage (numbers on top represent the number of modules in each category) with respect to Hot and Non-hot zone (a) 2014 Survey and (b) 2016 Survey.

134

4.6.4.2 Correlation of Interconnect Breakage with Linear P_{max} Degradation

The correlation of Linear P_{max} Degradation Rate (%/year) with the severity of interconnects breakage for Group A modules has been shown in Fig. 4.54 (a) for 2014 Survey and Fig. 4.54 (b) for 2016 Survey. It indicates that the output power degradation rate increases with the increase in the severity of interconnect breakage, as expected.

(a)   (b)
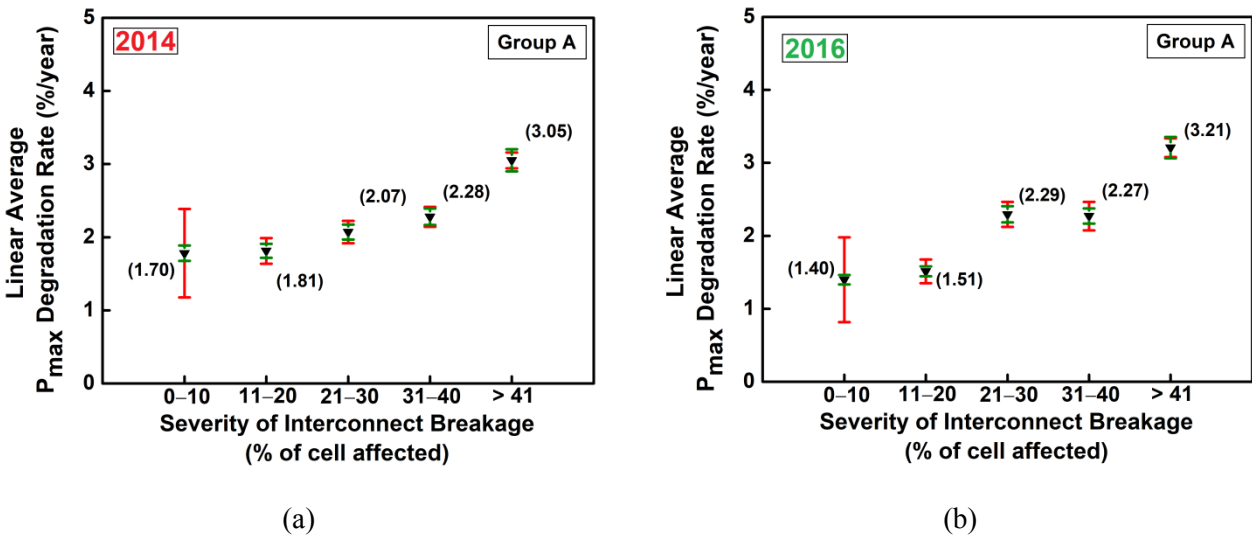
Fig. 4.54: Correlation of Linear P_{max} Degradation Rate (%/year) with severity of interconnects breakage for Group A (a) 2014 Survey and (b) 2016 Survey modules.

4.7   Analysis of Electroluminescence Data

The quality of the semiconductor material, the inactive regions, and cracks in the solar cells can be easily identified through EL imaging. In the field, during the survey, the EL imaging was performed using 2 cameras – (a) Silicon CCD based camera available from Sensovation, and (b) modified CMOS based digital camera developed at NCPRE in 2016 Survey. However, in 2014 Survey only Sensovation camera was used to capture the EL images. All the EL images were captured at a forward current equal to the short circuit current of the PV module under test.

The image difference technique was used, at some sites, to cancel the effect of ambient light on the EL images [245]. This method has been described in more detail in Chapter 5 of the thesis.

EL images of a total of 49 modules were taken in the field during the 2014 Survey whereas a total of 273 modules EL images were taken during the 2016 Survey. The reason for an increase in the number of EL images in 2016 Survey is due to the deployment of multiple in-house low-cost, portable, and compact modified CMOS based EL camera. The specification and the development of the modified camera are explained in more detail in Chapter 5. EL images of some of the Group X and Group Y site modules are shown in Fig. 4.55 and Fig. 4.56 respectively. The dark portions along the edges of the cells in Fig. 4.55 (a) and (b) probably appear in wafer because it has been taken from the ends of the ingots, but it does not affect the power output significantly [235]. The irregular dark patches in the cells shown in Fig. 4.56 (a) – (c), indicates the presence of cracks that affect the charge collection, and output power. In Fig. 4.56 (d), an entire string of cells is dark, which is due to the bypass diode failure (short – circuited). Also, it could be noticed in Fig. 4.56 that one half of two cells (top row) is bright while the other half is dark, which is attributed to interconnect breakage in these cells, which is forcing current crowding along the intact busbars. A typical impression is that the modules in Group Y sites have a much greater number of cracks in modules as compared to the modules in Group X sites, which, in general, show good EL images. This may be due to the poor manufacturing, transportation, or installation practices.

(a)

(b)

(c)

(d)
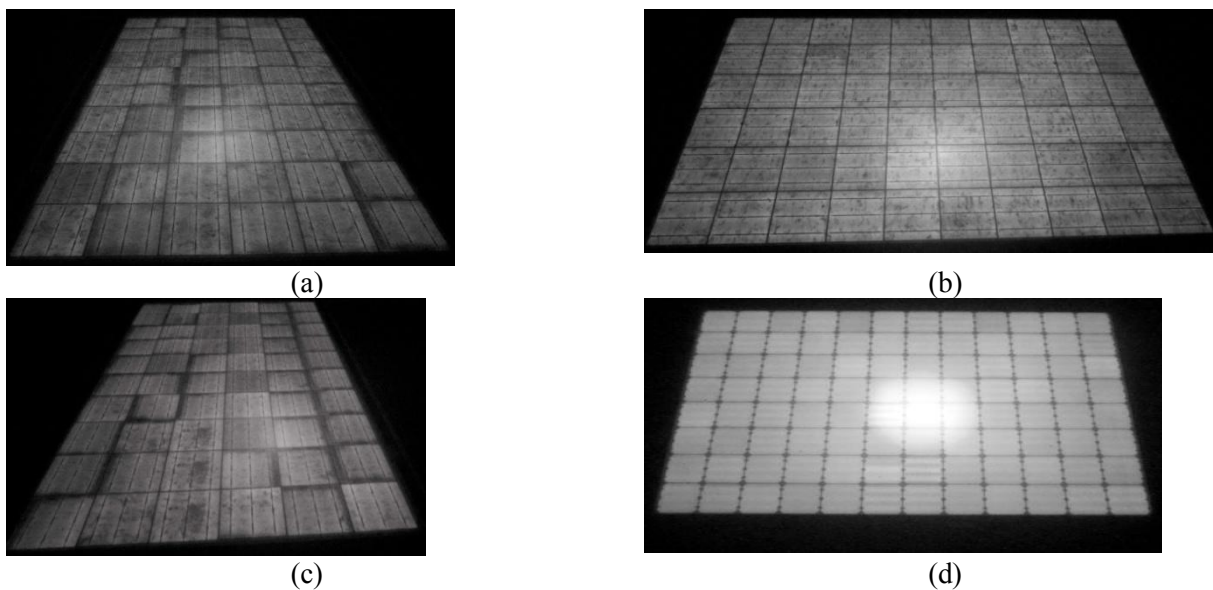
Fig. 4.55: EL images of some Group X modules taken in the field.

<center>(a)</center>

<center>(b)</center>

<center>(b)</center>

<center>(d)</center>
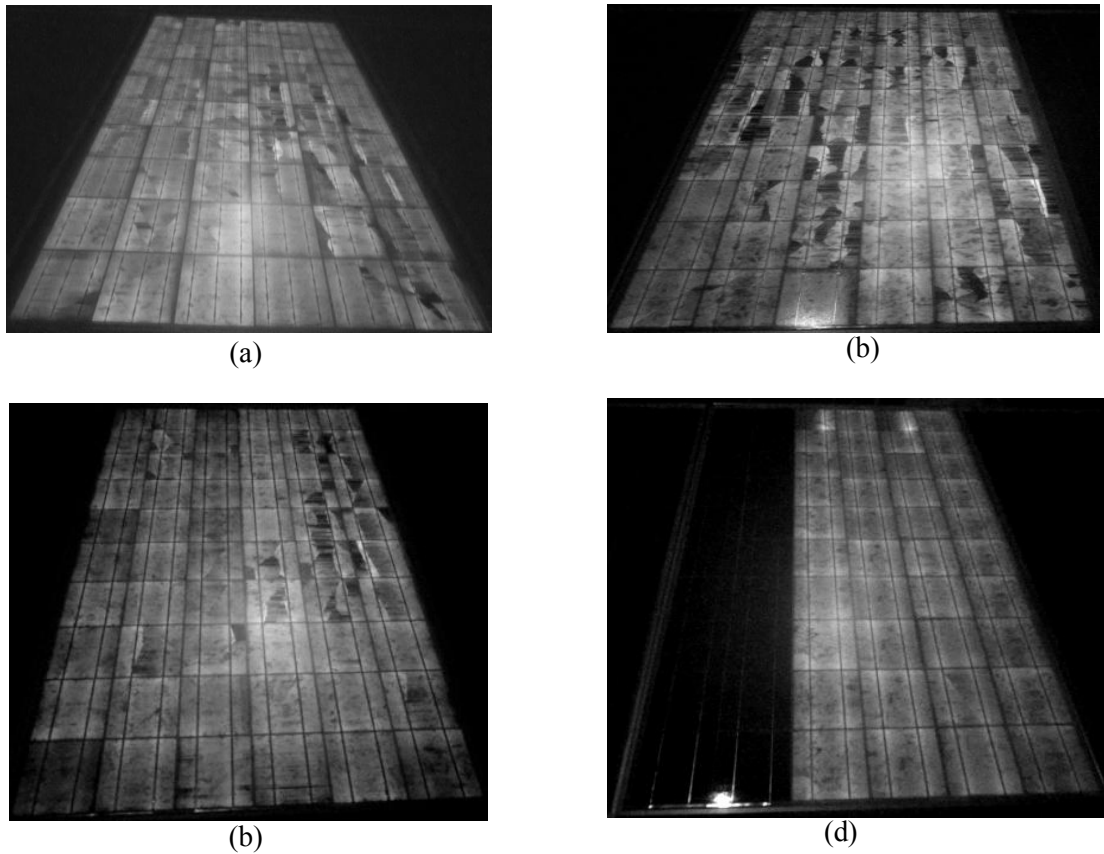
<center>Fig. 4.56: EL images of some Group Y modules taken in the field.</center>

4.7.1 Classification of Cracks

In this study cracks have been classified into 3 categories based on the area affected by the crack as visible in the EL image [207]:

a)   Mode A cracks which are basically hair-line cracks, not associated with any dark area

b)   Mode B cracks which are associated with a grey (not very dark) area in the cell

c)   Mode C cracks which are associated with a dark area in the cell

Figure 4.57 shows an example of all the 3 types of cracks [207]. Out of these 3 classifications, Mode C and Mode B types of cracks can lead to significant power loss since the dark areas mean that electrical connection to the affected area has been broken, whereas Mode A

<center>137</center>

cracks does not lead to a significant loss in power output. Table 4.14 shows the statistics of the number of cracks for 2014 Survey and 2016 Survey of different categories have been counted from the EL images taken during the survey and it is evident that modules in Group Y have a larger number of cracks (of all 3 types) as compared to Group X modules. It can also been seen that in each category the percentage of crack is more in the case of 2014 Survey as compared to 2016 Survey. This explains the reason for high Overall degradation rate (2.10%/year) for 2014 Survey as compared to Overall degradation rate (1.55%/year) for 2016 Survey. Also majority of Group Y and Outlier modules have higher percentage of cracks. This has been presented in more detail in Section 4.8. Table 4.15 shows the statistics for young and old modules for 2014 Survey and 2016 Survey EL data and it show that the percentage of cracks is higher in young modules as compared to old modules. This draws the attention towards possible hasty and improper transportation and/or installation practices and the starting quality of the modules for young modules. Furthermore, it could also be due the reduction in the cell thickness in younger modules. Table 4.16 shows that the rooftop installations have higher cracks as compared to ground mounted installations for both 2014 Survey and 2016 Survey. This explains the reason for the high degradation rate for rooftop systems. Table 4.17 shows that the small installations suffer from more cracks than large installations for 2016 Survey EL data (due to lack of large installation EL data for 2014 Survey). Since a large number of cracks can give rise to power loss, this could be the one reason for the high degradation for Group Y sites, young sites, rooftop sites, and small sites.
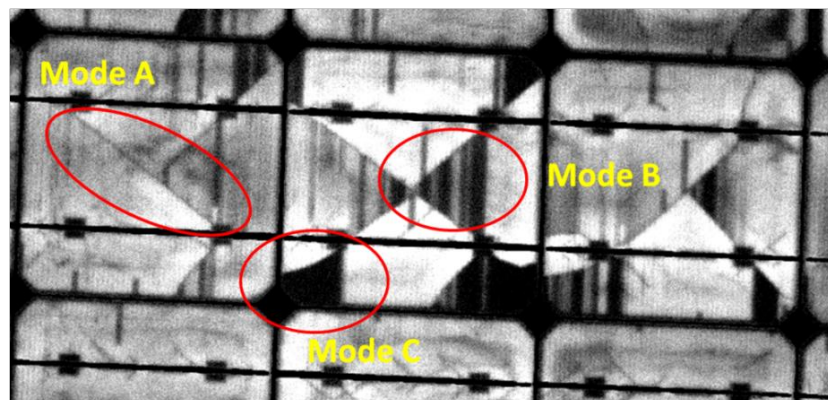
Fig. 4.57: Different types of cracks as visible in EL images [207].

138

Table 4.14: Percentage of cells affected by different types of cracks in Group X and Group Y modules.

| | Percentage of cells affected by different types of cracks | | | | | | Total no. of cells checked | |
| | Mode A cracks | | Mode B cracks | | Mode C cracks | | | |
	2014	2016	2014	2016	2014	2016	2014	2016
Group X	2.4%	1.23%	14.1%	1.46%	3.2%	0.83%	972	9464
Group Y	29.7%	7.58%	42.3%	9.48%	14.2%	3.39%	444	3300

Table 4.15: Percentage of cells affected by different types of cracks in young and old modules.

| | Percentage of cells affected by different types of cracks | | | | | | Total no. of cells checked | |
| | Mode A cracks | | Mode B cracks | | Mode C cracks | | | |
	2014	2016	2014	2016	2014	2016	2014	2016
Young	37.9%	3.19%	14.9%	4.14%	12.2%	1.62%	408	8952
Old	0%	2.10%	26.2%	2.10%	4.4%	1.21%	1008	3812

Table 4.16: Percentage of cells affected by different types of cracks in Roof top and Ground mounted installations.

| | Percentage of cells affected by different types of cracks | | | | | | Total no. of cells checked | |
| | Mode A cracks | | Mode B cracks | | Mode C cracks | | | |
	2014	2016	2014	2016	2014	2016	2014	2016
Roof-top	13.3%	3.07%	25%	3.97%	7.66%	2.22%	888	4860
Ground Mounted	7.01%	2.75%	19.51%	3.26%	4.92%	1.05%	528	7904

Table 4.17: Percentage of cells affected by different types of cracks in Large and Small size systems.

| | Percentage of cells affected by different types of cracks | | | Total no. of cells checked |
| | Mode A cracks | Mode B cracks | Mode C cracks | |
	2016	2016	2016	2016
Small Size Systems	3.01%	3.58%	1.85%	6920
Large Size Systems	2.70%	3.47%	1.08%	5844

4.7.2 Correlation of Snail Tracks and Interconnect Breakage with EL

In many young modules surveyed, snail tracks have been observed; this has been presented in detail in a separate thesis [241]. Snail tracks can be visually observed on the PV module as black or brown curved lines running across the solar cells, and sometimes bordering them (like a frame). Generally, cells affected by snail tracks shows cracks in the EL images, as shown in Fig. 4.58. The cracks in the solar cell facilitate the moisture to reach the top side of the solar cell, where it helps the migration of the silver ions from the gridlines to the encapsulant layer. Subsequently, the silver ions then react with several chemicals from the encapsulant and backsheet producing various compounds of silver, which are the cause of the snail tracks [246].

Figure 4.59 (a) shows interconnect breakage in the busbar of the cell (marked in red) which has been found using the Togami Cell Line Checker. The EL image of the same module and the effect of the breakage can be clearly seen in the EL image is shown in Fig. 4.59 (b). Breakage in the interconnect increases the series resistance of the module which subsequently reduces the power output of the module.

(a)   (b)
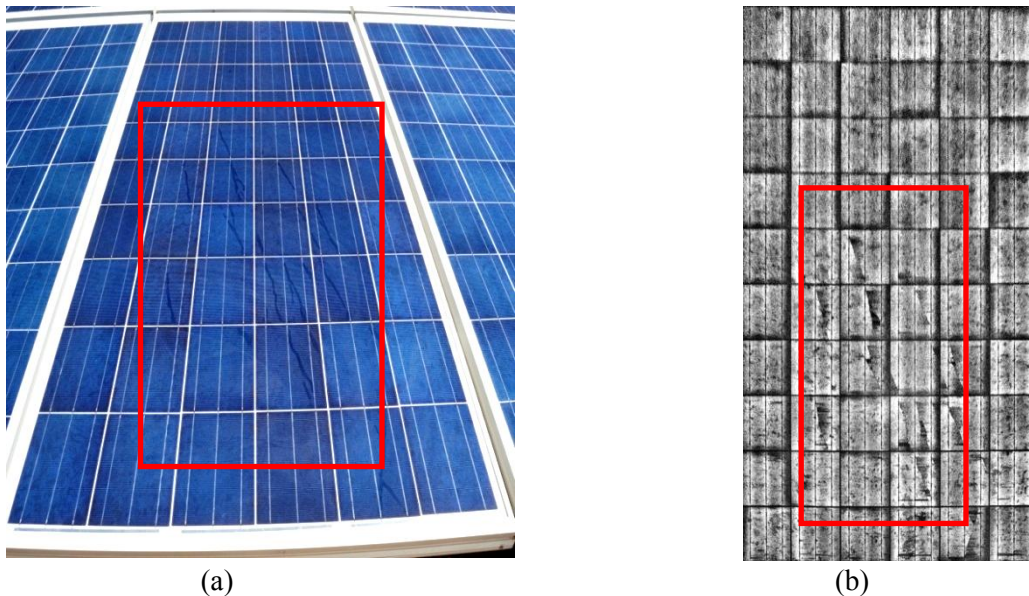
Fig. 4.58: (a) Snail tracks observed in a PV module in Hot & Dry climate, (b) EL image of the same module showing the cell cracks.

<div align="center">(a)   (b)</div>
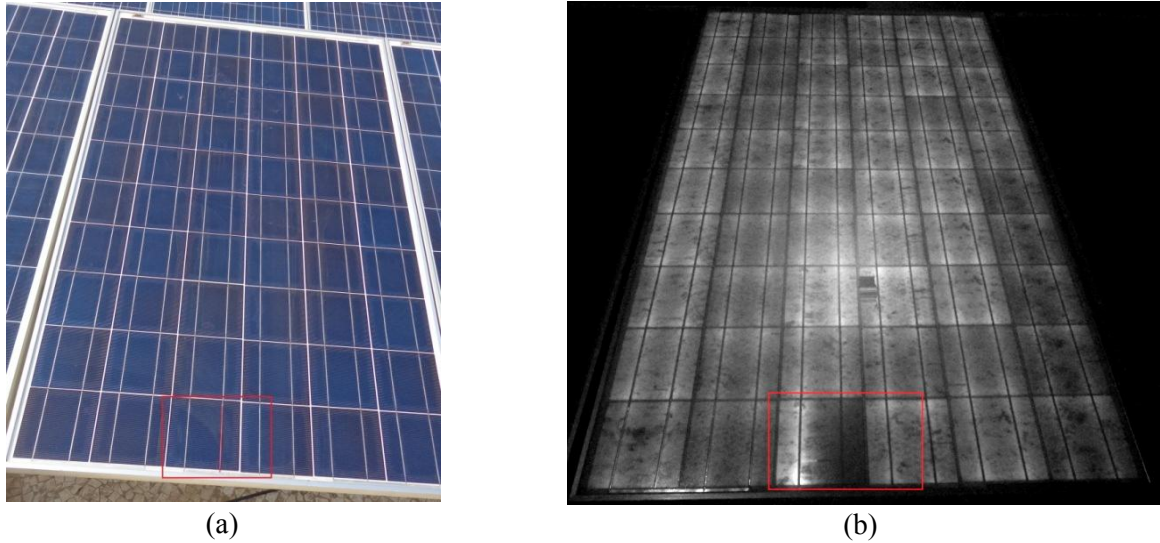
Fig. 4.59: (a) Interconnect breakage in a PV module, detected using Togami Cell Line checker (marked red on the cell interconnect), and (b) the EL image of the corresponding section.

4.7.3 Correlation of Cracks with Location

In order to understand the possible cause of cracks in the PV module, analysis with respect to the location of cracks can provide useful information. Due to the relatively few EL images captured during the 2014 Survey, the correlation of cracks with location is done only for the 2016 Survey. To do this analysis, every module was divided into three regions – the central zone, the intermediate zone, and the periphery, as shown in Fig. 4.60. In respective regions the percentage of cells cracked is computed for each module and the values are plotted in Fig. 4.61. From the figure, it is evident that the average value for Region 2 is higher than Regions 1 and 3. This is supported by the Mann-Whitney-Wilcoxon test which indicates that the data distribution for Region 3 is significantly different from Regions 1 and 2, therefore it can be concluded that the cracks are found more in the outer regions as compared to the central region of the PV modules.

<div align="center">141</div>
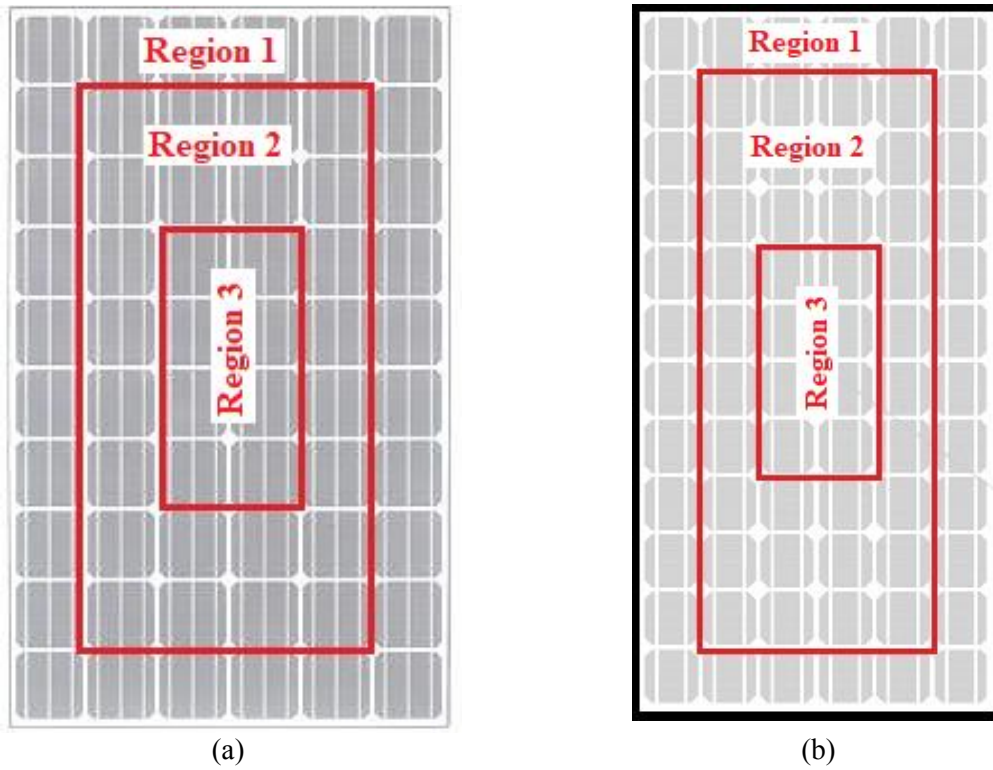
Fig. 4.60: Definition of the three regions in (a) 60 cell module, (b) 72 cell module.
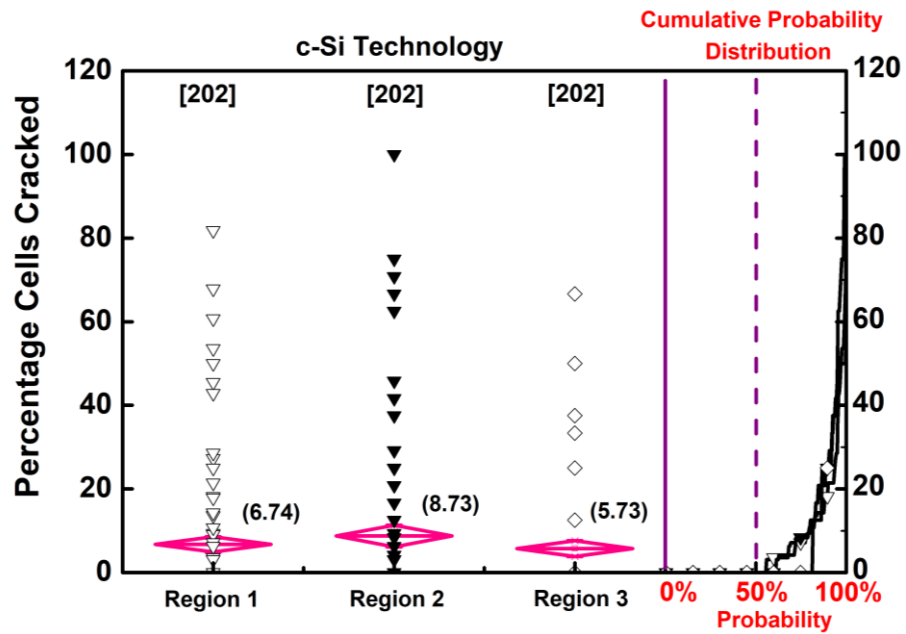
Fig. 4.61: Percentage cells cracked with position on PV module.

4.7.4 Correlation of P_{max} Degradation with Number of Cracks

The average Linear P_{max} Degradation Rate (% per year) versus the total number of cracks in the module has been shown in Fig. 4.62 (a) for 2014 Survey and Fig. 4.62 (b) for 2016 Survey. The number of cracks has been counted manually. From the figure, it can be seen that the degradation rate increases with an increase in the number of cracks. As explained earlier, this demonstrates that cracks and micro-cracks are definitely one of the causes of increased degradation seen in the poor-performing sites.

(a)   (b)
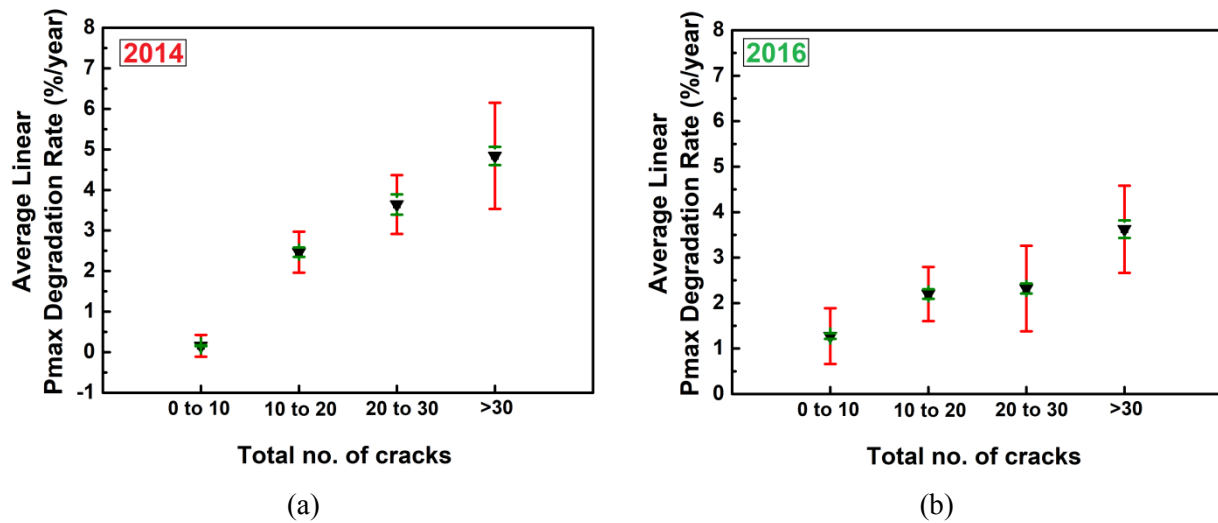
Fig. 4.62: P_{max} degradation rate (%/year) versus the total number of cracks in the module (a) 2014 Survey and (b) 2016 Survey. The green and red bars indicate the instrument/STC translation error and nameplate error respectively.

4.8 Analysis of Poorly Performing Group Y Modules and Outlier Modules

The results of the analysis of the All India Survey of PV Module Reliability indicate that some of the c-Si modules are performing quite well, whereas others are not; there are some 'good' sites and some 'problematic' sites (refer Section 4.5.1). Furthermore, a total of 254 modules in the 2014 Survey and 34 modules in the 2016 Survey showed high overall P_{max} degradation rates above 5.02 %/year and 5.12 %/year respectively, and these have been considered as 'outliers'. It was deemed important to understand the degradation modes prevalent in Group Y sites and outlier modules which are leading to such high degradation rates. In this section, the analysis of the poor-performing modules (in Group Y sites and outlier modules) observed in the All-India Surveys is presented.

Figure 4.63 shows that the average linear degradation rate of the Group Y modules is (a) 2.79 %/year for 2014 Survey and (b) 2.75 %/year for 2016 Survey which is very high, and hence this is a cause for concern.

(a)   (b)
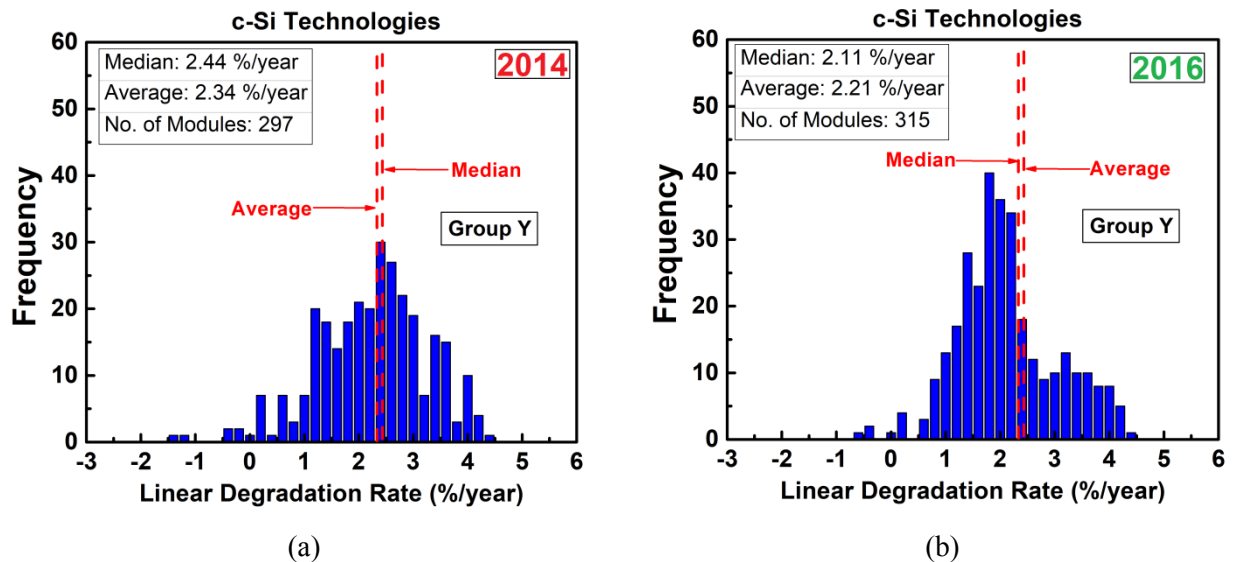
Fig. 4.63: Histogram of Overall P_{max} Degradation rate for (a) 2014 Survey Group Y modules and (b) 2016 Survey for Group Y modules.

Table 4.18 shows the age distribution of the modules belonging to Group Y sites. It has been consistently found for both the surveys that most of the Group Y site modules belong to the young age category, with less than 5 years of field exposure. Almost 63% of Group Y site modules for the 2014 Survey and 88% of Group Y site modules for the 2016 Survey belong to the young age category. This is a cause for concern and also substantiates the conclusion that young modules are showing a higher degradation rate than old modules (refer Section 4.5.4).

Table 4.18: Percentage of Group Y modules in different age categories.

	Age Group (years)											
	0 to 1		1 to 3		3 to 5		5 to 10		10 to 20		>20	
	2014	2016	2014	2016	2014	2016	2014	2016	2014	2016	2014	2016
Percentage of Group Y Modules	5%	0%	26%	49%	32%	39%	5%	0%	32%	8%	0%	4%

From Table 4.19 it is evident that 47% of the Group Y site modules for 2014 Survey and 68% of the Group Y site modules for 2016 Survey are found in Rooftop (rack-mounted on flat roofs) installations, while the rest are ground-mounted. Furthermore, 100% of the Group Y site modules for 2014 Survey and 77% of the Group Y site modules for 2016 Survey come from small installations of size < 100 kW (as shown in Table 4.20). All this data clearly indicates the poor performance of the small rooftop systems installed in recent years. In addition some evidences have also been obtained that a few large sites are not performing well and the reason could be due to the bad quality of modules/installation resulting from reverse bidding.

Table 4.19: Percentage of Group Y modules in different mounting categories.

	Roof Mounted		Ground Mounted	
	2014	2016	2014	2016
Percentage of Group Y Modules	47%	68%	53%	32%

Table 4.20: Percentage of Group Y modules in different system size categories.

	Small Sites (<100 kW)		Large Sites (>100 kW)	
	2014	**2016**	**2014**	**2016**
Percentage of Group Y Modules	100%	77%	0%	23%

The Linear Degradation Rate for P_{max}, I_{sc}, V_{oc}, and *FF*, for young and old modules in Group Y sites are shown in Fig. 4.64 (a) for 2014 Survey and (b) for 2016 Survey. It is evident from the figure that for the young modules, fill factor degradation is the main (and only) culprit, while for the older modules in Group Y, fill factor degradation and short circuit current degradation both significantly affect the degradation in P_{max}. It could be concluded that degradation in the fill factor is the main reason for the high degradation in Group Y modules. As a result, it is necessary to understand the degradation modes responsible for the high degradation in the performance of the Group Y modules. Cell cracks are observed to be one of the major degradation modes observed in the surveyed Group Y modules. Table 4.21 shows the percentage of cells affected by cracks in Groups X and Y. The cracks have been categorized as Mode A, B or C as per [207]. The percentage of cells affected by cracks is much higher in Group Y than in Group X, for all 3 types of cracks for both the surveys. The high fill factor degradation rates reported in Group Y site modules are attributed to the cell-to-cell mismatch caused due to the cracks in the PV modules.
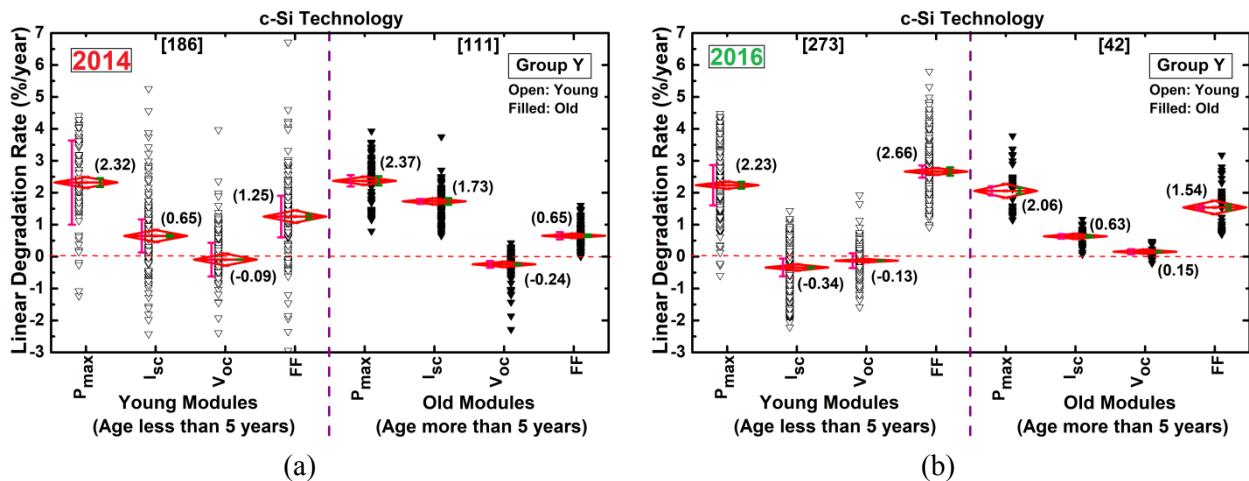
Fig. 4.64: Linear P_{max}, I_{sc}, V_{oc} and *FF* Degradation for young and old crystalline silicon modules in Group Y (a) 2014 Survey and (b) 2016 Survey.

Table 4.21: Percentage of cells affected by different types of cracks in Group X and Group Y modules.

| | Percentage of cells affected by different types of cracks | | | | | | Total no. of cells checked | |
| | Mode A cracks | | Mode B cracks | | Mode C cracks | | | |
	2014	2016	2014	2016	2014	2016	2014	2016
Group X	2.4%	1.23%	14.1%	1.46%	3.2%	0.83%	972	9464
Group Y	29.7%	7.58%	42.3%	9.48%	14.2%	3.39%	444	3300

As mentioned in Section 4.5.1, a total of 254 modules in the 2014 Survey and 34 modules in the 2016 Survey showed high overall P_{max} degradation rates above 5.02 %/year and 5.12 %/year respectively and these were considered as 'Outliers'. These were not included in the analyses presented in Section 4.5, but it is obviously important to understand the root causes for such high degradation rates. Figure 4.65 (a) for 2014 Survey and (b) for 2016 Survey shows the age distribution of the Outlier modules. It is evident from the figure that almost 99% of the modules in the Outlier category in 2014 Survey and 79% of the modules in the Outlier category are young modules, which have been in the field for less than 5 years. This fact raises concerns regarding the quality and nameplate rating of the modules, and installation practices in recent times.

(a)   (b)
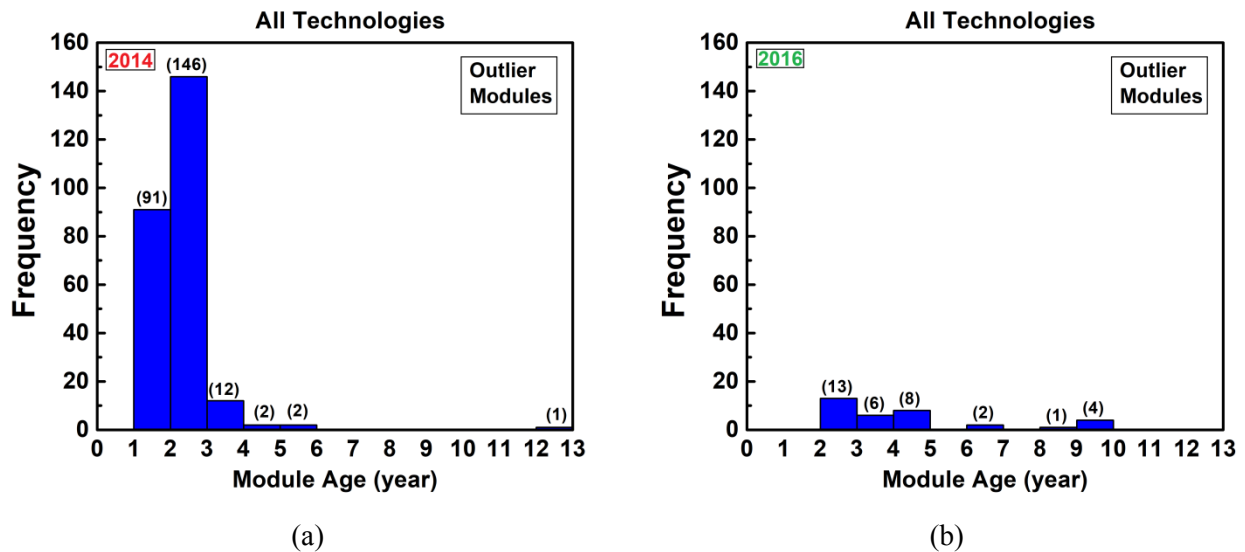
Fig. 4.65: Age distribution of the Outlier modules. (a) 2014 Survey and (b) 2016 Survey.

The histogram of the P_{max} degradation rates for the Outlier modules is shown in Fig. 4.66 (a) for 2014 Survey and (b) for 2016 Survey. The average degradation rate for these modules is 7.60 %/year for 2014 Survey and 6.62 %/year for 2016 Survey which is very high compared to 0.8%/year international benchmarks even after 2% initial LID discounting. Furthermore, it is also evident that the number of outlier modules (34) in 2016 Survey is much lower as compared to the 2014 Survey (number of outlier modules 254). This is attributed to the inclusion of more large sites (system size > 100kW) in the 2016 Survey. The degradation rates for Hot and Non-Hot climatic zones are shown in Fig. 4.67 (a) for 2014 Survey and (b) for 2016 Survey. The modules in the Hot zone are degrading at a slightly higher rate than modules in the Non-Hot zone. This tells us that climatic conditions do not seem to be the primary cause behind the high degradation rates of Outliers. Figure 4.68 gives the degradation rates of the various electrical parameters (P_{max}, I_{sc}, V_{oc}, and FF) for the Outlier modules. It is evident that FF degradation is the major contributing factor to power degradation in most of the Outlier modules.
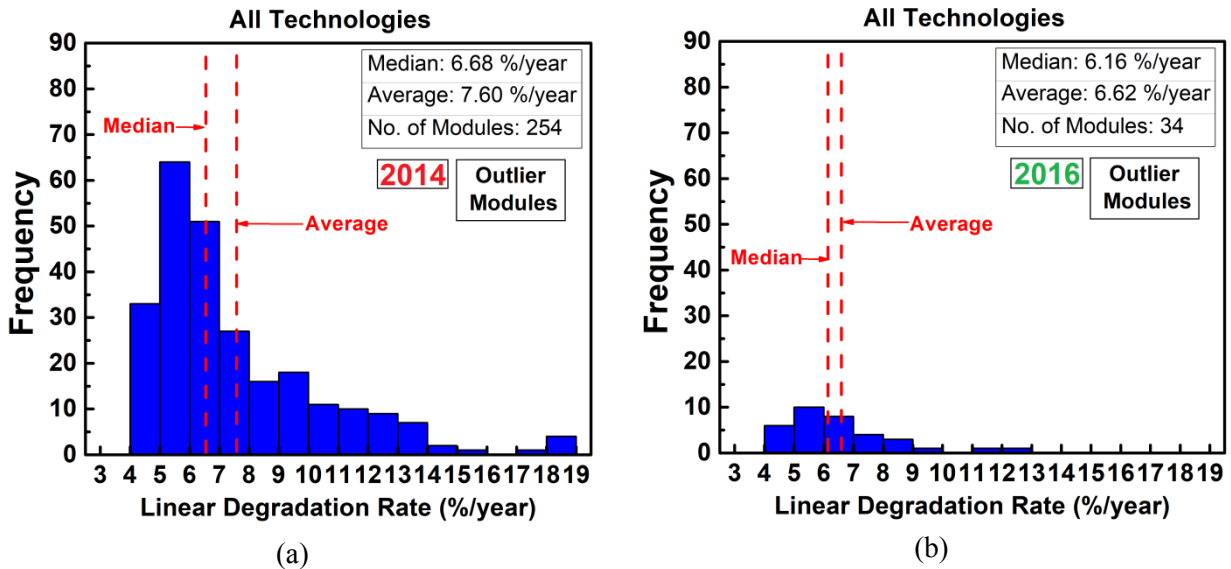
Fig. 4.66: Histogram of Outlier module Linear P_{max} Degradation Rate of crystalline silicon modules for (a) 2014 Survey, and (b) 2016 Survey.

148
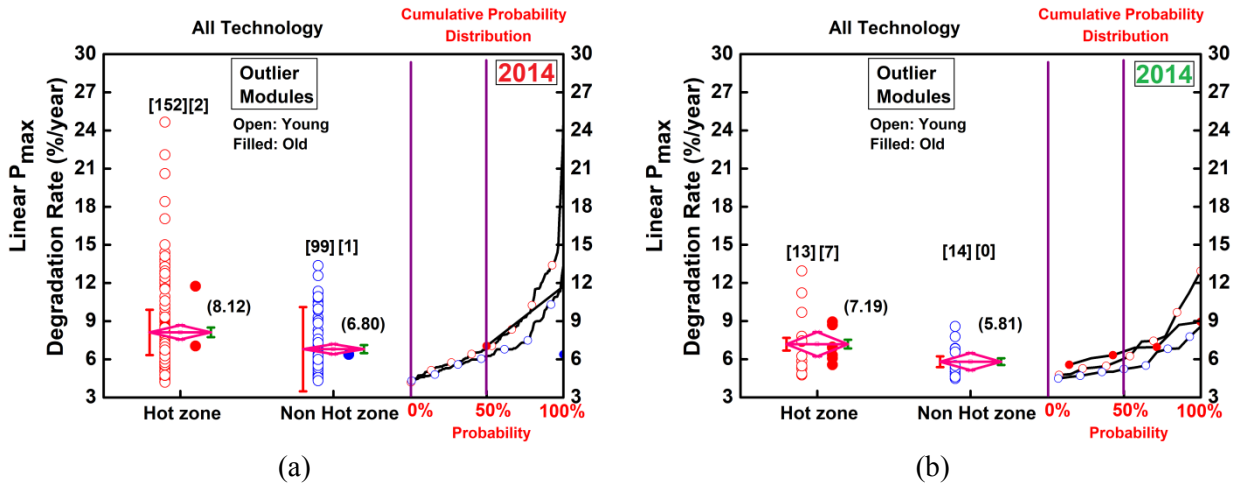
Fig. 4.67: Comparison of Linear P_{max} Degradation Rate with respect to Hot and Non-Hot zone for Outlier modules (a) 2014 Survey and (b) 2016 Survey.
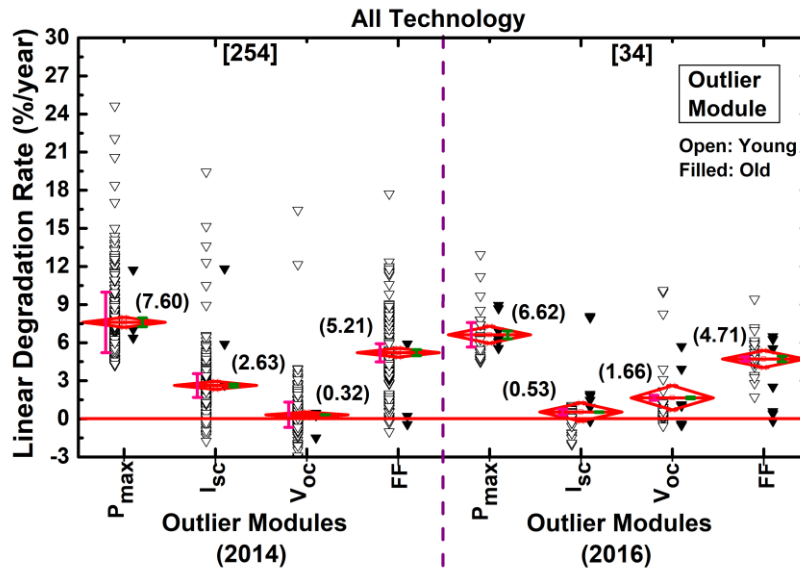
Fig. 4.68: Linear P_{max}, I_{sc}, V_{oc} and FF degradation for Outlier modules for 2014 Survey and 2016 Survey.

The EL images of the Outlier modules show signatures of different types of defects in the cells, as shown in Fig. 4.69. Figure 4.69(a) has no EL emission from 1 string of the module, which can occur due to the shorting of the bypass diode. In Fig. 4.69(b), the bottom row of cells and also 2 cells in the top row have low EL emission, suggesting potential induced degradation (PID) as the degradation mode. There were multiple modules at this site that fell in the Outlier

149

category and all showed low EL emission in the bottom row cells. In Fig. 4.69 (c), cracks can be seen in multiple cells, which lead to high loss of output power.

(a)   (b)   (c)
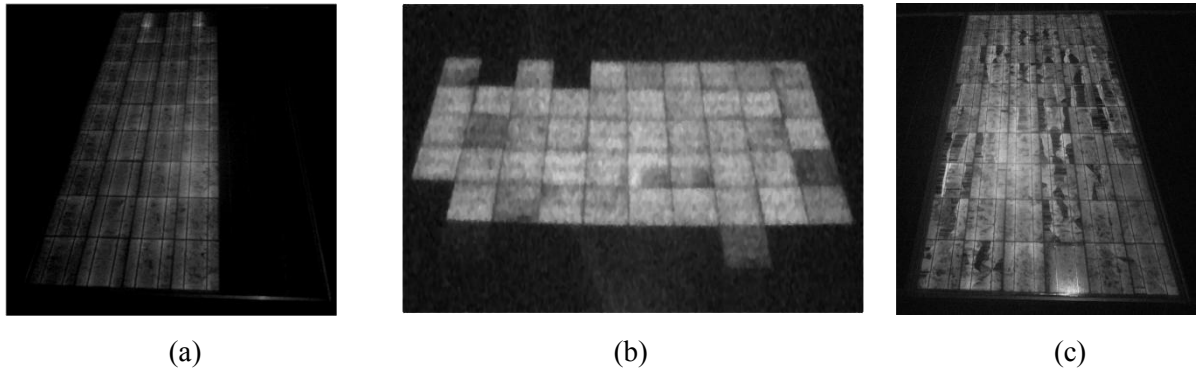
Fig. 4.69: EL images of some crystalline silicon Outlier modules – (a) module with 1 string shorted (probably bypass diode shunting), (b) module with edge cells defective (PID suspected), and (c) module with cracks in multiple cells.

The detailed analysis of the poorly performing modules (modules at Group Y sites and Outlier) shows that most of these are young modules having age less than 5 years. The analysis also shows that cracks are one of the main causes of the high degradation rates, which are leading to high fill factor degradation. Furthermore, it has been found that most of these poor performing modules are found in small rooftop systems installed in recent years. The presence of cracks is an indication that the quality of modules and/or installation procedures are not up to the mark in these sites.

4.9   Analysis of Risk Priority Number (RPN)

The Risk Priority Number (RPN) analysis can be used to quantify the reliability of the PV modules. PV modules undergo different failure modes based on the bill of material used for the construction of the module and the environmental condition in which it is deployed. RPN analysis is done to obtain a quantitative index for the identified failure modes and its effect on the system based on priority ranking. RPN analysis utilizes the Failure Modes, Effects, and Criticality Analysis (FMECA) as per IEC 60812. RPN is calculated as per the following equation:

$$RPN = S * O * D \qquad\qquad (4.11)$$

where:

S: Severity (representing the impact of failure mode or defects)

O: Occurrence (representing the probability of occurrence)

D: Detection (representing the recognizing or spotting and removing or preventing of failure modes)

The analysis of the Risk Priority Number (RPN) analysis has been presented in detail in a separate thesis [247], and is also available in the public domain as part of the report "*All India Survey of Photovoltaic Module Reliability 2016*" [20].

4.10   Comparison of 2014 and 2016 Survey Data

In this section, the comparison of the data collected in the 2014 and 2016 Surveys is presented. We will briefly mention also comparison with the results of the 2018 Survey. The broad trends are very similar, which re-affirms confidence in the data. Some figures which have been shown earlier are repeated here for convenience to highlight the comparison.

4.10.1 Comparison of Electrical and Electroluminescence Data

Figure 4.70 (a) for 2014 and (b) for 2016 Survey show that the average overall degradation rate of all the modules surveyed in the 2014 Survey (2.10%/year excluding the outliers) is higher as compared to the 2016 Survey (1.55%/year excluding the outliers). This is attributed to the inclusion of more large sites (system size > 100kW) in the 2016 Survey. This was to be expected, as we had noted even in the 2014 Survey that large sites showed a lower degradation rate site which was confirmed again in 2016 (see Fig. 4.34). A total of 11 large sites were surveyed in 2016 as compared to 6 large sites in the 2014. This shows that the large size power plants are degrading at a lower rate as compared to small (typically rooftop) systems. Similar conclusions are obtained after discounting for 2% LID (refer Fig. 4.71). However, from both the figures it can be concluded the modules (in Group A) are degrading at a higher rate than the international warranty limits provided by the manufactures. Figure 4.72 (a) for 2014 Survey and (b) for 2016 Survey show the Linear degradation rate for Group X modules. It is evident from the figure that Group X modules for the 2016 Survey (0.89%/year) have a degradation rate much lower than Group X modules for the 2014 Survey (1.25%/year). It substantiates our conclusions that the large sites are performing better since most of the large sites in the 2016 Survey fall in the Group X category. Furthermore, in 2014 Survey, a sizeable number of the small (system size<100 kW) rooftop sites fall in the Group X category as compared to 2016 Survey. These small sites are not performing well (though they are good enough to be in Group X), causing the high average Linear degradation rate for the 2014 Survey Group X modules. It is also comforting that good large sites do approach the international benchmark of 0.8 %/year. However, for Group Y modules in both 2014 and 2016 Surveys, comparable Linear degradation rates were obtained (refer Fig.4.72 (c) for 2014 Survey and (d) for 2016 Survey). This indicates that modules in bad sites degrade at a high rate which is a cause of great concern.   Figure 4.73 shows that the Linear degradation rate for Non-Hot zones (Cold & Cloudy and Cold & Dry) is much lower as compared to the Hot zones in both the surveys (refer Fig. 4.73 (a) for 2014 Survey and (b) for 2016 Survey). Furthermore, Fig. 4.74 shows that for both the surveys (Fig. 4.74 (a) for 2014 and Fig.4.67 (b) for 2016 Survey) modules in Hot Zones are having a high degradation rate as compared to modules deployed in Non-Hot zones. Figure 4.75 shows the technology dependence of Linear P_{max} Degradation Rate

(%/year) for Group A modules surveyed in 2014 (refer Fig.4.75 (a)) and 2016 (refer Fig.4.68 (b)). It is seen that in both the surveys the c-Si modules are having higher degradation rates as compared to CdTe and HIT modules. Whether this is an intrinsic technology effect or not was discussed earlier in Section 4.5.3. Table 4.22 shows the percentage of cracks in Group X and Group Y modules. It is evident from the table that Group Y modules show a higher percentage of cracks as compared to Group X modules.
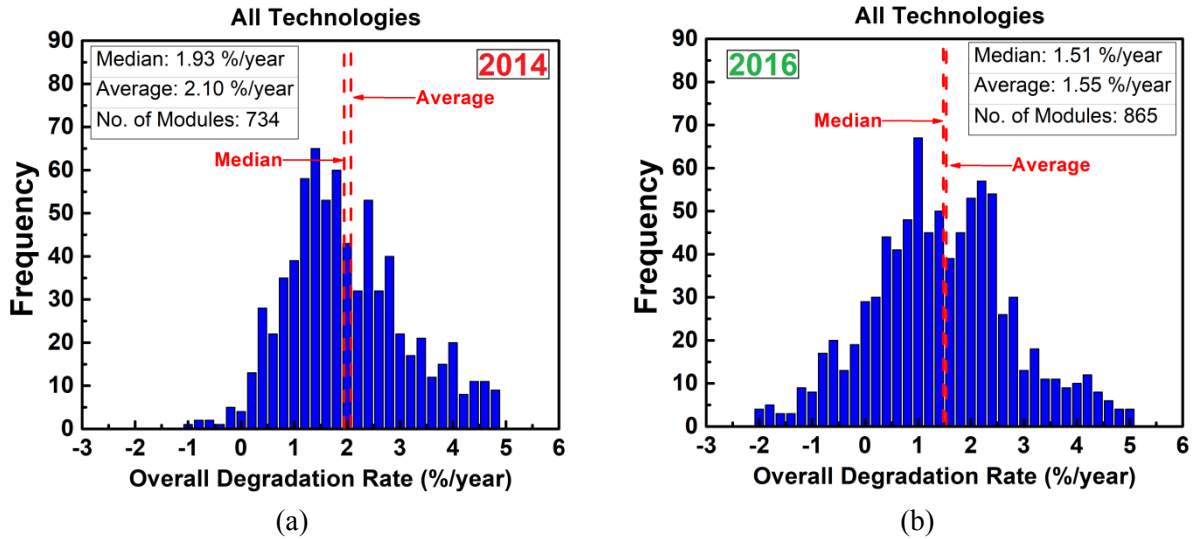
Fig. 4.70: Histogram of Overall P_{max} Degradation Rate of (a) 2014 Survey data (mean value of 2.10%/year), and (b) 2016 Survey data (mean value of 1.55%/year).
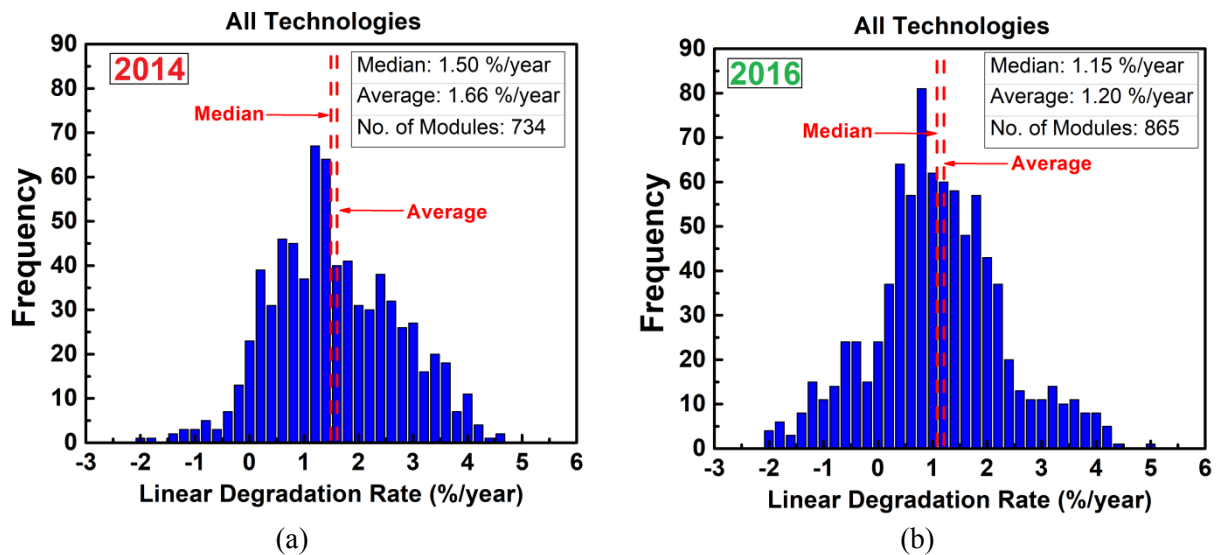
Fig. 4.71: Histogram of Linear P_{max} Degradation Rate of (a) 2014 Survey data (mean value of 1.66%/year), and (b) 2016 Survey data (mean value of 1.20%/year).
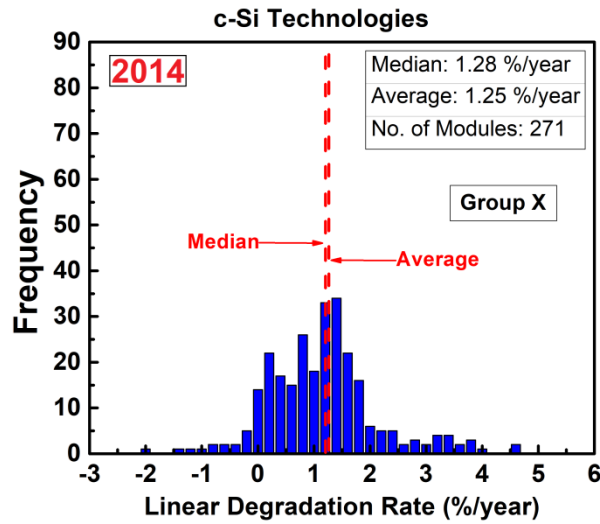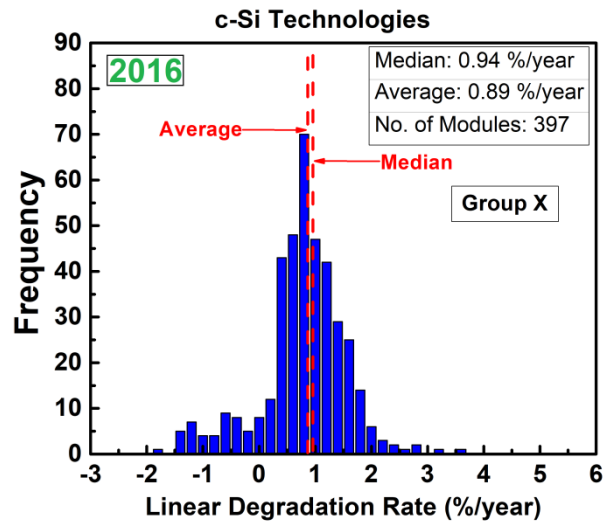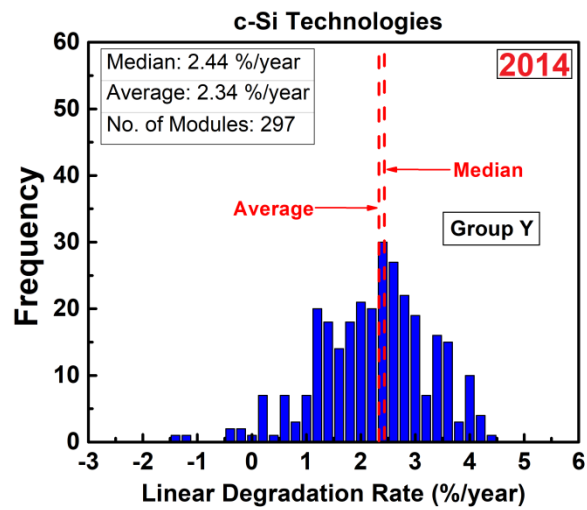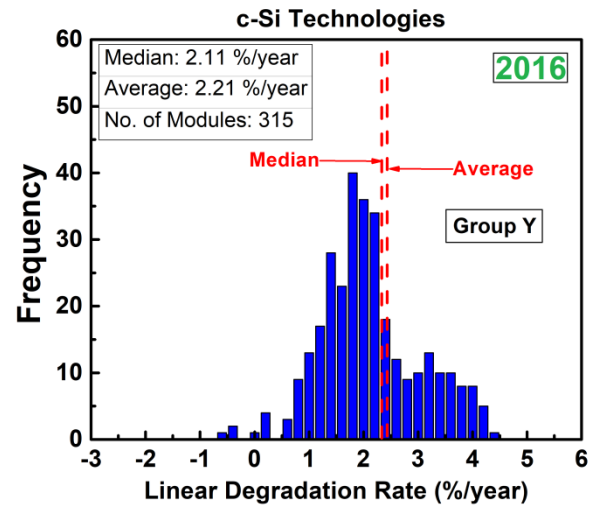
Fig. 4.72: Histogram of Linear P_{max} Degradation rate for (a) 2014 Survey Group X modules, (b) 2016 Survey Group X modules, (c) 2014 Survey Group Y modules and (d) 2016 Survey for Group Y modules.
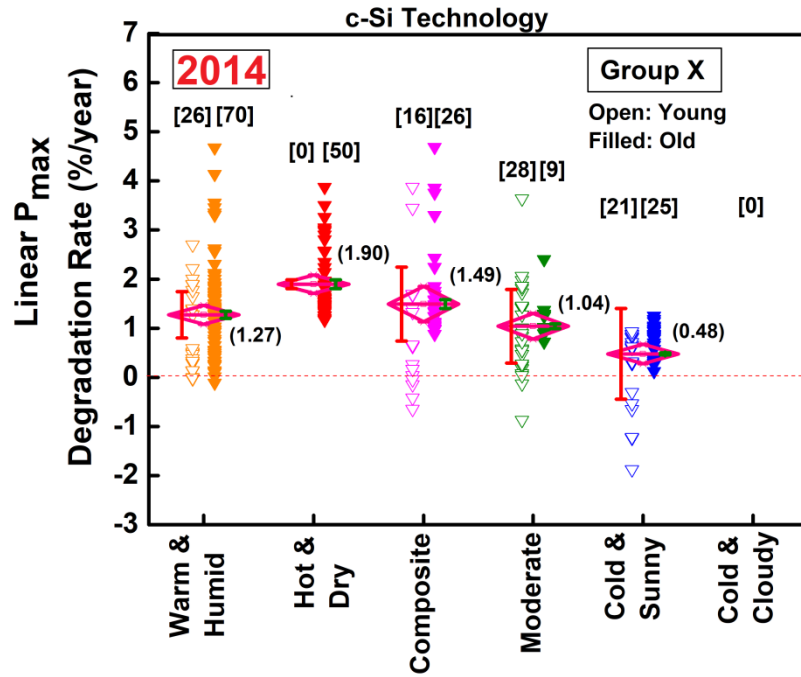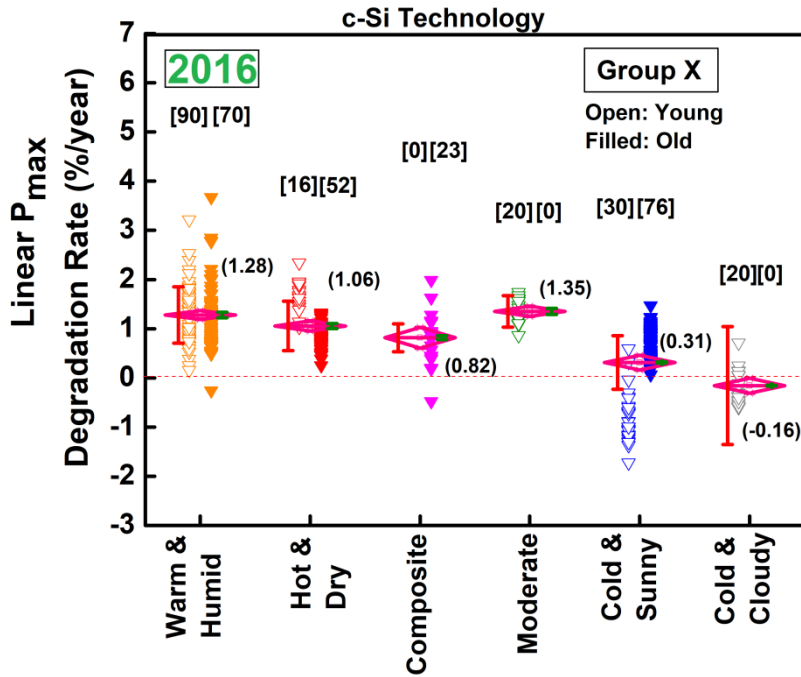
Fig. 4.73: Comparison of Linear *P*_{max} Degradation Rate with respect to six-zone classification system for Group X modules (a) 2014 Survey and (b) 2016 Survey. Warm and Humid and Hot and Dry have the highest degradation and Cold zones have the least value of degradation.
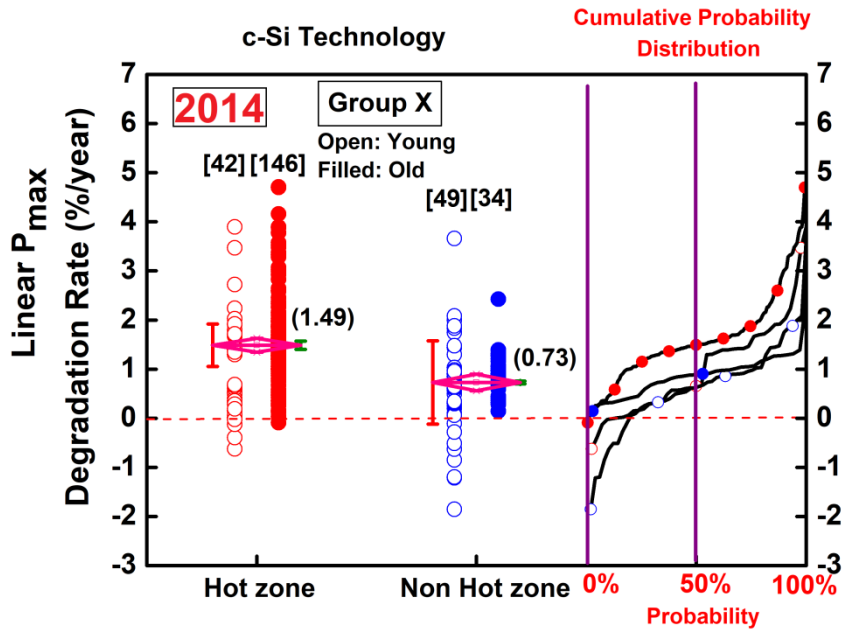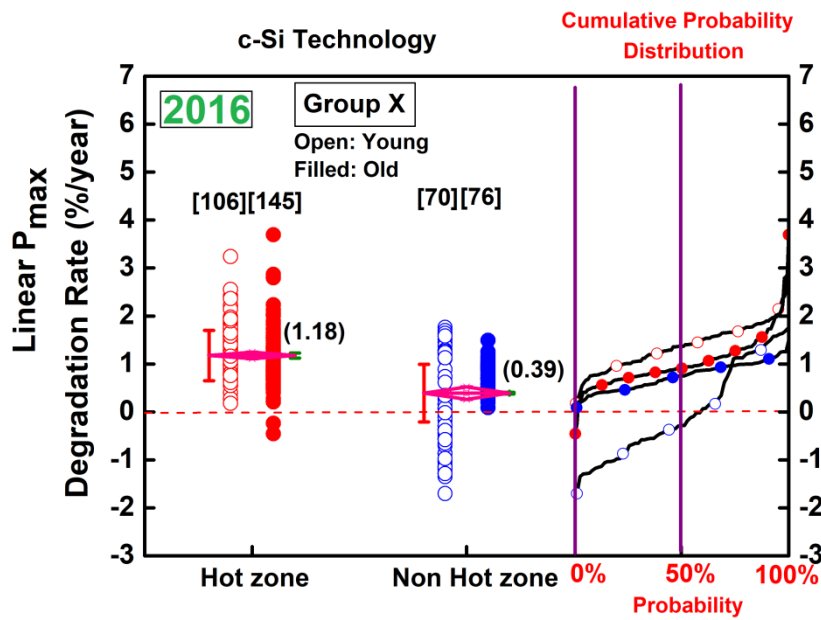
Fig. 4.74: Comparison of Linear P_{max} Degradation Rate with respect to Hot and Non-Hot zone for Group X modules (a) 2014 Survey and (b) 2016 Survey. Young modules in Hot zones have higher degradation rate and Young modules in Non-hot zones are showing the least degradation.

156
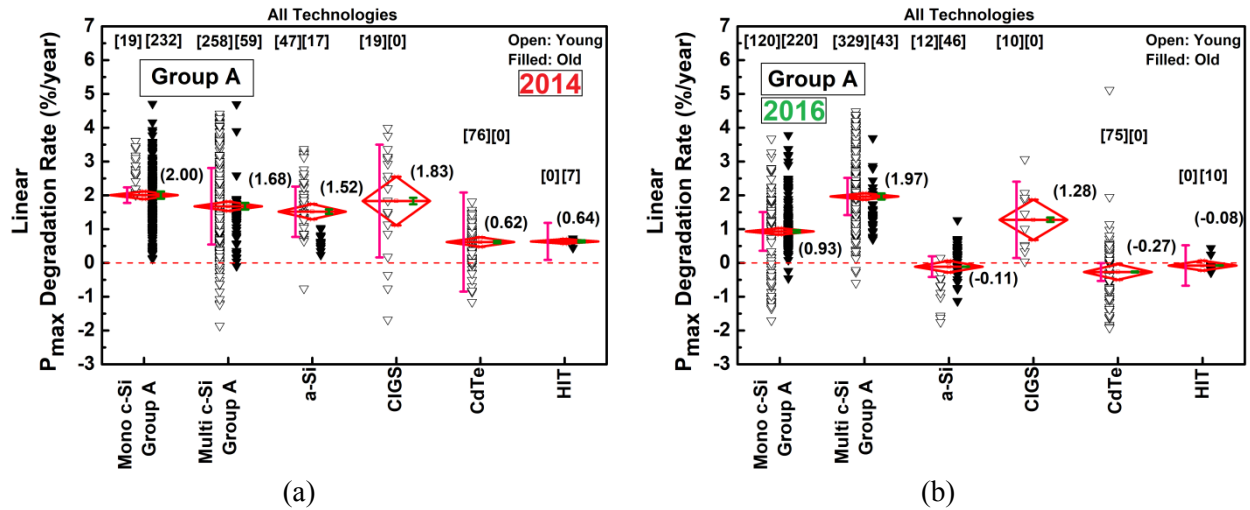
Fig. 4.75: Linear P_{max} Degradation per year for modules of different technologies (all (Group A) c-Si modules are considered) (a) 2014 Survey and (b) 2016 Survey. Crystalline silicon modules are degrading at a faster rate than thin-film modules.

Table 4.22: Percentage of cells affected by different types of cracks in Group X and Group Y modules.

	Percentage of cells affected by different types of cracks						Total no. of cells checked	
	Mode A cracks		Mode B cracks		Mode C cracks			
	2014	2016	2014	2016	2014	2016	2014	2016
Group X	2.4%	1.23%	14.1%	1.46%	3.2%	0.83%	972	9464
Group Y	29.7%	7.58%	42.3%	9.48%	14.2%	3.39%	444	3300

It is evident from the analysis of 2014 and 2016 Survey data that similar trends in the degradation rates are obtained with respect to the climatic zone, technology, system size, and mounting configurations (refer Section 4.5). It has been consistently observed that the modules surveyed in 2014 and 2016 Surveys have a higher degradation rate than the international warranty limits provided by the manufactures. However, it has been seen in both the Surveys that c-Si Group X modules are performing reasonably well, while the rest of the modules which are falling in the Group Y category are showing a higher rate of degradation. This leads us to the conclusion that some sites show excellent performance, whereas some show grave problems. These observations point to problems regarding module quality and/or installation procedures.

157

Consistent results obtained in both the surveys also substantiate the conclusion that high ambient temperatures are causing modules to degrade at a faster rate due to an increased encapsulant browning (discussed in a separate thesis [241] and also the All-India Survey report [20]) and interconnect breakage due to thermal cycling which contribute to high degradation in I_{sc} and FF respectively. In old crystalline silicon modules, the main contributor to the P_{max} degradation is I_{sc} followed by FF, whereas in the case of young crystalline silicon modules the main contributor to the P_{max} degradation is FF degradation. This has been observed in both the surveys (refer to Section 4.5.3). It has also been consistently obtained from both the surveys that modules deployed in Large ground-mounted sites show lower degradation rates as compared to Small sites and roof-tops (refer Section 4.5.5). The reason for the lower degradation rate for modules deployed in Large sites and ground-mounted systems is attributed to the lower percentage of cell cracks in both the surveys (refer Section 4.7).

There are a few significant differences that have been observed in the 2014 and 2016 Survey data. It was seen that the degradation rate of a-Si modules in 2014 Survey is higher as compared to the a-Si modules in 2016. This is due to the reason that in 2016 Survey most of the a-Si modules were surveyed from large power plants (where installation quality and maintenance are expected to be better). Also, it can be seen that the old modules for 2014 Survey have a higher degradation rate as compared to 2016 Survey since most of these old Group X c-Si modules in 2016 Survey fall in the category of the (better) Large sites.

The present author had a brief involvement in the 2018 Survey in planning, training the survey team, and in the discussion of survey results. It is worth presenting the data here to compare with the 2014 and 2016 Surveys. Figure 4.76 (a) shows the median overall degradation rate of all the modules surveyed in the 2018 Survey (1.56%/year excluding the outliers) which is similar to the 2016 Survey (1.51%/year excluding the outliers).   Figure 4.76 (b) shows the median linear degradation rate of all the modules surveyed in the 2018 Survey (1.21%/year excluding the outliers) which is similar to the 2016 Survey (1.15%/year excluding the outliers). The trend in the degradation rate observed in 2018 Survey is similar to the 2016 Survey due to the inclusion of many power plants (system size >100 kW) in the survey.
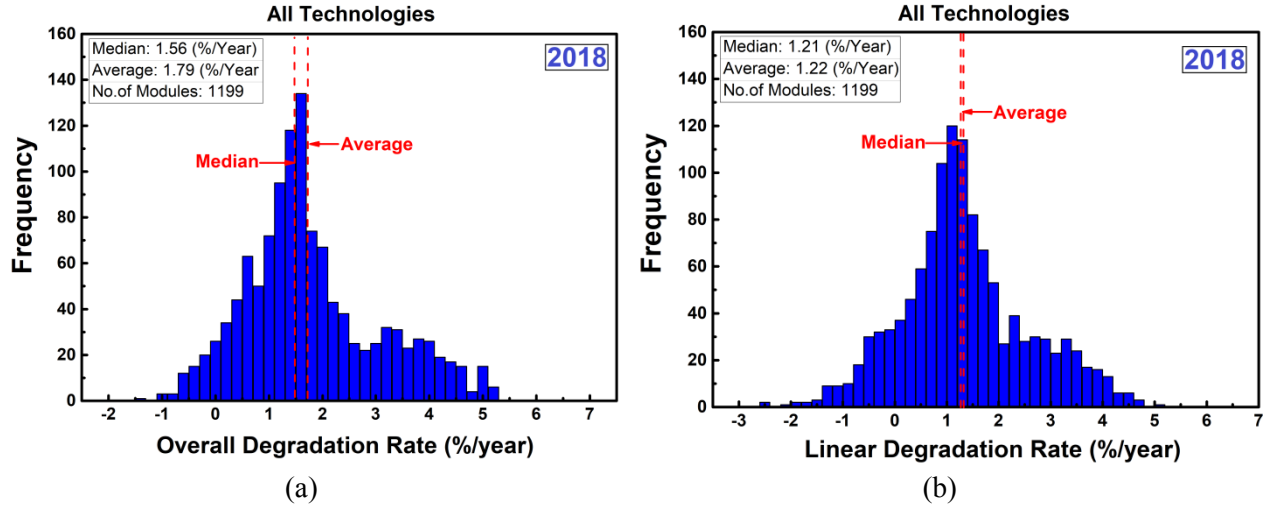
Fig. 4.76: (a) Histogram of Overall P_{max} Degradation Rate of 2018 Survey data (mean value of 1.79%/year), and (b) Histogram of Linear P_{max} Degradation Rate of 2018 Survey data (mean value of 1.22%/year).

4.10.2 Three Point Data Analysis for Repeat Sites

In the course of All India Survey 2013, 2014, and 2016 modules at a few sites were repeated. The reason for repeating these modules was to understand the degradation on a year-on-year basis. This would help in understanding the long-term reliability and durability of PV module from the field data. Figure 4.77 shows the STC power of the modules at sites which were repeated in 2014 and 2016 Survey. In the figure, each plot (a) to (j) represents a site which was measured in both 2014 and 2016 Surveys. The average power (after STC translation) of the modules inspected at the site is shown along with the translation/measurement error (green bar). In majority of cases, the average power is monotonically decreasing except for one site (refer Fig. 4.77(j)). The slope of the red line joining the 3 points on the plots represents the degradation rate. In several cases, this slope is larger between the nameplate and the 2014 measurement as compared to the slope between 2014 and 2016 measurements even after discounting 2% Light Induced Degradation in the initial years of field exposure.
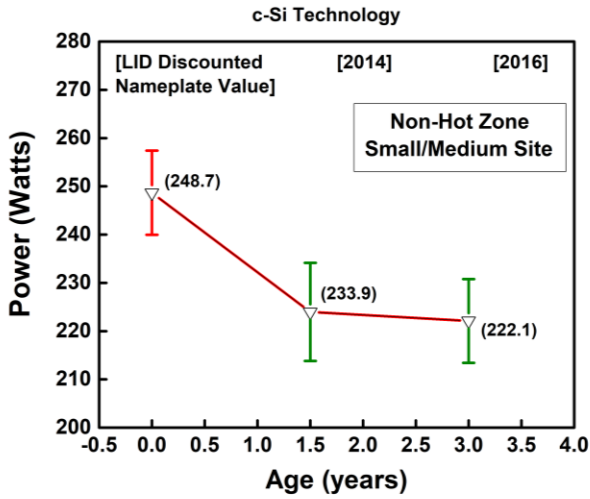
(a)
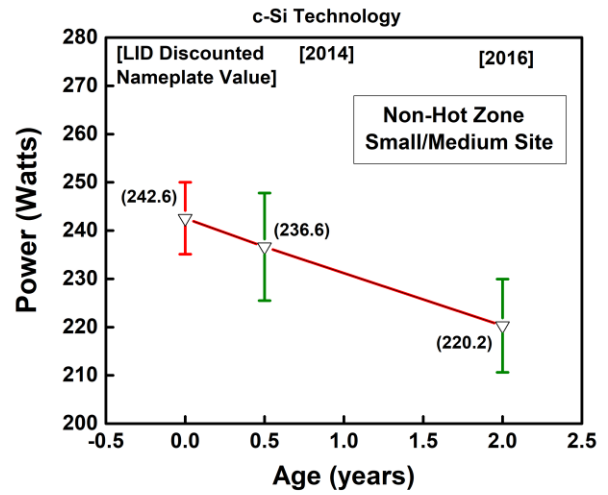
(b)
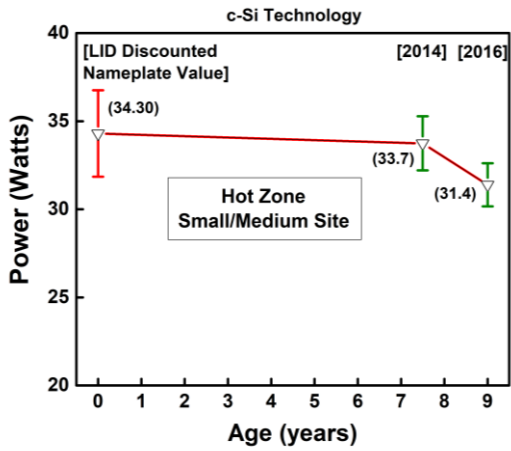
(c)
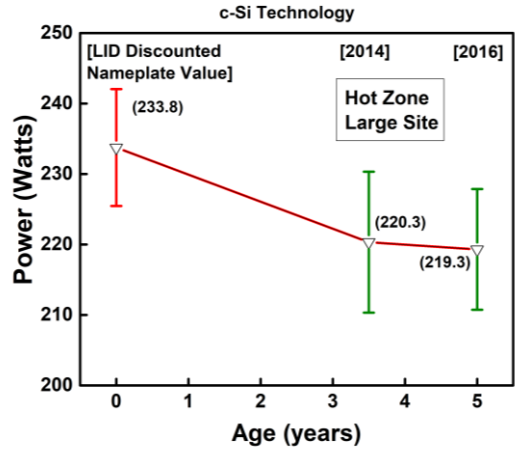
(d)
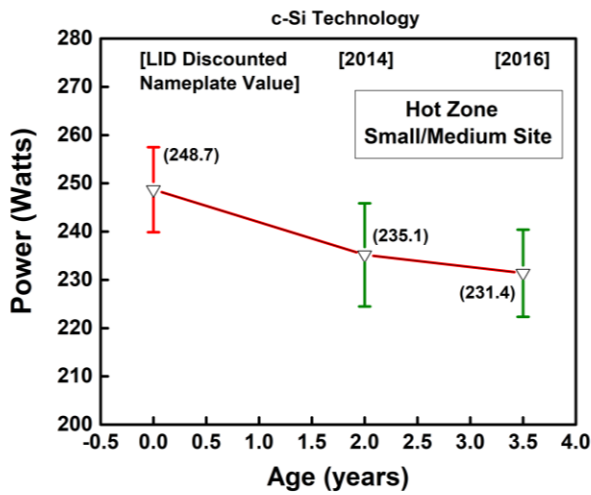
(e)
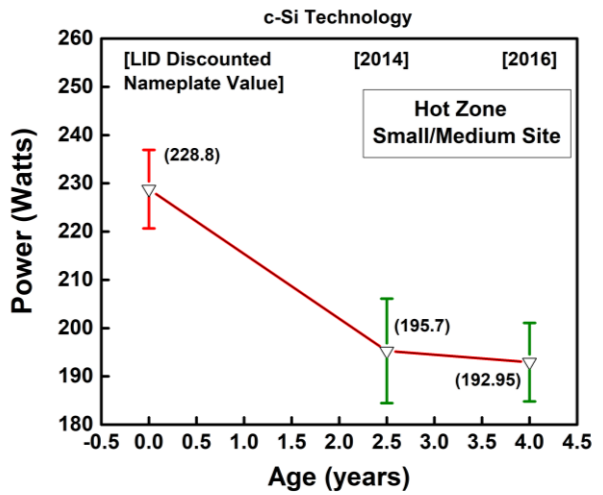
(f)
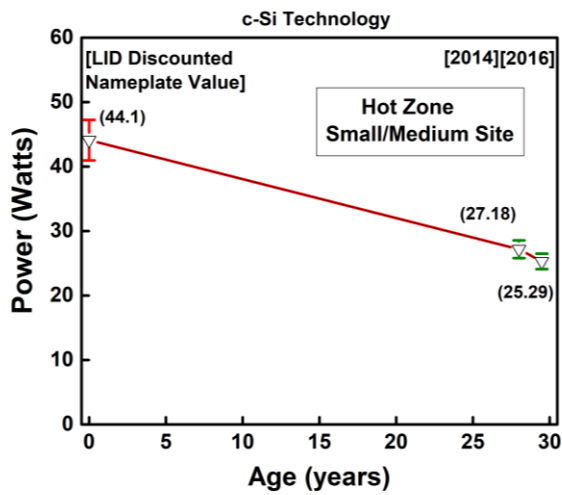
(g)
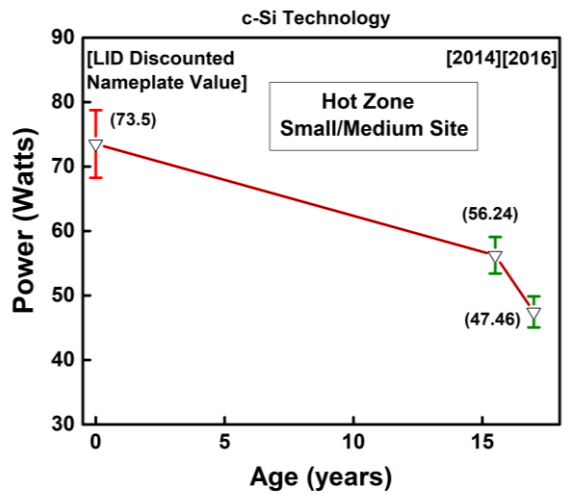
(h)
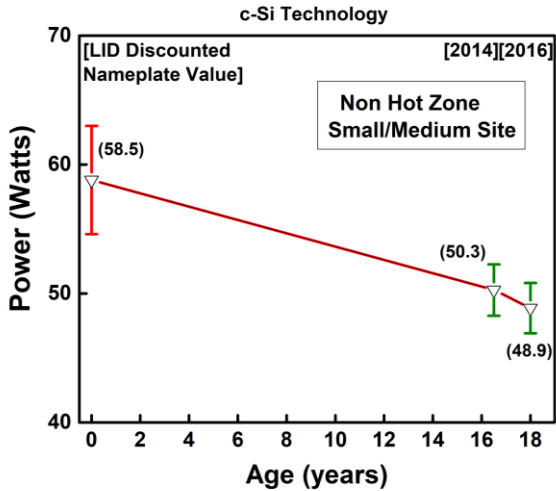
(i)
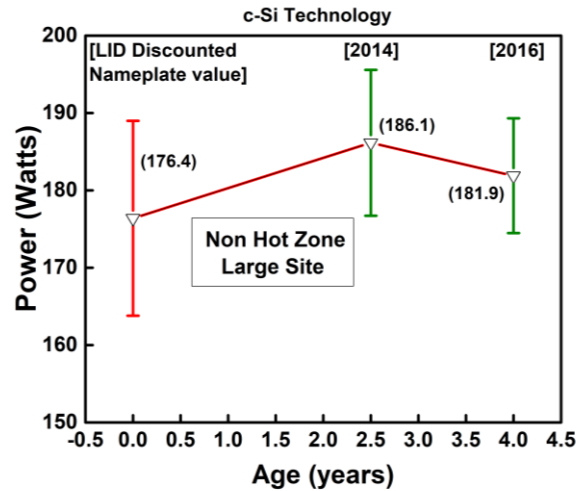
(j)

Fig. 4.77: Performance of the modules installed at 10 sites (a) through (j) which were repeated in 2014 and 2016 Survey.

Table 4.23 provides the average degradation rates of the repeat sites calculated by three different procedures:

a) LID discounted degradation rate based on 2016 Survey measurements

b) LID discounted degradation rate based on 2014 Survey measurements

c) LID degradation Rate based on difference in power output between 2014 and 2016 measurements

161

It can be seen that the degradation rates given in the second, and fourth columns of the table are mostly quite close to each other, but differ significantly from the values given in the third column. The average value of the LID discounted degradation rate as per 2016 measurements is 2.43 %/year. In some of the sites, the degradation rate between 2014 and 2016 are very high, which may be due to the error in translation and measurement. Also, it is important to note that the 2014 Survey was conducted in Sept-Nov (autumn) while the 2016 Survey was conducted in March-May (early summer).

Table 4.23: Degradation rates of repeat sites.

Figure Number	LID Discounted P_{max} (%/year) rate for modules measured in 2016	LID Discounted P_{max} (%/year) rate for modules measured in 2014	LID Discounted P_{max} (%/year) rate between 2014 & 2016
Fig. 4.72 (a)	3.99	3.31	3.56
Fig. 4.72 (b)	5.05	1.22	4.57
Fig. 4.72 (c)	1.03	0.18	0.71
Fig. 4.72 (d)	1.32	1.15	1.31
Fig. 4.72 (e)	2.14	1.55	2.03
Fig. 4.72 (f)	4.64	3.66	4.11
Fig. 4.72 (g)	2.52	1.30	1.41
Fig. 4.72 (h)	3.23	1.38	1.85
Fig. 4.72 (i)	1.13	0.81	0.91
Fig. 4.72 (j)	-0.76	-1.38	-0.92
Average of above sites	2.43	1.32	1.95

4.11 Summary

It is important to understand the performance of the PV modules in actual operating conditions in the field, considering the large investments which are being made for setting up utility scale PV power plants in the near future. The degradation rates have serious implications

on the return-on-investment calculations of investors, and can make the difference between a financially successful and an unsuccessful project. With the aim of understanding the long term reliability of PV modules in India, a comprehensive study was conducted for the first time in India. Field data obtained during the 2014 and 2016 All-India Surveys of Photovoltaic Module Reliability have been analyzed in detail. The analysis shows that there is a wide variability in the annual module degradation rate, and are generally higher than international benchmarks. It has been found that degradation rates degradation is higher in hot climates. Furthermore, the average power degradation rate for large installations is significantly lower than that for small installations. In addition cell cracks are the main reason for the high degradation rate in young modules falling in Group Y. Most of the Group Y modules are in young age category which implies low quality of these young modules.

The results which have emerged from this survey of PV module reliability in India provide useful indicators for future deployment in terms of location, technology type and due diligence required for module selection and handling during installation. The results from these surveys are very useful for the module manufactures, module installers, and operation and maintenance teams for improved performance of the PV module. The outcomes from the All India Survey of PV Modules Reliability have provided one of the most consistent observations of actual field performance anywhere in the world. From the analysis of the data collected in 2014 and 2016 Surveys, the following specific conclusions can be drawn:

- A total of 1148 and 925 modules have been inspected in 2014 and 2016 Survey respectively, which include good representations in most of categories like climate, site size, age, technology, and mounting configuration.

- The measurement and STC translation procedures together have been assessed and the maximum possible total error in P_{max} degradation rate has been found to be 9% and 5% for crystalline silicon modules measured above 500 W/m^2 and 700 W/m^2 respectively.

- It can be seen from both the surveys that there is a lot of variability in performance of crystalline silicon modules. Almost half of the surveyed sites of c-Si modules are performing reasonably well (Group X), while the rest of the c-Si sites (falling in Group Y) are not. Some sites show excellent performance, whereas some show

163

grave problems. These observations point to problems regarding module quality and/or installation procedures.

- Modules installed in Hot zones (Hot & Dry, Warm & Humid and Composite) show higher degradation rates compared to the modules deployed in Non-Hot zones (Moderate, Cold & Cloudy and Cold & Sunny). This warrants more attention to understanding the hot climate degradation mechanism, as well as accelerated testing and appropriate certification for these climates.

- In Group X, young modules (age <5 years) show a slightly lower degradation rate than old modules (age >5 years). However, if modules from Group A ('All' – Group X plus Group Y) are considered, young modules show a higher degradation rate than old modules. This indicates that young modules seem to have problems regarding quality of modules, installation, and/or possible over-rating.

- In old crystalline silicon modules the main contributor to the P_{max} degradation is I_{sc} followed by FF, whereas in the case of young crystalline silicon modules the main contributor to the P_{max} degradation is FF degradation. The fact that young modules show a higher degradation rate mainly due to FF degradation indicates the possibility of deliberate over-rating of the power of the module.

- Modules installed in large systems (size more than 100 kW) are degrading at a much lower rate (~0.7 %/year average Linear Degradation Rate for Group A) than modules installed in small systems of size less than 100 kW. All large systems fall in the 'good' Group X category. However, the modules from the large sites in only the Hot zone have an average Linear P_{max} Degradation Rate of 1.3 %/year which is much higher than the linear warranty. Also the young large systems are degrading at a higher rate than the old large systems in Hot zones. Hence, installers need to be cautious about the quality of materials and installation practices.

- Roof mounted modules suffer from a higher degradation rate as compared to ground mounted modules.

- Analysis of insulation resistance shows that more than 90% of the modules have passed the dry insulation resistance test. Also, 100% modules installed in the large system category have passed the dry insulation test which shows that large power plants are doing well with respect to the safety of the PV system.

- Modules in the Hot zones have shown larger percentage of interconnect failure as compared to the Non-Hot zones. Also the series resistance of the module increases with the increase in the severity of the interconnect failure which eventually reduces the power output of the module.

- Modules in Group Y sites have higher percentage of cracked cells than modules in Group X, which indicates poor handling of the modules during manufacturing, transportation and/or installation for Group Y sites. This conclusion is also supported by the higher percentage of mode A and mode C cracks observed in the young modules as compared to the old modules. Also, the quality of the materials (and possibly manufacturing processes) used in Group Y modules is a cause for concern, given that faster encapsulant and metallization discoloration is seen in these modules as compared to Group X modules.

- Rooftop sites show more cracked cells than ground-mounted sites, as are also seen in young sites compared to old sites. This again indicates poor handling of the modules during manufacturing, transportation and/or installation for rooftop and young sites.

- There is a good correlation between the total number of cracks in the module and the power degradation of the module.

- EL images are helpful in detecting cracked cells and broken interconnects in the module. Modules with snail trails have been found to have cracks in the corresponding cells.

This page is intentionally left blank.

This page is intentionally left blank.

Chapter 6

Accelerated Testing for Impact of Cell Cracks

6.1   Introduction

One of the key findings from the All India Surveys [248] [20] was that many modules, especially Group Y young modules (age less than 5 years), were suffering from high P_{max} degradation. The reason for this high value of P_{max} degradation was partly attributed to the development of a large number of cell cracks in the PV module. These cracks may have been developed during module manufacturing, or developed due to transportation or poor handling and installation. In our All-India Surveys, higher degradation is seen in the modules that have a large number of cracks. Hence, it was felt necessary to conduct a systematic study to understand the impact of cell cracks on the performance of the PV module over a wide range of mechanical

loading conditions. These accelerated tests have been performed by using the in-house Dynamic Mechanical Loading (DML) tool developed at NCPRE, IIT Bombay (refer Section 5.6). This tool can simulate the same types of loading on the PV module, which it experiences in the real field conditions, but with the possibility of accelerating the effects.

In this chapter, the sample selection and the test setup are presented first, followed by the results of the accelerated tests. Finally, the recommended parameters for performing dynamic mechanical testing parameters like pressure, frequency (number of cycles/minute) and number of cycles have been suggested.

6.2 Objectives of Accelerated Testing

The study on the impact of cell cracks on the performance of the PV modules was carried out by two sets of experiments. The aim of choosing these experiments was to experimentally validate that cracks in the PV module do lead to power loss, since cell cracks were found to be one of the most prominent degradation modes especially for the young modules. Furthermore, a methodology and test protocol was developed for the accelerated test in order to understand the impact of cracks on the performance of the PV module. In addition, this study also compares the response of two different interconnect designs to cracks. We have initiated the study to assess whether a different interconnect design can ameliorate the impact of cracks deployed in field in the future. The objectives of these experiments are described in Table 6.1.

Table 6.1: Objectives of the study on the impact of cell cracks on the performance of the PV module.

Sl. No.	Experiment Title	Objective
1	Effect of cracks on power loss of PV module with different interconnect designs	• To correlate the total dark area in the PV module EL image with the maximum power loss. • To compare the impact of cell cracks on the maximum power loss of the conventional busbar interconnect design and the mesh interconnect design (refer Fig. 6.1).
2	Effect of mechanical loading cycles' parameters on crack generation and power loss	• To find the effect of pressure/number of cycles/frequency on the transformation from Mode A to Mode B and Mode C cracks. • To compare the effect of frequency (number of cycles per minute) on the generation of cracks and the power loss.

6.3 Effect of Cell Cracks on Power Loss of PV Modules with Different Interconnect Designs

The field survey data have shown that cracks are more prevalent in power plants with high degradation rates. In order to understand the effect of cracks on the power loss, panels of two different interconnect design have been considered, which is discussed in detail in the following section. We have demonstrated the DML is an effective method for such an evaluation.

6.3.1 Methodology

6.3.1.1 Selection of Samples

The objective of the systematic study was to understand the effect of cell cracks on power loss of PV module and to correlate the power loss with the total dark area in the EL image. In addition, we also wish to explore how the different PV module interconnect designs affect the cracks and power loss. To conduct this experiment, two types of c-Si PV modules with different interconnect designs were examined. Of the two samples considered for the experiment, one was a mono c-Si PV module having a conventional busbar design (henceforth referred to as Sample A) having 4 busbars, and the other was mono c-Si PV module having the mesh type interconnect design (henceforth referred to as Sample B). The Sample A was procured in the year 2016 and Sample B was procured in the year 2018. Although both the samples were from the same manufacturer and were of the same technology, however, it is likely that the bill of material (BoM) for the samples would not be the same since they were manufactured in different years. The schematic of the two interconnect designs have been shown in Fig. 6.1 (a) for conventional busbar design and Fig. 6.1 (b) for mesh type interconnect design. The specifications of these samples have been described in Table 6.2, as initially measured on Spire Simulator at NCPRE, IIT Bombay.

Table 6.2: Specification of Sample A and Sample B.

Parameter	Sample A	Sample B
P_{max} (W)	330.80	333.35
I_{sc} (A)	9.15	9.10
V_{oc} (V)	46.35	46.38
FF (%)	77.96	78.94
No. of Cells	72	72

(a)   (b)
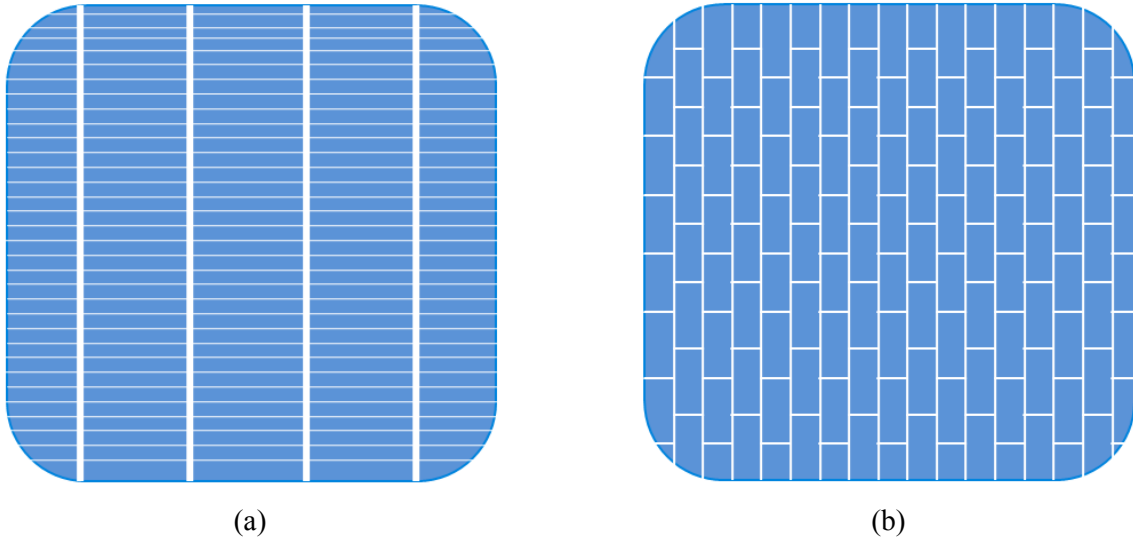
Fig. 6.1: The schematic of mono c-Si PV module cell having (a) conventional busbar interconnect design in Sample A and (b) mesh type interconnect design in Sample B.

6.3.1.2 Details of Test Protocol

To explore the effect of cell cracks on the power loss of the PV module, we adopted the test protocol as shown in Fig. 6.2 for the experiment. The two test samples (Sample A and Sample B) were initially characterized for lighted *I-V* and EL at I_{sc} and 10% of I_{sc} bias before applying any load. Subsequently, the test samples were subjected to mechanical loading by the DML tool in five different stages, operated with the set parameters described in Table 6.3. Figure 6.3 shows the

test sample (Sample A) placed on the DML tool. The test samples were characterized on Spire Solar Simulator 5200 SPL Blue for lighted *I-V* and Sensovation HR830 camera for EL imaging at the end of each Stage. Furthermore, EL video at short circuit current (using Sensors Unlimited SU320CSX InGaAs camera) has been captured continuously, while the test sample was under mechanical loading during every stage. EL images were also taken at every instance when the module was transported from DML setup for lighted *I-V* measurement to see if there are any cracks generated during handling.
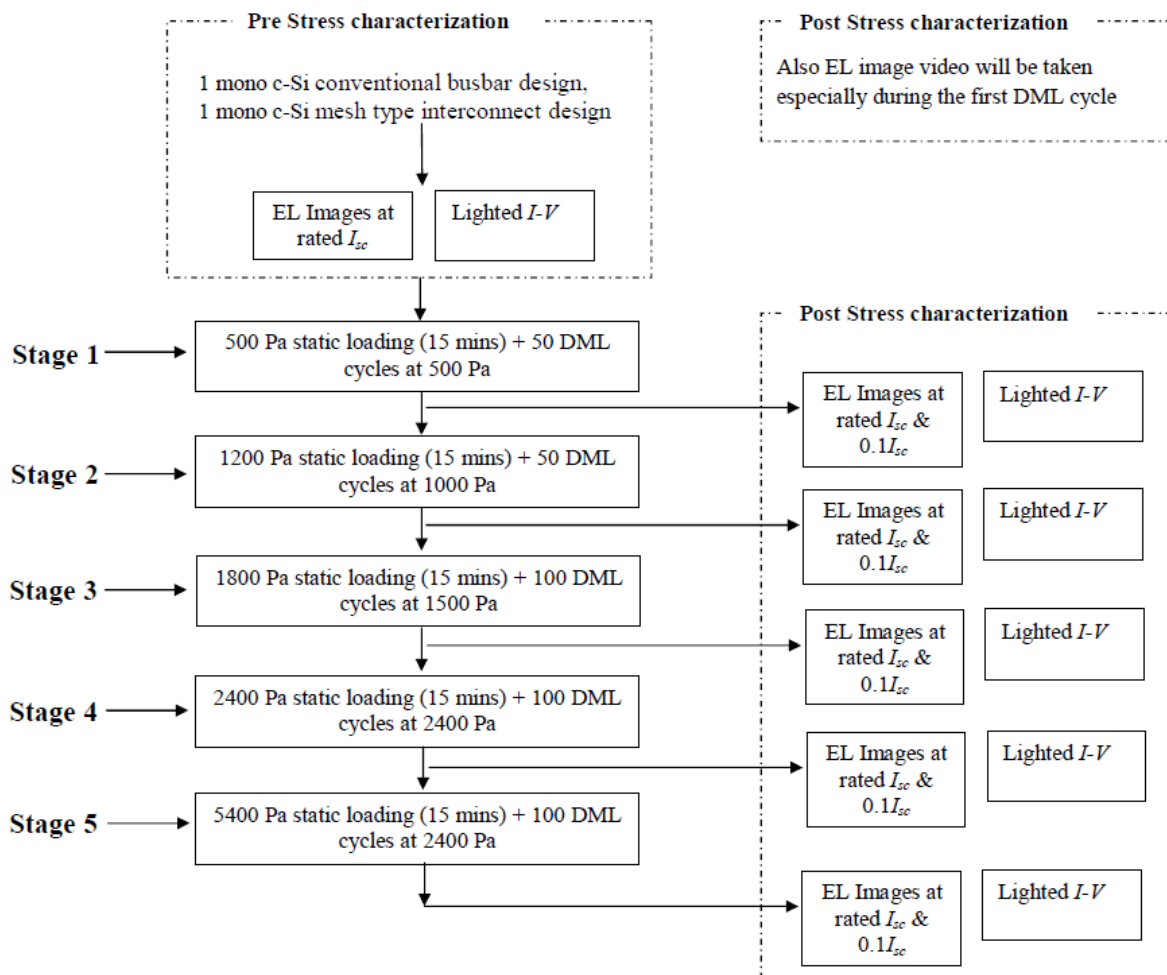
Fig. 6.2: Test protocol for the experiment.

Table 6.3: Operating parameters for the experiment.

	Operating Condition
Stage 1	500 Pa static loading for 15 minutes followed by 50 cycles of loading at 500 Pa
Stage 2	1200 Pa static loading for 15 minutes followed by 50 cycles of loading at 1000 Pa
Stage 3	1800 Pa static loading for 15 minutes followed by 50 cycles of loading at 1500 Pa
Stage 4	2400 Pa static loading for 15 minutes followed by 100 cycles of loading at 2400 Pa
Stage 5	5400 Pa static loading for 15 minutes followed by 100 cycles of loading at 2400 Pa

Fig. 6.3: Test module placed on the DML tool for accelerated testing.

6.3.2 Results and Discussion

In this section, the results of the experiments on two mono c-Si PV modules with different interconnect designs (conventional busbar interconnect and mesh type interconnect design) subjected to a combination of static and dynamic loading are presented. It was found that in both the interconnect designs that an increase in the loading (in terms of applied pressure or the number of cycles) causes an increase in the extent (number of cracks and the total dark area due to

the cracks) of the cracks. This is evident from the EL images of Sample A (conventional busbar interconnect design) and Sample B (mesh type interconnect design) shown in Fig. 6.4. It can be noticed from the EL images that at the lower magnitude (Stage 1 and Stage 2) of loading, Sample B is more affected as compared to Sample A. However, at the higher magnitude (Stage 3, Stage 4 and Stage 5) of loading both the samples are affected to a similar extent. Furthermore, from the EL images, it is seen that for both the interconnect designs (Sample A and Sample B) the cells at the corner of the modules show a higher extent of cracks whereas the cells in the center of the PV module are affected the least. Similar results have been reported by Gabor *et al.* [257].

Sample A

Sample B
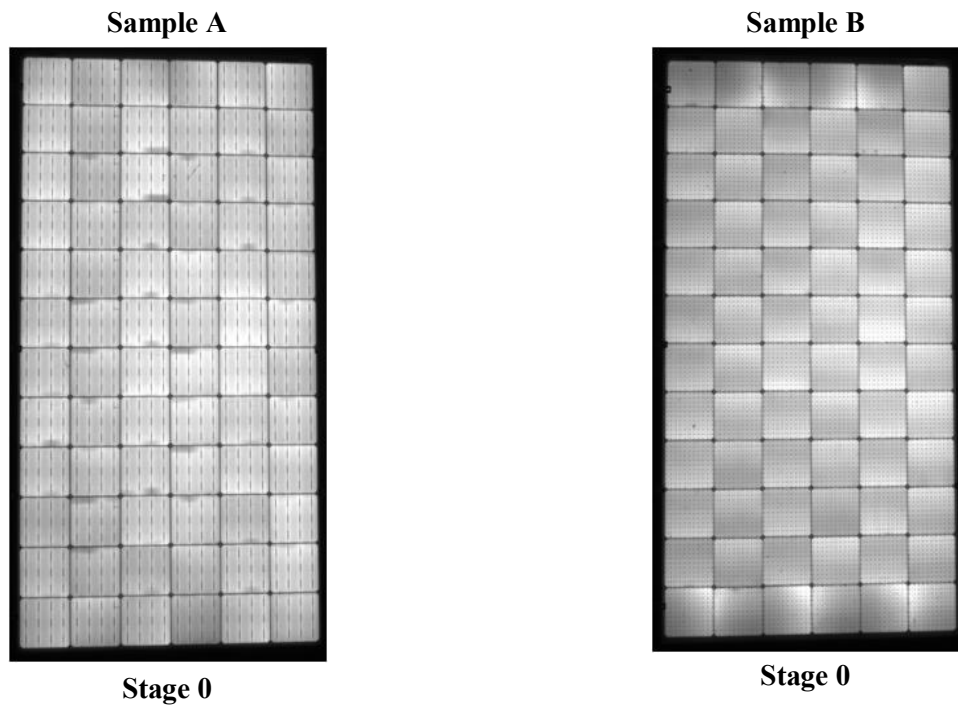
Stage 0

Stage 0

(a)
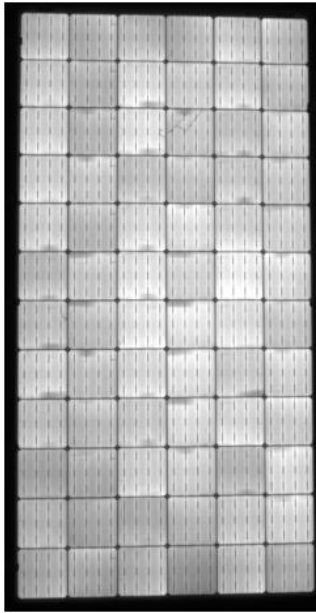
Sample A

Stage 1

Sample B
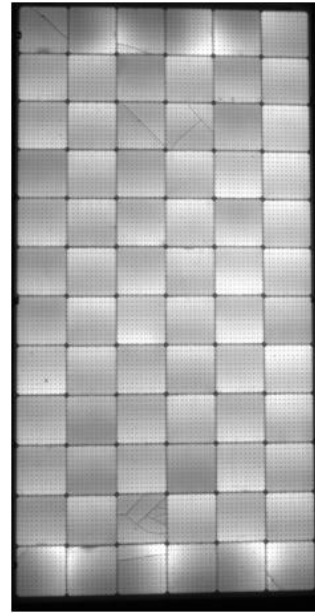
Stage 1

(b)

Sample A
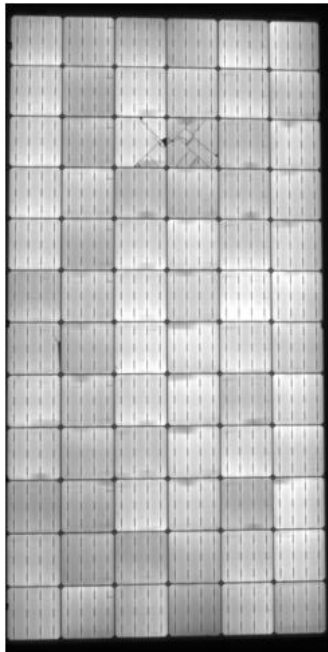
Stage 2

Sample B
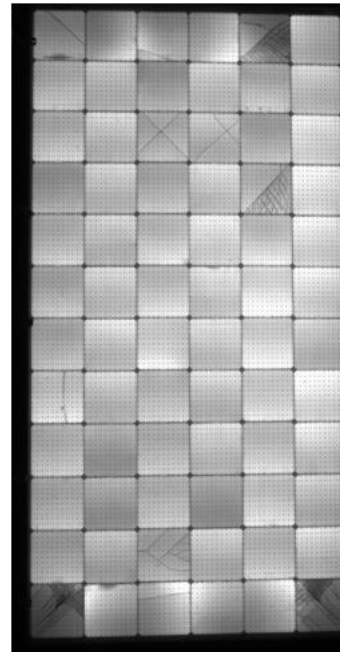
Stage 2

(c)

Sample A

Sample B

Stage 3

Stage 3

(d)

Sample A

Sample B

Stage 4

Stage 4

(e)

Sample A

Sample B

Stage 5

Stage 5

(f)
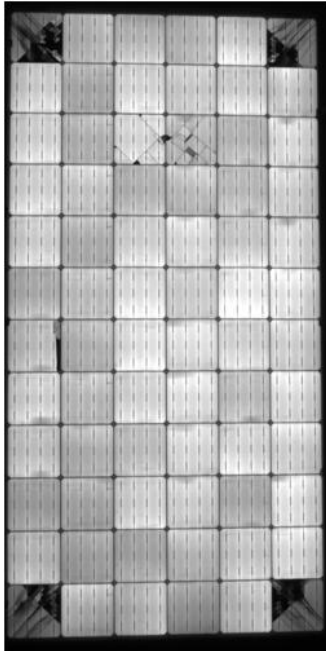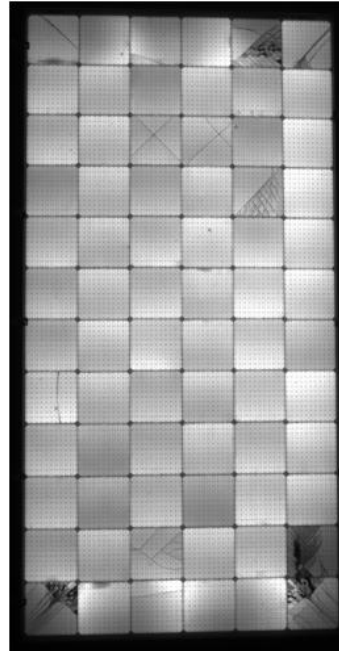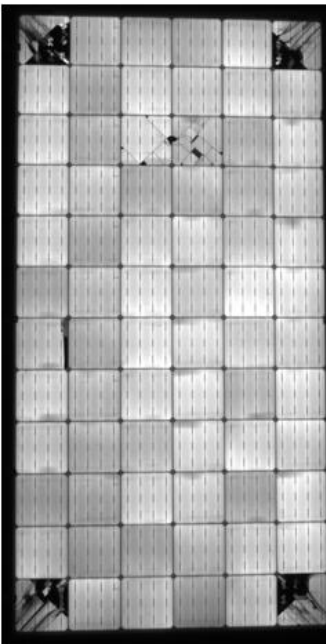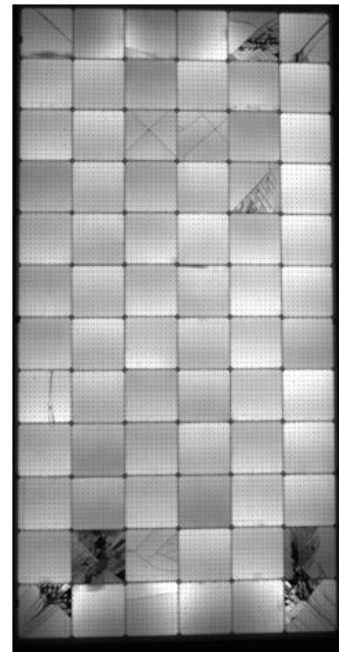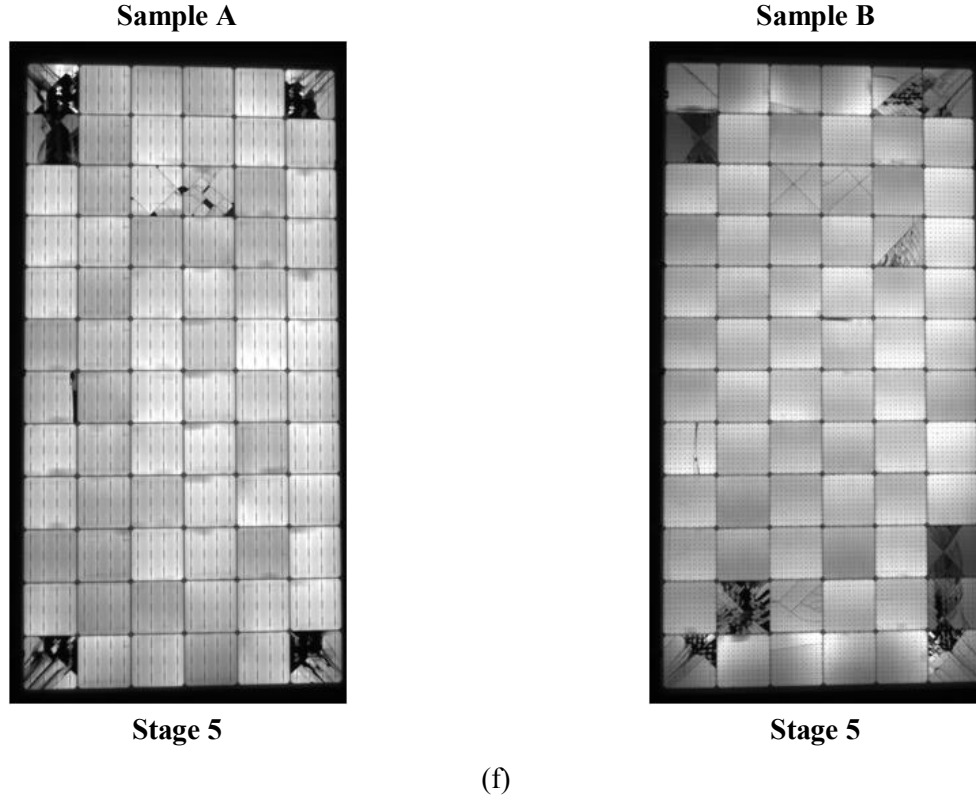
Fig. 6.4: EL images of Sample A (Left) and Sample B (Right) after (a) Stage 0, (b) Stage 1, (c) Stage 2, (d) Stage 3, (e) Stage 4 and (f) Stage 5

The current-voltage (*I-V*) characterization of the test samples was done at the end of each Stage (refer Section 6.3.1.2) on Spire Sun Simulator 5600 SPL Blue at STC. The *I-V* parameters such as P_{max}, I_{sc}, V_{oc}, and *FF* for both Sample A (pink) and Sample B (blue) were extracted and presented in Table 6.4. Figure 6.5 (a) for Sample A and Fig 6.5 (b) for Sample B shows the *I-V* plot at the end of Stage 5. From the Table 6.4, it can be seen at the lower magnitudes (Stage 1 and Stage 2) of loading Sample B shows higher P_{max} degradation as compared to Sample A which is due to the development of higher number of cracks in Sample B (refer Fig.6.4). However, the higher magnitude (Stage 3, Stage 4, and Stage 5) of loading Sample A shows higher P_{max} degradation as compared to Sample B. Even though from the EL images of the test samples (refer Fig. 6.4) it can be seen that Sample B shows slightly more number of cracks as compared to Sample A, however, Sample B shows lower P_{max} degradation. This leads to an inference that mesh type interconnect are better in collecting current and providing electrical contact even in the cracked cells. Furthermore, it can also be inferred as the mesh type interconnect minimizes the

electrically inactive region in the cracked cell. However, in order to substantiate the conclusion, this study needs to be repeated on more number of samples. The degradation in P_{max} in both the samples is mainly due to the degradation in FF, to a lower extent in V_{oc}, and the degradation in I_{sc} is least. This is attributed to the increase in the series resistance and cell mismatch due to the cracks in the cell. A similar observation has been found from the field survey data of the young modules showing cracks, measured during our All India Surveys [248] [20]. Furthermore, from the 2014 and 2016 Surveys, it has been found that the degradation rate increases with an increase in the number of cracks, which is also validated in this laboratory experiment. As explained earlier (refer to Chapter 4), this demonstrates that cracks and micro-cracks are definitely one of the causes of increased degradation seen in the poor-performing sites.

Table 6.4: *I-V* parameters for Sample A and Sample B after various stages.

	P_{max} % Degradation		I_{sc} % Degradation		V_{oc} % Degradation		FF % Degradation	
	Sample A	Sample B	Sample A	Sample B	Sample A	Sample B	Sample A	Sample B
Stage 1	0.46%	1.39%	0.07%	0.34%	0.36%	0.55%	0.04%	0.51%
Stage 2	0.59%	2.21%	0.11%	0.67%	0.34%	0.56%	0.13%	0.99%
Stage 3	3.84%	3.41%	0.24%	0.78%	0.89%	1.08%	2.74%	1.59%
Stage 4	5.48%	4.11%	0.26%	0.53%	1.00%	1.24%	4.28%	2.38%
Stage 5	6.58%	5.12%	0.28%	0.62%	0.69%	1.17%	5.66%	3.40%
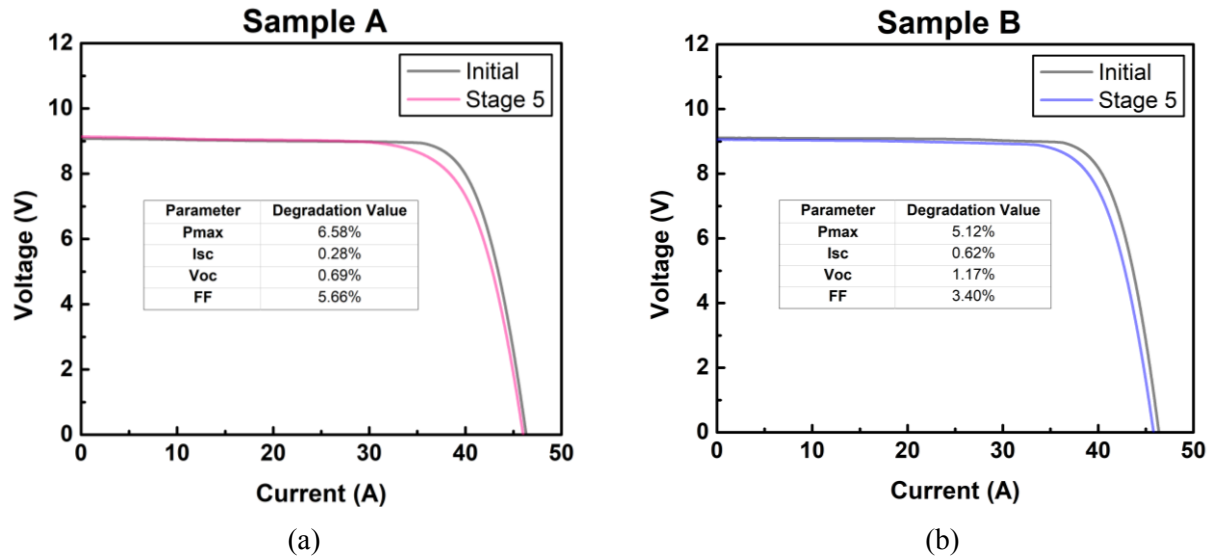
Fig. 6.5: *I-V* plot at the end of Stage 5 (a) Sample A, and (b) Sample B.

Figure 6.6 for Sample A and Fig. 6.7 for Sample B shows the screenshot of the EL video captured during the mechanical stress. These EL video was captured by using Sensors Unlimited (SU320CSX) InGaAs camera. Due to the low resolution of the EL camera, the EL video was captured for half of the PV sample. From Fig. 6.6 it is evident from the EL images (refer Fig. 6.6 (a) and (b)) that the cracks are closing when the outward pressure is applied (during blowing cycle) and they get open up (refer Fig. 6.6 (c) and (d)) when the inward pressure is applied (during the vacuum cycle). The opening of the cell crack is also confirmed by the current crowding at the corner of the cell which is evident from the EL image as it is bright. Similar observations were obtained for Sample B. This technique of capturing EL video while the PV module is under mechanical loading could help in understanding the origin and mechanism of the generation of cracks. A methodology for capturing the EL video has been described in this thesis.
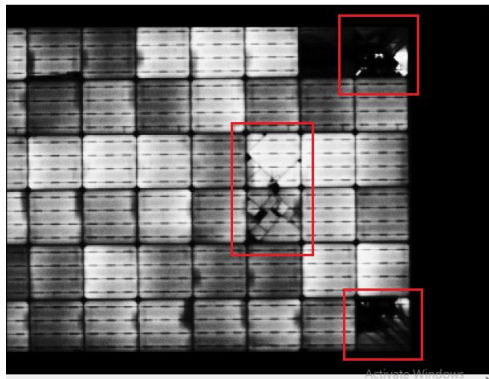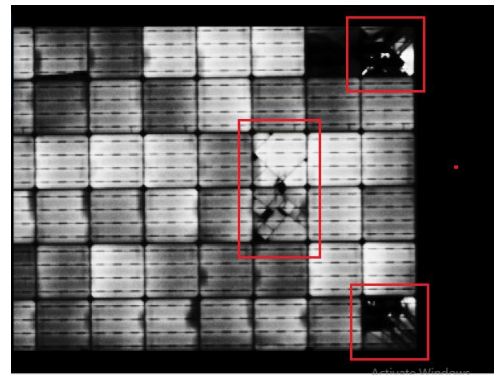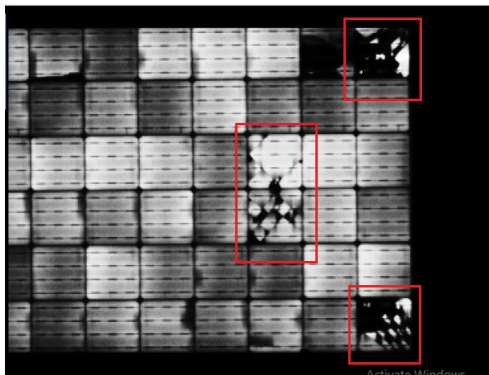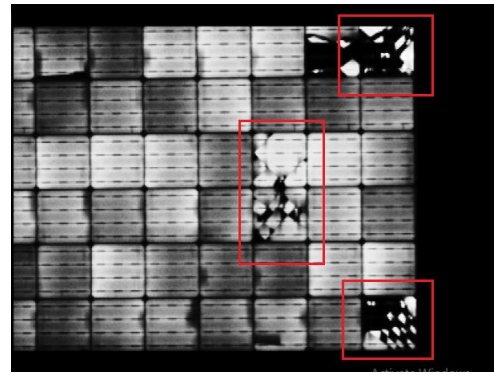
Fig. 6.6: Screenshot of EL video for Sample A (a), (b) for blowing cycling and (c), (d) for vacuum cycling. The cracks closed during blowing (outward pressure) appear bright in the EL image marked in red. The cracks open during the vacuum cycle (inward pressure) appear dark in the EL images marked in red. Also in (d) the corner appear bright due to current crowding confirms opening of cell cracks.
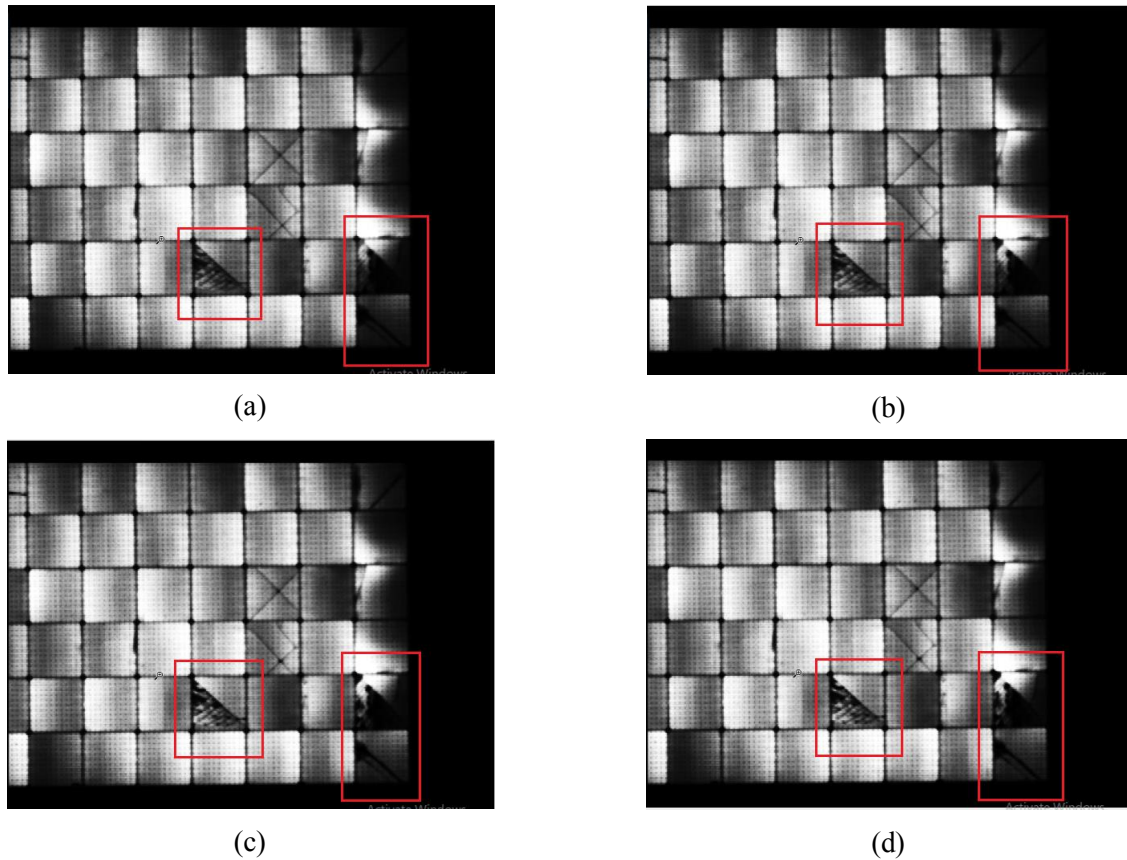
Fig. 6.7: Screenshot of EL video for Sample B (a), (b) for blowing cycling and (c), (d) for vacuum cycling. The cracks closed during blowing (outward pressure) appear bright in the EL image marked in red. The cracks open during the vacuum cycle (inward pressure) appear dark in the EL images marked in red. Also in (d) the corner appear bright due to current crowding confirms opening of cell cracks.

To correlate the total dark area in the PV module with the maximum power loss, the total inactive area in the PV module was calculated. To compute the total inactive area in the PV module using EL image, the pixel intensity at each point on the 8-bit EL image is compared with a threshold value, and it is considered to be inactive if the value is obtained to be less than the threshold. The threshold value is obtained manually by noting the pixel value which is considered to be inactive visually. Figure 6.8 shows an example of how the threshold value was identified manually. The value marked in red represents the pixel value considered for obtaining the threshold value. Subsequently, the total number of pixels less than the threshold in the EL image is obtained, and thus the percentage dark area is computed by comparing with the total number of pixels in the EL image. Figure 6.9 shows the percentage of degradation in P_{max} with the total inactive area in the EL images for Sample A and Sample B. The number on top of the data point in the figure represents the Stage at which the data was measured. The power degradation and the

percentage inactive area are obtained utilizing the *I-V* and EL characterization performed at the end of each stage. It is seen from the figure that increases in the extent of crack increases the power loss. It is also evident from the figure that Sample A (conventional busbar interconnect design) shows higher degradation in P_{max} compared to Sample B (mesh type interconnect) for similar inactive area. This may be attributed to the superior ability of mesh type interconnect design to collect current from the inactive regions compared to the conventional busbar interconnect design where the inactive region gets completely electrically separated. However, in order to substantiate the conclusion, this study needs to be repeated on more number of samples.

Fig. 6.8: Example for identifying threshold value in an EL image. The value marked in red represents the pixel value considered for obtaining the threshold value.
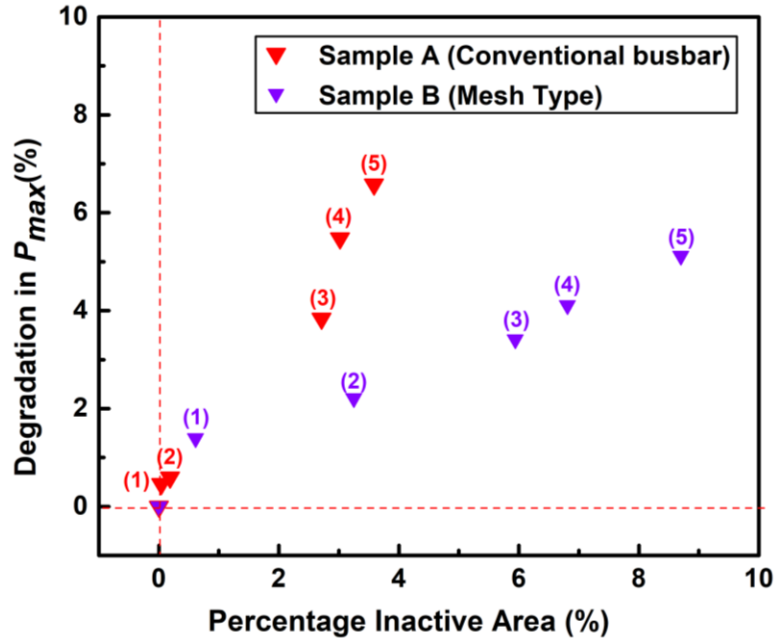
Fig. 6.9: Percentage degradation in P_{max} with the total inactive area in the EL images for Sample A and Sample B.

6.3.3 Conclusions of these Experiments

The effect of cracks on power loss of PV modules with different interconnect designs has been studied using the DML tool developed at NCPRE IIT Bombay. It was found that as the severity of cracks (in terms of total dark area in the cell and the number of cracks) increases, there is a reduction in P_{max} for both the designs of interconnects (conventional busbar and mesh type) examined in this study. The degradation in the P_{max} is mainly due to the degradation in *FF*. This is attributed to the increase in the series resistance and cell mismatch due to the cracks in the cell.

It has been found that both the interconnect designs develop cracks even at the low magnitude of loading (evident from EL images of Stage 1 and 2). It should be mentioned that Sample B shows more cracks under these conditions than Sample A, but this may be due to different (inferior) quality of the silicon wafers used for Sample B, and not the interconnect design itself. (As mentioned earlier the BoM used for the two cases is likely to be different.) At higher loading, where both samples show cracking, the power loss is *less* for Sample B, despite

Sample B showing higher number of cracks and larger inactive area. This seems to indicate that mesh type interconnect design is better in handling cracks, since the mesh interconnect design is better in collecting current from the cracked cells which leads to lower power loss inspite of having (possibly larger) inactive areas. The results shown above suggest that even with the large inactive or dark area in the module, the mesh type interconnect shows lesser degradation in power. However, this study needs to be repeated on more number of samples (ideally having the same BoM except for difference in interconnect), in order to substantiate the conclusion. If the result seen here based on 2 modules can be reproduced by further experiments, it may be possible to recommend the use mesh type interconnect modules for better power output when cracks in the cell cannot be completely avoided under some situations.

6.4 Effect of Mechanical Loading Cycle Parameters on Crack Generation and Power Loss

6.4.1 Methodology

6.4.1.1 Selection of Samples

The objective of this systematic study was to find the effect of the pressure, number of cycles, and frequency settings on the transformation from Mode A to Mode B and Mode C cracks, and also, to compare the effect of pressure, number of cycles, and frequency (number of cycles/minute) on the power loss and generation of cracks. To perform this study, a total of 3 sets of c-Si PV modules were examined. In each set, 1 mono c-Si with conventional busbar design, 1 mono c-Si with mesh type interconnect design, and 1 multi c-Si with conventional busbar design were considered. As mentioned in Section 6.3.1.1 the mono and multi c-Si conventional busbar design module was procured in the year 2016 and mono c-Si with mesh type interconnect design PV module was procured in the year 2018. Although all the samples were from the same

manufacturer and were of the same cell technology, it is likely that the BoM for the samples would not be the same since they were manufactured in different years. Table 6.5 summarizes the type and the number of samples used for this experiment.

Table 6.5: Type and total number of samples used in the experiment.

Type of Sample	Number
Mono c-Si PV module with conventional busbar design	3
Mono c-Si PV module with mesh type interconnect design	3
Multi c-Si PV module with conventional busbar design	3

6.4.1.2   Details of Test Protocol

To meet the objectives of this study, Fig. 6.10 shows the test protocol for conducting this experiment. This experiment has three Legs that define the three different sets of the conditions of applied pressure and frequency under which the test samples have been tested. In each Leg, three c-Si PV modules are tested. Table 6.6 shows the type of samples used in this experiment with assigned codes, henceforth used in this chapter. After every 1000 cycles, the test modules were characterized for lighted *I-V*, EL, dark *I-V*, and IR. Furthermore, the EL video at short circuit current has been captured continuously, while the test sample was under dynamic mechanical loading during the test.

Table 6.6: Test samples used in this experiment with assigned codes.

	Test Sample	Assigned Code
Leg 1	Mono c-Si PV module with conventional busbar design	L1MoCB
	Mono c-Si PV module with mesh type interconnect design	L1MoMT
	Multi c-Si PV module with conventional busbar design	L1MuCB
Leg 2	Mono c-Si PV module with conventional busbar design	L2MoCB
	Mono c-Si PV module with mesh type interconnect design	L2MoMT
	Multi c-Si PV module with conventional busbar design	L2MuCB
Leg 3	Mono c-Si PV module with conventional busbar design	L3MoCB
	Mono c-Si PV module with mesh type interconnect design	L3MoMT
	Multi c-Si PV module with conventional busbar design	L3MuCB
Note: L stands for Leg, Mo stands for mono c-Si, Mu stands for multi c-Si, CB stands for conventional busbar interconnect design and MT stands for mesh type interconnect design.		

EL, Lighted *I-V*, Dark *I-V*, Dark IR

Leg-1	Leg-2	Leg-3
1 mono c-Si (conventional busbar design)	1 mono c-Si (conventional busbar design)	1 mono c-Si (conventional busbar design)
1 mono c-Si (mesh type interconnect design)	1 mono c-Si (mesh type interconnect design)	1 mono c-Si (mesh type interconnect design)
1 multi c-Si (conventional busbar design)	1 multi c-Si (conventional busbar design)	1 multi c-Si (conventional busbar design)

(Slow DML as per IEC)

DML 1000 Pa, 10000 cycles, 5 cycles/min

(Fast DML)

DML 1000 Pa, 5000 cycles, 8 cycles/min

(Fast DML & High Pressure)

DML 2000 Pa, 5000 cycles, 5 cycles/min

Post Stress Characterization

EL (at I_{sc} and $0.1I_{sc}$), Lighted *I-V*, Dark *I-V*, Dark *IR* was measured after completion of every 1000 cycles.

EL video was captured continuously by the InGaAs detector camera, while test sample was under loading at I_{sc}.

EL, Lighted *I-V*, Dark *I-V*, Dark *IR*

Fig. 6.10: Test protocol for the study.

231

6.4.2 Results and Discussion

In this study, there are three Legs that define the three different sets of the condition of applied pressure and frequency under which the test samples have been tested. In each Leg, three c-Si PV modules were tested. Figure 6.11 (a) shows the total number of Mode C cracks and Fig 6.11 (b) shows total percentage inactive area in the test samples with an increasing number of cycles for Leg 1. It is evident from the figure that for all the three test samples (L1MoMT, L1MoCB, and L1MuCB) the number of Mode C cracks and the percentage inactive area initially increases with an increase in the number of cycles and gets almost saturated after 5000 cycles. It is supported, as an example, by the EL data of sample L1MuCB as shown in Fig. 6.12 (a) EL after 1000 cycles, Fig. 6.12 (b) EL after 5000 cycles and (c) after 10,000 cycles. From the figure, it is seen that there is an increase in the number of cracks upto 5000 cycles, and no change thereafter. Figure 6.13 shows the *I-V* parameter degradation of the test samples with an increase in the number of cycles for Leg 1. From the figure, it is evident that the degradation in the P_{max} gets saturated after 5000 cycles. Furthermore, it is seen from the figure that the main reason for the degradation in power is the degradation in *FF* whereas it is less affected by the degradation in V_{oc} and I_{sc}. Similar conclusions were obtained from our field studies that the main reason for the degradation in power for the young modules having cracks in the cell was the degradation in fill factor and least affected by the degradation in short circuit current. It is evident from the figure that L1MoMT shows the highest degradation in power and L1MoCB shows the least degradation in power. The reason for the higher degradation of L1MoMT as compared to the L1MoCB could be the higher percentage of inactive area in the module (refer Fig. 6.11 (a) and (b)). Furthermore, from the earlier Fig. 6.9, where it was seen that at the lower pressure of loading (500 Pa to 1000 Pa) mesh type interconnect shows higher degradation as compared to conventional busbar design. Since the pressure condition in Leg 1 is at 1000 Pa, a higher degradation in L1MoMT was observed as compared to L1MoCB. Furthermore, it should be noted that the degradation in power for all the test samples sees a saturating trend at 5000 cycles for the given test conditions (1000 Pa and 5 cycles/min) of Leg 1. Since it was observed that the number of cracks and the degradation in power gets saturated after 5000 cycles, it was decided to reduce the number of cycles for

testing the samples in Leg 2 and Leg 3, under the expectation that a similar saturation phenomenon would be seen in there.

(a)

(b)
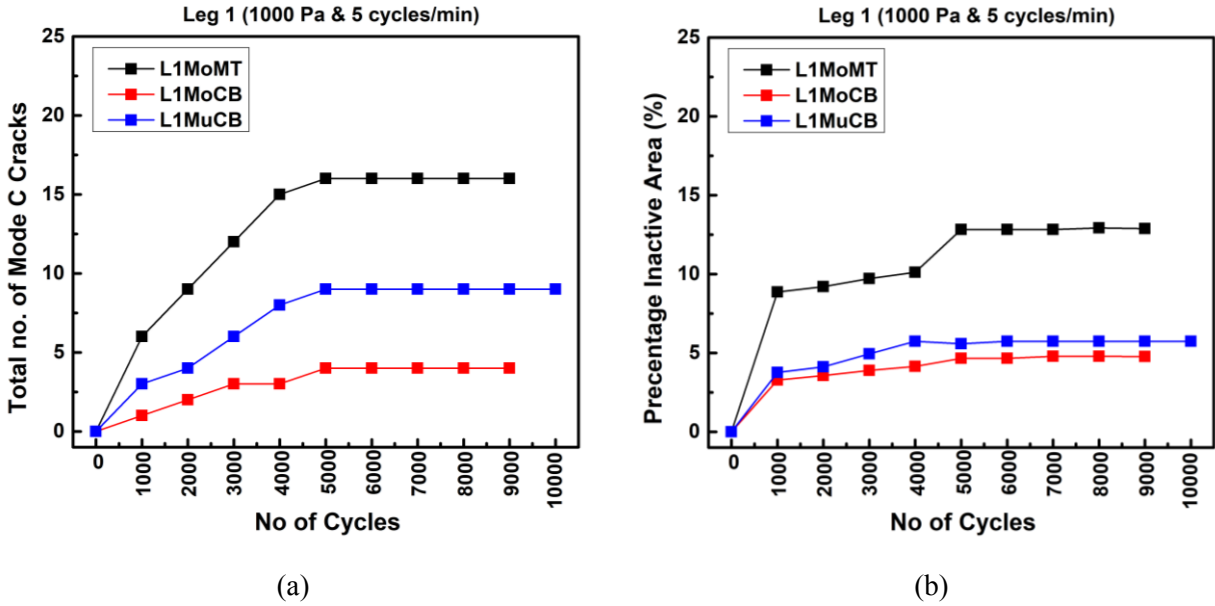
Fig. 6.11: (a) Total number of Mode C cracks and (b) Percentage inactive area in each test samples with the number of cycles for Leg 1.

(a)

(b)

(c)
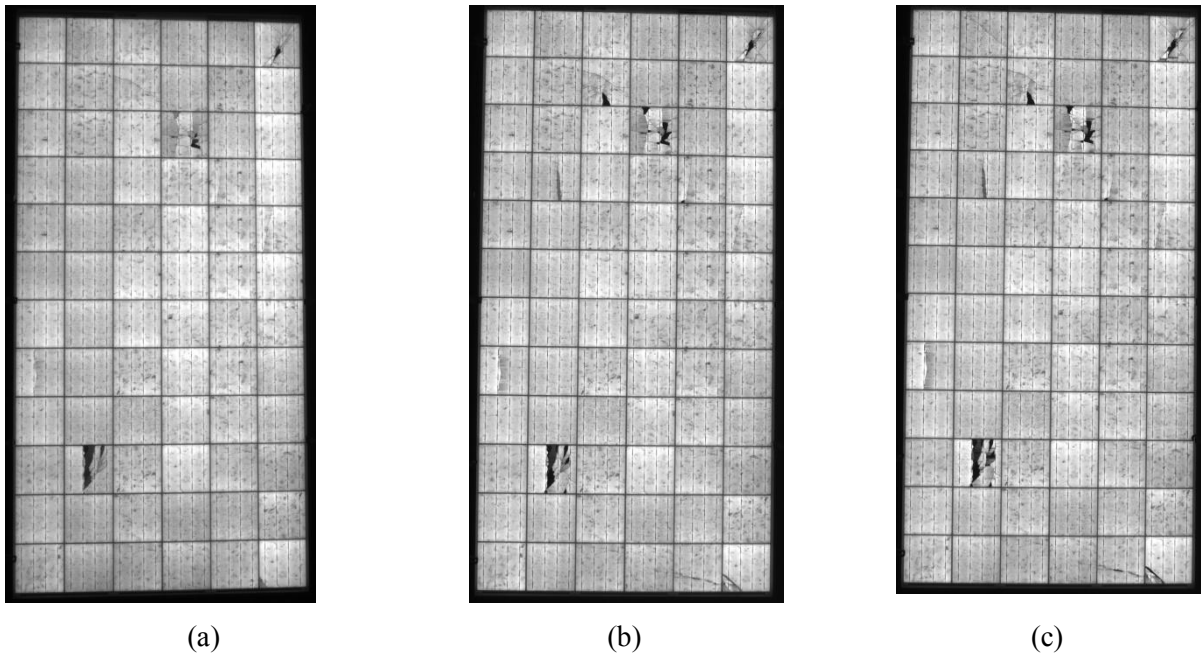
Fig. 6.12: EL image of L1MuCB after (a) 1000 cycles, (b) 5000 cycles and (c) 10000 cycles.
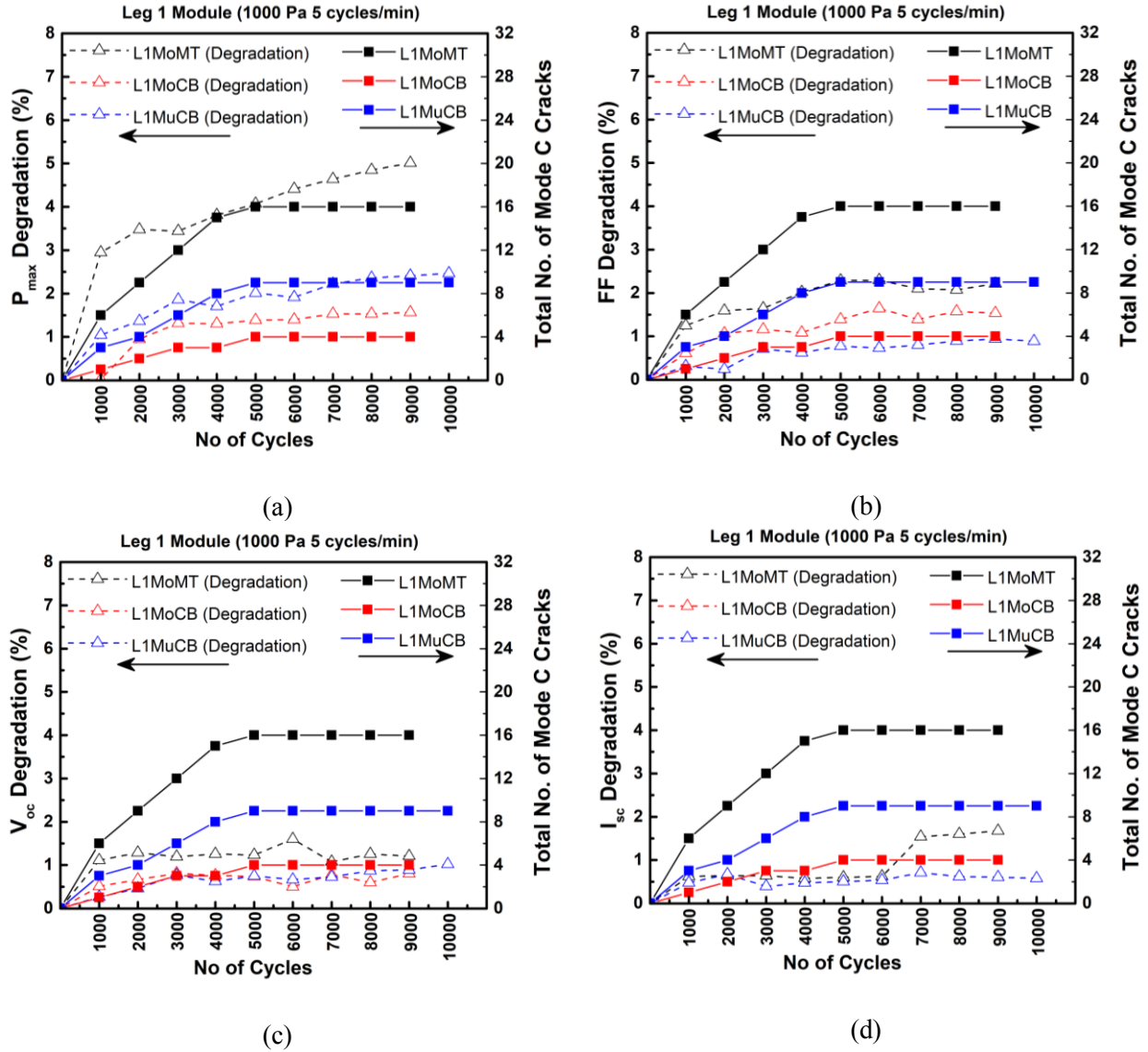
Fig. 6.13: Current-Voltage parameter *(I-V)* degradation with number of cycles (a) P_{max}, (b) *FF*, (c) V_{oc} and (d) I_{sc} for Leg 1.

To understand the effect of frequency (number of cycles/minute) another set of three c-Si modules (L2MoMT, L2MoCB, and L2MuCB) were tested in Leg 2 at the same pressure but increased frequency (1000 Pa and 8 cycles/min). Figure 6.14 shows the total number of Mode C cracks in the test samples with an increasing number of cycles for Leg 2. It is evident from the figure that for all the three test samples (L2MoMT, L2MoCB, and L2MuCB) the number of Mode C cracks initially increases with an increase in the number of cycles and gets saturated after 1000

234

cycles. The saturation occurs earlier here probably because of the increased frequency of cycling. Figure 6.15 shows the comparison of the total number of Mode C cracks with an increasing number of cycles for Leg 1 and Leg 2. It is evident from the figure that at a higher frequency the development of cracks in the test samples gets saturated at a lower number of cycles. Furthermore, it is also evident from the figure that the number of Mode C cracks in L1MoCB and L2MoCB is nearly equal when it gets saturated. Similar result was obtained from L1MuCB and L2MuCB. Table 6.7 summarizes the total number of Mode C cracks for the test samples in Leg 1 and Leg 2 when the number of cracks gets saturated.
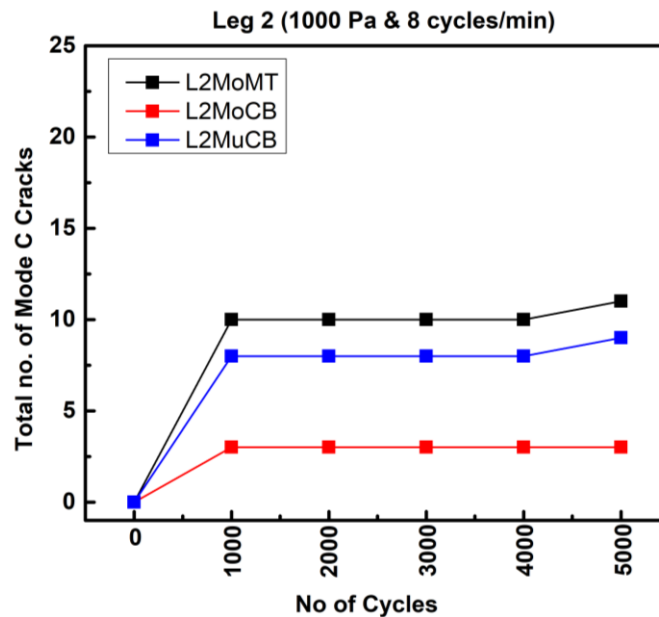
Fig. 6.14: Total number of Mode C cracks in each test samples with the number of cycles for Leg 2.
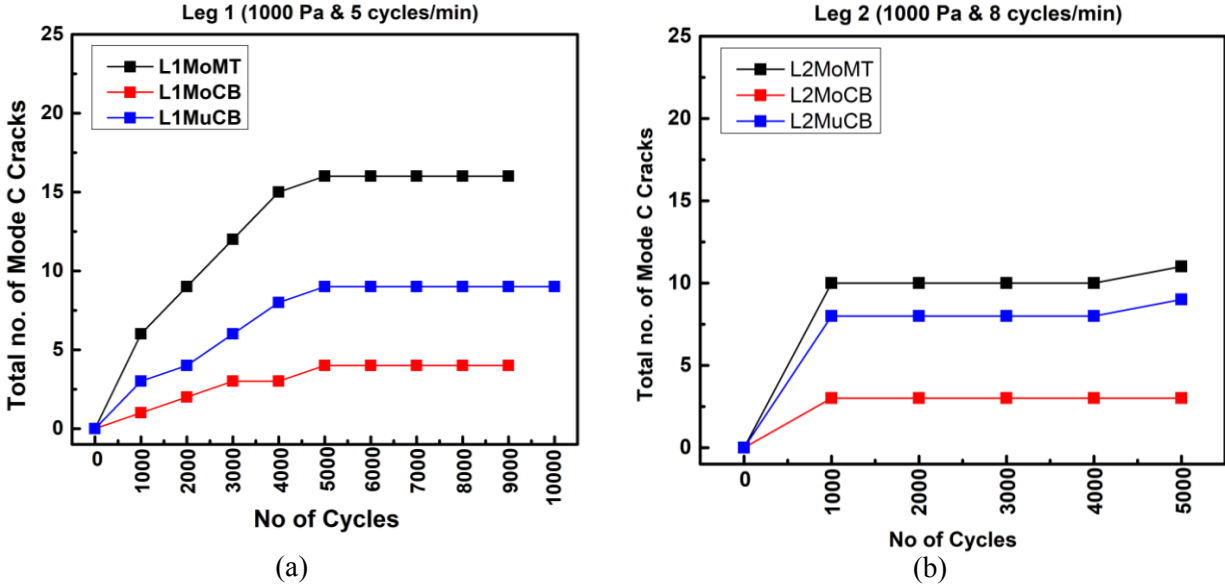
Fig. 6.15: Total number of Mode C cracks with the number of cycles for (a) Leg 1 and (b) Leg 2.

Table 6.7: Number of cracks for the test sample after saturation in Leg 1 and Leg 2.

	MoCB	MuCB	MoMT
	No. of cracks	No. of cracks	No. of Mode C cracks
Leg 1 (L1) (1000 Pa 5 cycles/min) after 5000 cycles	4	9	16
Leg 2 (L2) (1000 Pa 8 cycles/min) after 1000 cycles	3	8	11

The effect of frequency was also studied on the *I-V* parameters. Figure 6.16 shows the *I-V* parameter degradation of the test samples with an increase in the number of cycles for Leg 2. From the figure, it is evident that the degradation in the P_{max} gets saturated after 1000 cycles, consistent with the saturation in the number of cracks. Furthermore, it is seen from the figure that the main reason for the degradation in power is again the degradation in *FF*. Again for Leg 2 L2MoMT (mesh type interconnect) shows higher degradation in power compared to L2MoCB

and L2MuCB (conversational busbar design). As explained above the reason for the higher degradation of L2MoMT as compared to the L2MoCB could be the higher percentage of inactive area in the L2MoMT module. This leg is also at a low pressure of 1000 Pa, and as seen earlier, mesh type interconnect shows higher degradation as compared to conventional busbar design. Finally, it should be noted that the degradation in power saturates for all the test samples at 1000 cycles for the given test conditions (1000 Pa and 8 cycles/min) of Leg 2.

(a)

(b)

(c)

(d)
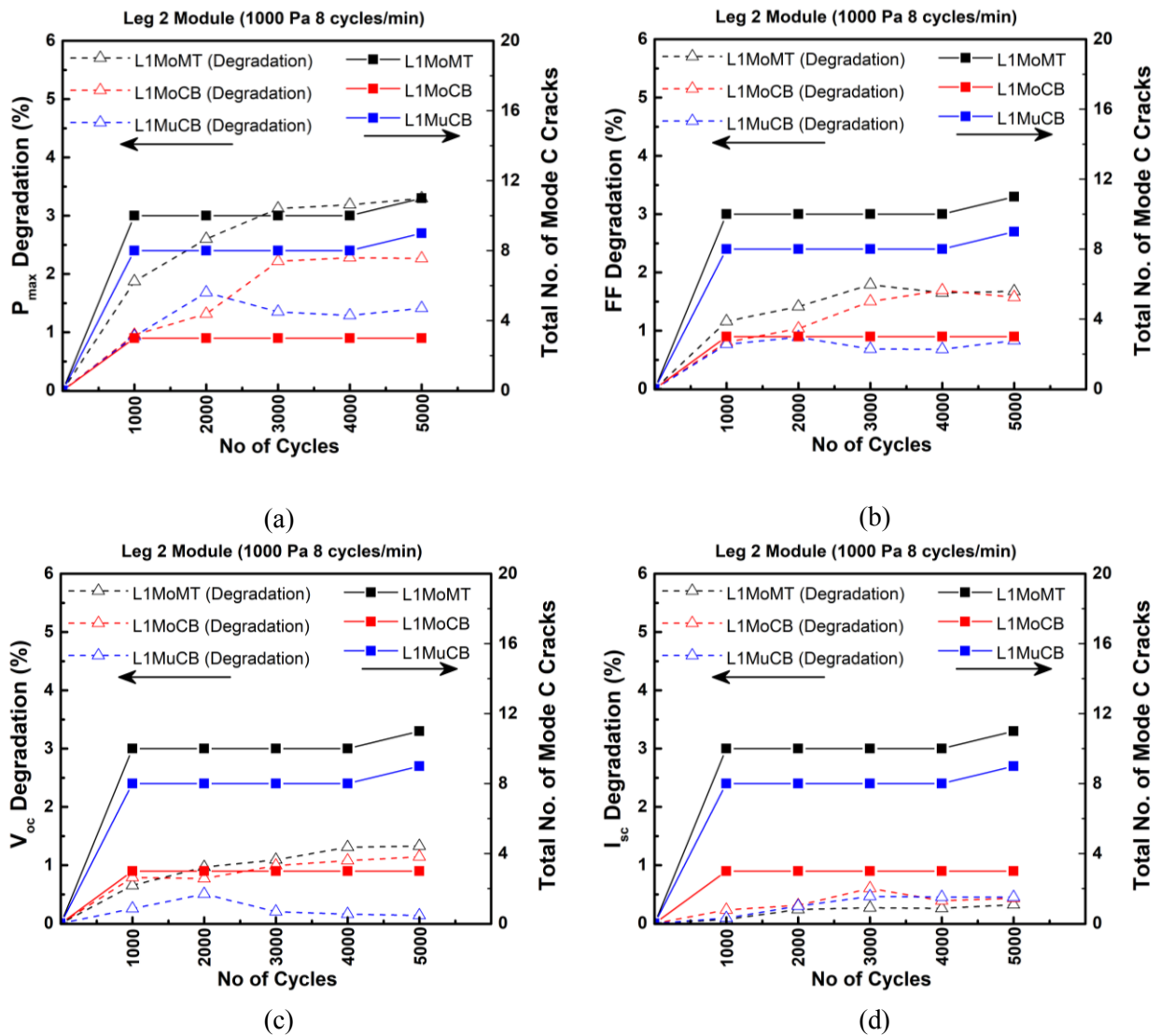
Fig. 6.16: *I-V* degradation with number of cycles (a) P_{max}, (b) *FF*, (c) V_{oc} and (d) I_{sc} for Leg 2.

In order to understand the impact of high loading pressure, another set of three c-Si modules (L3MoMT, L3MoCB, and L3MuCB) were tested in Leg 3 (2000 Pa and 5 cycles/min). Figure 6.17 shows the degradation in power for test samples with the number of cycles. It is evident from the figure that only mesh type interconnect L3MoMT sample could pass all the 5000 cycles at 2000 Pa pressure. The conventional busbar interconnect L3MuCB could pass only 1000 cycles, since the interconnect ribbon got disconnected (marked in red) as shown in the EL image in Fig. 6.18. Therefore no *I-V* data could be measured. This may be attributed to accelerated mechanical fatigue. It should be noted that there is no data point for L3MoCB since the glass of the test sample got broken during the DML cycle. Therefore no further test could be conducted. It could only be concluded that dynamic mechanical cycles at high pressure can cause a catastrophic effect (interconnect breakage and glass breakage) on the PV modules at high applied pressure.
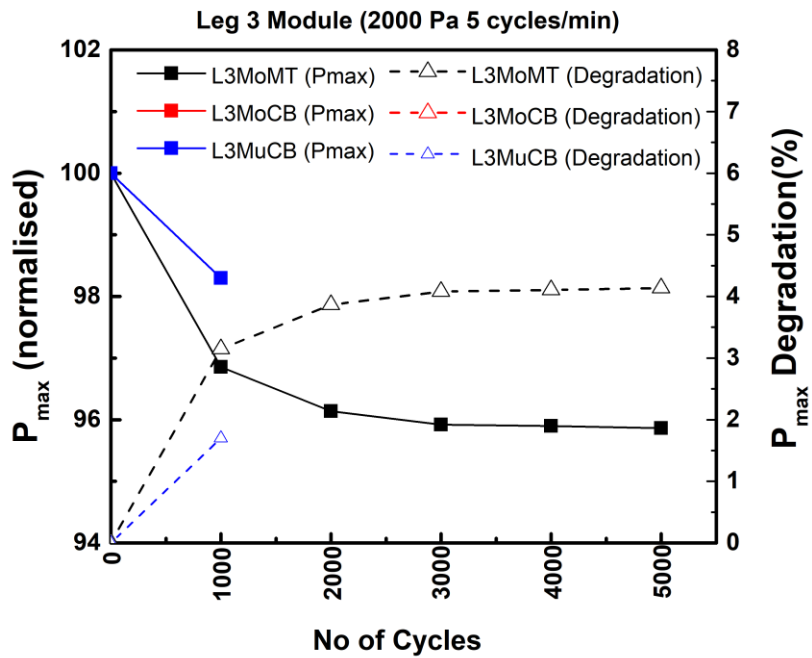
Fig. 6.17: *P_{max}* degradation with number of cycles for Leg 3.
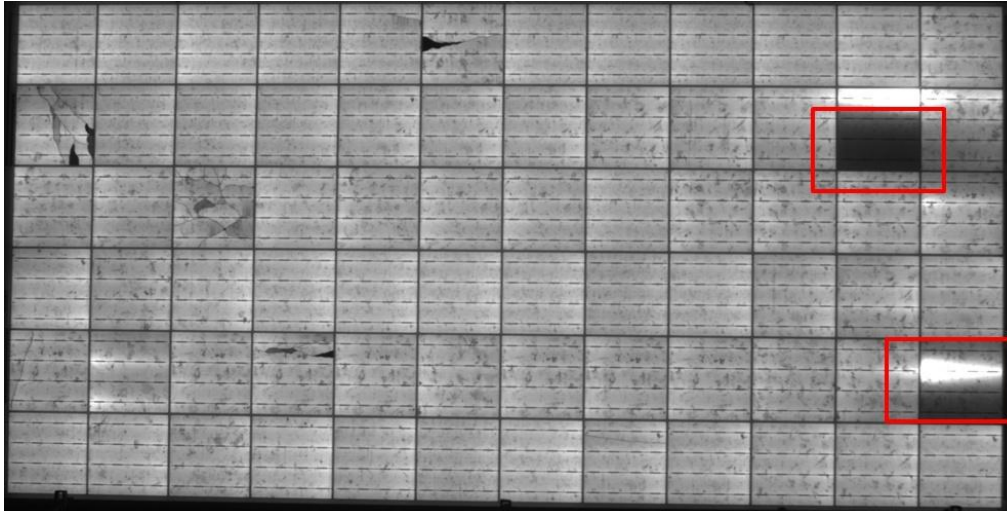
Fig. 6.18: EL image of L3MuCB after 1000 cycle. Interconnect failure (marked in red rectangle) can be seen in multiple cells.

Figure 6.19 (a) for L1MoMT, (b) L1MoCB, and (c) L1MuCB shows the dark *I-V* for test samples with the number of cycles. It is evident from the figure that for mesh type interconnect there is a deviation in the dark *I-V* curve between the initial pre-stress curve and after applying stress. The reason for this deviation in the L1MoMT could be the higher value of the dark area in the mesh type interconnect as compared to L1MoCB and L1MuCB (refer Fig. 6.11). Figure 6.20 (a) for L1MoMT, (b) L1MoCB, and (c) L1MuCB shows the comparison of dark *IR* (at short circuit current) and EL images after 5000 cycles. It can be seen from the figure that the dark area in the EL image can be seen as a cooler region in the dark *I-R* image (marked in red). This shows that the dark area in the EL image gets electrically isolated; hence it appears cooler in the dark *IR* image.
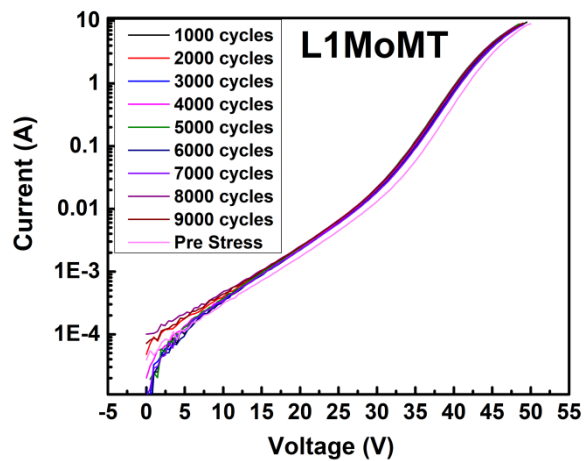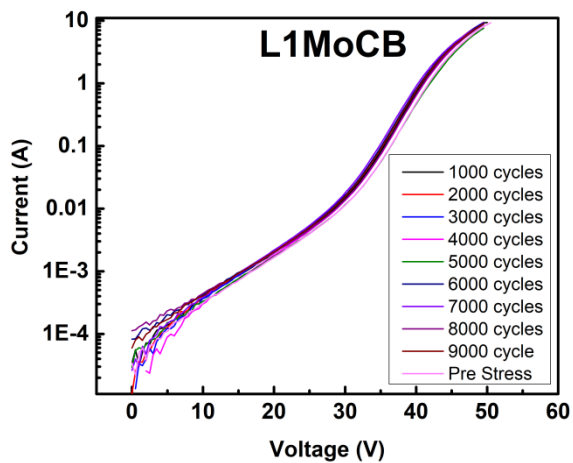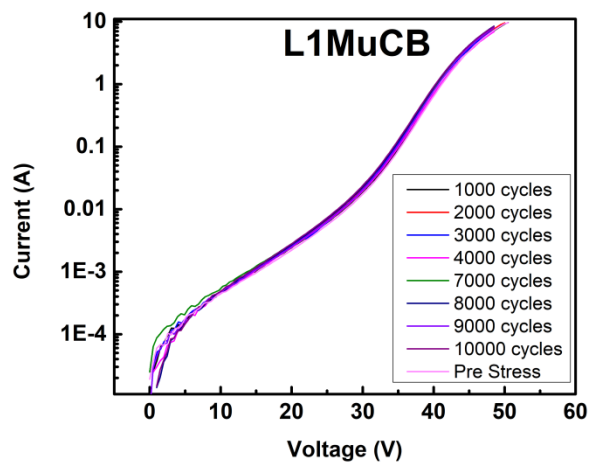
Fig. 6.19: Dark *I-V* (a) for L1MoMT, (b) L1MoCB and (c) L1MuCB shows the dark *I-V* for test samples with the number of cycles.
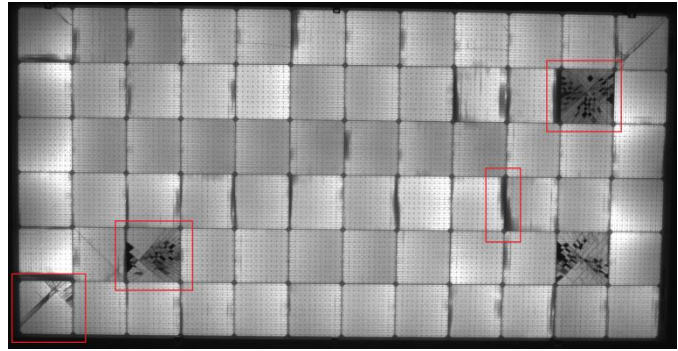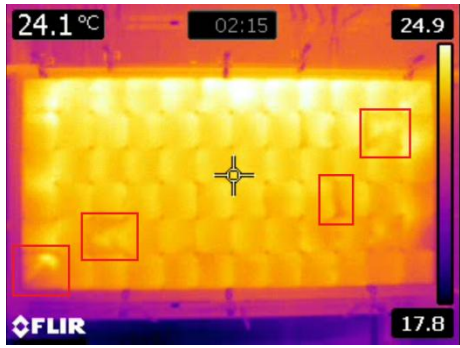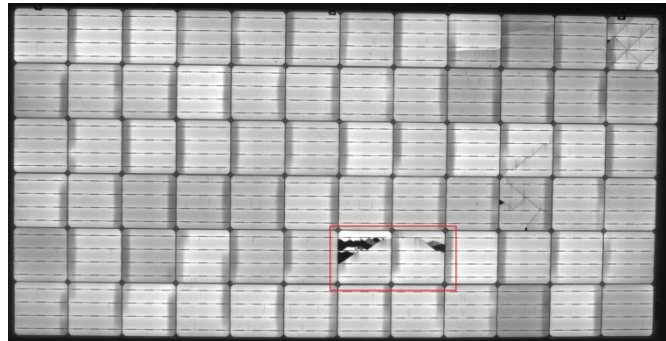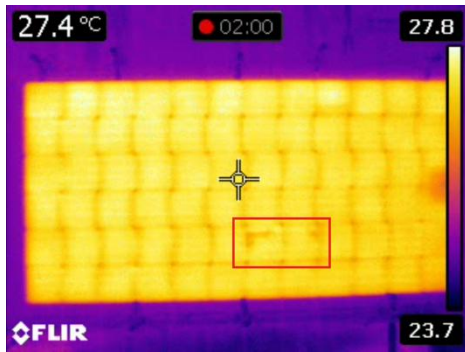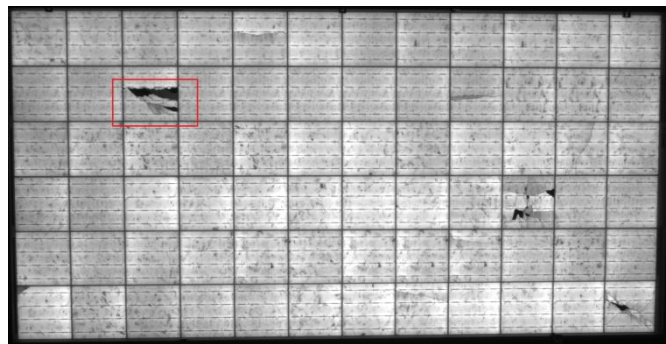
Fig. 6.20: Dark *I-R* (left) and EL (right) (a) for L1MoMT, (b) L1MoCB and (c) L1MuCB after 5000 cycles. Rectangle marked in red shows the similarity between the cracks in EL image and cooler region in dark *IR*.

6.4.3 Conclusions of these Experiments

The effect of mechanical loading cycle parameters on the crack generation and power loss has been studied using the DML tool. It has been found that mechanical loading at a lower pressure causes cracks in the cell, whereas a higher pressure causes cell cracks along with interconnects breakages. Furthermore, the degradation in power and the number of Mode C cracks both show a saturating trend (no impact on the crack generation and power loss after a certain number of cycles). Moreover, lower frequency (slow DML) requires more number of DML cycles to create cracks as compared to a higher frequency (fast DML). Since the saturation number of cracks is independent of number of cycles (at least for the conventional interconnect), accelerated testing in the laboratory appears to be a very feasible option, and this is an important conclusion. The degradation in P_{max} is mainly due to the degradation in FF and the degradation in I_{sc} is least. This is attributed to the increase in the series resistance and cell mismatch due to the cracks in the cell.

It has been apparently observed that mesh type interconnect showed higher degradation in power as compared to the conventional busbar design. As explained, the probable reason for the higher degradation of Sample B (mesh type interconnect) as compared to the conventional busbar design could be the higher percentage of inactive area in Sample B modules. Furthermore, it is evident from the earlier experiment (refer Fig.6.9) that at the lower pressure of loading (500 Pa to 1000 Pa) Sample B shows higher degradation as compared to Sample A (conventional busbar design) and since the pressure in both Leg 1 and Leg 2 is at 1000 Pa, this data set is consistent with that seen in Section 6.3. It should again be pointed out that the greater crack generation and higher power degradation seen for Sample B (mesh type) compared to Sample A(conventional) is possibly due to difference in cell and/or BoM quality, and not a function of type of interconnect. Our attempt to go to higher pressure unfortunately did not succeed. More comparative studies with increased number of samples on mesh type and conventional interconnects are required, but our limited data set shows that the mesh type or grid design may have the potential to minimize power degradation even in the presence of significant crack generation.

Finally an important observation for all types of samples was that the number of cracks generated and the corresponding power degradation saturates after a certain number of cycles. This provides a basis for the protocol to be followed in an accelerated mechanical loading test. Based on our results, the proposed recipe for the accelerated dynamic mechanical loading is 1000 Pa pressure at 8 cycles/min and 1000 number of cycles.

6.5   Connection of Field and Laboratory Studies

It was felt that the key results obtained in the field studies on the impact of cell cracks on the performance of the PV module may benefit by being further investigated through a systematic laboratory study. This became the motivation for the development of the Dynamic Mechanical Loading tool at NCPRE, IIT Bombay. In this section, the connection or the similarities between the key findings from field and the laboratory study is presented. Figure 6.21 shows the comparison of the impact of cell cracks on the power loss of the PV module by field and laboratory data. From both the studies it can be concluded that the degradation in power increases with an increase in the number of cracks in the PV module.
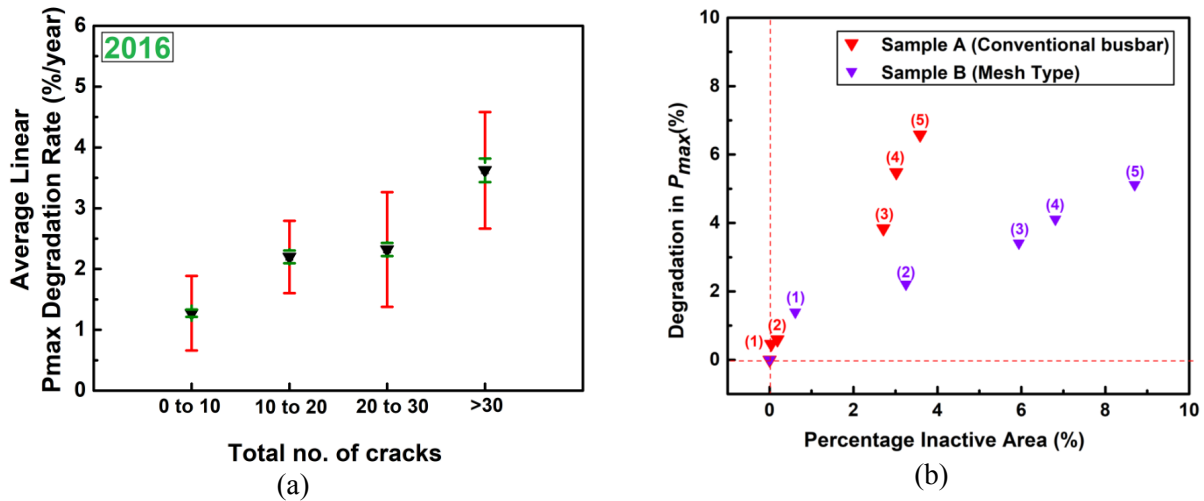
Fig. 6.21: Comparison of impact of crack on the power loss (a) 2016 field and (b) laboratory data.

To check which *I-V* parameter is responsible for the degradation in power due to cracks, we compare the field and laboratory data (of Fig. 6.9). In particular, the field data and the laboratory *FF* data are reproduced again in Fig. 6.22. It is seen from the figure that from both the studies, the main reason for the degradation in power modules is attributed to fill factor (*FF*) degradation. The correlation of power loss with number of cracks, and also the identification of *FF* as the main contributor to power loss are similar in both the field study and the laboratory study. We therefore have reasonable confidence in our ability to predict field phenomena (with respect to cracks) from laboratory studies. In addition, as our results in this chapter show, we can perform accelerated studies in the laboratory. The saturation effect is very pertinent, as it indicates the maximum effect which will be seen, and this can be achieved in a short time instead of waiting for years in the field. This will prove to be extremely useful, for example, in assessing the relative resistance to crack development in different types of modules (not just different interconnect designs) in the laboratory before deploying them in the field.
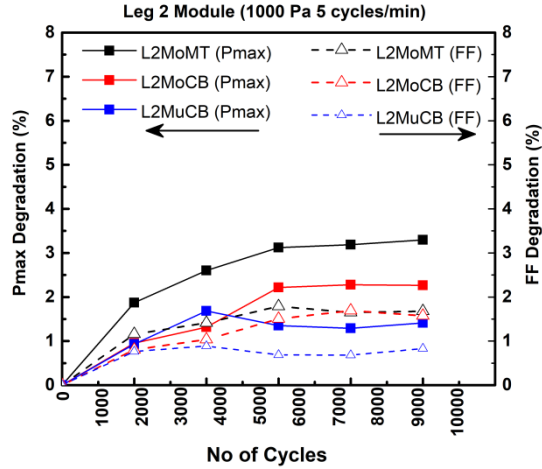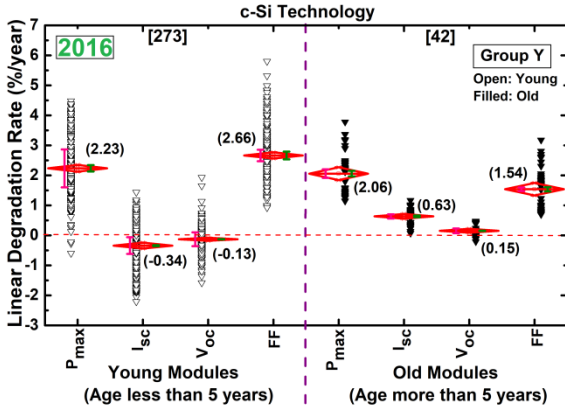
(a)

(b)
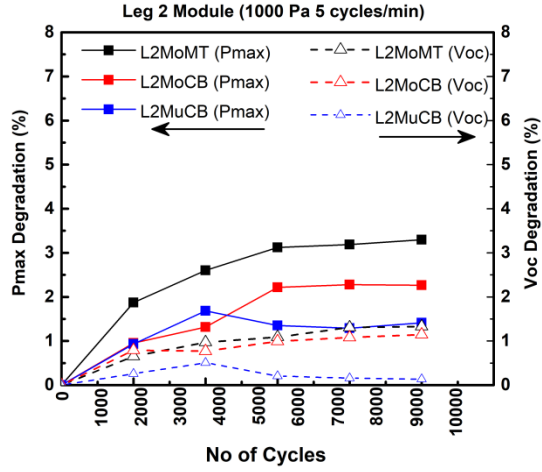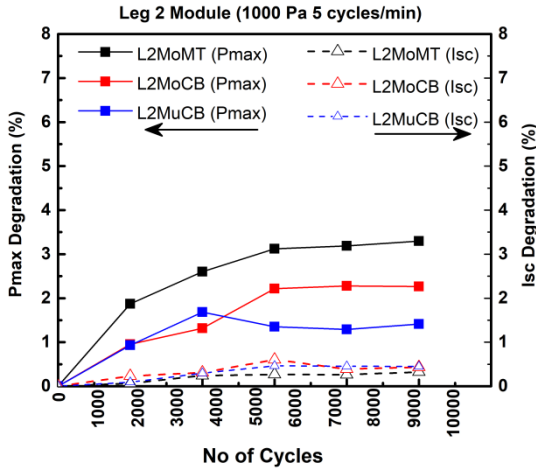
(c)

(d)

Fig. 6.22: Comparison of impact of crack on the *I-V* parameter (a) 2016 field, (b), (c) and (d) laboratory data.

6.6 Summary

The data from field surveys has indicated a relation between the cracks in the solar panels and the degradation rate of the panels. This relationship has been investigated in detail in this chapter, using the DML tool developed at NCPRE IIT Bombay. We have used the DML tool to study two types of modules with different interconnects. It has been found that the output power decreases with increase in severity of the crack (in terms of total dark area in the cell and the

number of cracks) for both the designs of interconnects (conventional busbar and mesh type) examined in this study. Fill factor degradation is the main contributor to the power degradation, followed by V_{oc} and I_{sc}. This degradation is attributed to the increase in the series resistance and cell mismatch due to the cracks in the cell. Of the two types of interconnects compared in this study, the mesh type interconnect is found to be less affected in power loss due to crack formation as compared to the conventional interconnect design for applied pressure of greater than 1000 Pa. This shows that mesh type interconnect design may be better in handling a higher magnitude of loading as compared to conventional interconnect design. However, more comparative studies with increased number of samples on mesh type and conventional interconnect are required to substantiate this observation.

The effect of mechanical loading cycle parameters on the crack generation and power loss has also been studied on both types of interconnects designs. Mechanical loading at a lower pressure has been found to cause cracks in the cell, whereas higher pressure causes cell cracks along with interconnects breakages. Furthermore, it has been found that there is saturation in the power loss after a certain number of cycles. Lower frequency (slow) DML requires more number of DML cycles to create same level of cracks as compared to high frequency (fast) DML. This helps us to identify an accelerated test protocol for dynamic mechanical loading. The proposed recipe for this accelerated testing is 1000 Pa pressure, 8 cycles/min and 1000 number of cycles. This accelerated testing of panels can be used to assess the resilience of modules from different manufacturers with different technologies and BoMs.

Chapter 7

Conclusions & Scope of Future Work

7.1   Conclusions

Currently, there is a worldwide push for renewable energy. As a result, utility-scale solar PV installations have increased significantly and also large investments are being made for setting up utility scale PV power plants in the near future. These PV modules undergo degradation upon exposure to the outdoor environment. Environmental factors like high operating temperature, humidity, and mechanical loading cause degradation in the individual components of the PV module. As a result, it affects the long term reliability and the durability of the PV module. The degradation rates have serious implications on the return-on-investment

calculations of investors, and can make the difference between a financially successful and an unsuccessful project. Hence, it is important to accurately measure the power generation of the deployed modules and determine the degradation which can help us to predict the actual performance over the long term.

With the aim of understanding the long term reliability of PV modules in India, a comprehensive study was conducted for the first time in India. This thesis reports the results of the comprehensive study. The study included collecting field data from solar PV installations under diverse conditions from all over the country, and a detailed analysis of the data. During the field trips, it was realized that specialized field-capable instruments are needed, and this thesis also describes the development of such instruments, and their use in the field. Furthermore, it was felt that some aspects of the degradation seen in the field need to be studied more systematically in the laboratory, and as a consequence, a novel lab-based equipment was developed, and used to conduct detailed accelerated tests on PV modules. The thesis describes this aspect as well.

The All-India Surveys of PV Module Reliability were conducted in 2014 and 2016 in different parts of the country to identify the major degradation modes in different climatic zones. It has been found from the surveys that there is a lot of variability in the performance of crystalline silicon modules. Almost half of the surveyed c-Si modules (Group X) are performing reasonably well, while the rest of the modules (falling in Group Y) are not. Some sites show excellent performance, whereas some show grave problems. The reason for poorly performing Group Y modules has been investigated. Cracks in the cell have been found to be a major degradation mode in the young modules. The effect of cell cracks on the electrical degradation of the surveyed modules has been studied. Several characterization tools such as an inexpensive and robust EL camera and temperature co-efficient device have been developed. Besides, field characterization methodologies like daylight electroluminescence imaging and temperature coefficient measurement of PV module have also been developed. These characterization tools and methodologies have assisted in measuring useful data in the field and helped in a better understanding of the various degradation modes prevalent in different climatic zones. Furthermore, a novel DML tool was developed which can simulate similar conditions of loading on the PV module in the laboratory. Accelerated tests in the laboratory using the in-house developed DML tool have been performed to understand the effect of cracks on power loss of PV

248

module with different interconnect designs, and also the effect of the mechanical loading cycle's parameters on the crack generation and power loss. Furthermore, it establishes the importance of the DML tool which enables similar and repeatable loading conditions on the test samples. This helps in developing a good test protocol for accelerated testing. The major conclusions from our study are summarized below.

1. **Effect of various degradation modes prevalent in Indian climatic conditions**

- A lot of variability in performance of crystalline silicon modules has been found which leads to a conclusion that there are some sites which are performing reasonably well (which we classified as Group X sites). However, there are modules in Group Y sites which show grave problems. The average Linear Degradation Rate is 1.25%/year for 2014 Survey and 0.89 %/year for 2016 Survey for Group X sites. The average degradation rate even after LID discounting for the Group Y sites is high – 2.34%/year for 2014 Survey and 2.21%/year for 2016 Survey which is a matter of concern. These observations point to problems regarding module quality, installation procedures and/or transportation issues.

- Modules installed in Hot zones (Hot & Dry, Warm & Humid and Composite) show higher degradation rates compared to the modules deployed in Non-Hot zones (Moderate, Cold & Cloudy and Cold & Sunny). This warrants more attention to understanding the hot climate degradation mechanism, as well as accelerated testing and appropriate certification for these climates.

- In Group X, young modules (age < 5 years) show a slightly lower degradation rate than old modules (age > 5 years). However, if modules from Group Y are considered, young modules show a higher degradation rate than old modules. This indicates that young modules seem to have problems regarding quality of modules, installation, and/or possible over-rating.

- In old crystalline silicon modules the main contributor to the P_{max} degradation is I_{sc} followed by FF, whereas in the case of young crystalline silicon modules the main

249

contributor to the P_{max} degradation is *FF* degradation. The fact that young modules show a higher degradation rate mainly due to *FF* degradation indicates the possibility of deliberate over-rating of the power of the module.

- Modules installed in large systems (size more than 100 kW) are degrading at a much lower rate (~1 %/year average Linear Degradation Rate for Group A) than modules installed in small systems of size less than 100 kW. All large systems fall in the 'good' Group X category. However, the modules from the large sites in only the Hot zone have an average Linear P_{max} Degradation Rate of 1.28 %/year which is much higher than the linear warranty. Also the young large systems are degrading at a higher rate than the old large systems in Hot zones. Hence, installers need to be cautious about the quality of materials and installation practices.

- Analysis of insulation resistance shows that more than 90% of the modules have passed the dry insulation resistance test. Also, 100% modules installed in the large system category have passed the dry insulation test which shows that large power plants are doing well with respect to the safety of the PV system , and there does not appear to be any safety hazard issue.

- Modules in the Hot zones have shown larger percentage of interconnect failure as compared to the Non-Hot zones. Also the series resistance of the module increases with the increase in the severity of the interconnect failure which eventually reduces the power output of the module.

- Modules in Group Y sites have higher percentage of cracked cells than modules in Group X, which indicates poor handling of the modules during manufacturing, transportation and/or installation for Group Y sites. This conclusion is also supported by the higher percentage of mode A and mode C cracks observed in the young modules as compared to the old.

- Rooftop sites show more cracked cells than ground-mounted sites, and higher number of cracks is also seen in young sites compared to old sites. This again indicates poor handling of the modules during manufacturing, transportation and/or installation for rooftop and young sites.

250

- There is a good correlation between the total number of cracks in the module and the power degradation of the modules.

2.   Development of characterization tools and methodology

- The development of two innovative and advantageous field characterization tools namely, inexpensive EL camera and PV module's temperature co-efficient measurement has been done. This development was motivated by our experience during the first broad scale field survey in 2014.

- Laboratory validation of these two characterization tools shows that these are eminently suitable for outdoor measurements, and are even acceptable for more demanding laboratory measurements.

- The development of field characterization methodologies (besides the development of actual devices or tools) like daylight Electroluminescence imaging and field-based temperature coefficient measurement of PV modules has been done.   These characterization methodologies are very effective in field studies, and again, their development was based on the need felt during the first broad scale (2014) All-India Survey.

- Due to the observation of many cracked cells during the All-India Surveys, we wished to investigate in the laboratory the effect of various loading effects in the field which occur during handling, shipping, installation, and also during deployment due to snow and wind loading. As a result, a Dynamic Mechanical Tool (DML) was developed, by extending the design developed by the author at NREL. This novel tool can simulate the similar conditions of loading on the PV module in the laboratory.

- The DML tool developed can perform both static and dynamic loading tests as defined in IEC 61215 and IEC TS 62782 respectively. Testing of any size of commercially available PV modules can be performed on this DML tool – making this the first of its kind in the world.

3. Effect of cracks on power loss of PV module with different interconnect designs

- The effect of cracks on power loss of PV module with different interconnect designs (conventional busbar and mesh type) has been studied using the DML tool developed at NCPRE IIT Bombay.

- It has been found that as the severity of cracks (in terms of total dark area in the cell and the number of cracks) increases, there is a reduction in P_{max} for both the designs of interconnects.

- The degradation in the P_{max} is mainly due to the degradation in FF and the degradation in I_{sc} is least. This is attributed to the increase in the series resistance and cell mismatch due to the cracks in the cell.

- It has been found that modules with both the interconnect designs develop cracks even at the low magnitude of loading (evident from EL images of Stage 1 and 2). This raises concern because various types of loading occur during handling, shipping, installation and during deployment, causing mechanical loading and bending of the PV modules.

- It has been observed that conventional busbar design shows higher degradation in P_{max} compared to mesh type interconnect with similar values of dark inactive area. This leads to an inference that mesh type interconnect may be superior in handling mechanical stress which can cause cracks. However, this conclusion is tentative, and more detailed studies are required.

4. Effect of mechanical loading cycles parameters on crack generation and power loss methodology

- The degradation in power and the number of Mode C cracks shows a saturating trend with number of cycles used in the DML accelerated testing. Mechanical loading at lower frequency (slow DML) requires more number of cycles to create cracks as compared to a higher frequency (fast DML). Therefore the recommended recipe for

the dynamic mechanical loading for accelerated testing is 1000 Pa pressure at 8 cycles/min and 1000 number of cycles.

- The degradation in the P_{max} is mainly due to the degradation in *FF* and the degradation in I_{sc} is least. This is attributed to the increase in the series resistance and cell mismatch due to the cracks in the cell.

- Mechanical loading at a lower pressure causes cracks in the cell, whereas a higher pressure causes cell cracks along with interconnects breakages, and sometimes shows a catastrophic effect.

- An excellent connection has been found between the field and laboratory studies. It has been found that the degradation in power increases with an increase in the number of cracks in the PV module. Furthermore, from both field and laboratory studies, it was concluded that the main reason for the degradation in power in young modules is attributed to fill factor degradation.

Based on the above conclusions, it is recommended that the installers and the module manufacturers put sufficient emphasis on the quality of the materials that are being used in the solar panels, especially for PV modules intended to be installed in Hot climates and in Indian conditions. Further, the quality and protocol for transportation and installation should also be given due emphasis. It is recommended to perform EL of the PV modules before and after the installation to reduce the possibility of microcracks in the modules which may have developed during transportation and installation. Our preliminary results have found that mesh interconnect design is more robust than conventional busbar design; however, further investigation of this is required.

7.2 Scope of Future Work

Field surveys and reliability assessment of PV installations is yet in its early stages in India. This thesis has made valuable contributions, but much work will need to be done to enable India's solar energy target of 300 GW by 2030. Some points for future work, arising out of this thesis, are mentioned below.

The All-India Survey of PV module reliability has been performed to understand the degradation of PV modules in the field in different climatic zones of India. In many cases, the signs of initial degradation have been found and many modules show higher than benchmark (0.8%/year) degradation rates, even after discounting for LID. It is advisable to regularly monitor the degradation of such modules, which will provide important feedback for future installations. The data collected on a year-on-year basis over several years shall provide accurate degradation rates, which can be used to fine-tune the financial models of the power plant owners. Also, a financial model based on the degradation rates needs to be built for better risk management, and it would enhance the confidence of the business community on the performance of PV modules.

Based on our field survey data, a correlation has been done for the loss in electrical power with physical degradation. It has been shown that modules with a higher number of cracks tend to have higher power degradation, which is mostly due to fill factor degradation (originating from cell cracks). However, further work is needed to establish an accurate correlation between the cell cracks and the power output, which will enable estimation of the power degradation of modules based on EL images alone (without the need for intrusive contact-based I-V measurements). Unmanned aerial vehicles (drones) are nowadays being tried for EL images of large power plants spread across acres of land, and the determination of the module power loss through aerial EL imaging is the logical next step for the PV industry.

The accelerated testing of mesh type interconnect versus conventional busbar interconnect design on the DML tool has shown the potential superiority of the mesh type. It will be beneficial to continue such accelerated tests on more samples and different interconnect designs to understand the suitable interconnect technology for achieving 25 years warranted life of PV modules. It is important to conduct a study to find a systematic correlation between the equivalent parameter of thermal cycles and mechanical cycles. This would help in reducing the time and cost

in order to perform the failure test analysis of interconnects ribbon and busbar. Further, the accelerated mechanical loading testing protocols developed in this thesis can be used for different module structures (besides just interconnect design) to test for variations in glass type and thickness, cell type, frame/frameless, etc.

In a separate study done by Mr. Devan P. V. was found that the vibration profile data obtained for the transportation of PV modules on India roads are substantially higher than the values defined in ASTM D4169 Assurance level II. A separate study needs to be done to determine the test parameters of DML which would correlate with these conditions. Some of these tests have already been started at our laboratory by other students as part of their Ph.D. and M.Tech. work.

This page is intentionally left blank.

Appendix I

Analysis of All-India Survey 2013 Data

I.1.   Background

Before the All-India Surveys of 2014 and 2016, which have been described in detail in this thesis, we had conducted a shorter All-India Survey on PV module degradation in 2013. The background for that, and indeed for the genesis of the bi-annual Surveys conducted by us, is described in this Appendix. A summary of the results obtained is also described.

The 2013 Survey was conducted with the objective of assessing the degradation of visually degraded PV modules installed in India between 3 to 30 years ago. As recommended by the "High Powered Task Force under JNNSM for Solar Photovoltaics" in its meeting held on March 4, 2013, such a survey would give valuable data on how existing installations in India have fared over the past decades, and thus give insight into the path forward for JNNSM. The National Centre for Photovoltaic Research and Education (NCPRE) was requested to undertake this

survey, together with Solar Energy Centre (SEC). Accordingly, the survey was initiated within a short time in May 2013, encompassing PV modules of different ages and technologies, located in five different climatic zones in India. In this survey, a total of 63 PV modules, spread across 26 different sites (shown in Fig. I.1) were inspected. The electrical data collected for 5 PV modules in Patna (Bihar) had to be discarded owing to low irradiation levels due to rain, so the electrical analysis was performed on the data of 58 PV modules (52 crystalline silicon modules and 6 thin film modules). Given the relatively few number of modules measured, as well as the preliminary nature of this Survey, we decided to view the 2013 Survey as a 'trial' survey, antedating the more complete and rigorous 2014, 2016 (and 2018) Surveys.

The technology-wise and age-wise distributions of the inspected modules are shown in Fig. I.2 (a) and Fig. I.2 (b) respectively. As expected, due to the age of the modules, many of them were of crystalline silicon, and there were none of newer technologies like Cadmium Telluride (CdTe). Further, although most of the modules were between 5 to 20 years old, there were a few less than 5 years old, and some more than 20 years old.
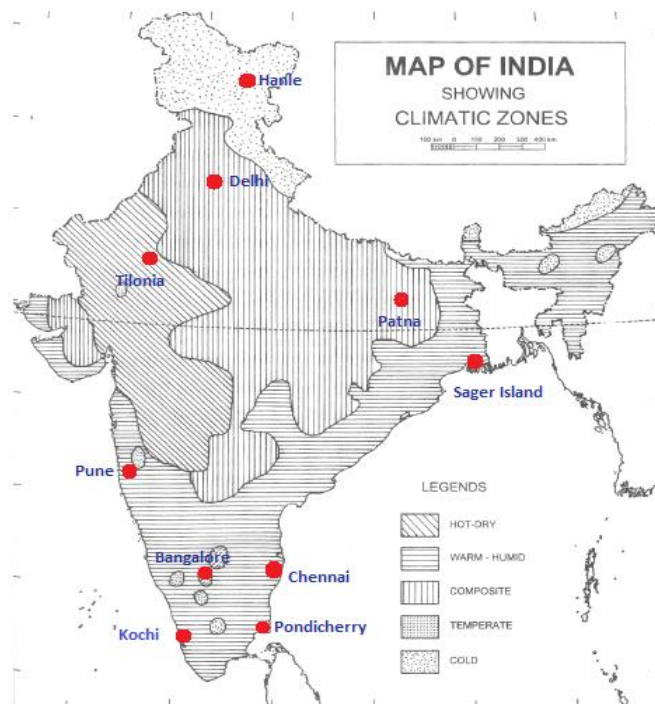
Fig. I.1: Outline map of India showing the various inspection sites (marked in red) in five different climatic zones.
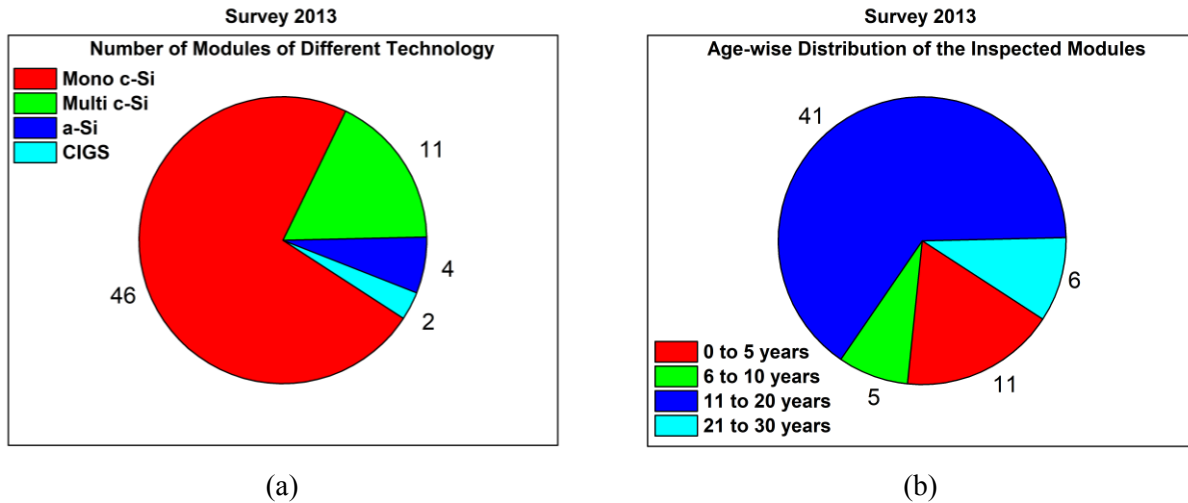
Fig. I.2: (a) Technology-wise distribution and (b) age-wise distribution of the inspected PV Modules.

The electrical performance of the modules was recorded using MECO 9018 Solar System Analyzer, a portable *I-V* curve tracer. A visual inspection checklist [29] was also filled in on site, consisting of the physical characteristics of the module, information on balance of system components like inverter and battery, and some socio-economic information. At some of the sites, infrared thermography was also performed using Wuhan Guide Infrared Co. Ltd. - EasIR-4on the PV Modules. The electrical performance data was extrapolated to Standard Test Conditions (STC) as per IEC standard 60891. Error analysis indicates that the uncertainty associated with the extrapolation is within 13.5% (for crystalline silicon modules) for data taken at irradiance level greater than 550 W/m^2.

I.2. Degradation in Electrical Performance

The analysis of electrical degradation of the inspected modules has shown that the degradation rate of mono c-Si is marginally better than that of multi c-Si (refer to Fig. I.3 (a)). This (and following figures) shows the spread in the calculated values of average degradation per year of all of the modules measured in that category, based on the name-plate value and the currently measured value. The green horizontal line shows the median value. It should be noted

that since this survey focused mainly on visibly degraded modules, the average degradation rates should not be taken as representative for that class of technology. The degradation values reported for this survey are generally higher than the typical values reported in the literature, for this reason. The degradation of the power output of mono-crystalline silicon modules has been found to be mainly due to degradation in the short circuit current (refer to Fig. I.3 (b)), which can be attributed to the physical degradation of the encapsulant, like discoloration and delamination of the EVA used. On the other hand, degradation in thin film modules (a-Si and CIGS) is mainly due to degradation in the fill factor (refer to Fig. I.3 (c)).
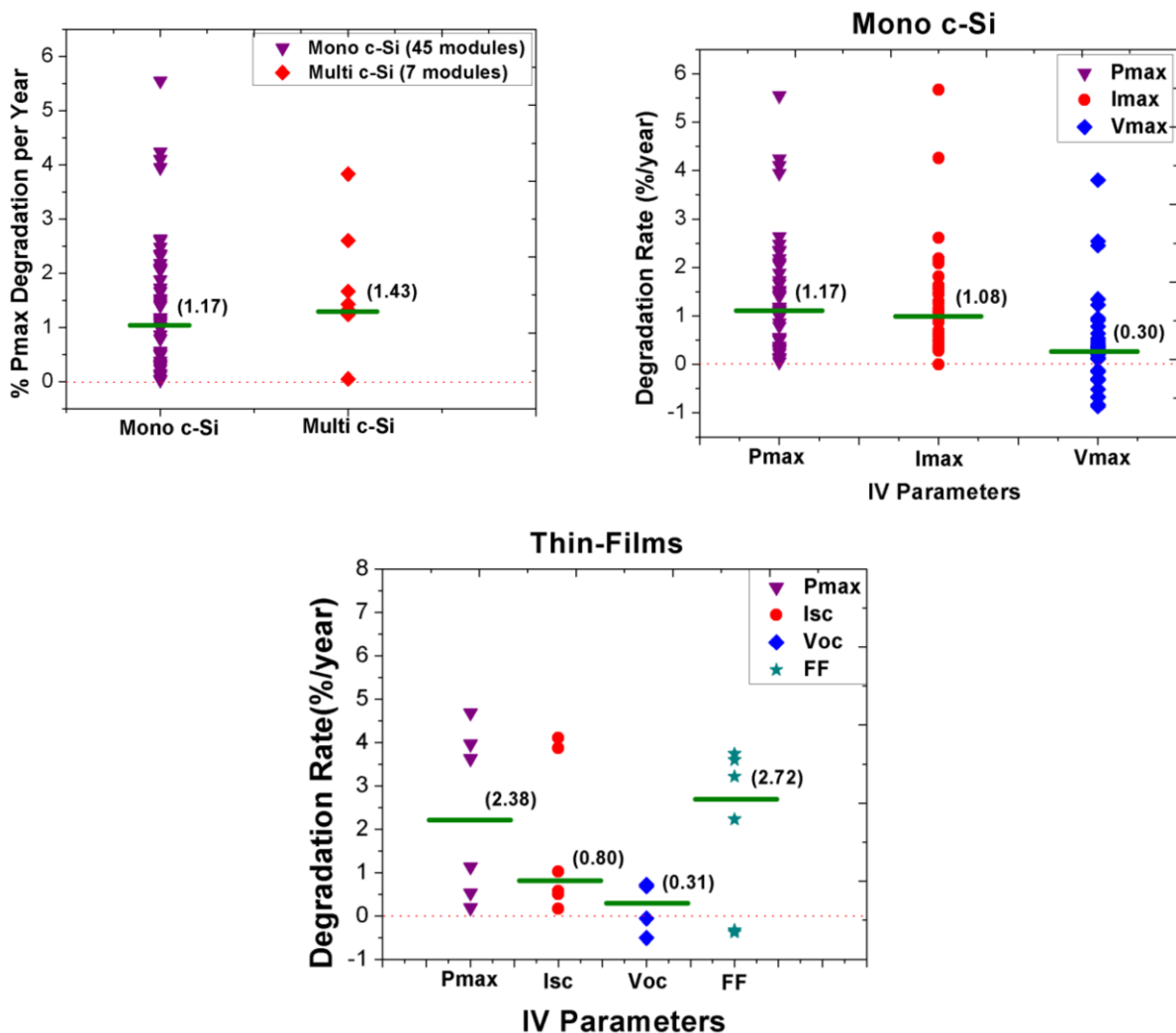
Fig. I.3: Degradation rates of (a) mono-crystalline silicon and multi-crystalline silicon modules, (b) various *I-V* parameters for mono-crystalline silicon modules, and (c) various *I-V* parameters for thin film modules.

The highest levels of module degradation have been seen in the Hot climatic zones (Hot & Dry as well as Hot & Humid zones) as compared to other climatic zones (refer to Table I.1 and Fig. I.4). Particularly interesting is that the Hot & Dry climate has a more deleterious effect on the modules than the Hot & Humid climate. Modules placed in the Hot & Dry zone are most susceptible to encapsulant discoloration, with the Hot & Humid zone coming second in the list. Corrosion of metallization and output terminals is most prevalent in the Hot & Humid zone as compared to other zones. Modules in the cooler climates perform much better (although the row for temperate climate should be discounted because of the paucity of data for that zone).

Table I.1: Degradation rates of various *I-V* parameters by climatic zone.

Climatic Zone	P_{max}(%/year)	I_{sc}(%/year)	V_{oc}(%/year)	FF(%/year)
Hot and Humid	1.40	0.98	-0.34	0.89
Temperate	0.24	-0.34	0.04	0.46
Composite	0.56	0.45	-0.17	0.64
Hot and Dry	1.55	0.78	0.20	0.51
Cold and Dry	0.19	0.72	-0.11	0.21
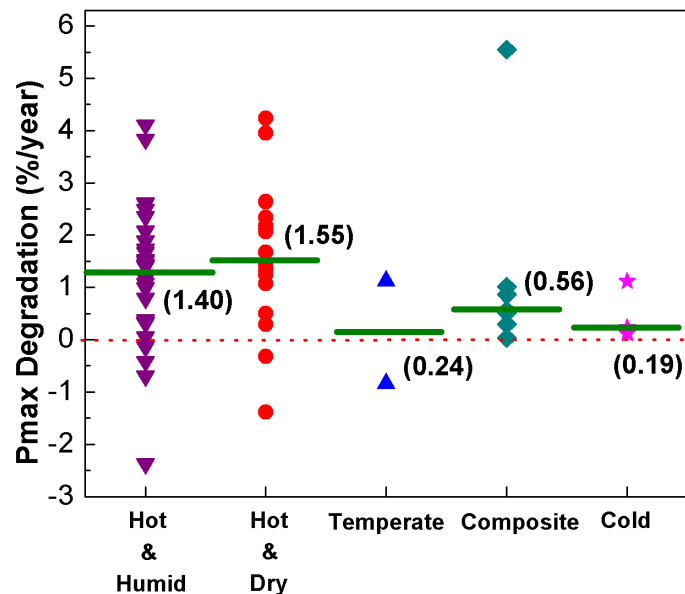
Fig. I.4: Comparison of P_{max} degradation rates in different climatic zones.

261

I.3. Conclusions

Based on the results of the 2013 Survey, some of the major conclusions which emerged are:

- Mono-crystalline silicon performs slightly better than multi-crystalline silicon.
- Power degradation for c-Si in the hot zones (Hot & Dry as well as Hot & Humid) is significantly higher than in the other climatic zones (Temperate, Composite and Cold).
- Modules in Hot & Dry zones show more degradation in power than in Hot & Humid zones.
- Across climatic zones, the major causes for power degradation for c-Si are a reduction in short-circuit current, followed by a reduction in fill factor.
- In Hot & Dry zones, reduction in short-circuit current dominates, while in Hot & Humid zone, the reduction in fill factor also contributes significantly.

Note that these conclusions are broadly consistent with the results of the subsequent 2014 and 2016 Surveys. Based on these initial results, it was decided that it would be very valuable to conduct a series of more detailed and extensive Surveys, starting in 2014.

Appendix II

Results from Accelerated Test at NREL

II.1   Background

In order to study the physical reason for the development of cracks and to understand the growth of these cracks with time, it was felt necessary to undertake a systematic study on impact of cracks on the power loss. Since in our field surveys, we have found that one of the main reasons for the loss in power of the young modules was due to the development of cracks, subsequently a study on cell cracks and impact of these cracks on the power loss was conducted by the author as a part of an internship at the National Renewable Energy Laboratory (NREL), in USA in 2016. During this internship, a stress test tool was developed which could simulate the same effect on the PV module which it experiences in the real field conditions. In this section the test methodology, test sequence through which the PV modules were subjected and the test results of the accelerated test are presented. Furthermore, the author's contribution was to rebuild

the fixture for a new set of modules, add new powerful vacuum pumps, and add the data logging part in the setup.

II.2 Impact of Cracks on Different Module Designs

In this section, we shall discuss the impact of cell cracks on PV modules of different make and design. Furthermore, the experiment methodology, sample selection, and test protocol used for this experiment are presented, and the results of this experiment are discussed.

II.2.1 Selection of Samples

In this experiment, four modules each of manufacturer A, B, and C were taken. Out of these four modules for each manufacturer, one sample was subjected to heavy steps (by walking 10 steps on the top of the module from the glass side), one sample was dropped from a 12-inch height, one sample was dropped from a 24-inch height and one sample was not subject to any kind of initial stress. Table II.1 summarizes the group of modules and the number of modules in each group subjected to initial stress for the experiment.

Table II.1: Summary of Modules considered for the experiment.

Manufacturer	No of Modules in each group of initial stress			
	Heavy Steps	12 inch drop	24 inch drop	No initial damage or control module
A	1	1	1	1
B	1	1	1	1
C	1	1	1	1

II.2.2 Test Protocol

The test sequence which was chosen comprises 1000 cycles of dynamic mechanical loading at 1000 Pa pressure followed by 50 cycles of thermal cycles and 10 cycles of humidity

freeze. At the end of each stress (namely mechanical stress, thermal cycles and humidity freeze), lighted *I-V*, dark *I-V*, EL, *IR* were measured. Figure II.1 shows the test protocol used in the experiment.
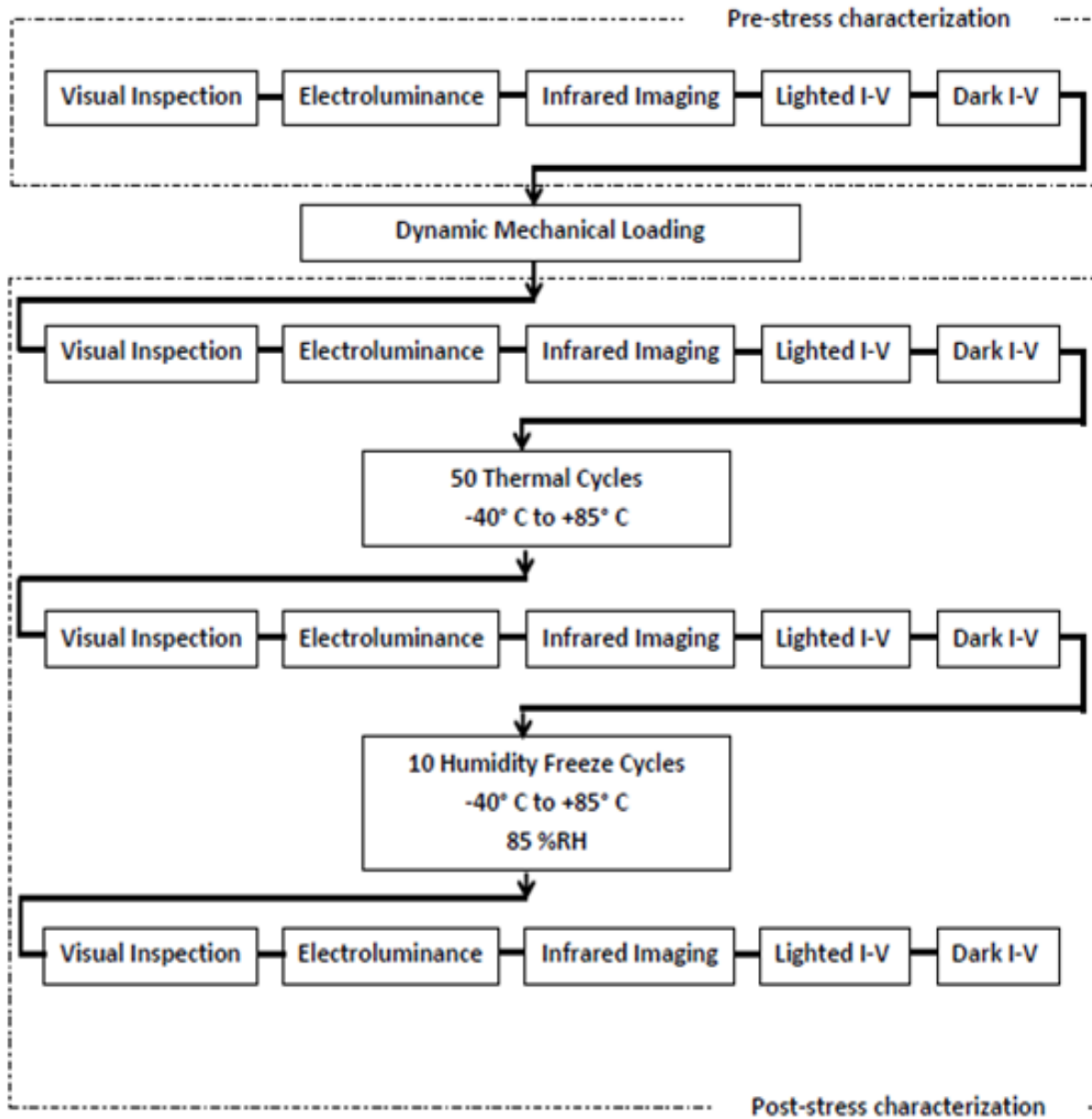
Fig. II.1: Test protocol used for the experiment.

II.2.3 Results

Table II.2 shows the percentage change in the P_{max} after subjecting the PV module to 1000 cycles of DML, 50 thermal cycles and 10 cycles of humidity freeze. It shows that in each category of initial stress (24-inch drop, 12-inch drop, heavy step, and no initial stress or control module), the module initially subjected to 24-inch drop has suffered maximum change in the value of P_{max}. Furthermore, manufacturer A has suffered the least in the value of P_{max} as compared to B, C in each category of initial stress. Figure II.2 shows the *I-V* parameter degradation at the end of the test sequence (after 10 cycles of Humidity Freeze). It can be clearly seen that the main reason for the degradation of power is degradation in the *FF*.

Table II.2: Percentage change in P_{max} at the end of the test protocol.

Manufacture	% P_{max} change after 10 cycles of Humidity Freeze			
	No initial damage or control module	Heavy Steps	12 – inch drop	24 – inch drop
A	1.47	4.15	4.44	7.26
B	No Data (as module front glass got broken)	4.90	5.68	7.89
C	5.63	6.87	8.10	10.77
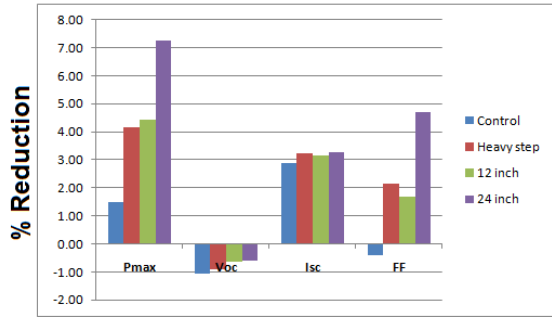
(a)
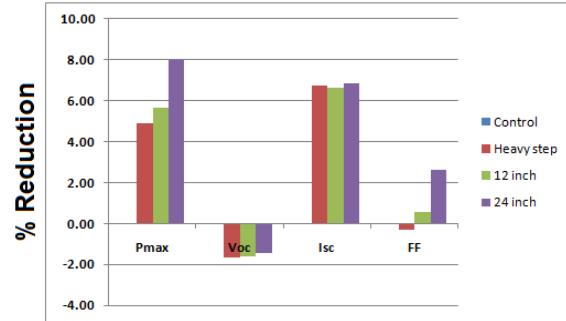
(b)
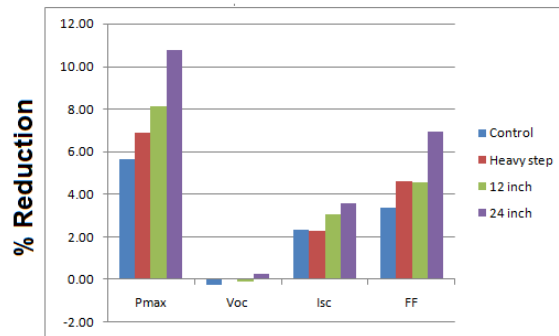
(c)

Fig. II.2: *I-V* parameter degradation at the end the test sequence for manufacture (a) A, (b) B, and (c) C.

Table II.3 shows the value of the series resistance at the end of each stress in each group of initial stress. It can be noticed that the series resistance increases after each stress test. This explains the reason for the high degradation in the value of *FF*, which is responsible for the degradation in P_{max}. Table II.4 shows the value of the shunt resistance at the end of each stress. The value of shunt resistance decreases after the mechanical stress, however, it recovers after 50 thermal cycles. The reason for the recovery in the shunt resistance after thermal cycles was unknown. Figure II.3 shows the EL images for manufacturer C at the end of the test sequence for each category of initial stress. It is evident from the figure that the module having a large number of cracks initially also has a large number of cracks at the end of the test sequence and suffers the maximum power loss. Similar results were obtained for manufacturers A and B. This substantiates our finding that the presence of cracks in the cell would degrade the performance of the PV module in long term.

Table II.3: Value of the series resistance after each stress in each group.

		Pre DML Stress	Post DML Stress	Post 50 TC Stress	Post 10 HF Stress
Module Type	Initial Stress	Pseudo Series resistance (ohms)	Pseudo Series resistance (ohms	Pseudo Series resistance (ohms	Pseudo Series resistance (ohms
Manufacture A	No damage	0.47	0.48	0.49	0.49
	Heavy step	0.48	0.49	0.49	0.52
	12 inch	0.48	0.49	0.50	0.51
	24 inch	0.51	0.51	0.54	0.56
Manufacture B	No damage	0.99	NA	NA	NA
	Heavy step	0.97	0.98	0.98	0.98
	12 inch	0.98	0.99	1.00	1.00
	24 inch	1.02	1.03	1.05	1.02
Manufacture C	No damage	0.62	0.62	0.62	0.68
	Heavy step	0.62	0.63	0.64	0.67
	12 inch	0.62	0.63	0.67	0.64
	24 inch	0.63	0.63	0.66	0.68

Table II.4: Value of the shunt resistance after each stress test in each category.

		Pre DML Stress	Post DML Stress	Post 50 TC Stress	Post 10 HF Stress
Module Type	Initial Stress	Pseudo Shunt resistance (ohms)	Pseudo Shunt resistance (ohms)	Pseudo Shunt resistance (ohms)	Pseudo Shunt resistance (ohms)
Manufacture A	No damage	555	462	800	561
	Heavy step	211	214	224	157
	12 inch	398	350	370	327
	24 inch	327	263	457	225
Manufacture B	No damage	715	NA	NA	NA
	Heavy step	357	244	398	525
	12 inch	792	652	728	1130
	24 inch	529	539	704	988
Manufacture C	No damage	966	376	871	376
	Heavy step	419	275	169	364
	12 inch	780	410	666	406
	24 inch	732	722	752	384

(a)   (b)

(c)   (d)
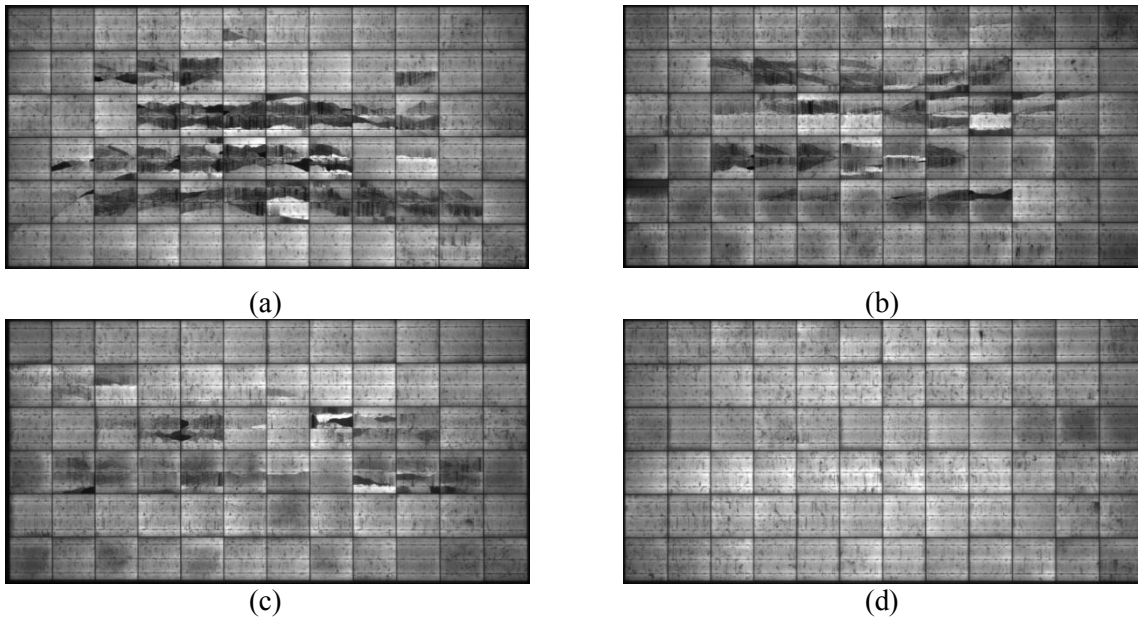
Fig. II.3: EL images for the manufacture C after the end of test sequence (a) 24- inch drop, (b) 12 – inch drop, (c) heavy steps and (d) no initial damage or control module.

Figure II.4 shows the EL image for the 24-inch drop module after each stress for manufacturer C. It is evident from the figure that after each stress the number and the area of cracks are increased. Similar results were obtained for Manufacture A and B.

(a)   (b)

(c)   (d)
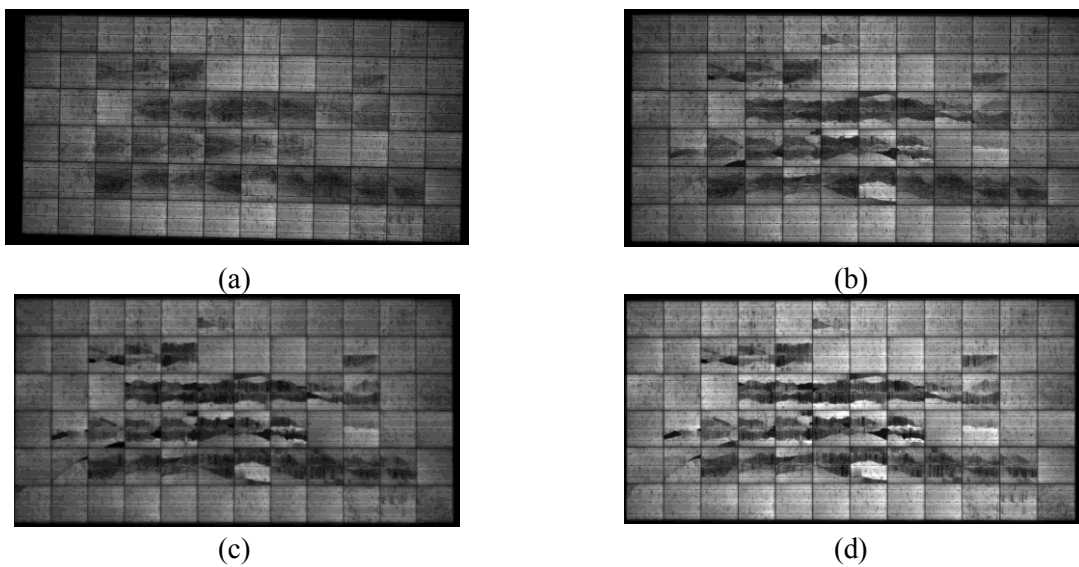
Fig. II.4: EL image for 24-inch drop module after each stress for manufacture C after (a) Pre DML, (b) Post DML, (c) 50 thermal cycles and (d) 10 humidity cycles.

II.3 Conclusions

The data from field surveys have indicated a relationship between the cracks in the solar panels and the degradation rate of the panels. This relationship has been investigated in detail in this appendix, using the DML tool developed by the author at NREL as a part of the internship. We have used the DML tool to study three different types of modules with different levels of initial stress. It has been found that the output power decreases with an increase in severity of the crack (in terms of total dark area in the cell and the number of cracks). From this accelerated testing we can conclude the following:

- Dropping of modules can cause more reduction in power loss than heavy steps on them.
- EL images also confirm that the dropping causes more damage to the modules.
- Manufacturers A and B modules are less affected by cracks than Manufacturer C.
- The main contributor to the power loss is reduction in fill factor and open circuit voltage is least affected.
- The reduction in power is due to series resistance.
- Shunt resistance improves after the thermal cycle stress.

{Note: Due approval was taken from NREL to present this data in the current thesis.}

270

Appendix III

Electrical Checklist

The electrical checklist has been developed into a two page checklist for quick evaluation of the condition of a solar panel through electrical inspection at site. The checklist is provided in the following pages. It is based on the NREL checklist [29].

ELECTRICAL CHECKLIST (GROUP – A)

A1. Module & System Information

Manufacturer _____ Model # _____ Serial # _____

Year of Installation_____

Module Nameplate Data: ☐ Available ☐ Missing

P_{max} _____ V_{oc} _____ I_{sc} _____

Sys Volt_____ V_{max} _____ I_{max} _____

Bypass diode, I_f _____ Series fuse _____

Temperature Coefficients:

Voltage: _____ Current: _____ Power: _____

System design: ☐ single module ☐ multiple modules (a) ☐ unknown

(a.) Multiple module system:
Module location/number in a series string (from negative) _____
No of modules in series (string) _____ No of strings in parallel (array) _____
No of bypass diodes_____ Rating & Model No. of Bypass Diodes: _____
No of modules per blocking diode _____ Rating & Model No. of Bypass Diodes: _____

System Bias: ☐ open circuit ☐ resistive load ☐ max. power tracked ☐ short circuit

☐ unknown

Frame Grounding: ☐ grounded ☐ not grounded

System Grounding – DC Side: ☐ grounded (a.) ☐ not grounded ☐ unknown

(a.) ☐ negative ☐ positive ☐ center of string ☐ unknown

System Grounding – AC Side: ☐ grounded ☐ not grounded ☐ unknown

Comments: _____
_____

Filed by: Page 1   Date:

Site No.:   **ELECTRICAL CHECKLIST (GROUP – A)**

A2. I-V Characteristics   (☐ Not applicable   ☐ Applicable)

Tracer used   ☐ Solmetric 1   ☐ Solmetric 2
                  ☐ PVPM I-V curve tracer   ☐ Meco System Analyzer

I-V Curve File number/name & Time: _____

Relative Humidity (%) _____ Ambient Temperature (º C) _____

Comments on I-V curve: _____

_____

A3. Bypass Diode Test   (☐ Not applicable   ☐ Applicable)

No. of Bypass Diodes: _____

No. of solar cells per Bypass Diode: _____

Diode position from (+) terminal	1	2	3	4	5
Status (√, X, NA)					
If not working (open/short)					

No. of Diodes functioning properly: _____

A4. Interconnect Failure Test   (☐ Not applicable   ☐ Applicable)

Interconnect Failure Present: ☐ Yes (a)   ☐ No (b)

(a) No. of interconnect failure sites: _____

(a) Visual Image File No. : _____

(b) Max signal strength (No. of LED glowing 1 to 10) _____

     Min signal strength (No. of LED glowing 1 to 10) _____

Comments: _____

_____

Filed by: Page 2   Date:

This page is intentionally left blank.

Appendix IV

Dark *I-V* Parameter Extraction Methodology

In order to calculate the dark *I-V* parameters of the module we converted the dark *I-V* of the module into the dark *I-V* of an equivalent solar cell by dividing the voltage (at each *I-V* data point) by the number of cells in the module. This of course assumes that all cells in the module are identical. Figure IV.1 graphically demonstrates the concept of dark *I-V* of the equivalent cell. It should be noted that the module's cell-to-cell interconnect resistance gets subsumed into an equivalent solar cell series resistance.
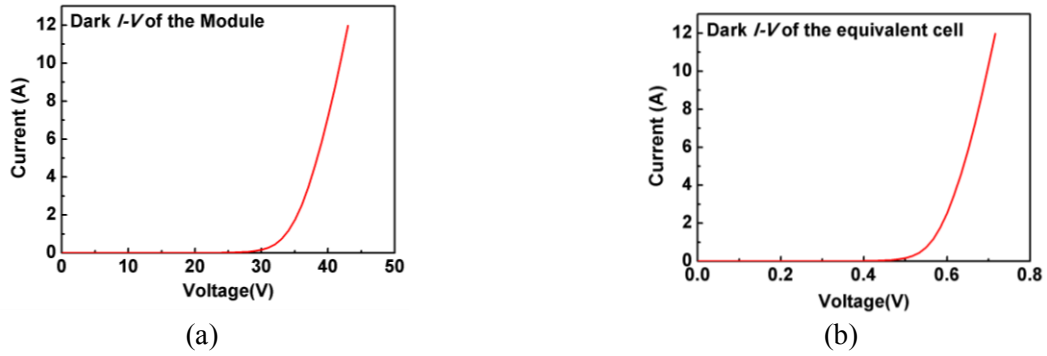
Fig. IV.1: (a) Measured dark *I-V* of the module and, (b) dark *I-V* of an equivalent cell obtained by dividing the module *I-V* voltages by number of cells (here 60).

Ideality factor *n* of the equivalent solar cell diode is calculated from slope obtained by drawing a tangent at the maximum power point voltage V_{mp}, (as shown in Fig. IV.2). Figure IV.3 shows the procedure to calculate the dark *I-V* parameters from the slope at V_{mp} point, and the y-axis intercept.
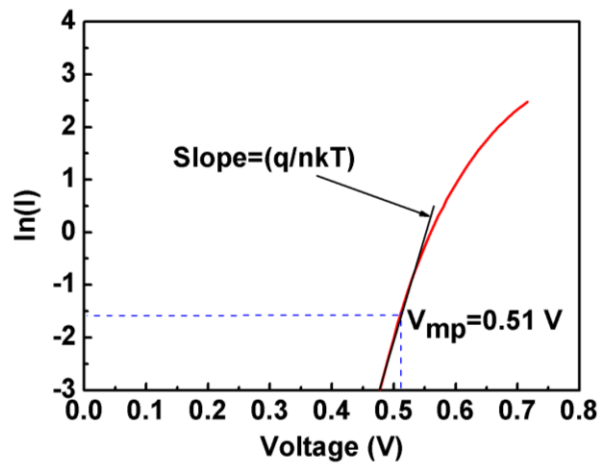
Fig. IV.2: ln(*I*) vs. Voltage plot, showing also the tangent at V_{mp}, from which *n* can be found.

276
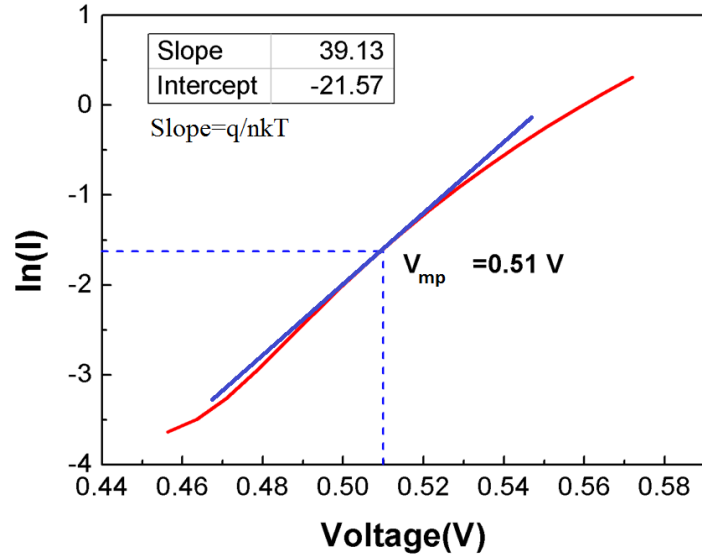
Fig. IV.3: Enlarged plot of ln(I) vs. Voltage around V_{mp}, also showing the tangent at V_{mp}, from which n and I_o can be calculated.

This page is intentionally left blank.

References

[1] "U.S. Energy Information Administration, International Energy Outlook 2019". [Online]. Available: https://www.eia.gov/todayinenergy/detail.php?id=41433 [Accessed: June 14, 2020]

[2] "National Aerospace and Space Administration, 'World of Change – Global Temperatures', National Aeroscpace and Space Administration" [Online]. Available: https://earthobservatory.nasa.gov/world-of-change/DecadalTemp. [Accessed: Feb. 5, 2019]

[3] "Global energy demand rose by 2.3% in 2018, its fastest pace in the last decade". [Online]. Available: https://www.iea.org/news/global-energy-demand-rose-by-23-in-2018-its-fastest-pace-in-the-last-decade [Accessed: June 14, 2020]

[4] United Nations Organization, "The Paris Agreement", United Nations Framework Convention on Climate Change (UNFCCC). [Online]. Available: https://unfccc.int/process-and-meetings/the-paris-agreement/the-paris-agreement [Accessed: Feb. 5, 2019]

[5] V. Masson-Delmotte, P. Zhai, H.-O. Pörtner, D. Roberts, J. Skea, P.R. Shukla, A. Pirani, W. Moufouma-Okia, C. Péan, R. Pidcock, S. Connors, J.B.R. Matthews, Y. Chen, X. Zhou, M.I. Gomis, E. Lonnoy, T. Maycock, M. Tignor, and T. Waterfield (eds.), "IPCC, 2018: Summary for Policymakers. In: Global Warming of 1.5°C," Intergovernmental Panel on Climate Change, 2018. [Online]. Available: https://www.ipcc.ch/site/assets/uploads/sites/2/2019/05/SR15_SPM_version_report_LR.pdf [Accessed: Feb. 10, 2019]

[6] Government of India, "Revision of cumulative targets under National Solar Mission from 20,000 MW by 2021-22 to 1,00,000 MW," Press Information Bureau (PIB), June 17, 2015. [Online]. Available: http://pib.nic.in/newsite/PrintRelease.aspx?relid=122566 [Accessed: March 10, 2020]

[7] Staff Reporter, "India India will have 227 Gigawatt of renewable energy capacity by 2022: Vice President," Economic Times, 15 April 2019 [Online]. Available: https://energy.economictimes.indiatimes.com/news/renewable/india-will-have-227-gigawatt-of-renewable-energy-capacity-by-2022-vice-president/68887932 [Accessed: Feb 10, 2019]

[8] T. Wang, "Global cumulative installed solar PV capacity 2000-2018", May 24, 2019. [Online]. Available: https://www.statista.com/statistics/280220/global-cumulative-installed-solar-pv-capacity/ [Accessed: June 14, 2020]

[9] Z. Shahan, '13 Charts On Solar Panel Cost & Growth Trends', Cleantechnica, September 4, 2014. [Online]. Available: https://cleantechnica.com/2014/09/04/solar-panel-cost-trends-10-charts/ [Accessed: June 14, 2020]

[10] J. Trube, 'International Technology Roadmap for Photovoltaic – 2018 Results', Verband

Deutscher Maschinen- und Anlagenbau, Frankfurt, Germany. [Online]. Available: https://pv-manufacturing.org/wp-content/uploads/2019/03/ITRPV-2019.pdf [Accessed: June 14, 2020]

[11] US Energy Information Administration, "Coal Explained," US Energy Information Administration. [Online]. Available: https://www.eia.gov/energyexplained/index.php?page=coal_home [Accessed: Feb. 12, 2020]

[12] "Solar Photovoltaic Technology Basics", [Online]. Available: https://www.nrel.gov/research/re-photovoltaics.html. [Accessed: June 14, 2020]

[13] C. S. Solanki, *Solar Photovoltaics: Fundamentals, Technologies And Applications*, PHI Learning Pvt. Ltd., Delhi, 2015.

[14] S. R. Wenham, M. A. Green, M. E. Watt, and R. Corkish, *Applied photovoltaics, 2d ed.* Earthscan, 2007.

[15] "Clean Energy Review", [Online]. Available: https://www.cleanenergyreviews.info/blog/solar-panel-components-construction. [Accessed: Nov 1, 2020]

[16] TSEC Corporation, "Solar Overview" [Online]. Available: http://www.tsecpv.com/en-global/solar_knowledge/index/zero_house_02 [Accessed: Feb. 7, 2019]

[17] *Crystalline Silicon Terrestrial Photovoltaic (PV) Modules – Design qualification and type approval,* IEC 61215-2005, 2005.

[18] J. Wohlgemuth, "IEC 61215: What it is and isn't," NREL PV Module Reliability Workshop, Golden, Colorado, 2012. [Online]. Available: https://www.nrel.gov/docs/fy12osti/54714.pdf [Accessed: Feb. 15, 2019]

[19] S. Chattopadhyay *et al.*, "All India Survey of Photovoltaic Module Degradation 2014: Survey Methodology and Statistics," in *Proceedings of the 42nd IEEE Photovoltaics Specialists Conference*, New Orleans, 2015, pp. 1-6. DOI: 10.1109/PVSC.2015.7355712

[20] S. Chattopadhyay, R. Dubey, Vivek K., S. Zachariah, S. Bhaduri, C. Mahapatra, S. Rambabu, F. Ansari, A. Chindarkar, A. Sinha, H. K. Singh, N. Shiradkar, B. M. Arora, A. Kottantharayil, K. L. Narasimhan, S. Sabnis, B. Bora, G. Kumar, Y. K. Singh, M. Bangar, M. Kumar, A. Kum, "All-India Survey of Photovoltic Module Reliability: 2016," 2017. [Online]. Available: http://www.ncpre.iitb.ac.in/research/pdf/All_India_Survey_of_Photovoltaic_Module_Reliability_2016.pdf. [Accessed: June. 15, 2020]

[21] B. P. Lockridge, O. Lavrova, and W. B. Hobbs, "Comparison of electroluminescence image capture methods," in *Proceedings of the 44th IEEE Photovoltaic Specialist Conference,* Washington, 2017, pp. 1–4, doi: 10.1109/PVSC.2017.8366143.

[22] *Photovoltaic devices – Procedures for temperature and irradiance corrections to measured I-V characteristics,* IEC 60891 Ed. 2.0. 2003

[23] E. Lee, A. Chodos, "Bell Labs demonstrates the first practical silicon solar cell," APS News, 2009. [Online]. Available: https://www.aps.org/publications/apsnews/200904/physicshistory.cfm#:~:text=April 25%2C 1954%3A Bell Labs,First Practical Silicon Solar Cell&text=Solar cells%2C which convert sunlight,to be of much use. [Accessed: June. 15, 2020]

[24] M. A. Green, K. Emery, Y. Hishikawa, and W. Warta, "Solar cell efficiency tables (version 36)," *Prog. Photovoltaics Res. Appl.*, vol. 18, no. 5, pp. 346–352, 2010, doi: 10.1002/pip.1021.

[25] D. C. Jordan and S. R. Kurtz, "Photovoltaic Degradation Rates — An Analytical Review," *Prog. Photovoltaics Res. Appl.*, vol. 21, no. 1, pp. 12–29, 2013, doi: 10.1002/pip.1182.

[26] A Powerful Measure of Confidence. [Online]. Available: https://www.spectrolab.com/company.html#history [Accessed: June 18, 2020]

[27] M. Kempe, "Overview of scientific issues involved in selection of polymers for PV applications," in *Proceedings of the 37th IEEE Photovoltaic Specialists Conference*, Washington, DC, 2011, pp. 000085–000090, doi: 10.1109/PVSC.2011.6185851.

[28] C. Peike, I. Hädrich, K. Weiß and I. Dürr, "Overview of PV module encapsulation materials," *Photovoltaics International*, vol. 22, November 2015, pp. 85–92, 2013.

[29] C. E. Packard, J. H. Wohlgemuth, and S. R. Kurtz, "Development of a Visual Inspection Data Collection Tool for Evaluation of Fielded PV Module Condition," in *NREL Technical Report*, 2012, August, pp. 1–52.

[30] K. Kato, "PV module failures observed in the field: solder bond and bypass diode failures", in *Proceedings of the Photovoltaic Module Reliability Workshop*, Golden, Colorado, USA, 2012. [Online]. Available: http://ieapvps.org/index.php?id=223&eID=dam_frontend_push&docID=1275. [Accessed March 14, 2014]

[31] W. Herrmann, "Current-Voltage Translation Procedure for PV Generators in the German 1000 Roofs Programme" [Online]. Available: http://www.f09.fhkoeln.de/imperia/md/content/personen/wiesner_wolfgang/veroeffentlichungen/26_proceed.pdf, [Accessed Feb. 20, 2020]

[32] D. Dirnberger, J. Bartke, A. Steinhüser, K. Kiefer, and F. Neuberger, "Uncertainty of field IV Curve measurements in Large Scale PV systems," in *Proceedings of the 25th European Photovoltaic Solar Energy Conference and Exhibition / 5th World Conference on Photovoltaic Energy Conversion*, Valencia, Spain, 2010, pp. 4587 - 4594, doi: 10.4229/25thEUPVSEC2010-4BV.1.62.

[33] D. C. Jordan, S. R. Kurtz, K. VanSant, and J. Newmiller, "Compendium of photovoltaic degradation rates," *Prog. Photovoltaics Res. Appl.*, vol. 24, no. 7, pp. 978–989, 2016, doi: 10.1002/pip.2744.

[34] D. C. Jordan, M. G. Deceglie, and S. R. Kurtz, "PV degradation methodology comparison - A basis for a standard," in *Proceedings of the 44th IEEE Photovoltaic Specialist*

Conference, Washington, DC, 2017, pp. 1–6, doi: 10.1109/PVSC.2017.8366644.

[35]   D. C. Jordan, "Methods for Analysis of Outdoor Performance Data," in *Proceedings of the NREL PV Module Reliability Workshop,*Golden CO, USA*, 2011, pp. 1–37, [Online]. Available: http://www.nrel.gov/docs/fy11osti/51120.pdf. [Accessed March 14, 2020]

[36]   S. Kurtz, J. Granata and M. Quintana "Photovoltaic Reliability R&D toward a Solar-Powered World.", in *Proceedings of the SPIE,* San Diego, 2009, pp. 7412-104, doi: 10.1117/12.825649.

[37]   J. H. Wohlgemuth, "Reliability testing of PV modules," in *Proceedings of the 24th IEEE Photovoltaic Specialists Conference and 1st World Conference on Photovoltaic Energy Conversion (WCPEC)*, Waikoloa, HI, 1994, vol. 1, pp. 889–892, doi: 10.1109/wcpec.1994.520104.

[38]   D. Jordan, J. Wohlgemuth, and S. Kurtz, "Technology and Climate Trends in PV Module Degradation", in *Proceedings of the 27th European Photovoltaic Solar Energy Conference and Exhibition*, Frankfurt, Germany, 2012, pp. 3118–3124, doi: 10.4229/27thEUPVSEC2012-4DO.5.1

[39]   C. R. Osterwald and T. J. McMahon, "History of accelerated and qualification testing of terrestrial photovoltaic modules: A literature review," *Prog. Photovoltaics Res. Appl.*, vol. 17, no. 1, pp. 11–33, 2009, doi: 10.1002/pip.861.

[40]   D. J. Roesler, D. D. Faehn, and L. R. Suelzle, "Analysis of a 60kW PV power plant after the first year of operation," in *Proceedings of the 3rd European Photovoltaic Solar Energy Conference*, Cannes, France, 1980, pp. 505–512.

[41]   A. L. Rosenthal, M. G. Thomas, and S. J. Durand, "Ten year review of performance of photovoltaic systems," in *Proceedings of the 23rd IEEE Photovoltaic Specialists Conference*, Louisville, KY, 1993, pp. 1289–1291, doi: 10.1109/pvsc.1993.346934.

[42]   G. H. Atmaram, G. G. Ventre, C. W. Maytrott, J. P. Dunlop, and R. Swamy, "Long-term performance and reliability of crystalline silicon photovoltaic modules," in *Proceedings of the 26th IEEE Photovoltaic Specialists Conference*, Washington, DC, 1996, pp. 1279–1282, doi: 10.1109/pvsc.1996.564366.

[43]   R. DeBlasio, D. Waddington, and L. Mrig, "Outdoor performance and stability testing of thin film devices," *Sol. Cells*, vol. 21, no. 1–4, pp. 343–351, 1987, doi: 10.1016/0379-6787(87)90133-5.

[44]   M. J. Hahn, W. B. Berry, and L. Mrig, "Comparative short term/long term field test performance and stability of tandem and single junction a-Si modules," in *Proceedings of the 21st IEEE Photovoltaic Specialists Conference*, Kissimmee, FL, 1990, vol. 2, pp. 1057–1061, doi: 10.1109/pvsc.1990.111779.

[45]   D. Berman, S. Biryukov, and D. Faiman, "EVA laminate browning after 5 years in a grid-connected, mirror-assisted, photovoltaic system in the Negev desert: effect on module efficiency," *Sol. Energy Mater. Sol. Cells*, vol. 36, no. 4, pp. 421–432, 1995, doi: 10.1016/0927-0248(94)00198-7.

[46] G. Iliceto A, Belli G, Buonarota A and P. A. S, Patane R, "Long term operational experience at Vulcano PV plant," in *Proceedings of the 13th European Photovoltaic Solar Energy Conference*, Nice, France, 1995, pp. 351–355.

[47] Nyman C., "Photovoltaics in Finland," in *Proceedings of the 14th European Photovoltaic Solar Energy Conference*, Barcelona, Spain, 1997, pp. 1145–1147.

[48] M. K. Chenlo F, Rebollo L, Matas A, Zarauza L, Valera P, Garcia P, "Three years of operation and experience of the 1MW photovoltaic plant," in *Proceedings of the 14th European Photovoltaic Solar Energy Conference*, Barcelona, Spain, 1997, pp. 705–708.

[49] K. Fukae *et al.*, "Outdoor performance of triple stacked a-Si photovoltaic module in various geographical locations and climates," in *Proceedings of the 25th IEEE Photovoltaic Specialists Conference*, Washington, DC, 1996, pp. 1227–1230, doi: 10.1109/pvsc.1996.564353.

[50] K. Akhmad, A. Kitamura, F. Yamamoto, H. Okamoto, H. Takakura, and Y. Hamakawa, "Outdoor performance of amorphous silicon and polycrystalline silicon PV modules," *Sol. Energy Mater. Sol. Cells*, vol. 46, no. 3, pp. 209–218, 1997, doi: 10.1016/S0927-0248(97)00003-2.

[51] M. Ikisawa, A. Nakano, S. Igari, and H. Terashima, "Outdoor exposure tests of photovoltaic modules in Japan and overseas," *Renew. Energy*, vol. 14, no. 1–4, pp. 95–100, 1998, doi: 10.1016/s0960-1481(98)00053-6.

[52] K. Machida, T. Yamazaki, and T. Hirasawa, "Secular degradation of crystalline photovoltaic modules," *Sol. Energy Mater. Sol. Cells*, vol. 47, no. 1–4, pp. 149–153, 1997, doi: 10.1016/S0927-0248(97)00035-4.

[53] S. Dongaonkar and M. A. Alam, "Geometrical design of thin film photovoltaic modules for improved shade tolerance and performance," *Prog. Photovoltaics Res. Appl.*, vol. 23, no. 2, pp. 170–181, 2015, doi: 10.1002/pip.2410.

[54] N. Cereghetti, E. Burà, D. Chianese, G. Friesen, A. Realini, and S. Rezzonico, "Power and energy production of PV modules statistical considerations of 10 years activity," in *Proceedings of the IEEE 3rd World Conference on Photovoltaic Energy Conversion*, WCPEC-3, Osaka, Japan , 2003, vol. 2, pp. 1919–1922.

[55] C. R. Osterwald, J. Adelstein, J. A. Del Cueto, B. Kroposki, D. Trudell, and T. Moriarty, "Comparison of degradation rates of individual modules held at maximum power," in *Proceedings of the IEEE 4th World Conference on Photovoltaic Energy Conversion, WCPEC-4*, Waikoloa, Hawaii, 2006, vol. 2, pp. 2085–2088, doi: 10.1109/WCPEC.2006.279914.

[56] M. Vázquez and I. Rey-Stolle, "Photovoltaic module reliability model based on field degradation studies," *Prog. Photovoltaics Res. Appl.*, vol. 16, no. 5, pp. 419–433, 2008, doi: 10.1002/pip.825.

[57] W. Vaassen, "Qualitätsmerkmale photovoltaischer Module", in *Proceedings of the 6th Symposium Photovoltaïque National*, Geneva, Switzerland, 2005.

283

[58] Becker G, Bettinger H. Degrationsmessungen, Solarenergieförderverein Bayern e.V., München, 2005. IBB-SOLAR. [Online]. Available: http://www.sev-bayern.de/index.php?entryid=14.[Accessed: June 14, 2020]

[59] D. C. Jordan, R. M. Smith, C. R. Osterwald, E. Gelak, and S. R. Kurtz, "Outdoor PV degradation comparison," in *Proceedings of the 35th IEEE Photovoltaic Specialists Conference*, Honolulu, HI, 2010, pp. 2694–2697, doi: 10.1109/PVSC.2010.5616925.

[60] A. M. Reis, N. T. Coleman, M. W. Marshall, P. A. Lehman, and C. E. Chamberlin, "Comparison of PV module performance before and after 11-years of field exposure," in *Proceedings of the 29th IEEE Photovoltaic Specialists Conference*, New Orleans, LA, 2002, pp. 1432–1435, doi: 10.1109/PVSC.2002.1190878.

[61] S. Sakamoto and T. Oshiro, "Field test results on the stability of crystalline silicon photovoltaic modules manufactured in the 1990s.," in *Proceedings of the 3rd World Conference on Photovoltaic Energy Conversion*, Osaka, Japan, 2003, vol. 2, pp. 1888–1891.

[62] D. L. King, M. A. Quintana, J. A. Kratochvil, D. E. Ellibee, and B. R. Hansen, "Photovoltaic module performance and durability following long-term field exposure," *Prog. Photovoltaics Res. Appl.*, vol. 8, no. 2, pp. 241–256, 2000, doi: 10.1002/(SICI)1099-159X(200003/04)8:2<241::AID-PIP290>3.0.CO;2-D.

[63] J. H. Wohlgemuth, D. W. Cunningham, A. M. Nguyen, and J. Miller, "Long term reliability of PV modules," in *Proceedings of the 20th European PV Solar Energy Conference*, Spain, 2005, pp. 1942–1948, [Online]. Available: http://citeseerx.ist.psu.edu/viewdoc/download;jsessionid=F0050C879CAA1F0BD54880F4EE1AEC40?doi=10.1.1.496.984&rep=rep1&type=pdf.

[64] M. G. Tamizhmani, "Performance losses and reliability of photovoltaic modules," in *Proceedings of the International PV Reliability Workshop*, Tempe, AZ, USA, 2009.

[65] P. Sánchez-Friera, M. Piliougine, J. Peláez, J. Carretero, and M. S. De Cardona, "Analysis of degradation mechanisms of crystalline silicon PV modules after 12 years of operation in Southern Europe," *Prog. Photovoltaics Res. Appl.*, vol. 19, no. 6, pp. 658–666, 2011, doi: 10.1002/pip.1083.

[66] Realini A. Mean time before failure of photovoltaic modules, Federal Office for Education and Science, *Final report BBW 99.0579*, June 2003.

[67] A. Realini, E. Burá, N. Cereghetti, D. Chianese, and S. Rezzonico, "Study of a 20 year old PV plant," in *Proceedings of the 17th European Photovoltaic Solar Energy Conference*, Munich, Germany, 2001, pp. 447–450.

[68] Hedström J, Palmblad L, "Performance of old PV modules: measurement of 25 years old crystalline silicon modules", *Elforsk Rapport 06:71,* October 2006.

[69] Saleh IM, Abouhdima I, Gantrari MB, "Performance of Thirty Years Stand Alone Photovoltaic System," in *Proceedings of the 24th European Photovoltaic Solar Energy Conference,* Hamburg, Germany, 2009, pp. 3995–3998, doi:

284

10.4229/24thEUPVSEC2009-5DO.7.6.

[70]   F. Vignola, F. Mavromatakis, J. Krumsick, and R. Walwyn, "Measuring degradation of photovoltaic module performance in the field," in *Proceedings of the 38th ASES National Solar Conference* , Buffalo, NY, USA 2009, vol. 5, pp. 2611–2633.

[71]   M. Alonso-Abella, F. Chenlo, N. Vela, J. Chamberlain, R. Arroyo, and F. J. Alonso-Martínez, "Toledo PV plant 1MWp-10 years of operation," in *Proceedings of the 20th European Photovoltaic Solar Energy Conference*, Barcelona, Spain, 2005, pp. 2454–2457.

[72]   McNutt P, Adelstein J, SekulicW, "Performance evaluation of a 1.5-kW a-Si PV array using the PVUSA power rating method at NREL's outdoor test facility", *DOE Solar Energy Technologies Program Review Meeting*, Denver, CO, USA, 2005, NREL/CP-520-38971, November .

[73]   Adelstein J, Sekulic W, "Small PV systems performance evaluation at NREL's outdoor test facility using the PVUSA power rating method", *DOE Solar Energy Technologies Program Review Meeting*, Denver, CO, USA, 2005, NREL/CP-520-39135, November 2005.

[74]   A. Gregg, R. Blieden, A. Chang, and H. Ng, "Performance analysis of large scale, amorphous silicon, photovoltaic power systems," in *Proceedings of the 31st IEEE Photovoltaic Specialists Conference*, Buena, FL, 2005, pp. 1615–1618, doi: 10.1109/PVSC.2005.1488454.

[75]   F. Apicella, S. Ferlito, V. Giglio, M. Pellegrino, Y. Okamoto, and F. Tanikawa, "Thin Film PV Tile: Long Term Operational Experience in Mediterranean Climate," in *Proceedings of the 23rd European Photovoltaic Solar Energy Conference*, Valencia, Spain, 2008, pp. 4261–4264, doi: 10.4229/ 23rdEUPVSEC2008-5BV.2.21.

[76]   S. M. Pietruszko, B. Fetlinski, and M. Bialecki, "Analysis of the performance of grid connected photovoltaic system," in *Proceedings of the 34th IEEE Photovoltaic Specialists Conference*, Philadelphia, PA, 2009, pp. 000048–000051, doi: 10.1109/PVSC.2009.5411757.

[77]   Dirnberger D, Heydenreich W and Kiefer K, 'Performance of thin film PV technologies—Fraunhofer ISE experience form field and laboratory measurements", in *Proceedings of the 6th International Thin Film Conference*, Würzburg, Germany, 2010.

[78]   B. Marion, J. A. del Cueto, P. McNutt, and D. Rose, "Performance Summary for the First Solar CdTe 1 kW System," in *NREL/CP-520-30942, Lakewood, CO, USA*, 2001, no. October, pp. 1–4.

[79]   M. Ross, G. Rich, L. Petacci, and J. Klammer, "Improvement in reliability and energy yield prediction of thin-film CdS/CdTe PV modules," in *Proceedings of the 4th World Conference on Photovoltaic Energy Conversion, WCPEC-4*, Waikoloa, HI, 2006, vol. 2, pp. 2148–2151, doi: 10.1109/WCPEC.2006.279930.

[80]   R. E. Foster, L. M. G. Rocha, V. P. Gupta, Á. Sánchez-Juárez, J. O. Cruz, and J. C. Rosas, "Field testing of CdTe PV modules in Mexico," in *Proceedings of the International Solar*

Energy Conference, Denver, CO, 2006.

[81] D. Jordan, J. Wohlgemuth, and S. Kurtz, "Technology and Climate Trends in PV Module Degradation", in *Proceedings of the 27th European Photovoltaic Solar Energy Conference*, Frankfurt, Germany, 2012, pp. 3118–3124.

[82] D. C. Jordan and S. R. Kurtz, "Field performance of 1.7 GW of photovoltaic systems," *IEEE J. Photovoltaics*, vol. 5, no. 1, pp. 243–249, 2015, doi: 10.1109/JPHOTOV.2014.2361667.

[83] M. G. Deceglie, D. C. Jordan, A. Nag, A. Shinn, and C. Deline, "Fleet-Scale Energy-Yield Degradation Analysis Applied to Hundreds of Residential and Nonresidential Photovoltaic Systems," *IEEE J. Photovoltaics*, vol. 9, no. 2, pp. 476–482, 2019, doi: 10.1109/JPHOTOV.2018.2884948.

[84] A. Suleske, J. Singh, J. Kuitche, and G. Tamizh-Mani, "Performance degradation of grid-tied photovoltaic modules in a hot-dry climatic condition," in *Proceedings of Reliability of Photovoltaic Cells, Modules, Components, and Systems IV*, 2011, vol. 8112, p. 81120P, doi: 10.1117/12.894928.

[85] C. Raupp *et al.*, "Degradation rate evaluation of multiple PV technologies from 59,000 modules representing 252,000 modules in four climatic regions of the United States," in *Proceedings of the 44th IEEE Photovoltaic Specialist Conference*, Washington, DC, 2017, pp. 1–6, doi: 10.1109/PVSC.2017.8366611.

[86] Honnurvali M.S., Gupta N., Goh K., et al. 'Case study of PV output power degradation rates in Oman', *IET Renew. Power Gener.*, 2018, 13, pp. 352–360.

[87] J. H. Wohlgemuth, O. S. Sastry, A. Stokes, Y. K. Singh, and M. Kumar, "Characterization of field exposed thin film modules," in *Proceedings of the 38th IEEE Photovoltaic Specialists Conference*, Texas, AU, 2012, pp. 2411–2415, doi: 10.1109/PVSC.2012.6318083.

[88] O. S. Sastry *et al.*, "Performance analysis of field exposed single crystalline silicon modules," *Sol. Energy Mater. Sol. Cells*, vol. 94, no. 9, pp. 1463–1468, 2010, doi: 10.1016/j.solmat.2010.03.035.

[89] O. S. Sastry, A. Kumar, R.K. Singh, D. Adiraju, A. Anand, R. Kumar, "Performance Comparision of Three Technology Modules Under Similar Outdoor Conditions," in *Proceedings of the 26th European Photovoltaic Solar Energy Conference and Exhibition*, Hamburg, Germany, 2011, pp. 3566–3568.

[90] A. Sinha, O. S. Sastry, Y. K. Singh, M. Kumar, and R. Gupta, "Performance of Champion Module's of PV Lighting Systems in India," in *Proceedings of the 27th European Photovoltaic Solar Energy Conference and Exhibition*, Frankfurt, Germany, 2012, pp. 3507–3510, doi: 10.4229/27thEUPVSEC2012-4BV.3.36.

[91] V. Sharma, O. S. Sastry, A. Kumar, B. Bora, and S. S. Chandel, "Degradation analysis of a-Si, (HIT) hetro-junction intrinsic thin layer silicon and mc-Si solar photovoltaic technologies under outdoor conditions," *Energy*, vol. 72, pp. 536–546, 2014, doi:

10.1016/j.energy.2014.05.078.

[92] B. Bora, O. S. Sastry, A. Kumar, Renu, and M. Bangar, "Performance modeling of three pv module technologies based on clearness index and air-mass using contour map," in *Proceedings of the 42nd IEEE Photovoltaic Specialists Conference,* New Orleans, LA, 2015, pp. 1-4, doi: 10.1109/PVSC.2015.7356008.

[93] S. Rai *et al.*, "Modeling the performance of HIT technology for composite climatic zone of India", in *Proceedings of the 42nd IEEE Photovoltaic Specialists Conference,* New Orleans, LA , 2015, doi: 10.1109/PVSC.2015.7355999.

[94] V. Sharma, A. Kumar, O. S. Sastry, and S. S. Chandel, "Performance assessment of different solar photovoltaic technologies under similar outdoor conditions," *Energy*, vol. 58, pp. 511–518, 2013, doi: 10.1016/j.energy.2013.05.068.

[95] R. Singh *et al.*, "Effect of series resistance on degradation of isc, power output and fill factor of HIT technology", in *Proceedings of the 42nd IEEE Photovoltaic Specialists Conference,* New Orleans, LA , 2015, doi: 10.1109/PVSC.2015.7356032.

[96] G. Makrides, B. Zinsser, A. Phinikarides, M. Schubert, and G. E. Georghiou, "Temperature and thermal annealing effects on different photovoltaic technologies," *Renew. Energy*, vol. 43, pp. 407–417, 2012, doi: 10.1016/j.renene.2011.11.046.

[97] D. B. Magare *et al.*, "Effect of seasonal spectral variations on performance of three different photovoltaic technologies in India," *Int. J. Energy Environ. Eng.*, vol. 7, no. 1, pp. 93–103, 2016, doi: 10.1007/s40095-015-0190-0.

[98] M. Bangar, B. Bora, Renu, A. Kumar, and O. S. Sastry, "Analysis of spectrum variations in different seasons in composite climate zone of India," in *Proceedings of the 42nd IEEE Photovoltaic Specialists Conference,* New Orleans, LA, 2015, pp. 1–4, doi: 10.1109/PVSC.2015.7356007.

[99] Y. K. Singh *et al.*, "Effect of spectrum and temperature on seasonal performance of CdTe technology in composite climate of India," in *Proceedings of the 42nd IEEE Photovoltaic Specialists Conference,* New Orleans, LA*,* 2015, pp. 1–3, doi: 10.1109/PVSC.2015.7355820.

[100] O. S. Sastry, R. Chandel, R. K. Singh, R. B. Stephen, P. K. Dash, R. Kumar, B. Bandhopadhyay, "Degradation Analysis of Different PV Modules After Prolonged Field Operation", in *Proceedings of the 26th European Photovoltaic Solar Energy Conference and Exhibition*, Hamburg, Germany, 2011, pp. 3495–3499, doi: 10.4229/26thEUPVSEC2011-4AV.2.6.

[101] V. Schacht, A. Häberle, I. Mitra, A. K. Kumar, and A. N. Srivastava, "PV Performance Benchmarking in India. Results from the Project 'Solar Mapping and Monitoring-SolMap,'" in *Proceedings of the ISES Conference*, 2015, pp. 1–10, doi: 10.18086/eurosun.2014.02.03.

[102] A. Pooppal and H. te Heesen, "Survey on Yield of Photovoltaic Systems in India 2014," in *Proceedings of the 31st European Photovoltaic Solar Energy Conference and*

Exhibition, Hamburg, Germany, 2015, pp. 2307–2310, doi: 10.4229/EUPVSEC20152015-5BV.2.45 [Online]. Available: http://www.eupvsec-proceedings.com/proceedings?paper=34485.

[103] S. Roy and B. Ghosh, "Performance of a 10MWp Grid-Integrated PV System in Salty Warm and Humid Ambience in India," in *Proceedings of the 28th European Photovoltaic Solar Energy Conference and Exhibition*, Paris, France, 2013, pp. 3678–3681, doi: 10.4229/28thEUPVSEC2013-5CO.5.5.

[104] B. Ghosh and S. Bardhan, "Impacts and uncertainties of a 10 MWp grid integrated PV power plant in salt marsh land of India," in *Proceedings of the 27th European Photovoltaic Solar Energy Conference and Exhibition*, Frankfurt Germany, 2012, pp. 4638–4641, doi: 10.4229/27thEUPVSEC2012-6CV.4.2

[105] B. Tripathi, P. Yadav, S. Rathod, and M. Kumar, "Performance analysis and comparison of two silicon material based photovoltaic technologies under actual climatic conditions in Western India," *Energy Convers. Manag.*, vol. 80, pp. 97–102, 2014, doi: 10.1016/j.enconman.2014.01.013.

[106] R. Srivastava, A. N. Tiwari, and V. K. Giri, "An overview on performance of PV plants commissioned at different places in the world," *Energy Sustain. Dev.*, vol. 54, pp. 51–59, 2020, doi: 10.1016/j.esd.2019.10.004.

[107] O. Dupré, R. Vaillon, M. A. Green, *Thermal Behavior of Photovoltaic Devices*, Springer, Cham, Switzerland, 2017.

[108] J. Y. Ye, T. Reindl, A. G. Aberle, and T. M. Walsh, "Effect of solar spectrum on the performance of various thin-film PV module technologies in tropical Singapore," *IEEE J. Photovoltaics*, vol. 4, no. 5, pp. 1268–1274, 2014, doi: 10.1109/JPHOTOV.2014.2328585.

[109] N. Strevel, L. Trippel, M. Gloeckler, "Performance characterization and superior energy yield of first solar PV power plants in high-temperature conditions", *Photovoltaics International*, vol. 17, pp. 1-6, 2012.

[110] D. A. Quansah, M. S Adaramola and G. Takyi, 'Reliability and degradation of solar PV modules – case study of 19-year-Old polycrystalline modules in Ghana', MDPI, 2017, 5, (2), p. 22. [Online]. Available: https://doi.org/ 10.3390/technologies5020022. [Accessed: Feb. 12, 2020]

[111] Rehman, S. and El-Amin, "Performance evaluation of an off-grid photovoltaic system in Saudi Arabia", *Energy*, 2012, 46, (1), pp. 451–458. [Online].Available: http://dx.doi.org/10.1016/j.energy.2012.08.004 [Accessed: July 16, 2018].

[112] M. S. Honnurvali, N. Gupta, K. Goh, *et al.* 'Case study of PV output power degradation rates in Oman', *IET Renew. Power Gener.*, 2018, 13, pp. 352–360.

[113] J. Singh, J. Belmont, and G. Tamizhmani, "Degradation analysis of 1900 PV modules in a hot-dry climate: Results after 12 to 18 years of field exposure," in *Proceedings of the 39th IEEE Photovoltaic Specialists Conference*, Tampa, FL, 2013, pp. 3270–3275, doi: 10.1109/PVSC.2013.6745149.

[114] S. V. Janakeeraman, J. Singh, J. Kuitche, J. K. Mallineni, and G. Tamizhmani, "A statistical analysis on the cell parameters responsible for power degradation of fielded pv modules in a hot-dry climate," in *Proceedings of the 40th IEEE Photovoltaic Specialist Conference,* Denver, CO,2014, pp. 3234–3238, doi: 10.1109/PVSC.2014.6925624.

[115] K. Yedidi, S. Tatapudi, J. Mallineni, B. Knisely, J. Kutiche, and G. Tamizhmani, "Failure and degradation modes and rates of PV modules in a hot-dry climate: Results after 16 years of field exposure," in *Proceedings of the 40th IEEE Photovoltaic Specialist Conference,* Denver, CO,2014, pp. 3245–3247, doi: 10.1109/PVSC.2014.6925626.

[116] Jonathan Belmont, "26+ Year Old Photovoltaic Power Plant- Degradation and Reliability Evaluation of Crystalline Silicon Modules – North Array," Ph.D. dissertation, Arizona State University, 2013. [Online]. Available: https://repository.asu.edu/attachments/110532/content/Belmont_asu_0010N_12950.pdf. [Accessed: June 16, 2020].

[117] K. Olakonu, "26+ Year Old Photovoltaic Power Plant- Degradation and Reliability Evaluation of Crystalline Silicon Modules – South Array," Ph.D. dissertation, Arizona State University, 2013. [Online]. Available: https://repository.asu.edu/attachments/97788/content//tmp/package-bZMb48/Olakonu_asu_0010N_12428.pdf [Accessed: June 16, 2020].

[118] K. Olakonu, J. Belmont, S. Tatapudi, J. Kuitche, and G. Tamizhmani, "Degradation and failure modes of 26-year-old 200 kW power plant in a hot-dry desert climate," in *Proceedings of the 40th IEEE Photovoltaic Specialist Conference,* Denver, CO,2014, pp. 3207–3210, doi: 10.1109/PVSC.2014.6925618.

[119] N. Umachandran, J. Kuitche, and G. Tamizhmani, "Statistical methods to determine dominant degradation modes of fielded PV modules," in *Proceedings of the 42nd IEEE Photovoltaic Specialists Conference,* New Orleans, LA*,* 2015, doi: 10.1109/PVSC.2015.7355699.

[120] J. M. Kuitche, R. Pan, and G. Tamizhmani, "Investigation of dominant failure mode(s) for field-aged crystalline silicon PV modules under desert climatic conditions," *IEEE J. Photovoltaics*, vol. 4, no. 3, pp. 814–826, 2014, doi: 10.1109/JPHOTOV.2014.2308720.

[121] D. C. Jordan, C. Deline, M. Deceglie, T. J. Silverman, and W. Luo, "PV Degradation - Mounting Temperature," in *Proceedings of the 46th IEEE Photovoltaic Specialists Conference*, Chicago, IL, 2019, pp. 673–679, doi: 10.1109/PVSC40753.2019.8980767.

[122] A. C. Wenham *et al.*, "Hydrogen-Induced Degradation," in *Proceedings of the 7th World Conference on Photovoltaic Energy Conversion (WCPEC) (A Joint Conference of 45th IEEE PVSC, 28th PVSEC & 34th EU PVSEC)*, Waikoloa Village, HI, 2018, pp. 0001-0008, doi: 10.1109/PVSC.2018.8548100.

[123] S. Kurtz *et al.*, "Evaluation of high-temperature exposure of photovoltaic modules," *Prog. Photovoltaics Res. Appl.*, vol. 19, no. 8, pp. 954–965, 2011, doi: 10.1002/pip.1103.

[124] A. Sinha *et al.*, "Prediction of Climate-Specific Degradation Rate for Photovoltaic Encapsulant Discoloration," *IEEE J. Photovoltaics*, vol. 10, no. 4, pp. 1093–1101, 2020,

doi: 10.1109/JPHOTOV.2020.2989182.

[125] M. Cocca, L. D'Arienzo, and L. D'Orazio, "Effects of Different Artificial Agings on Structure and Properties of Whatman Paper Samples," *ISRN Mater. Sci.*, vol. 2011, pp. 1–7, 2011, doi: 10.5402/2011/863083.

[126] "PV Relibilty Workshop on Hot-climates," 2016. [Online]. Available: https://www.seriius.org/pdfs/pv-module-reliability-in-hot-climates.pdf [Accessed Jun. 14, 2020].

[127] M. A. Mikofski *et al.*, "PVLife: An integrated model for predicting PV performance degradation over 25+ years," in *Proceedings of the 38th IEEE Photovoltaic Specialists Conference*, Austin, Texas, 2012, pp. 1744–1749, doi: 10.1109/PVSC.2012.6317932.

[128] D. C. Jordan, T. J. Silverman, B. Sekulic, and S. R. Kurtz, "PV degradation curves: non-linearities and failure modes," *Prog. Photovoltaics Res. Appl.*, vol. 25, no. 7, pp. 583–591, 2017, doi: 10.1002/pip.2835.

[129] G. H. Kang, K. S. Kim, H. E. Song, G. J. Yu, H. Ahn, and D. Y. Han, "Investigation of aging phenomenon and power drop rate with field exposed PV modules," in *Proceedings of the 25th European Photovoltaic Solar Energy Conference and Exhibition / 5th World Conference on Photovoltaic Energy Conversion*, Valencia, Spain, 2010, pp. 4015–4018.

[130] M. A. Hossion, "Visual and electrical degradation data of five years aged rooftop photovoltaic modules," *Data in Brief*, vol. 31, 2020, doi: 10.1016/j.dib.2020.105762.

[131] H. Hashigami, Y. Itakura, and T. Saitoh, "Effect of illumination conditions on Czochralski-grown silicon solar cell degradation," *J. Appl. Phys.*, vol. 93, no. 7, pp. 4240–4245, 2003, doi: 10.1063/1.1559430.

[132] K. Bothe, R. Hezel, and J. Schmidt, "Recombination-enhanced formation of the metastable boron-oxygen complex in crystalline silicon," *Appl. Phys. Lett.*, vol. 83, no. 6, pp. 1125–1127, 2003, doi: 10.1063/1.1600837.

[133] R. L. Crabb, "Photon Induced Degradation of Electron and Proton Irradiated Silicon Solar Cells.," in *Proceedings of the IEEE Transactions on Nuclear Science*, vol. 20, no. 6, pp. 243-249, Dec. 1973, doi: 10.1109/TNS.1973.4327402.

[134] K. Graff and H. Pieper, "Carrier lifetime measurements on electron-irradiated silicon crystals," *Phys. Status Solidi*, vol. 30, no. 2, pp. 593–599, 1975, doi: 10.1002/pssa.2210300220.

[135] H. Fischer and W. Pschunder, "Investigation of Photon and Thermal Induced Changes in Silicon Solar Cells.," in *Proceedings of the 10th IEEE Photovoltaic Specialist Conference*, Palo Alto, CA, 1974, pp. 404–411.

[136] J. Schmidt, A. G. Aberle, and R. Hezel, "Investigation of carrier lifetime instabilities in Cz-grown silicon," in *Proceedings of the 26th IEEE Photovoltaic Specialists Conference*, Anaheim, CA, 1997, pp. 13–18, doi: 10.1109/pvsc.1997.653914.

[137] S. W. Glunz, S. Rein, W. Warta, J. Knobloch, and W. Wettling, "Degradation of carrier

lifetime in Cz silicon solar cells," *Sol. Energy Mater. Sol. Cells,* vol. 65, no. 1, pp. 219–229, 2001, doi: 10.1016/S0927-0248(00)00098-2.

[138] S. W. Glunz, S. Rein, J. Knobloch, W. Wettling, and T. Abe, "Comparison of boron- and gallium-doped p-type Czochralski silicon for photovoltaic application," *Prog. Photovoltaics Res. Appl.,* vol. 7, no. 6, pp. 463–469, 1999, doi: 10.1002/(SICI)1099-159X(199911/12)7:6<463::AID-PIP293>3.0.CO;2-H.

[139] H. Savin, M. Yli-Koski, and A. Haarahiltunen, "Role of copper in light induced minority-carrier lifetime degradation of silicon," *Appl. Phys. Lett.,* vol. 95, no. 15, 2009, doi: 10.1063/1.3250161.

[140] J. Lindroos, M. Yli-Koski, A. Haarahiltunen, M. C. Schubert, and H. Savin, "Light-induced degradation in copper-contaminated gallium-doped silicon," *Phys. Status Solidi - Rapid Res. Lett.,* vol. 7, no. 4, pp. 262–264, 2013, doi: 10.1002/pssr.201307011.

[141] K. Ramspeck, S. Zimmermann, H. Nagel, A. Metz, Y. Gassenbauer, B. Birkmann and A. Seidl, "Light Induced Degradation of Rear Passivated mc-Si Solar Cells Klaus," in *Proceedings of the 27th European Photovoltaic Solar Energy Conference and Exhibition,* Frankfurt, Germany, 2017, vol. 8, no. 9, pp. 1–58, doi: 10.1017/CBO9781107415324.004.

[142] S. Pingel, D. Koshnicharov, O. Frank, and T. Geipel, "Initial degradation of industrial silicon solar cells in solar panels'," 2010, [Online]. Available: http://www.solon.com/export/sites/default/solonse.com/_downloads/global/article-pid/Pingel_et_al_Initial_Degradation.pdf.

[143] F. Fertig, K. Krauß, and S. Rein, "Light-induced degradation of PECVD aluminium oxide passivated silicon solar cells," *Phys. Status Solidi - Rapid Res. Lett.,* vol. 9, no. 1, pp. 41–46, 2015, doi: 10.1002/pssr.201409424.

[144] D. L. Staebler and C. R. Wronski, "Reversible conductivity changes in discharge-produced amorphous Si," *Appl. Phys. Lett.,* vol. 31, no. 4, pp. 292–294, 1977, doi: 10.1063/1.89674.

[145] R. Rüther and J. Livingstone, "Seasonal variations in amorphous silicon solar module outputs and thin film characteristics," *Sol. Energy Mater. Sol. Cells,* vol. 36, no. 1, pp. 29–43, 1995, doi: 10.1016/0927-0248(94)00165-O.

[146] S. Demtsu, S. Bansal, and D. Albin, "Intrinsic stability of thin-film CdS/CdTe modules," in *Proceedings of the 35th IEEE Photovoltaic Specialists Conference,* Honolulu, HI, 2010, pp. 1161–1165, doi: 10.1109/PVSC.2010.5614753.

[147] J. A. Del Cueto and B. Von Roedern, "Long-term Transient and Metastable Effects in Cadmium Telluride Photovoltaic Modules," *Prog. Photovoltaics Res. Appl.,* vol. 14, no. 7, pp. 615–628, 2006, doi: 10.1002/pip.687.

[148] T. J. Silverman, U. Jahn, G. Friesen, M. Pravettoni, M. Apolioni, A. Louwen, W van Sark, M. Schweiger, G. Belluardo, J. Wagner, A. Tetzlaff, P. Ingenhoven, D. Moser, "Characterization of Performance of Thin Film Photovoltaic Technologies", *International Energy Agency,* Report number: IEA-PVPS T13-02:2014. [Online]. Available:

http://dspace.library.uu.nl/handle/1874/306324 [Accessed: March 6, 2019]

[149] Vikram Solar, "Limited and Linear Warranty for PV Modules." [Online]. Available: https://www.vikramsolar.com/wp-content/uploads/2016/03/Warranty-Certificate_Dec16.pdf [Accessed Jul. 20, 2020].

[150] Jinko Solar, "Limited Warranty." [Online]. Available: https://www.jinkosolar.com/download.html?downid=223 [Accessed Jul. 20, 2020].

[151] JA Solar, "Limited Warranty." [Online]. Available: http://en.jasolar.com/site/pdf/594 [Accessed Jul. 20, 2020].

[152] PVSyst, "LID (Light Induced Degradation) Loss." [Online]. Available: http://files.pvsyst.com/help/lid_loss.htm [Accessed Jul. 20, 2020].

[153] V. G. Weizer, H. W. Brandhorst, J. D. Broder, R. E. Hart, and J. H. Lamneck, "Photon-degradation effects in terrestrial silicon solar cells," *J. Appl. Phys.*, vol. 50, no. 6, pp. 4443–4449, 1979, doi: 10.1063/1.326437.

[154] J. H. Reiss, R. R. King, and K. W. Mitchell, "Characterization of diffusion length degradation in Czochralski silicon solar cells," *Appl. Phys. Lett.*, vol. 68, no. 23, pp. 3302–3304, 1996, doi: 10.1063/1.116581.

[155] D. R. Tobergte and S. Curtis, "Light Induced Degradation in Multicrystalline Solar Grade Silicon Solar Cells Evaluated Using Accelerated Lid," in *Journal of Chemical Information and Modeling*, 2013, vol. 53, no. 9, pp. 1689–1699, doi: 10.4229/26thEUPVSEC2011-2BV.4.21.

[156] K. M. Broek, I. J. Bennett, M. J. Jansen, N. J. C. M. van der Borg and W. Eerenstein, "Light and Current Induced Degradation in p-Type Multi-Crystalline Cells and Development of an Inspection Method and a Stabilisation Method," in *Proceedings of the 27th European Photovoltaic Solar Energy Conference and Exhibition*, Frankfurt Germany, 2012, pp. 3167–3171, doi: 10.4229/27thEUPVSEC2012-4DO.6.5.

[157] B. Sopori *et al.*, "Understanding light-induced degradation of c-Si solar cells," in *Proceedings of the 38th IEEE Photovoltaic Specialists Conference*, Austin, Texas, 2012, pp. 1115–1120, doi: 10.1109/PVSC.2012.6317798.

[158] K. Ramspeck, "Light induced degradation of rear passivated mc-Si solar cells," in *Proceedings of the 27th European Photovoltaic Solar Energy Conference and Exhibition,* Frankfurt, Germany, 2012, vol. 91, no. 5, pp. 1689–1699.

[159] F. Fertig *et al.*, "Fully solderable large-area screen-printed Al-BSF p-type MC-Si solar cells from 100 % solar grade feedstock yielding > 17 %: Challenges and potential on cell and module level," in *Proceedings of the 27th European Photovoltaic Solar Energy Conference and Exhibition,* Frankfurt, Germany, 2012, pp. 1031–1038, doi: 10.4229/27thEUPVSEC2012-2AV.4.42

[160] G. Dingemans *et al.*, "Stability of Al2O3 and Al2O3/a- SiNx:H stacks for surface passivation of crystalline silicon," *J. Appl. Phys.*, vol. 106, no. 11, 2009, doi: 10.1063/1.3264572.

[161] B. Liao, R. Stangl, T. Mueller, F. Lin, C. S. Bhatia, and B. Hoex, "The effect of light soaking on crystalline silicon surface passivation by atomic layer deposited Al2O3," *J. Appl. Phys.*, vol. 113, no. 2, 2013, doi: 10.1063/1.4775595.

[162] F. Kersten *et al.*, "Degradation of multicrystalline silicon solar cells and modules after illumination at elevated temperature," *Sol. Energy Mater. Sol. Cells*, vol. 142, pp. 83–86, 2015, doi: 10.1016/j.solmat.2015.06.015.

[163] S. Pingel *et al.*, "Potential induced degradation of solar cells and panels," in *Proceedings of the 36th IEEE Photovoltaic Specialists Conference*, Honolulu, HI, 2010, pp. 2817–2822, doi: 10.1109/PVSC.2010.5616823.

[164] P. Hacke *et al.*, "Test-to-failure of crystalline silicon modules," in *Proceedings of the 36th IEEE Photovoltaic Specialists Conference*, Honolulu, HI, 2010, pp. 244–250, doi: 10.1109/PVSC.2010.5614472.

[165] M. Rojen, S. Schönberger, J. Mayer, and M. Kasemann, "Techno-Economic Analysis of Utility Scale PV Power Plants with Up to +/-1500 VDC," in *Proceedings of the 29th European Photovoltaic Solar Energy Conference and Exhibition*, Amsterdam, The Netherlands, 2014, pp. 1689–1699, doi: 10.4229/EUPVSEC20142014-5CO.12.5

[166] G. Mon, L. Wen, R. Ross and D. Adent, "Effects of temperature and moisture on module leakage current" in *Proceedings of the 18th IEEE Photovoltaic Specialists Conference*, Las Vegas, NV, USA, 1985, pp. 1179–1185.

[167] G. Mon and R. Ross, "Electrochemical Degradation of Amorphous-Silicon Photovoltaic Modules," in *Proceedings of the 18th IEEE Photovoltaic Specialists Conference*, Las Vegas, Nevada, October 21-25, 1985, pp. 1142-1149.

[168] C. R. Osterwald, T. J. McMahon, and J. A. Del Cueto, "Electrochemical corrosion of SnO2:F transparent conducting layers in thin-film photovoltaic modules," *Sol. Energy Mater. Sol. Cells*, vol. 79, no. 1, pp. 21–33, 2003, doi: 10.1016/S0927-0248(02)00363-X.

[169] N. G. Dhere, S. M. Bet, and H. P. Patil, "High-voltage bias testing of thin-film PV modules," in *Proceedings of the 3rd World Conference on Photovoltaic Energy Conversion*, Osaka, Japan, 2003, vol. 2, pp. 1923–1926.

[170] T. J. McMahon and G. J. Jorgensen, "Electrical Currents and Adhesion of Edge-Delete Regions of EVA-to-Glass Module Packaging," in *Proceedings of the 2001 NCPV Program Review Meeting*, Lakewood, CO, 2001, [Online]. Available: http://www.nrel.gov/docs/fy02osti/30819.pdf.

[171] R. Swanson , M. Cudzinovic , D. DeCeuster , V. Desai , J. Jürgens , N. Kaminar , W. Mulligan , L. Barbarosa , D. Rose and D. Smith,"The surface polarization effect in high efficiency silicon solar cells", in *Proceedings of 15th International Photovoltaic Science and Engineering Conference*, Shanghai, China, 2005, pp. 410–411.

[172] P. Hacke *et al.*, "Acceleration factor determination for potential-induced degradation in crystalline silicon PV modules," in *Proceedings of 2013 IEEE International Reliability Physics Symposium (IRPS)*, Anaheim, CA, 2013, pp. 4B.1.1–4B.1.5 2013, doi:

293

10.1109/IRPS.2013.6532009.

[173] P. Hacke, R. Smith, K. Terwilliger, G. Perrin, B. Sekulic, and S. Kurtz, "Development of an IEC test for crystalline silicon modules to qualify their resistance to system voltage stress," *Prog. Photovoltaics Res. Appl.*, vol. 22, no. 7, pp. 775–783, 2014, doi: 10.1002/pip.2434.

[174] P. Hacke *et al.*, "System voltage potential-induced degradation mechanisms in PV modules and methods for test," in *Proceedings of the 37th IEEE Photovoltaic Specialists Conference*, Seattle, WA, 2011, pp. 000814–000820, doi: 10.1109/PVSC.2011.6186079.

[175] Z. Xiong, T. M. Walsh, and A. G. Aberle, "PV module durability testing under high voltage biased damp heat conditions," *Energy Procedia*, vol. 8, pp. 384–389, 2011, doi: 10.1016/j.egypro.2011.06.154.

[176] J. Berghold, S. Koch, B. Frohmann, P. Hacke, and P. Grunow, "Properties of encapsulation materials and their relevance for recent field failures," in *Proceedings of the 40th IEEE Photovoltaic Specialist Conference,* Denver, CO, 2014, pp. 1987–1992, doi: 10.1109/PVSC.2014.6925315.

[177] M. Schütze *et al.*, "Laboratory study of potential induced degradation of silicon photovoltaic modules," in *Proceedings of the 37th IEEE Photovoltaic Specialists Conference*, Washington, DC, 2011, pp. 000821–000826, doi: 10.1109/PVSC.2011.6186080.

[178] N. G. Dhere, N. S. Shiradkar, and E. Schneller, "Evolution of leakage current paths in MC-Si PV modules from leading manufacturers undergoing high-voltage bias testing," *IEEE J. Photovoltaics*, vol. 4, no. 2, pp. 654–658, 2014, doi: 10.1109/JPHOTOV.2013.2294764.

[179] P. Hacke, P. Burton, A. Hendrickson, S. Spataru, S. Glick, and K. Terwilliger, "Effects of photovoltaic module soiling on glass surface resistance and potential-induced degradation," in *Proceedings of the 42nd IEEE Photovoltaic Specialists Conference*, New Orleans, LA, 2015, pp. 1-4, doi: 10.1109/PVSC.2015.7355711.

[180] N. Shiradkar, E. Schneller, and N. G. Dhere, "Finite element analysis based model to study the electric field distribution and leakage current in PV modules under high voltage bias," in *Reliability of Photovoltaic Cells, Modules, Components, and Systems VI*, 2013, vol. 8825, p. 88250G, doi: 10.1117/12.2024740.

[181] S. Hoffmann and M. Koehl, "Effect of humidity and temperature on the potential-induced degradation," *Prog. Photovoltaics Res. Appl.*, vol. 22, no. 2, pp. 173–179, 2014, doi: 10.1002/pip.2238.

[182] H. Nagel, A. Metz, and K. Wangemann, "Crystalline si solar cells and modules featuring excellent stability against potential-induced degradation," in *Proceedings of the 26th European Photovoltaic Solar Energy Conference and Exhibition*, Hamburg, Germany, 2011, pp. 3107–3112, doi: 10.4229/26thEUPVSEC2011-4CO.5.6.

[183] N. G. Dhere, A. Kaul, and S. A. Pethe, "Long-term performance analysis of CIGS thin

film PV modules," in *Reliability of Photovoltaic Cells, Modules, Components, and Systems IV*, 2011, vol. 8112, p. 81120R, doi: 10.1117/12.893864.

[184] P. Hacke *et al.*, "Testing and analysis for lifetime prediction of crystalline silicon PV modules undergoing degradation by system voltage stress," in *Proceedings of the 38th Photovoltaic Specialists Conference*, Austin, TX, 2012, pp. 1–8, doi: 10.1109/pvsc-vol2.2012.6656746.

[185] J. Bauer, V. Naumann, S. Großer, C. Hagendorf, M. Schütze, and O. Breitenstein, "On the mechanism of potential-induced degradation in crystalline silicon solar cells," *Phys. Status Solidi - Rapid Res. Lett.*, vol. 6, no. 8, pp. 331–333, 2012, doi: 10.1002/pssr.201206276.

[186] V. Naumann *et al.*, "Explanation of potential-induced degradation of the shunting type by Na decoration of stacking faults in Si solar cells," *Sol. Energy Mater. Sol. Cells*, vol. 120, no. PART A, pp. 383–389, 2014, doi: 10.1016/j.solmat.2013.06.015.

[187] V. Naumann, D. Lausch, and C. Hagendorf, "Sodium Decoration of PID-s Crystal Defects after Corona Induced Degradation of Bare Silicon Solar Cells," *Energy Procedia*, vol. 77, pp. 397–401, 2015, doi: 10.1016/j.egypro.2015.07.055.

[188] *Photovoltaic (PV) modules - Test methods for the detection of potential-induced degradation - Part 1-1: Crystalline silicon - Delamination,* IEC TS 62804-1, Edition 1.0, 2015.

[189] T. M. Walsh, Z. Xiong, Y. S. Khoo, A. A. O. Tay, and A. G. Aberle, "Singapore modules-optimised PV modules for the tropics," *Energy Procedia*, vol. 15, pp. 388–395, 2012, doi: 10.1016/j.egypro.2012.02.047.

[190] J. Hattendorf *et al.*, "Potential induced degradation in mono-crystalline silicon based modules: An acceleration model," in *Proceedings of the 27th European Photovoltaic Solar Energy Conference and Exhibition*, Frankfurt Germany, 2012, pp. 3405–3410, doi: 10.4229/27thEUPVSEC2012-4BV.2.51

[191] P. Hacke *et al.*, "Accelerated Testing and Modeling of Potential-Induced Degradation as a Function of Temperature and Relative Humidity," *IEEE J. Photovoltaics*, vol. 5, no. 6, pp. 1549–1553, 2015, doi: 10.1109/JPHOTOV.2015.2466463.

[192] M. Kambe *et al.*, "Chemically strengthened cover glass for preventing potential induced degradation of crystalline silicon solar cells," in *Proceedings of the 39th IEEE Photovoltaic Specialists Conference*, Tampa, FL, 2013, pp. 3500–3503, doi: 10.1109/PVSC.2013.6744441.

[193] J. Oh, S. Bowden, and G. S. TamizhMani, "Potential-Induced Degradation (PID): Incomplete Recovery of Shunt Resistance and Quantum Efficiency Losses," *IEEE J. Photovoltaics*, vol. 5, no. 6, pp. 1540–1548, 2015, doi: 10.1109/JPHOTOV.2015.2459919.

[194] K. Hara, H. Ichinose, T. N. Murakami, and A. Masuda, "Crystalline Si photovoltaic modules based on TiO2-coated cover glass against potential-induced degradation," *RSC Adv.*, vol. 4, no. 83, pp. 44291–44295, 2014, doi: 10.1039/c4ra06791f.

[195] J. Kapur, K. M. Stika, C. S. Westphal, J. L. Norwood, and B. Hamzavytehrany,

"Prevention of potential-induced degradation with thin ionomer film," *IEEE J. Photovoltaics*, vol. 5, no. 1, pp. 219–223, 2015, doi: 10.1109/JPHOTOV.2014.2365465.

[196] T. Kirchartz, A. Heibig, W. Reetz, M. Reuter, J. H. Werner, and U. Rau, "Reciprocity between electroluminescence and quantum efficiency used for the characterization of silicon solar cells," *Prog. Photovoltaics Res. Appl.*, vol. 17, no. 6, pp. 394–402, 2009, doi: 10.1002/pip.895.

[197] P. Würfel, *Physics of Solar Cells: From Principles to New Concepts*. 2007.

[198] J. Colvin, "Comparative failure analysis of photovoltaic devices," in *Proceedings of the 35th International Symposium for Testing and Failure Analysis*, San Jose, CA, 2009, pp. 149–156.

[199] T. Fuyuki and A. Kitiyanan, "Photographic diagnosis of crystalline silicon solar cells utilizing electroluminescence," *Appl. Phys. Lett.*, vol. 96, pp. 189–196, 2008.

[200] M. Israil, S. A. Anwar, and M. Z. Abdullah, "Automatic detection of micro-crack in solar wafers and cells: A review," *Trans. Inst. Meas. Control*, vol. 35, no. 5, pp. 606–618, 2013, doi: 10.1177/0142331212457583.

[201] L. Stoicescu, M. Reuter and J. H. Werner, "Daylight Luminescence for Photovoltaic System Testing," in *Proceedings of the 22nd International Photovoltaic Science and Engineering Conference*, Hanghzhou, China, 2012.

[202] L. Stoicescu, M. Reuter and J. H. Werner, "Method and device for inspecting photovoltaic modules," Patent no. WO 2014023823 A1, 2013.

[203] M. Köntges, M. Siebert, and D. Hinken, "Quantitative analysis of PV-modules by electroluminescence images for quality control," in *Proceedings of the 24th European Photovoltaic Solar Energy Conference and Exhibition*, Hamburg, Germany, 2009, pp. 21–24, [Online]. Available: http://www.isfh.de/institut_solarforschung/files/24eupvsec_koentges_4co.2.3.pdf. [Accessed: Feb. 12, 2020]

[204] S. P. Phang, H. C. Sio, and D. Macdonald, "Applications of carrier de-smearing of photoluminescence images on silicon wafers," *Prog. Photovoltaics Res. Appl.*, vol. 24, no. 12, pp. 1547–1553, 2016, doi: 10.1002/pip.2747.

[205] K. G. Bedrich, "Quantitative Electroluminescence Measurements of PV Devices.", Ph.D. dissertation, Centre for Renewable Energy Systems Technology (CREST), Loughborough University, 2017. [Online]. Available: https://hdl.handle.net/2134/27303 [Accessed: Feb. 12, 2020]

[206] A. Mansouri, M. Zettl, O. Mayer, M. Lynass, M. Bucher, and O. Stern, "Defect detection in photovoltaic modules using electroluminescence imaging," in *Proceedings of the 27th European Photovoltaic Solar Energy Conference and Exhibition*, Frankfurt, Germany, 2012, vol. 64617926, pp. 3374–3378, doi: 10.4229/27thEUPVSEC2012-4BV.2.45

[207] M. Köntges, I. Kunze, S. Kajari-Schröder, X. Breitenmoser, B. Bjørneklett, "The risk of power loss in crystalline silicon based photovoltaic modules due to micro-cracks," *Sol.*

Energy Mater. Sol. Cells, vol. 95, no. 4, pp. 1131–1137, 2011, doi: 10.1016/j.solmat.2010.10.034.

[208] Y. Kaji, Y. Takahashi, A. Ogane, Y. Uraoka, and T. Fuyuki, "Characterization of Polycrystalline Silicon Solar Cells by Electroluminescence," in *Proceedings of the 15th International Photovoltic Science & Engineering Conference*, 2005, pp. 153–154.

[209] T. Fuyuki, Y. Kaji, A. Ogane, and Y. Takahashl, "Analtic findings in the photographic characterization of crystalline silicon solar cells using electroluminescence," in *Proceedings of the 4th IEEE World Conf. Photovolt. Energy Conversion, WCPEC-4*, Waikoloa, HI, 2006, vol. 1, pp. 905–907, doi: 10.1109/WCPEC.2006.279602.

[210] S. Takamoto, E. Sugimura, S. Tsujii, and K. Hirata, "Evaluation of Substrate Defects By Temperature Dependence of Spectroscopic Electroluminescence," in *Proceedings of the 21st International Photovoltaic Science and Engineering Conference*, Fukuoka, Japan, 2011, pp. 1–2.

[211] S. Khatavkar, M. Kulasekaran, C. V. Kannan, V. Kumar, P. Nair, and B. M. Arora, "Modulated electroluminescence technique for determination of the minority carrier lifetime of solar cells," in *Proceedings of the 39th IEEE Photovoltaic Specialists Conference*, Tampa, FL, 2013, pp. 631–634, doi: 10.1109/PVSC.2013.6744230.

[212] V. Gazuz and C. Buerhop, "Electroluminescence imaging for detection of power losses in solder contacts between busbar and interconnect in solar cells," in *Proceedings of the 25th European Photovoltaic Solar Energy Conference and Exhibition*, Valencia, Spain, 2010, pp. 4219–4222, doi: 10.4229/25thEUPVSEC2010-4AV.3.76.

[213] Crozier FJ, van Dyk EE and Vorster FJ., "High Resolution Spatial Electroluminescence Imaging of Photovoltaic Modules." [Online]. Available: http://www.crses.sun.ac.za/files/services/conferences/annual-student-symposium-2012/23_November/11_Crozier.pdf [Accessed Jul. 20, 2020].

[214] Y. Takahashi, Y. Kaji, A. Ogane, Y. Uraoka, and T. Fuyuki, "-"Luminoscopy"- Novel tool for the diagnosis of crystalline silicon solar cells and modules utilizing electroluminescence," in *Proceedings of the 4th World Conference on Photovoltaic Energy Conversion, WCPEC-4*, Waikoloa, Hawaii, 2006, vol. 1, pp. 924–927, doi: 10.1109/WCPEC.2006.279607.

[215] A. Kitiyanan, K. Bothe, Y. Takahashi, A. Ogane, and T. Fuyuki, "Detection of Crack Location Indetection of Crack Location in Multicrystalline Silicon Solar Cells By Electroluminescence Imagesubtraction Technique Multicrystalline Silicon Solar," in *Solar Energy*, 2007, pp. 706–707.

[216] P. Würfel, T. Trupke, T. Puzzer, E. Schäffer, W. Warta, and S. W. Glunz, "Diffusion lengths of silicon solar cells from luminescence images," *J. Appl. Phys.*, vol. 101, no. 12, 2007, doi: 10.1063/1.2749201.

[217] A. Helbig, T. Kirchartz, and U. Rau, "Quantitative Information of Electroluminescence Images," in *Proceedings of the 23rd European Photovoltaic Solar Energy Conference and Exhibition*, Spain, 2008, pp. 1–4.

[218] W. Warta, J. Sutter, B. F. Wagner, and R. Schindler, "Impact of diffusion length distributions on the performance of mc-silicon solar cells," in *Proceedings of the 2ⁿᵈ World Conference on Photovoltaic Solar Energy Conversion*, Vienna, Austria, 1998, vol. 2, pp. 1650–1653.

[219] J. Walter, D. Eberlein, J. Haunschild, M. Tranitz, and U. Eitner, "A method to detect defective solder joints by RS- electroluminescence imaging," *Energy Procedia*, vol. 27, pp. 652–657, 2012, doi: 10.1016/j.egypro.2012.07.124.

[220] D. M. Tsai, S. C. Wu, and W. C. Li, "Defect detection of solar cells in electroluminescence images using Fourier image reconstruction," *Sol. Energy Mater. Sol. Cells*, vol. 99, pp. 250–262, 2012, doi: 10.1016/j.solmat.2011.12.007.

[221] *Terrestrial photovoltaic (PV) modules - Design qualification and type approval - Part 1: Test requirements*, IEC 61215, Edition 1.0, 2016.

[222] A. M. Gabor, R. Janoch, A. Anselmo, J. L. Lincoln, H. Seigneur, and C. Honeker, "Mechanical load testing of solar panels - Beyond certification testing," in *Proceedings of the 43ʳᵈ IEEE Photovoltaic Specialists Conference*, Portland, OR, 2016, pp. 3574–3579, doi: 10.1109/PVSC.2016.7750338.

[223] B. Weller and L. Tautenhahn, "Mechanical challenge of frameless PV-modules," in *Proceedings of the 12ᵗʰ IEEE Intersociety Conference on Thermal and Thermomechanical Phenomena in Electronic Systems,* Las Vegas, NV, 2010, pp. 1-5, doi: 10.1109/ITHERM.2010.5501292.

[224] S. Koch, J. Kupke, D. Tornow, M. Schoppa, S. Krauter, and P. Grunow, "Dynamic Mechanical Load Tests on Crystalline Silicon Modules," in *Proceedings of the 25ᵗʰ European Photovoltaic Solar Energy Conference and Exhibition / 5ᵗʰ World Conference on Photovoltaic Energy Conversion*, Valencia, 2010, pp. 3998–4001, doi: 10.4229/25thEUPVSEC2010-4AV.3.11.

[225] N. Bosco *et al.*, "Evaluation of Dynamic Mechanical Loading as an accelerated test method for ribbon fatigue," in *Proceedings of the 39ᵗʰ IEEE Photovoltaic Specialists Conference*, Tampa, FL, 2013, pp. 3173–3178, doi: 10.1109/PVSC.2013.6745128.

[226] R. Mickiewicz *et al.*, "Effect of Encapsulation Modulus on the Response of PV Modules to Mechanical Stress," in *Proceedings of the 26ᵗʰ European Photovoltaic Solar Energy Conference and Exhibition*, Hamburg, Germany, 2011, pp. 3157–3161, doi: 10.4229/26thEUPVSEC2011-4CO.7.4.

[227] H. Seigneur, E. Schneller, J. Lincoln, and A. M. Gabor, "Cyclic Mechanical Loading of Solar Panels - A Field Experiment," in *Proceedings of the 7ᵗʰ World Conference on Photovoltaic Energy Conversion, WCPEC 2018 - A Joint Conference of 45ᵗʰ IEEE PVSC, 28th PVSEC and 34th EU PVSEC*, Waikoloa, HI, 2018, pp. 3810–3814, doi: 10.1109/PVSC.2018.8548153.

[228] D. P. Vasudevan, P. Bhatt, and A. Kottantharayil, "Impact of Transportation on Indian Roads, on PV Modules," in *Proceedings of the 46ᵗʰ IEEE Photovoltaic Specialists Conference*, Chicago, IL, 2019, pp. 1529–1532, doi: 10.1109/PVSC40753.2019.8980720.

[229] *Standard Practice for Performance Testing of Shipping Containers and Systems*, ASTM International, ASTM D4169-16.

[230] *Photovoltaic (PV) modules - Transportation testing - Part 1: Transportation and shipping of module package units*, IEC 62759, Edition 1, 2015.

[231] Solmetric, "PVA-1000S PV Analyzer Kit," *Solmetric*, 2016. [Online]. Available: http://www.solmetric.com/pvanalyzermatrix.html [Accessed Mar. 11, 2020].

[232] Spire Solar, "Spire Solar 5600SLP Blue 230ms - Spire Solar." [Online]. Available: https://www.spiresolar.com/products/solar-simulators/spi-sun-simulator-5600slp-blue/ [Accessed Mar. 11, 2019].

[233] *Photovoltaic devices - Part 9: Solar simulator performance requirements,* IEC Standard 60904-9, 2007.

[234] Sensovation, "Laboratory microscope camera SensoCam HR-830." [Online]. Available: http://www.sensovation.com/bausteine.net/f/10697/140129_SensoCamA4single_HR-830dis.pdf?fd=2 [Accessed Oct. 20, 2020].

[235] G. F. M. Kontges, S. Kurtz, C. Packard, U. Jahn, K. A. Berger, K. Kato, T. Friesen, H. Liu, M. V. Iseghem, J. Wohlgemuth, D. C. Miller, M. Kempe, P. Hacke, F. Reil, N. Bogdanski, W. Herrmann, C. Buerhop, G. Razongles, "Review of Failures of Photovoltaic Modules," International Energy Agency, Report number: IEA-PVPS T13-01:2014." [Online]. Available: http://www.iea-pvps.org/fileadmin/dam/intranet/ExCo/IEA-PVPS_T13-01_2014_Review_of_Failures_of_Photovoltaic_Modules_Final.pdf [Accessed Mar. 06, 2020].

[236] R. Dubey, S. Chattopadhyay, V. Kuthanazhi, J. John, C. S. Solanki, A. Kottantharayil, B. M. Arora, K. Narsimhan, J. Vasi, B. Bora, Y. Singh and O.S. Sastry, "All India Survey of Photovoltaic Module Degradation: 2013", [Online] Available: http://www.ncpre.iitb.ac.in/research/reports.html [Accessed Mar. 06, 2020].

[237] R. Dubey, S. Chattopadhyay, V. Kuthanazhi, J. John, F. Ansari, S. Rambabu, B. M. Arora, A. Kottantharayil, K. L. Narasimhan, J. Vasi, B. Bora, Y. K. Singh, K. Yadav, M. Banger, R. Singh and O.S. Sastry," All India Survey of Photovoltaic Module Reliability: 2014", [Online] Available: http://www.ncpre.iitb.ac.in/research/reports.html [Accessed Mar. 06, 2020].

[238] R. Dubey *et al.*, "Measurement of temperature coefficient of photovoltaic modules in field and comparison with laboratory measurements," in *Proceedings of the 42nd IEEE Photovoltaic Specialist Conference*, New Orleans, LA, 2015, pp. 1-5, doi: 10.1109/PVSC.2015.7355852.

[239] N. K. Bansal and G. Minke*, Climatic Zones and Rural Housing in India.* Julich: Forschungszentrum Julich GmbH, 1995.

[240] D. George and P. Mallery, "Skewness and kurtosis" [Online] Available: https://portal.regenesys.net/course/discussions/editors/kcfinder/upload/files/MBA9_BRES_SLIDES_v17.5_Class_4a.pdf [Accessed Oct. 20, 2020].

[241] S. Chattopadhyay, "Encapsulant Discoloration in Photovoltaic Modules in Different Indian Climates and its correlation with Hot Cells and Electrical Degradation," Ph.D. dissertation, ESE Department, IIT Bombay, 2020.

[242] S. V. Spataru, D. Sera, P. Hacke, T. Kerekes, and R. Teodorescu, "Fault identification in crystalline silicon PV modules by complementary analysis of the light and dark current-voltage characteristics," *Prog. Photovoltaics Res. Appl.*, vol. 24, no. 4, pp. 517–532, 2016, doi: 10.1002/pip.2571.

[243] K. Bouzidi, M. Chegaar, and M. Aillerie, "Solar cells parameters evaluation from dark I-V Characteristics," *Energy Procedia*, vol. 18, pp. 1601–1610, 2012, doi: 10.1016/j.egypro.2012.06.002.

[244] O. Breitenstein, P. Altermatt, K. Ramspeck, M. A. Green, J. Zhao, and A. Schenk, "Interpretation of the commonly observed I-V characteristics of c-Si cells having ideality factor larger than two," in *Proceedings of the IEEE 4th World Conference on Photovoltaic Energy Conversion, WCPEC-4*, Waikoloa, HI, 2006, vol. 1, pp. 879–884, doi: 10.1109/WCPEC.2006.279597.

[245] R. Dubey, S. Chattopadhyay, V. Kuthanazhi, J. John, C. S. Solanki, A. K., B. M. Arora, K. Narsimhan and J. Vasi, "Daylight Electroluminiscence Imaging of Photovoltaic Modules by Image Difference Technique," in *Proceedings of the IEEE 6th World Conference on Photovoltaic Energy Conversion, WCPEC-6*, Kyoto, Japan, 2014.

[246] S. Meyer *et al.*, "Silver nanoparticles cause snail trails in photovoltaic modules," *Sol. Energy Mater. Sol. Cells*, vol. 121, pp. 171–175, 2014, doi: 10.1016/j.solmat.2013.11.013.

[247] B. Bora, "Energy Rating and Assessment of Reliabilty of PV Module," Ph.D. dissertation,TERI, 2020.

[248] R. Dubey *et al.*, "Comprehensive study of performance degradation of field-mounted photovoltaic modules in India," *Energy Sci. Eng.*, vol. 5, no. 1, pp. 51–64, 2017, doi: 10.1002/ese3.150.

[249] Y. R. Golive *et al.*, "Analysis of Field Degradation Rates Observed in All-India Survey of Photovoltaic Module Reliability 2018," *IEEE J. Photovoltaics*, vol. 10, no. 2, pp. 560–567, 2020, doi: 10.1109/JPHOTOV.2019.2954777.

[250] *Photovoltaic devices - Part 13: Electroluminescence of photovoltaic modules*, IEC TS 60904-13, 2018.

[251] *Photovoltaic devices - Procedures for temperature and irradiance corrections to measured I-V characteristics*, IEC 60891:2009.

[252] M. G. Deceglie, T. J. Silverman, B. Marion, and S. R. Kurtz, "Metastable changes to the temperature coefficients of thin-film photovoltaic modules," in *Proceedings of the 40th IEEE Photovoltaic Specialist Conference,* Denver, CO, 2014, pp. 337–340, doi: 10.1109/PVSC.2014.6924926.

[253] D. L. King, W. E. Boyson, and J. A. Kratochvil, "Analysis of factors influencing the annual energy production of photovoltaic systems," in *Proceedings of the 29th IEEE*

Photovoltaic Specialists Conference, New Orleans, LA, 2002, pp. 1356–1361, doi: 10.1109/pvsc.2002.1190861.

[254] G. Friesen, D. Pavanello, and a. Virtuani, "Overview of Temperature Coefficients of Different Thin Film Photovoltaic Technologies," in *Proceedings of the 25th European Photovoltaic Solar Energy Conference and Exhibition / 5th World Conference on Photovoltaic Energy Conversion*, Valencia, 2010, pp. 4248–4252, doi: 10.4229/25thEUPVSEC2010-4AV.3.83.

[255] D. L. King, J. A. Kratochvil, and W. E. Boyson, "Temperature coefficients for PV modules and arrays: Measurement methods, difficulties, and results," in *Proceedings of the 26th IEEE Photovoltaic Specialists Conference*, Anaheim, CA, pp. 1183–1186, 1997, doi: 10.1109/pvsc.1997.654300.

[256] B. Kroposki, W. Marion, D. L. King, W. E. Boyson, and J. A. Kratochvil, "Comparison of module performance characterization methods," in *Proceedings of the 28th IEEE Photovoltaic Specialists Conference*, Anchorage, AK, 2000, pp. 1407–1411, doi: 10.1109/PVSC.2000.916156.

[257] A. M. Gabor, R. Janoch, A. Anselmo, J. L. Lincoln, H. Seigneur, and C. Honeker, "Mechanical load testing of solar panels - Beyond certification testing," in *Proceedings of the 44th IEEE Photovoltaic Specialist Conference,* Washington, DC, 2017, pp. 1–6, doi: 10.1109/PVSC.2017.8366848.

This page is intentionally left blank.

List of Publications

International Journals

1. **R. Dubey**, S. Chattopadhyay, V. Kuthanazhi, Anil K., C. S. Solanki, B. M. Arora, K. L. Narasimhan, J. Vasi, B. Bora, Y. K. Singh, O. S. Sastry, "Comprehensive study of performance degradation of field-mounted photovoltaic modules in India", *Energy Science & Engineering*, vol. 5, 51-64. 2016. DOI: 10.1002/ESE3.150. (Cited 40 times)

2. S. Chattopadhyay, **R. Dubey**, S. Bhaduri, S. Zachariah, H. K. Singh, C. S. Solanki, Anil K., N. Shiradkar, B. M. Arora, K. L. Narasimhan, J. Vasi, "Correlating Infrared Thermography with Electrical Degradation of PV Modules Inspected in All-India Survey of Photovoltaic Module Reliability 2016", *IEEE Journal of Photovoltaics*. vol. 8, issue 6, pp. 1800-1808, 2018. DOI: 10.1109/JPHOTOV.2018.2859780. (Cited 12 times)

3. S. Chattopadhyay, **R. Dubey**, Vivek K., J. John, C. S. Solanki, A. Kottantharayil, B.M. Arora, K.L. Narasimhan, V. Kuber, J. Vasi, A. Kumar, O.S. Sastry, "Visual Degradation in Field-aged Crystalline Silicon PV Module in India and Correlation with electrical degradation", *IEEE Journal of Photovoltaics*, vol. 4 Issue 6, pp. 1470 - 1476. 2014. DOI: 10.1109/JPHOTOV.2014.2356717 [**Oral presentation** at 41st *IEEE Photovoltaic Specialists Conference*, Denver, 2014]. (Cited 53 times)

4. Y. R. Golive, S. Zachariah, **R. Dubey**, S. Chattopadhyay, S. Bhaduri, H. K. Singh, B. Bora, S. Kumar, A.K. Tripathi, A. Kottantharayil, J. Vasi, Narendra S., "Analysis of Field Degradation Rates Observed in All-India Survey of Photovoltaic Module Reliability 2018," in *IEEE Journal of Photovoltaics*, vol. 10, no. 2, pp. 560-567, March 2020, doi: 10.1109/JPHOTOV.2019.2954777.

International Conferences

1. **R. Dubey**, S. Chattopadhyay, Vivek K., J. John, C. S. Solanki, A. Kottantharayil, B. M. Arora, K. L. Narasimhan, J. Vasi, B. Bora, Y. K. Singh, O.S. Sastry, "Correlation of Electrical and Visual Degradation Seen in Field Survey in India", in *Proceedings of the 43rd IEEE Photovoltaics Specialists Conference (PVSC)*, Portland, OR, 2016, pp. 1692-1696, doi: 10.1109/PVSC.2016.7749912. [**Best Poster Award**]

2. **R. Dubey**, S. Chattopadhyay, Vivek K., Jim John, C.S. Solanki, Anil K., B.M. Arora, K.L. Narasimhan, J. Vasi, A. Kumar, O.S. Sastry, "Performance Degradation of Field-aged crystalline silicon PV Modules in different Indian climatic conditions," in *Proceedings of the 40th IEEE Photovoltaics Specialists Conference (PVSC),* Denver, 2014, pp. 3182 - 3187, doi: 10.1109/PVSC.2014.6925612. (Cited 26 times)

3. **R. Dubey**, S. Chattopadhyay, Vivek K., Jim John, C. S. Solanki, Anil K., B.M. Arora, K.L. Narasimhan, J. Vasi, "Daylight Electroluminescence Imaging of Photovoltaic Modules by Image Difference Technique," presented at the *6th World Conference on Photovoltaic Energy Conversion,* Kyoto*, 2014*

4. **R. Dubey**, P. Batra, S. Chattopadhyay, A. Kottantharayil, B. M. Arora, K. L. Narasimhan, J. Vasi, "Measurement of Temperature Coefficient of Photovoltaic Modules in Field and Comparison with Laboratory Measurements", in *Proceedings of the 42nd Photovoltaic Specialist Conference (PVSC)*, New Orleans, LA, 2015, pp. 1-5, doi: 10.1109/PVSC.2015.7355852. (Cited 9 times)

5. **R. Dubey**, S. Zachariah, S. Chattopadhyay, V. Kuthanazhi, S. Rambabu, S. Bhaduri, Hemant K. Singh, A. Sinha, C. S. Solanki, A. Kottantharayil, Brij M. Arora, K. L. Narasimhan, J. Vasi, B. Bora, Rajesh Kumar, O. S. Sastry, "Performance of Field-Aged PV Modules in India: Results from 2016 All India Survey of PV Module Reliability", in *Proceedings of the 44th Photovoltaic Specialist Conference (PVSC)*, Washington, DC, 2017, pp. 3478-3481, doi: 10.1109/PVSC.2017.8366143.

6. **R. Dubey**, S. Chattopadhyay, S. Zachariah, V. Kuthanazhi, S. Rambabu, S. Bhaduri, H. K. Singh, C. S. Solanki, Anil K., B. M. Arora, K. L. Narasimhan, N. Shiradkar, B. Bora, O. S. Sastry, J. Vasi, "Investigation of Poor Performing PV Modules observed in All-India Survey of Photovoltaic Module Reliability 2016," in *Proceedings of the 7ᵗʰ World Conference on Photovoltaic Energy Conversion (WCPEC) (A Joint Conference of 45ᵗʰ IEEE PVSC, 28ᵗʰ PVSEC & 34ᵗʰ EU PVSEC)*, Waikoloa Village, HI, 2018, pp. 690-694. DOI: 10.1109/pvsc.2018.8548000

7. **Rajiv Dubey**, S. Chattopadhyay, S. Zachariah, V. Kuthanazhi, S. Rambabu, S. Bhaduri, H. K. Singh, C. S. Solanki, Anil K., B. M. Arora, K. L. Narasimhan, N. Shiradkar, B. Bora, O. S. Sastry, J. Vasi, "On-Site Electroluminescence Study of Field-Aged PV Modules", in *Proceedings of the 7ᵗʰ World Conference on Photovoltaic Energy Conversion (WCPEC) (A Joint Conference of 45ᵗʰ IEEE PVSC, 28ᵗʰ PVSEC & 34ᵗʰ EU PVSEC)*, Waikoloa Village, HI, 2018, pp. 0098-0102, doi: 10.1109/PVSC.2018.8548080.[Oral]

8. S. Chattopadhyay, **R. Dubey**, Vivek K., J. John, C. S. Solanki, A. Kottantharayil, B. M. Arora, K.L. Narasimhan, J. Vasi, B. Bora, Y. K. Singh, O.S. Sastry, "Effect of Hot Cells on Power Degradation of PV Modules," in *Proceedings of the NREL PV Module Reliability Workshop*, Golden, 2016. [**Best Poster Award** in "Module Reliability in Extreme Climates" category]

9. S. Chattopadhyay, **R. Dubey**, Vivek K., J. John, C. S. Solanki, A. Kottantharayil, B. M. Arora, K.L. Narasimhan, J. Vasi, B. Bora, Y. K. Singh, O.S. Sastry, "All India Survey of Photovoltaic Module Degradation 2014: Survey Methodology and Statistics," in *Proceedings of the 42ⁿᵈ IEEE Photovoltaics Specialists Conference (PVSC)*, New Orleans, LA, 2015, pp. 1-6, doi: 10.1109/PVSC.2015.7355712. (Cited 12 times)

10. Vivek K., **R. Dubey**, S. Chattopadhyay, J. John, C. S. Solanki, Anil K., B.M. Arora, K.L. Narasimhan, J. Vasi, A. Kumar, O.S. Sastry, "Linking Performance of PV Systems in India with Socio-economic Aspects of Installation," in *Proceedings of the 40ᵗʰ IEEE*

Photovoltaics Specialists Conference (PVSC), Denver, 2014, pp. 1448 - 1451, doi: 10.1109/PVSC.2014.6925188

11. J. John, S. Chattopadhyay, **R. Dubey**, Anil K., J. Vasi, "Evaluation of Soiling Loss Measurement Methodologies for Different PV Module Technologies," presented at the *6th World Conference on Photovoltaic Energy Conversion,* Kyoto, 2014

12. C. Mahapatra, **R. Dubey**, S. Chattopadhyay, S. Zachariah, S. Sabnis, "Statistical Analysis of Degradation Data for c-Si modules observed in India in 2016", in *Proceedings of the 44th IEEE Photovoltaics Specialists Conference (PVSC)*, Washington, DC, 2017, pp. 2849-2853, doi: 10.1109/PVSC.2017.8366657.

13. S. Bhaduri, S. Chattopadhyay, **R. Dubey**, S. Zachariah,V. Kuthanazhi, C. S. Solanki, B. M. Arora, K. L.Narsimhan, A. Kottantharayil, J. Vasi, "Correlating Infrared Thermography with Electrical Degradation of Modules inspected in All India Survey of Photovoltaic Module Reliability 2016", presented at NREL Photovoltaic Reliability Workshop, Colorado, USA, 2017 **[Best Poster Award]**

14. Hemant K. Singh, **R. Dubey**, S. Zachariah, K. L. Narasimhan, B. M. Arora, A. Kottantharayil, J. Vasi, "Modified STC Correction Procedure for Assessing PV Module Degradation in Field Surveys", in *Proceedings of the 44th IEEE Photovoltaic Specialists Conference (PVSC)*, Washington, DC, 2017, pp. 1995-1999, doi: 10.1109/PVSC.2017.8520933.

15. S. Bhaduri, S. Zachariah, Y. R. Golive, S. Chattopadhyay, **R. Dubey**, R. Ingle, A. Kottantharayil, A. A. Khattab, H. K. Singh, S. Mallick, J. Vasi and N. Shiradkar, "Correlating the Hot Spots and Power Degradation seen in crystalline silicon modules in All India Survey of PV Module Reliability 2018", in *Proceedings of the 46th IEEE Photovoltaics Specialists Conference (PVSC)*, Chicago, IL, USA, 2019, pp. 0861-0865, doi: 10.1109/PVSC40753.2019.8980514.

16. S. Zachariah, **R. Dubey**, G. Y. Rao, S. Bhaduri, S. Chattopadhyay, C. S. Solanki, A. Kottantharayil, B. M. Arora, K.L. Narasimhan, H. K. Singh, J. Vasi and N. Shiradkar,

"Electroluminescence Study of over 700 Fielded PV Modules in All India Survey 2018," in *Proceedings of the 46th IEEE Photovoltaics Specialists Conference (PVSC)*, Chicago, IL, USA, 2019, pp. 1414-1419, doi: 10.1109/PVSC40753.2019.8981208.

Reports

1. S. Chattopadhyay, **R. Dubey**, Vivek K., S. Zachariah, S. Bhaduri, C. Mahapatra, S. Rambabu, F. Ansari, A. Chindarkar, A. Sinha, H. K. Singh, N. Shiradkar, B. M. Arora, A. Kottantharayil, K. L. Narasimhan, S. Sabnis, B. Bora, G. Kumar, Y. K. Singh, M. Bangar, M. Kumar, A. Kumar Haldkar, R. Singh, S. Raghava, M. Morampudi, G. Ganesh, R. Kumar, O. S. Sastry and J. Vasi, "All-India Survey of PV Module Reliability: 2016," National Centre for Photovoltaic Research and Education, Mumbai, India, 2015. [Online]   Available: http://www.ncpre.iitb.ac.in/research/pdf/All_India_Survey_of_Photovoltaic_Module_Rel iability_2016.pdf. (Cited 19 times)

2. **R. Dubey**, S. Chattopadhyay, Vivek K., J. John, C.S. Solanki, Anil K., B.M. Arora, K.L. Narasimhan, V. Kuber, J. Vasi, B. Bora, Y. K. Singh, O.S. Sastry, "All-India Survey of PV Module Reliability: 2014," National Centre for Photovoltaic Research and Education, Mumbai,   India,   2015   [Online]   Available: www.ncpre.iitb.ac.in/uploads/All_India_Survey_of_Photovoltaic_Module_Reliability_20 14.pdf. (Cited 14 times)

3. **R. Dubey**, S. Chattopadhyay, Vivek K., J. John, C.S. Solanki, Anil K., B.M. Arora, K.L. Narasimhan, V. Kuber, J. Vasi, A. Kumar, O.S. Sastry, "All-India Survey of PV Module Degradation: 2013," National Centre for Photovoltaic Research and Education, Mumbai, India,   Mar.   2014   [Online]   Available: www.ncpre.iitb.ac.in/uploads/All_India_Survey_of_Photovoltaic_Module_Degradation_2 013.pdf. (Cited 25 times)

This page is intentionally left blank.

Resume

Rajeev Dubey

Ph. D. Student
Electrical Engineering Department
Indian Institute of Technology, Bombay
Specialization: Microelectronics
rajiv.knit.09@gmail.com
+91 9167546188

Education

Ph. D. Electrical Engineering (thesis submitted)
Indian Institute of Technology, Bombay
- Guides: Prof. Anil Kottantharayil, Prof. Juzer Vasi.
- CPI: 9.11/10

B. E. Electronics Engineering (6/2009)
K. N. I. T. Sultanpur, Uttar Pradesh Technical University, Lucknow.
- Percentage: 70%

Intermediate/+2 (7/2003)
St. John's School, I. C. S. E.
- Percentage: 77%

Matriculation (7/2001)
St. John's School, I. C. S. E.
- Percentage: 76%

Note: Joined IIT Bombay as a M. Tech. student in 2011, and converted to joint M. Tech. – Ph. D. program in 2014. (This option is available to selected research-oriented students with high CPI.)

Area of Interest

- Photovoltaic Modules (Characterization & Modelling)
- Reliability of Photovoltaic Modules
- Accelerated Testing and Lifetime Prediction
- Photovoltaic Power Plant Inspection

Research Work

Ph. D Thesis: Electrical Degradation of Crystalline Silicon PV modules in Indian Climates and its correlation with Cell Cracks: Field and Laboratory Studies
[June – 2014 to 2020]
Project aims at characterizing photovoltaic modules of various technologies and studying its reliability aspects.

Work Completed
- Essential electrical parameters of PV modules (like P_{max}, V_{oc}, I_{sc}, FF) is measured across different climatic zones in India and the degradation in those parameters are calculated and

studied. Study of maximum power degradation of PV modules in different climatic conditions especially the hot zones.

- Correlation of maximum power degradation with cracks, hot spot and degradation in device parameters (ideality factor, recombination parameters) has been done.
- Characterization technique has been developed to obtain the EL images of the fielded PV modules in the presence of ambient light.
- Impact of cracks on the PV modules performance and its correlation with essential electrical parameters of PV modules (like P_{max}, V_{oc}, I_{sc}, FF) has been studied from the field data.
- Laboratory validation of extent of crack with performance of PV modules and comparing various design of PV module.
- Correlate the mechanical stress generated during dynamic mechanical loading (DML) test PV module with different interconnect designs.
- To find the pressure/number of cycles/frequency on the transformation from Mode A to Mode B and Mode C cracks.

Professional Experience

SolarMarQ Engineering LLP (Co-founder and CEO)
[May. 2019 to present]
- Solar Panel Testing Products
  - EL-Pro Portable EL Tester (suitable for lab and field EL testing): Supplied to Sterling & Wilson, SunEdison, IISc Bangalore, NISE, ARCI Hyderabad, ASU-PSL Arizona USA.
  - Mini-Module EL Tester (suitable for mini modules and as an educational kit): Supplied to Barefoot College, Tilonia.
  - Dynamic Mechanical Loading Tool (suitable for static and dynamic loading of the PV module as per IEC 61215 and IEC TS 62782)
- On-site EL Inspection & Reporting Services
  - EL inspection for more 10,000 modules at different location of India.
  - Some of our valuable clients are Mahindra TEQO, Arbutus Consultants, YelloSky, Sustainfy Energy LLP, Clean Energy Associates (USA), IRCLASS.

Work Experience

- Lecturer in the department of Electronics & Communication in S.I.T.M Lucknow (Affiliated to U.P.T.U, Lucknow approved by AICTE, Government of India, New Delhi. [August 2009 – June 2011].
- Research Assistant, Nanoelectronics Device Characterization Lab, IIT Bombay. [July-2011-June 2014].

Internships

Research Intern at National Renewable Energy Laboratory (NREL) under Dr. Sarah Kurtz
[Nov. 2016 to Feb. 2017]
- The aim of this internship was to understand the impact of crack on the PV module performance and various other electrical parameters (V_{oc}, I_{sc}, FF, series and shunt resistance). Also, to

understand the origin of different types of cracks and how these cracks grow over time. One of the key aspects during this internship was to collect data as per the new IEC 61215 standards (where dynamic mechanical loading is included).

Research Intern at National Renewable Energy Laboratory (NREL) under Dr. Ingrid Repins
[Nov. 2017 to Dec. – 2017]
- The aim of this internship was to develop a laboratory technique to age PV modules. We compared the performance of PV modules of different contact designs (conventional versus IBC and others) under similar stress sequence (dynamic mechanical stress followed by thermal cycles and humidity freeze). Our focus was on determining which PV design will perform better in presence of similar types of cracks.

Field Surveys

All India Survey of PV Module Degradation: 2013 Team Lead
[May 2013 to June – 2013]
- All India survey of PV module degradation is done for the "first time" in India under the authority of Ministry of New and Renewable Energy (MNRE), Solar Energy Centre & NCPRE (IIT Bombay), across 26 different sites in 10 states of India, examining 63 different modules.
- On field *I-V* measurement & IR thermography of PV modules were done and visual degradation was recorded.
- A comprehensive data record of the entire work is submitted as "All India Survey of PV Module Degradation: 2013" report [http://www.ncpre.iitb.ac.in/uploads/All_India_Survey_of_Photovoltaic_Module_Degradation_2013.pdf] to MNRE for the first time.

All India Survey of PV Module Degradation: 2014 Team Lead
[September 2014 to November – 2014]
- All India survey of PV module degradation was done for the second time in collaboration with National Institute of Solar Energy (NISE) & NCPRE (IIT Bombay) on a massive scale in terms of number of modules and characterization done on modules, across 51 different sites in 15 states of India, examining 1148 different modules.
- On field lighted & dark *I-V* measurement, IR thermography, EL imaging, insulation resistance of PV modules was done and visual degradation was recorded.
- A comprehensive data record of the entire work is submitted as "All India Survey of PV Module Reliability: 2014" report [http://www.ncpre.iitb.ac.in/research/pdf/All_India_Survey_of_Photovoltaic_Module_Reliability_2014.pdf] to MNRE.

All India Survey of PV Module Degradation: 2016 Team Lead
[March 2016 to May – 2016]
- All India survey of PV module degradation was done for the third time in collaboration with National Institute of Solar Energy (NISE) & NCPRE (IIT Bombay) on a massive scale in terms of number of modules and characterization done on modules, across 37 different sites in 18 states of India, examining 925 different modules.

- On field lighted & dark *I-V* measurement, IR thermography, EL imaging, insulation resistance and temperature co-efficient of PV modules was done and visual degradation was recorded.
- A comprehensive data record of the entire work is submitted as "All India Survey of PV Module Reliability: 2016"report [http://www.ncpre.iitb.ac.in/research/pdf/All_India_Survey_of_Photovoltaic_Module_Reliability_2016.pdf] to MNRE.

Journal Publications

- Chattopadhyay S., **Dubey R**., Kuthanazhi V., John J .J. , Solanki C.S. , Kottantharayil A. , Arora B. M., Narasimhan, K. L. , Kuber V., Vasi, J. , Kumar A. , Sastry O. S., "Visual Degradation in Field-Aged Crystalline Silicon PV Modules in India and Correlation With Electrical Degradation", *IEEE Journal of Photovoltaics*, vol. 4, pp. 1470 – 1476, 2014.
- **Dubey R**, Chattopadhyay S. R., Kuthanazhi V., Kottantharayil A. , Arora B. M., Narasimhan, K. L. , Kuber V., Bora B., Sastry O. S. , Vasi, J. "Comprehensive study of performance degradation of field-mounted PV modules in India", *Energy Science and Engineering*, vol. 5, pp. 51, 2017.
- Chattopadhyay C ,**Dubey R**, Sonali Bhaduri , Sachin Zachariah, Hemant Kumar Singh , Chetan Singh Solanki, Anil Kottantharayil, Narendra Shiradkar, Brij M. Arora, K. L. Narasimhan, Juzer Vasi, "Correlating Infrared Thermography With Electrical Degradation of PV Modules Inspected in All-India Survey of Photovoltaic Module Reliability 2016", IEEE Journal of Photovoltaics, Vol. 8 Issue 6, pp. 1800 - 1808.
- G. Yogesh**,** Zachariah S., **Dubey R**, Chattopadhyay S., Bhaduri S., Singh H., Bora B., Kumar S., Tripathi A, Kottantharayil A., Vasi, J., Shiradkar N, "Analysis of Field Degradation Rates Observed in All-India Survey of Photovoltaic Module Reliability 2018", *IEEE Journal of Photovoltaics*, vol. 10, pp. 560 – 567, 2020.

Conference Publications

- **Dubey R**., Chattopadhyay S., Kuthanazhi V., John J. J, Kottantharayil A., Solanki C. S., Arora B. M., Narasimhan K. L., Vasi J., Kumar A., Sastry O.S., "Performance Degradation of Field-aged crystalline silicon PV Modules in different Indian climatic conditions", in *Proceedings of the 40th IEEE Photovoltaic Specialists Conference,* Denver, CO, 2014.
- **Dubey R**., Chattopadhyay S., Kuthanazhi V., John J. J, Kottantharayil A., Solanki C. S., Arora B. M., Narasimhan K. L., Vasi J., "Day Light Electroluminescence Imaging of Photovoltaic Modules by Image Difference Technique", in *Proceedings of 6th World Conference on Photovoltaic Energy Conversion*, Kyoto, Japan, 2014.
- **Dubey R**., Batra P., Chattopadhyay S., Kottantharayil A., Arora B. M., Narasimhan K. L., Vasi J., "Measurement of Temperature Coefficient of Photovoltaic Modules in Field and Comparison with Laboratory Measurements", in *Proceedings of the 42nd IEEE Photovoltaic Specialists Conference,* New Orleans, LA, 2015.
- Chattopadhyay S., **Dubey R**., Kuthanazhi V., John J. J, Solanki C. S., Arora B. M., Narasimhan K. L., Kottantharayil A., Vasi J., Bora B. , Singh Y., Sastry O. S., "All India Survey of Photovoltaic Module Degradation 2014: Survey Methodology and Statistics", in *Proceedings of the 42nd IEEE Photovoltaic Specialists Conference,* New Orleans, LA, 2015.

- **Dubey R.**, Chattopadhyay S., Kuthanazhi V., John J. J, Solanki C. S., Arora B. M., Narasimhan K. L., Kottantharayil A., Vasi J., Bora B. , Singh Y., Sastry O. S, "Correlation of Electrical and Visual Degradation Seen in Field Survey in India", *Proceedings of the 43rd IEEE Photovoltaic Specialist Conference,* Portland, USA, 2016.
- Kuthanazhi V., Santhosh J., Prachi J., Kamlesh K. Akhilesh M., Ameya P., Vasi J., Kottantharayil A., Krithi R., Narayanan N., Vinit K., **Dubey R.** , "Estimating Mumbai's Rooftop PV Potential through Mobilization of IEEE Student Community", *Proceedings of the 43rd IEEE Photovoltaic Specialist Conference,* Portland, USA, 2016.
- **Dubey R**., Zachariah S., Chattopadhyay S., Kuthanazhi V., Rambabu S., Bhaduri S., Singh H., Sinha A., Bora B., Kumar R., Sastry O., Chetan S. S., Kottantharayil A., Brij M. A., Narasimhan K., Vasi J., "Performance of Field-Aged PV Modules in India: Results from 2016 All India Survey of PV Module Reliability", *Proceedings of the 44th IEEE Photovoltaic Specialist Conference,* Washington DC, USA, June 2017.
- **Dubey R.** Chattopadhyay S., Zachariah S., Rambabu S., Singh H., Kottantharayil A., Arora B., Narasimhan K., Shiradkar N., Vasi J., "On-Site Electroluminescence Study of Field-Aged PV Modules", *presented at the 7th World Conference on Photovoltaic Energy Conversion*, Hawaii, USA, 2018.
- **Dubey R.** Chattopadhyay S., Zachariah S.,Kuthanazhi V., Rambabu S., Bhaduri S., Singh H., Kottantharayil A., Arora B., Narasimhan K., Shiradkar N, Solanki C., Bora B., Sastry O.S, Vasi J., "Investigation of Poor Performing PV Modules Observed in All-India Survey of PV Module Reliability", *presented at the 7th World Conference on Photovoltaic Energy Conversion*, Hawaii, USA, 2018.

Conferences Attended

- 40th IEEE Photovoltaic Specialist Conference held in June, 2014 at Denver, Colorado.
- 6th World Conference on Photovoltaic Energy Conversion held in November, 2014 at Kyoto, Japan.
- 42nd IEEE Photovoltaic Specialist Conference held in June, 2015 at New Orleans, Louisiana, USA.
- 43rd IEEE Photovoltaic Specialist Conference held in June, 2016 at Portland, Oregon, USA.
- 44th IEEE Photovoltaic Specialist Conference held in June, 2017 at Washington D.C. Washington, USA.
- 7th World Conference on Photovoltaic Energy Conversion held in June, 2018 at Hawaii, USA.

Awards/Fellowships

- Best poster award at the PV Module Reliability Workshop 2016 for the poster: "Effect of Hot Cells on Electrical Degradation of PV Modules", by Shashwata Chattopadhyay, Rajiv Dubey, Vivek Kuthanazhi, Jim Joseph John, Juzer Vasi, Anil Kottantharayil, Brij M. Arora, K. L. Narsimhan, Chetan S. Solanki, Birinchi Bora, Yogesh Kumar Singh and O.S. Sastry.
- Best poster award at the 43rd IEEE Photovoltaic Specialist Conference for the poster: "Correlation of Electrical and Visual Degradation Seen in Field Survey in India", by Dubey R., Chattopadhyay S., Kuthanazhi V., John J. J, Solanki C. S., Arora B. M., Narasimhan K. L., Kottantharayil A., Vasi J., Bora B. , Singh Y., Sastry O. S.

- Best poster award at the 43rd IEEE Photovoltaic Specialist Conference for the poster: "Estimating Mumbai's Rooftop PV Potential through Mobilization of IEEE Student Community", by Kuthanazhi V., Santhosh J., Prachi J., Kamlesh K. Akhilesh M., Ameya P., Vasi J., Kottantharayil A., Krithi R., Narayanan N., Vinit K., Dubey R.
- Received SERIIUS MAGEEP fellowship in year 2016 for perusing three months internship at NREL.

PV Characterization Tools Developed

Dynamic Mechanical Loading

- It can simulate wind, snow loading on any size commercial available PV module.
- Can do static (as per IEC 61215) and dynamic (as per IEC TS 62782) mechanical loading.

Low Cost Electroluminance (EL) Camera

- Developed a low cost EL camera by modifying a regular digital camera.
- Developed an EL camera under $100

Low Cost Temperature Co-efficient Device

- Developed a low cost temperature co-efficient device which could measure the temperature co-efficient of a PV module in field.

Technical Skills

Characterization Tools/Instruments	:	Solmetric PVA 1000S, FLIR thermal IR Imaging, Spire SPI- Sun Simulator 5600 SPL Blue, Sensovation HR-830, Daystar Multicurve *I-V* tracer, Fluke 1550C, Keithley 4200, Agilent B1500, Agilent 8110 PGU, Agilent 4284/4285 LCR
Design Tools	:	NgSpice, Magic, Ghdl.
Programming Skills	:	MATLAB, Python, LabVIEW, C, C++, GPIB programming.

Acknowledgements